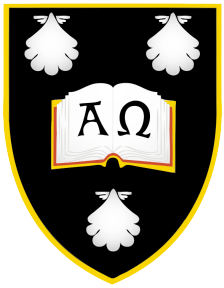
Orchestration of the Ubiquitin-Dependent DNA Damage Response by the p97 System

DPhil Thesis

Supervised by
Prof Kristijan Ramadan



Judith K. Oehler

Linacre College



CRUK/MRC Oxford Institute for Radiation Oncology
Department of Oncology
University of Oxford

Trinity Term 2016





OXFORD INSTITUTE FOR RADIATION ONCOLOGY



FONDS NATIONAL SUISSE
SCHWEIZERISCHER NATIONALFONDS
FONDO NAZIONALE SVIZZERO
SWISS NATIONAL SCIENCE FOUNDATION

ACKNOWLEDGMENTS

First of all, I would like to thank Kristijan Ramadan for giving me the opportunity to perform my DPhil in his laboratory including lots of fruitful discussions, idea exchanges and motivation speeches. His mind is a source of knowledge and fountain of ideas, which can be very inspiring. Thanks Kristijan!

Additionally, I would like to express my thanks to all the members (current and past) of the Ramadan lab. Bruno(lino), who was always there inside and outside the lab, helping me through those four years but also making it a fun ride. You have also been (and still are) a great source of knowledge both in science and politics. Swagata, who started out with me as a DPhil student and therefore accompanied me on the way from the start to the end on, cooking the very best biryani on the run. Abhay, with whom I shared a protein of interest and therefore had many fruitful chats about how to best work with it. Thanks for sharing your data openly with me. Katy, who sacrificed time to share the chore of ordering with me and drinking coffee/tea/water. Additionally, I thank her for proofreading the thesis and keep me motivated whenever it became very hard. Marta who knows everything about IPs and cloning, thanks for many a squash fight, coffee and beer chats but also for the hours spent in the library with you! Ignacio, the peace-center and most organised person possible, who also happens to have organised the best BBQ ever! Thank you for discovering Ataxin-3 in your SILAC and sharing your data! John, who has just the right sense of humor and science smartness but also for feeding me on weekends and late nights in the lab. Jenny, Domenik and Divya, who enriched our lab for a while with their enthusiasm.

Thanks to all the people in the ORCRB that have helped me one way or the other. Especially a big, hearty thank you goes to Boris Vojnovic, Ian Tullis and Pam for setting up the UV-A laser system.

Moreover, a thank you to Israel and the group of Yossi Shiloh, especially Keren, for offering me the opportunity to work with them on UBE4A/B and sharing their data with me.

Mirjam, Selina and Jeannette, who have been great friends throughout this time even though being far away. Danke, er liebe! Thanks also to Naga Raja who was more than a great friend and would always be on my side, no matter what.

Thanks also to my family, who have been a constant support throughout.

DECLARATION

I declare that this thesis and the work described in it is my work, aside from the results presented in Fig 4.1, Fig 4.2, partially in Fig 4.6, Fig 6.5B and Fig. 6.9. In the corresponding figure legends, the individual person who created the work is credited.

ABSTRACT

The DNA damage response (DDR) is a highly organised process, which involves the spatial and temporal orchestrated removal and recruitment of proteins, achieved by the use of dynamic posttranslational modifications (PTMs). Ubiquitination has emerged as one of the major PTMs in the DDR after DNA double strand breaks. Intensive studies have been performed to understand the regulation and impact of ubiquitination in the DDR. Regulation of important DDR players such as 53BP1, BRCA1 or RAD51 strictly depend on the signaling cascade initiated by the two main ubiquitin E3 ligases RNF8 and RNF168 at the site of DNA damage. Recently, it has emerged that the AAA ATPase p97 (VCP/Cdc48) plays a crucial role in the ubiquitin axis of the DDR. p97 interacts with a vast set of cofactors that target p97 to specific substrates and assist it in its function as a molecular segregase. However, the exact role of p97 and its cofactors in the response to ionising radiation induced DSBs and ubiquitination is still poorly understood. In this thesis, three p97 cofactors and their role in the DSB-triggered ubiquitination have been studied. The results show that the so-far poorly characterised UBE4A and UBE4B, two E3/E4 ubiquitin enzymes and p97 associated proteins (cofactors), play critical roles in the regulation of ubiquitination at the sites of DNA damage and absence of either affects both K48- and K63-linked ubiquitin chains. Furthermore, another cofactor of p97, the deubiquitinating enzyme Ataxin-3, affects the regulation of RNF8 and RNF168 at the sites of DNA damage. All three proteins, therefore, help to fine-tune the DDR and the recruitment of critical DDR proteins including BRCA1 or 53BP1. Together, the results of this thesis discover and characterise three new players

to the ubiquitination axis at the site of DNA damage. Moreover, Ataxin-3 appears to be an interesting druggable target for two-hit radiotherapy for cancer treatment, namely, the inhibition of Ataxin-3 deubiquitinating activity in combination with ionising radiation.

TABLE OF CONTENTS

ACKNOWLEDGMENTS ..... **I**

DECLARATION ..... **II**

ABSTRACT ..... **III**

TABLE OF CONTENT ..... **I**

LIST OF FIGURES ..... **VI**

LIST OF TABLES ..... **VII**

LIST OF ABBREVIATIONS ..... **VIII**

1 INTRODUCTION **1**

1.1 UBIQUITIN 1

1.2 THE UBIQUITIN CHEMISTRY 1

1.2.1 The Ubiquitin Code *2*

1.2.2 Writers Of The Ubiquitin Code: Ubiquitin Ligases *3*

1.2.3 Ubiquitin E4 Chain Assembly Enzymes *5*

1.2.4 Reading The Ubiquitin Code: Ubiquitin Binding Domains *6*

1.2.5 Eraser Of The Ubiquitin Code: Deubiquitinating Enzymes (DUBs) *7*

1.2.6 Regulation Of Dubs *8*

1.2.7 The Proteasome *8*

1.2.8 The Ubiquitin-Proteasome System (UPS) *10*

1.3 P97 11

1.3.1 p97 And Its Cofactors *12*

1.3.2 p97 Inside The Nucleus *15*

1.3.3 p97's Role In Replication *16*

1.4 P97 ADAPTORS CONNECTED TO THIS THESIS 17

1.4.1 Ataxin-3 (ATXN3) *17*

1.4.1.1 ATXN3 Structure And Activity 17

1.4.1.2 Machado-Joseph Disease (MJD) 19

1.4.1.3 ATXN3 And PolyQ ATXN3 Features 19

1.4.2 Yeast Ufd2 And Its Mammalian Orthologues UBE4A And UBE4B *21*

1.5 DNA DAMAGE RESPONSE 23

1.5.1 Base Excision Repair (BER) *23*

1.5.2 Mismatch Repair (MMR) *24*

1.5.3 Nucleotide Excision Repair (NER) *24*
1.5.4 DNA Double Strand Break Repair *26*
1.5.4.1 Canonical NHEJ (cNHEJ) 27
1.5.4.2 Homologous Recombination (HR) 28
1.5.4.3 Alternative NHEJ (aNHEJ) Or Microhomology-Mediated End Joining (MMEJ) 30
1.5.4.4 Single Strand Annealing (SSA) 31
1.5.5 FA Pathway To Repair Interstrand Crosslinks *32*
1.5.6 Chromatin Response To Orchestrate DSB Repair *34*
1.6 THE UBIQUITINATION SYSTEM IN THE ORCHESTRATION OF THE DDR 36
1.6.1 RNF8 ..... *36*
1.6.2 Stabilisation Of RNF8 And MDC1 Interaction *39*
1.6.3 RNF168 ..... *40*
1.6.4 Regulation Of RNF168 Pool And Activity *44*
1.6.5 RNF169, A RNF168 Paralogue *44*
1.6.6 Dubs Involved In The Regulation Of The DDR *45*
1.6.6.1 BRCC36 45
1.6.6.2 Members Of The USP Family 46
1.6.6.3 Proteasome Associated DUB POH1/RPN11 48
1.6.6.4 OTUB1 And OTUB2 48
1.6.7 Regulation Via SUMO-Dependent Ubiquitination *49*
1.6.8 p97 Dependent Processes At The Site Of DNA Damage *50*
1.6.9 Events Downstream Of RNF8 And RNF168 ..... *53*
1.6.9.1 Regulation Of 53BP1 53
1.6.9.2 BRCA1-RAP80 Complex 54
1.6.10 Regulation Of DSB Repair And Pathway Choice *56*
1.7 GENOMIC INSTABILITY AND CANCER 57
1.7.1 The Components Of DDR As Druggable Targets *58*
1.7.2 Targeting The UPS *60*
1.8 AIM OF THE THESIS 62
2 MATERIALS AND METHODS 63
2.1 BUFFERS: 63
2.1.1 10x Phosphate Buffered Saline (PBS) *63*
2.1.2 10x TBS (Tris-buffered saline) *63*
2.1.3 10x Tris/Glycine Buffer *64*
2.1.4 1x Running Buffer For Western Blots *64*
2.1.5 1x Transfer Buffer For Western Blots *64*
2.1.6 5x Laemmli Buffer (LB) *64*

2.2 MAMMALIAN CELL CULTURE 65
2.2.1 Human Cell Lines 65
2.2.2 Maintenance Of Human Cell Lines 65
2.3 MANIPULATING HUMAN CELLS 66
2.3.1 siRNA Transfections 66
2.3.2 Plasmid transfection 67
2.3.3 Cycloheximide Chases, Proteasome Inhibitor And p97 Inhibitor 68
2.4 ANALYSIS OF PROTEINS 68
2.4.1 Preparation Of Cell Lysates 68
2.4.2 SDS-Polyacrylamide Gel Electrophoresis (PAGE) 70
2.4.3 Western Blotting 71
2.5 DNA DAMAGE INDUCTION 73
2.5.1 Preparation Of Cells For And Performance Of UV-A Laser Damage Induction 73
2.5.2 Ionising Radiation (IR) 74
2.6 COLONY FORMING ASSAY 74
2.7 IMMUNOFLUORESCENCE (IF) 75
2.7.1 Immunofluorescence Microscopy And Image Quantifications 76
2.8 PROTEIN CO-IMMUNOPRECIPITATIONS (CO-IPS) 77
2.9 STABLE ISOTOPE LABELING WITH AMINO ACIDS IN CELL CULTURE (SILAC) MASS SPECTROMETRY 78
2.10 PLASMID MANIPULATION AND CLONING 79
2.10.1 Transformation Of Bacteria 80
2.10.2 Mini/Maxiprep Plasmid Purification 80
2.10.3 Site-Directed Mutagenesis 82
2.10.4 Sub-Cloning 82
2.11 STATISTICAL ANALYSIS 85

3 RESULTS 1: UBE4A AND UBE4B: TWO NOVEL E3-UBIQUITIN LIGASES IN DSB REPAIR 86

3.1 UBE4A HELPS TO MAINTAIN K63-LINKED UBIQUITIN CHAINS 87
3.2 UBE4A REGULATES K48-LINKED UBIQUITIN CHAINS AT SITES OF DSBS 92
3.3 UBE4B HELPS TO FINE-TUNE THE K48- AND K63- LINKED UBIQUITIN CHAINS AT THE SITE OF DNA DAMAGE 95
3.4 ABSENCE OF UBE4B LEADS TO PROLONGED K48-LINKED UBIQUITINATION 96
3.5 UBE4B HELPS TO MAINTAIN THE K63-LINKED UBIQUITIN CHAINS AT THE SITE OF DNA DAMAGE 98
3.6 DISCUSSION 100

4 RESULTS 2: ATXN3 IS A NEW PLAYER IN THE DNA DAMAGE RESPONSE 103

4.1 ATXN3 DEPLETION HYPERSENSITISES CELLS TO IR 105

4.2 ATXN3 IS RECRUITED TO SITES OF DNA DAMAGE 107

4.3 ABSENCE OF ATXN3 DELAYS INITIAL 53BP1 RECRUITMENT AND LEADS TO IMPAIRED 53BP1 FOCI RESOLUTION 110

4.4 ATXN3 IS NECESSARY FOR ACCURATE UBIQUITINATION AT DSBS 116

4.5 ABSENCE OF ATXN3 LEADS TO INCREASED BRCA1 RETENTION AT A LATER TIME POINT AFTER DNA DAMAGE INDUCTION 119

4.6 DISCUSSION 121

5 RESULTS 3: ATXN3 PHYSICALLY INTERACTS WITH CRUCIAL DDR FACTORS 123

5.1 ATXN3 FORMS A COMPLEX WITH IMPORTANT PLAYERS OF THE DDR IN UNCHALLENGED CELLS 123

5.2 ATXN3 INTERACTION WITH RNF168 CHANGES UPON DSB INDUCTION 127

5.3 INTERACTION WITH RNF168, RNF8 AND KU80 IS MEDIATED OVER THE JOSEPHIN DOMAIN OF ATXN3 128

5.3.1 Creation Of Different ATXN3 Mutants 128

5.3.2 Mutation Of Putative SIM Does Not Abolish Interaction With The DDR Proteins 132

5.3.3 Interaction Of ATXN3 With The DDR Proteins Is Facilitated Over The Josephin Domain 134

5.4 DISCUSSION 136

6 RESULTS 4: ATXN3 REGULATES BOTH RNF8 AND RNF168 AT SITES OF DNA DAMAGE 138

6.1 RNF8 HYPERACCUMULATES AT SITES OF DNA DAMAGE UPON ATXN3 DEPLETION 138

6.2 ATXN3 FINE-TUNES RNF168 RECRUITMENT 142

6.3 P97 REGULATES RNF168 HOMEOSTASIS IN UNDAMAGED CELLS 145

6.3.1 ATXN3 depletion does not affect p97 recruitment to sites of DNA damage .. 147

6.4 ATXN3 RECRUITMENT TO SITES OF DNA DAMAGE DEPENDS ON P97 149

6.5 ATXN3 FORMS A PHYSICAL COMPLEX WITH $P97^{UFD1-NPL4}$ 152

6.6 DISCUSSION 153

7 DISCUSSION 156

7.1 UBE4A AND UBE4B FINE-TUNE UBIQUITINATION AT THE SITE OF DNA DAMAGE 156

7.2 ATXN3, A NEW DUB INVOLVED IN THE FINE-TUNING OF DSB REPAIR 161

7.3 ATXN3 AS A POSSIBLE DRUGGABLE TARGET FOR CANCER THERAPY 166

7.4 FUTURE WORK 167

REFERENCES **168**

APPENDIX – PUBLICATIONS **199**

LIST OF FIGURES

Figure 1-1 The Ubiquitin Code. 4
Figure 1-2. p97 and its cofactors. 14
Figure 1-3. Schematic representation of ATXN3 18
Figure 1-4. RNF8 induced ubiquitination at the site of DSBs. 38
Figure 1-5. Regulation of RNF168 and its role at the site of DNA damage. 43
Figure 1-6. p97 orchestrates the removal of proteins from the site of DNA damage. 52
Figure 3-1. Representative control Western blots 89
Figure 3-2. UBE4A helps to maintain K63-linked ubiquitin chains at the site of DNA damage. 91
Figure 3-3. UBE4A helps to maintain K48-linked ubiquitin chains at the site of DNA damage. 94
Figure 3-4. Representative Western blot for p97 and UBE4B depletion efficiency in U2OS cells. 95
Figure 3-5. UBE4B is involved in the turnover of K48-linked chains ubiquitinated proteins at later time point after damage induction. 97
Figure 3-6. UBE4B helps to maintain the K63-linked ubiquitin signal at the site of DNA damage. 99
Figure 4-1. p97 shows increased interaction with ATXN3 inside the nucleus upon IR. 104
Figure 4-2. ATXN3 protects HeLa cells from IR induced DSBs. 106
Figure 4-3. Endogenous ATXN3 is instantly recruited to sites of DNA damage. 108
Figure 4-4. Non-commercial ATXN3 antibody recognises ATXN3 specifically. 109
Figure 4-5. ATXN3 and p97 are efficiently knocked down performing siRNA transfection in U2OS. 111
Figure 4-6. Depletion of p97 or ATXN3 affects the repair of DSB indicated by delayed initial formation of 53BP1 foci and retention of them at later time points. 112
Figure 4-7. Efficacy of siRNA depletion. 114
Figure 4-8. 53BP1 recruitment to sites of DNA damage is affected upon ATXN3 depletion at 30 min but not 5 hrs of recovery. 115
Figure 4-9. ATXN3 regulates ubiquitination at the site of DSB. 117
Figure 4-10. ATXN3 depletion leads to increased ubiquitination at the site of DNA damage. 118
Figure 4-11. ATXN3 depletion leads to BRCA1 hyperaccumulation at the site of DNA damage at the later time point. 120
Figure 5-1. ATXN3 interacts with important players of the DDR. 124
Figure 5-2. ATXN3 is pulled down over RNF8, RNF168 and KU80 reciprocally. 125
Figure 5-3. ATXN3 interacts specifically with RNF8 and RNF168. 126

Figure 5-4. ATXN3 interactions with the tested proteins do not change upon IR except for RNF168. 128
Figure 5-5. Schematic depiction of ATXN3. 129
Figure 5-6. Different mutant constructs of ATXN3 do not abolish the interaction with the proteins of interest except for ATXN3 UIM* and RNF168. 131
Figure 5-7. Creation of SIM mutant ATXN3 SIM*. 132
Figure 5-8. Mutating the putative SIM in ATXN3 does not abolish interaction with RNF8, RNF168 nor KU80. 134
Figure 5-9. Schematic representation of the different fragments produced. 135
Figure 5-10. Interaction with RNF8, RNF168 and KU80 is facilitated over the N-terminal Josephine domain. 136
Figure 6-1. Non-commercial RNF8 antibody recognises RNF8 at sites of DNA damage specifically. 139
Figure 6-2. ATXN3 or p97 depletion leads to hyperaccumulation of RNF8 at the site of DNA damage. 141
Figure 6-3. The non-commercial RNF168 antibody recognises RNF168 specifically at the site of DNA damage by IF. 142
Figure 6-4. ATXN3 fine-tunes RNF168 turnover at the sites of DNA damage. 144
Figure 6-5. p97 stabilises RNF168 in unchallenged mammalian cells. 147
Figure 6-6. ATXN3 depletion does not affect p97 recruitment at sites of DNA damage. 149
Figure 6-7. ATXN3 recruitment to the site of DNA damage depends partially on p97. 151
Figure 6-8. ATXN3 is part of the $p97^{UFD1\text{-}NPL4}$ complex. 153
Figure 6-9. ATXN3 is involved in stabilising RNF8 and RNF168 in unstressed cells. 154
Figure 7-1. UBE4A and UBE4B are important new players in the maintenance of ubiquitination at the site of DNA damage. 160
Figure 7-2. ATXN3 is a fine-tuner of RNF8 and RNF168 turnover at the site of DNA damage. 165

LIST OF TABLES

Table 1 Summary of siRNA sequences 67
Table 2 Plasmid transfection using PEI 68
Table 3 List of inhibitors 70
Table 4 Protocol for running and stacking gels 71
Table 5 List of antibodies used for Western blotting 72
Table 6 Number of HeLa cells seeded for colony forming assay 75
Table 7 List of antibodies used for immunofluorescence 76
Table 8 IP beads used and their washing buffers 78

Table 9 List of plasmids used **79**
Table 10 Set-up of over-night double digestion of insert and plasmid for sub-cloning of ATXN3 ..... **84**
Table 11 List of primers **85**

LIST OF ABBREVIATIONS

53BP1	p53-Binding Protein 1
AAA ATPase	ATPase Associated With Diverse Cellular Activities
aNHEJ	Alternative Non-Homologous End-Joining
APC	Anaphase Promoting Complex
APE1/2	Apurinic-Apyrimidinic Endonuclease 1/2
APEX1	Apurinic/Apyrimidinic Endodeoxyribonuclease 1
APLF	Aprataxin-And-PNK-Like Factyor
ATM	Ataxia-Telangiectasia Mutated
ATP	Adenosine Triphosphate
ATR	ATM And Rad3-Related
ATXN3	Ataxin-3
BACH1	BRCA1-Associated C-Terminal Helicase
BARD1	BRCA1-Associated RING Domain Protein 1
Bcl-2	B-Cell Lymphoma 2
BER	Base Excision Repair
BLM	Bloom Syndrome Protein
BRCA1/2	Breast Cancer Type 1/2 Susceptibility Protein
BRCC	BRCA1/BRCA2-Containing Complex
BRCT	BRCA1 Carboxyl Terminus
CAD	Chromatin Associated Degradation
Cdc	Cell Division Cycle
CDK1	Cyclin-Dependent Kinase 1
CDT1	Chromatin Licensing And DNA Replication Factor 1
CHFR	Checkpoint With The Forkhead And RING Finger
CHIP	C Terminus Of HSC7-Interacting Protein
CHX	Cycloheximide
CK2	Casein Kinase 2
cNHEJ	Canonical Non-Homologous End-Joining
co-IP	Coimmunoprecipitation
CPD	Cyclobutane-Pyrimidine Dimers
Crb2	Cut5-Repeat Binding Protein 2
CSA/B	Cockayne Syndrome Proteins A/B
CtIP	Ctbp-Interacting Protein
CUL-3	Cullin-3
DAPI	4',6-Diamidino-2-Phenylindole

DDB2	DNA Damage-Binding Protein 2
DDR	DNA Damage Response
DMSO	Dimethyl Sulfoxide
DNA	Deoxyribonucleic Acid
DNA-PKcs	DNA-Dependent Protein Kinase Catalytic Subunit
DNA2	DNA Replication ATP-Dependent Helicase-Like Homolog 2
DSB	Double Strand Break
DUB	Deubiquitination Enzyme
EME1	Essential Meiotic Endonuclease 1
ERAD	Endoplsmic Reticulum-Associated Degradation
ERCC1	Excision Repair Cross-Complementing 1
EXO1	Exonuclease 1
FA	Fanconi Anemia
FAF1	Fas Associated Factor 1
fALS	Familial Amyotrophic Lateral Sclerosis
FANC	Fanconi Anemia Group Protein
FEN1	Flap Endonuclease 1
FHA	Forkhead-Associated
Fig	Figure
GFP	Green Fluorescent Protein
GG-NER	Global Genome-NER
GINS	Go-Ichi-Ni-San
HCC	Hepatocellular Carcinoma
HDAC6	Histone Deacetylase 6
HECT	Homologous To The E6-AP Carboxyl Terminus
HERC2	HECT Domain And RCC1-Like Domain-Containing Protein 2
HNPCC	Hereditary Non-Polyposis Colorectal Cancer
HR	Homologous Recombination
hrs	Hours
IBMPFD	Inclusion Body Myopathy With Paget's Disease Of The Bone And Frontotemporal Dementia
ICL	Interstrand Crosslink
IDL	Insertion/Deletion Loop
IF	Immunofluorescence
IR	Ionising Radiation
JAMM	JAB1/MPN/MOV34
JD	Josephine Domain
JMJD	Jumonji Domain-Containing Protein
KAP1	KRAB-Associated Protein 1
L3MBTL1	Lethal(3)Malignant Brain Tumor-Like Protein 1
LIG	Ligase
LRM	LR Motifs
Luc	Luciferase
Lys	Lysine
MBT	Malignant Brain Tumour
MBTD1	MBT Domain-Containing Protein 1

MCM	Minichromosome Maintenance
MDC1	Mediator Of DNA Damage Checkpoint Protein 1
MDM2	Double Minute 2 Protein
MERIT40	Mediator Of RAP80 Interactions And Targeting Subunit Of 40 kDa
Met	Methionine
min	Minute(s)
MINDY	Motif Interacting With Ubiquitin Containing Novel DUB Family
MIU	Motif Interacting With Ubiquitin
MJD	Machado-Joseph Disease
MMEJ	Microhomology-Mediated End Joining
MMR	Mismatch Repair
Mps1	Monopolar Spindle 1
MRE11	Meiotic Recombination 11
MRG15	MORF-Related Gene 15 Protein
MRN	MRE11, RAD50, NBS4 Complex
MSH	Muts Homolog
MTOC	Microtubule-Organisation Center
MUS81	MMS And UV-Sensitive Protein 81
NBS1	Nijmegen Breakage Syndrome Protein 1
NCS	Neocarzinostatin
NER	Nucleotide Excision Repair
NES	Nuclear Export Signal
NLS	Nuclear Localisation Signal
NPL4	Nuclear Protein Localisation Protein 4
OTU	Ovarian Tumour
OTULIN	OTU Domain-Containing Deubiquitinase With Linear Linkage Specificity
PALB2	Partner And Localiser Of BRCA2
PARP1	Poly(ADP-Ribose)Polymerase 1
PAXX	Paralog Of XRCC4 And XLF
PBS	Phosphate Buffered Saline
PCNA	Proliferating Cell Nuclear Antigen
PFGE	Pulse-Field Gel Electrophoresis
PI-3	Phosphatidylinositol-3
PIAS	Protein Inhibitor Of Activated STAT X
PIKK	Phosphatidylinositol-3 Kinase-Like Kinase
PLK1	Polo-Like Kinase 1
PMSF	Phenylmethylsulfonyl Fluoride
PNKP	Polynucleotide Kinase 3'-Phosphatase
POH	Pad One Homolouge 1
PP4C	Serine/Threonine-Protein Phosphatase 4 Catalytic Subunit
PST	Proline-Serine-Threonine
PTIP	PAX Transactivation Activation Domain-Interacting Protein
PTM	Posttranslational Modifications
RAD	Ribosomal Associated Degradation
RAD23	Radiation Sensitive 23
RAP80	Receptor-Associated Protein 80

RBR	RING-Between-RING
RFC	Replication Factor C
RIDDLE	Radiosensitivity, Immunodeficiency, Dysmorphic Features And Learning Difficulties
RIF1	Rap1-Interacting Factor 1
RING	Really Interesting New Gene
RIPA	Radioimmunoprecipitation Assay Buffer
RMI1/2	Recq-Mediated Genome Instability Protein 1/2
RNA	Ribonucleic Acid
RNF	RING Finger
RPA	Replication Protein A
RPB1	RNA Polymerase II Subunit 1
rpm	Revolutions Per Minute
RPN	Regulatory Particle Non-Atpase
RPT	Regulatory Particle Atpase
RT	Room Temperature
RTEL1	Regulator Of Telomere Elongation Helicase 1
SCA3	Spinocerebellar Ataxia Type 3
SDS	Sodium Dodecyl Sulfate
SDSA	Synthesis-Dependent Strand Annealing
SENP	Sentrin-Specific Protease
SLX1/4	Synthetic Lethal Of Unknown Function Protein 1/4
SPRTN	Spartan Protein
SQSTM1	Sequestosome-1
SSA	Single-Strand Annealing
ssDNA	Single-Stranded DNA
Strep	Streptactin
STUbL	Sumo-Targeted Ubiquitin Ligase
SUMO	Small Ubiquitin-Related Modification
SVIP	Small VCP/P97-Interacting Protein
TBS	Tris-Buffered Saline
TC-NER	Transcription Coupled NER
TDP1/2	Tyrosyl-DNA Phosphodiesterase 1/2
TFIIH	Transcription Initiation Factor IIH
TIP60	60 kDa Tat-Interactive Protein
TLS	Translesion Synthesis
TopoIIIα	Topoisomerase III α
TRIP12	Thyroid Receptor-Interacting Protein 12
UBA	Ubiquitin-Associated Domain
UBC	Ubiquitin-Conjugating Enzyme
UBD	Ubiquitin Binding Domain
UBE4	Ubiquitination Factor E4
UBR5	Ubiquitin Protein Ligase E3 Component N-Recognin 5
UbS	Ubiquitin Binding Site
UBX	Ubiquitin Regulatory X
UBXL	UBX-Like

UBZ	Ubiquitin-Binding Zinc Finger
UCH	Ubiquitin C-Terminal Hydrolase
UDM	Ubiquitin-Dependent DSB Recruitment Module
UEV1A	Ubiquitin-Conjugating Enzyme E2 Variant 1
UFD	Ubiquitin Fusion Degradation
Ufd2	Ubiquitin Fusion Degradation Protein 2
UHRF1	Ubiquitin-Like PHD And RING Finger Domain-Containing Protein 1
UIM	Ubiquitin-Interacting Motif
UMI	UIM- And MIU- Related UBD
UPS	Ubiquitin-Proteasome System
USP	Ubiquitin-Specific Protease
UV	Ultraviolet
VBM	VCP Binding Motif
VCP	Valosin-Containing Protein
VIM	VCP-Interaction Motif
WCE	Whole Cell Extracts
WRAP53β	WD Repeat-Containing Protein
WRN	Werner Syndrome ATP-Dependent Helicase
XLF	XRCC40-Like Factor
XPC	Xeroderma Pigmentosum, Complementation Group C
XRCC	X-Ray Repair Cross Complementing 1
γH2AX	S139 Phosphorylated Histone 2A.X

1 INTRODUCTION

1.1 Ubiquitin

Cellular pathways and protein homeostasis are tightly regulated and organised. To this end, posttranslational modifications (PTMs) play an essential role. PTMs, like phosphorylation, acetylation, SUMOylation, neddylation or ubiquitination, are protein modifications which can be dynamically added to and removed from substrates. Besides phosphorylation, ubiquitination is one of the most prevalent and conserved PTMs in eukaryotes, whereas it is inexistent in prokaryotes.

In 1978, Ciehanover, Hod and Hershko published their initial manuscript in which they tried to answer the question of how intracellular proteins are degraded. This later led to the discovery of ubiquitin (Ciechanover, 2015). In 2004, Aaron Ciechanover, Avram Hershko and Irwine Rose were rewarded with the Nobel Prize in Chemistry "for the discovery of ubiquitin-mediated protein degradation". Ubiquitin is a small, 76-amino acid, 8-kDa protein, that is added to its substrate in a three step enzymatic cascade, involving a ubiquitin activating enzyme (E1), a ubiquitin conjugating enzyme (E2) and a ubiquitin ligase (E3) (Hershko et al., 1983) and is removed by deubiquitinating enzymes (DUBs). It has emerged that ubiquitination is a highly dynamic and complex process used in virtually all cellular pathways.

1.2 The Ubiquitin Chemistry

Ubiquitin ligases promote the formation of an isopeptide bond between the C terminus of ubiquitin and the ε-amino group of a lysine residue in the targeted protein, which can be both a substrate or a proximal ubiquitin. The

ubiquitination reaction occurs through a series of enzymatic steps (Fig 1.1A). The E1 binds the ubiquitin C terminus in an ATP dependent manner, resulting in a thioester intermediate. The E2 takes the activated ubiquitin and, together with the catalysing E3 ligase, the ubiquitin is conjugated to the substrate via an isopeptide formation reaction (Spasser and Brik, 2012).

1.2.1 The Ubiquitin Code

Ubiquitin can be conjugated to other ubiquitin moieties and its substrates via multiple different linkages and in different patterns (Fig 1.1B).

Addition of only a single ubiquitin moiety leads to monoubiquitination of the substrate, or multi-monoubiquitination if several different lysines of the substrate are monoubiquitinated (Fig 1.1B).

Each ubiquitin contains seven lysine residues (Lys6, Lys11, Lys27, Lys29, Lys33 Lys48 and Lys63), as well as Methionine 1 (Met1), over which it can build ubiquitin chains. Homogeneous ubiquitin chains refer to the creation of polymeric chains, where two or more moieties are linked to form a chain conjugated to a single lysine on the substrate. All types of possible homogeneous chains have been observed in living organisms, with the K48- and K11- linked chains being the most abundant ones in yeast (Xu et al., 2009). E3-ubiquitin ligases can also create mixed ubiquitin chains where more than one kind of lysine in the different subunits in the chain is used for linkage. Furthermore, ubiquitin chains can be branched if more than one linkage is present on a single ubiquitin molecule. Overall, ubiquitination is the most complex PTM, and the various ubiquitin modifications constitute a highly sophisticated code used to regulate virtually all cellular processes (Komander and Rape, 2012).

The different ubiquitin tags affect the fate of a substrate in specific ways. For instance, during replication stress, PCNA can be monoubiquitinated at K164, which facilitates the association of translesion DNA polymerases. This monoubiquitination can be further extended to a K63-linked ubiquitin chain leading to DNA replication template switching (Zhang et al., 2011). Monoubiquitination of histone H2B is a signal for transcription, while monoubiquitination of receptor tyrosine kinases initiates their endocytosis followed by the transport to the lysosome (Biel et al., 2004).

K48-linked ubiquitin chains are mainly known to trigger the proteasomal degradation of the substrate, while K63-linked chains are involved in cell signaling, endocytosis and the DNA damage response (Chen and Sun, 2009).

1.2.2 Writers Of The Ubiquitin Code: Ubiquitin Ligases

The mammalian genome encodes two E1 enzymes, 30-40 E2 enzymes and more than 600 E3 ligases (Grabbe et al., 2011). There are different classes of ubiquitin E3 ligases, differing in the way in which the ubiquitin molecule is transferred from the E2 onto the substrate.

HECT (Homologous to the E6-AP Carboxyl Terminus) E3 ubiquitin ligases contain a catalytic cysteine that forms a transient thioester intermediate with ubiquitin before the ubiquitin is transferred onto the substrate (Fig 1.1A). Therefore, their linkage specificity does not depend on the E2 but is conferred by the E3 ligase itself (Komander and Rape, 2012).

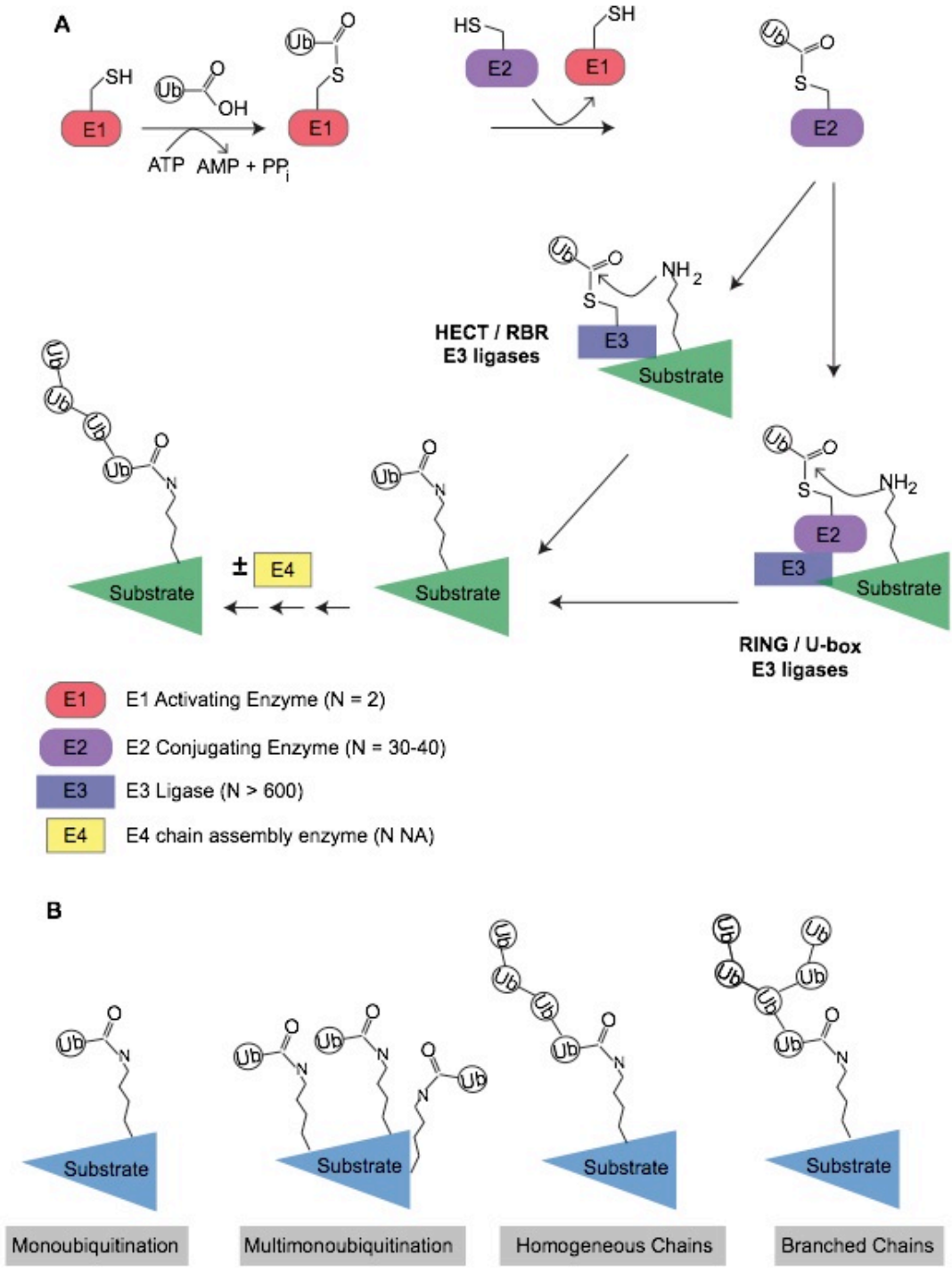


Figure 1-1 The Ubiquitin Code. A: Chemistry of Ubiquitination. The E1 binds the ubiquitin C terminus in an ATP dependent manner, resulting in a thioester intermediate. The E2 takes the activated ubiquitin and, together with the catalysing E3 ligase, the ubiquitin is added to the substrate in an isopeptide formation step. Depending on the E3, the E2 is (RING / U-box ligases) or is not (HECT ligases) involved in the transfer of the ubiquitin onto the substrate. Several ubiquitin moieties can be added to a chain, and this mechanism can involve the addition of an E4 enzyme. The numbers of each enzymes encoded in the mammalian genome is depicted. B: The Ubiquitin code. Ubiquitin can be added to a substrate in different ways. Depicted are four different ways of how ubiquitination can occur.

RING (really interesting new gene) and U-box domain containing E3 ligases serve as scaffold proteins for the E2 and the substrate by binding to both of them and stimulating the transfer of ubiquitin onto the substrate. Hence, they lack a classical catalytic active site and their linkage specificity depends on the E2 while substrate specificity usually depends on the E3 ligase. Most ubiquitin E3 ligases belong to the family of RING domain containing ligases (Komander and Rape, 2012). The two main ubiquitin ligases found at the site of DNA damage, RNF8 and RNF168 are members of the RING family of ligases. Their function in the repair of DNA damage is discussed in detail in chapter 1.6.

Another group of E3s are the RING-between-RING (RBR) that are RING/HECT hybrids. The name originates from the fact that they encode two RING domains that flank the conserved in-between-RING domain. The RING1 domain recruits the E2 and the ubiquitin is transferred onto a cysteine in the RING2 domain before addition to the substrate. These ligases usually have very strong linkage specificity (Spratt et al., 2014). Parkin is a member of this family and catalyses monoubiquitination as well as Lys27, Lys48 and Lys63-linked chains.

1.2.3 Ubiquitin E4 Chain Assembly Enzymes

Ubiquitin E4 ligases, also known as chain assembly enzymes, enhance multiubiquitination in collaboration with E1, E2 and E3 (Fig 1.1A) (Hoppe, 2005). The laboratory of Stefan Jentsch was the first to report on the E4-ubiquitin ligase Ufd2 (ubiquitin fusion degradation protein 2) in yeast in 1999. In their reconstituted *in vitro* system for the UPS (ubiquitin-proteasome system), they used model substrates to investigate the requirement for ubiquitination in the proteasomal degradation pathway. They observed that the absence of Ufd2

in the reaction did not abolish the formation of ubiquitin chains but instead resulted in much shorter ubiquitin chains being formed. In collaboration with an E1, E2 and E3 enzyme, the yeast Ufd2 is therefore able to increase the length of existing ubiquitin chains (Koegl et al., 1999). Another E4 enzyme, CHIP (C terminus of Hsc70-interacting protein), polyubiquitinates the Pael receptor together with the E3 Parkin (Imai et al., 2002).

1.2.4 Reading The Ubiquitin Code: Ubiquitin Binding Domains

The ubiquitin code is recognised by proteins that contain specific reader domains referred to as ubiquitin binding domains (UBDs). At least 20 UBDs have been discovered so far that confer their carrier specificity towards ubiquitin. Proteins can encode more than one UBD as well as different kinds of UBDs. These specific UBD arrays can give rise to strong linkage specificity (Dikic et al., 2009). For instance, two ubiquitin-interacting motifs (UIMs) in receptor-associated protein 80 (RAP80) are responsible for its strong specificity for K63-linked ubiquitin chains (Sims and Cohen, 2009). On the other hand, Ataxin-3 (ATXN3) contains three UIMs, which have been reported to give it K48-linkage specificity. Exchanging the patterns of the two UBD arrays in RAP80 and ATXN3 leads to inverted ubiquitin-linkage specificity (Sims and Cohen, 2009).

Other UBDs include MIU (motif interacting with ubiquitin), UMI (UIM- and MIU-related UBD), UBA (ubiquitin-associated domain) and UBZ (ubiquitin-binding zinc finger). RNF168 contains two MIUs and one UMI, which targets RNF168 to the sites of DNA damage (Pinato et al., 2009). RNF168 also served as a model protein to show how short sequences adjacent to the UBDs have an impact on

the recognition of ubiquitinated substrates (Panier et al., 2012) as discussed in chapter 1.6.3.

1.2.5 Eraser Of The Ubiquitin Code: Deubiquitinating Enzymes (DUBs)

Ubiquitination is a reversible modification. Specialised isopeptidases, DUBs, posses the ability to cleave off ubiquitin molecules from ubiquitin chains or remove entire chains from substrates, thus leading to recycling of the ubiquitin moieties as well as the eradication of the signal on the substrate. Around 100 DUBs are encoded in the human genome. They are classified in six families, five of which encode cysteine proteases and one encodes metalloproteases (Amerik and Hochstrasser, 2004).

Members of the cysteine isopeptidases are further classified into families according to the domains they contain: the ubiquitin C-terminal hydrolase domain (UCH), the ubiquitin-specific protease domain (USP), the ovarian tumour domain (OTU), Machado-Joseph Disease protein domain (MJD) and the very recently discovered motif interacting with ubiquitin containing novel DUB family (MINDY) (Arif et al., 2016). ATXN3 (Ataxin-3), discussed more detailed in chapter 1.4, is one of the four members of the MJD DUB family. With 56 members, USP makes up the largest family.

The metalloprotease family of isopeptidases contains the JAB1/MPN/Mov34 metalloenzyme domain (JAMM) (Amerik and Hochstrasser, 2004).

It has been shown that some DUBs exhibit strong linkage specificity while others do not. Furthermore, the cleavage can be either endo (within the chain) or exo (from the end). Some DUBs are substrate-specific and remove the entire ubiquitin chain in one step (Spasser and Brik, 2012).

1.2.6 Regulation Of Dubs

At any given time, a vast number of proteins are ubiquitinated inside the cell. Therefore, cells have to tightly regulate the activity of DUBs to avoid unwanted deubiquitination events. This can be achieved by many different means.

Many DUBs are regulated by PTMs. For instance, monoubiquitination of UCH-L1 inhibits its DUB function (Meray and Lansbury, 2007). Regulation can be achieved by protein interaction. For instance, USP14 is a proteasome-associated DUB and interaction with the proteasome increases its DUB activity 500-fold. Therefore, the DUB activity is regulated by its interactor and the resulting conformational changes in USP14 (Hu et al., 2005).

1.2.7 The Proteasome

Ubiquitination, especially via K48-linked chains, is a signal for substrate degradation. Degradation of marked proteins is performed by the 26S proteasome, which consists of a catalytic 20S component that is closed on both sides by a regulatory 19S particle. Overall, the 26S proteasome is a megacomplex consisting of around 50 subunits and has a combined molecular weight of approximately 2.5 MDa (Bhattacharyya et al., 2014).

The 20S subunit, consisting of 28 subunits, has a barrel-like shape with two α-rings on each side, regulating substrate entrance, and a catalytic center located in the two β-rings. The active sites are β1, β2 and β5 which exclusively face the inside of the 20S barrel (Finley, 2009).

The 19S component recognises the ubiquitinated substrate, cleaves off the ubiquitin and unfolds it before handing it over to the 20S component. Thus, substrates targeted for degradation are attached to the 26S proteasome over

their ubiquitin chains, which are, in turn, recognised by UBD containing receptor proteins. Some of these receptor proteins are permanent components of the 19S subunit, such as RPN10 (regulatory particle non-ATPase) and RPN13, while others can move on and off, such as RAD23 (Radiation sensitive protein 23). Ten subunits make up the base of the 19S particle, and six of them (RPT1-RPT6, regulatory particle ATPase) are AAA ATPases. By hydrolysing ATP, these ATPases can unfold substrates, open the usually closed molecular gate of the 20S component and translocate the substrate into the 20S chamber. POH1, a DUB associated with the 19S proteasome subunit and member of the JAMM family, cleaves off the ubiquitin chains from the passing substrate, thus enabling the substrate to properly enter the proteasome without clogging it (Yao and Cohen, 2002).

Degradation is a highly regulated mechanism. For instance, the DUB USP14 can associate with the RPN1 subunit of the 19S particle, which enhances the activity of USP14 by inducing a conformational change. Once bound, USP14 can remove ubiquitin from proteasome-bound substrate molecules. In this way, not only are the ubiquitin moieties recycled, but the substrate might be released from the proteasome without degradation (Hanna et al., 2006). A similar mechanism has been found for a second DUB, UCH-L5, that can also bind to the proteasome temporarily and deubiquitinate substrates, thus preventing their degradation (Koulich et al., 2008).

After substrate degradation by the proteasome, peptides with a length of 3 to 25 amino acids remain, while the ubiquitin is recycled. The proteasome is located both in the cytoplasm and nucleus (Biel et al., 2004). The ubiquitin-proteasome

system is essential for the proper coordination of many basic processes, such as cell cycle progression, cell proliferation, and protein quality control.

1.2.8 The Ubiquitin-Proteasome System (UPS)

The turnover of proteins is a tightly regulated process. This is illustrated in the fact that around 30% of all proteins have a lifespans of less than 10 minutes and more than 80% of the cellular proteins are eventually degraded by the proteasome (D'Arcy et al., 2015). If protein turnover is not accurately maintained, it can lead to protein aggregation, which is known to contribute to the pathogenesis of severe neurodegenerative diseases such as Alzheimer's, Parkinson's and Machado-Joseph disease, as well as ageing and cancer. Therefore, maintaining balanced levels of proteins inside a cell is of uttermost importance for a cell's well being.

K48-linked ubiquitin chains are considered to be the main signal for proteasomal degradation, but other chains (such as K11 or K29) and even monoubiquitination have also been implicated as degradation signals (Kravtsova-Ivantsiv et al., 2013).

The UPS is a part of the protein quality control system, which controls protein stability from the moment a protein is translated until it has served its function and is no longer needed. Endoplasmic reticulum-associated degradation (ERAD), where misfolded and short-lived proteins are retro-translocated from the ER into the cytoplasm and degraded by the proteasome, is one of the important cytoplasmic UPS functions. Defective ERAD leads to the aggregation of proteins and, in worms, has been observed to reduce lifespan (Kevei and Hoppe, 2014).

An important player in the UPS is p97, also known as valosin containing protein (VCP) in mammals, or Cdc48 in lower eukaryotes.

1.3 p97

p97 is a member of the family of type II ATPases associated with various cellular activities (AAA+) that is fundamentally important for various subcellular processes. p97 is an abundant protein located throughout the cell and makes up approximately 1% of total cytoplasmic protein.

It is a key player in the maintenance of protein homeostasis, and its function in the ERAD has been thoroughly studied. p97 is located at the ER membrane, where it extracts proteins from the membrane via ATP hydrolysis and hands them over to the proteasome (Xia et al., 2016).

However, over the last decade, p97 has emerged as an essential regulator of the UPS related to various other cellular processes like transcriptional and metabolic regulation, chromatin remodeling, cell cycle progression, apoptosis, DNA replication and the DNA damage response. Moreover, mutations in the human p97 gene are the cause of two separate diseases: Inclusion Body Myopathy with Paget's disease of the bone and Frontotemporal Dementia (IBMPFD), and familial Amyotrophic Lateral Sclerosis (fALS). IBMPFD is a progressive adult-onset autosomal dominant deadly disorder which affects the muscles (myopathy), the bones and the brain (Kimonis et al., 2000). The autosomal dominant disease fALS manifests in progressive malfunction in motor neurons, leading to death from respiratory failure. However, only around 1-2% of all fALS cases are caused by mutations in p97 (Johnson et al., 2010).

Structurally, p97 is a homohexameric protein, where each of the six subunits is arranged in a ring around a central pore. Each subunit contains four domains: an N-terminal domain and a C-terminal tail, separated by two conserved AAA domains referred to as D1 and D2 (Fig 1.2A). The 6 ATPase active sites of the D2 domain are highly active under physiological conditions, and ATP hydrolysis induces a conformational change of p97 that enables it to extract proteins from various protein complexes, membranes and chromatin (Stolz et al., 2011; Rouiller et al., 2002; Song et al., 2003). Hence, inhibition of the ATPase active sites of p97 leads to inhibition of its function (Esaki and Ogura, 2010).

1.3.1 p97 And Its Cofactors

p97 gains its multi-tasking ability by interacting with various cofactor proteins (also known as adaptors) that target p97 to the different cellular pathways and help p97 to recognise and process client proteins. Around 30 cofactors are known to be involved in regulating p97-dependent processes (Fig 1.2C). Several different p97 interaction motifs exist, and most of them interact with the N-terminal part of p97 (Fig 1.2C). The main cofactors of p97 are UFD1-NPL4 (Nuclear protein localisation protein 4), p47 and UBXD1 (ubiquitin regulatory X protein D1), which are mutually exclusive, and thus form three main p97 complexes in the cell (Fig 1.2B). Interaction with p47 targets p97 mainly for membrane fusion events, important for the formation of Golgi stacks, transitional ER compartments and the nuclear envelope during cell division (Buchberger et al., 2015; Kondo et al., 1997). UFD1-NPL4 targets p97 for its role in ERAD, ribosomal associated degradation (RAD) and chromatin associated degradation (CAD). p97 and UBXD1 together play a role in mediating the sorting

of ubiquitinated cargo in endolysosomal trafficking (Ritz et al., 2011). Moreover, a common mutation found in the p97 disease, IBMPFD, leads to abolishment of the interaction with UBXD1 but not UFD1-NPL4 or p47, indicating that loss of this specific complex is causative for the disorder (Ritz et al., 2011).

As most of the cofactors bind to the N-terminal part of p97, a maximum of six different adaptors can bind to a homohexameric assembled p97 at any given time. *In vitro* analysis of cofactor binding competition has shown that only one cofactor, the VIM (VCP-interaction motif)-containing SVIP (small VCP-interactin protein), efficiently outcompetes all the other cofactors, thus interacting with all six p97 subunits (Hänzelmann et al., 2011). Furthermore, several cofactors, such as UFD1-NPL4, UBXD1 or p47, contain more than one p97-interacting motif and thus can occupy more than one subunit, thereby reducing the number of other potential cofactors (Fig 1.2). The so-called "hierarchical cofactor binding concept" describes the idea that the general activity of p97 with its core-adaptors UFD1-NPL4 in the UPS is further specified by interacting with additional cofactors (Schuberth and Buchberger, 2008).

The majority of cofactors contain at least one UBD that links p97 with ubiquitinated substrates.

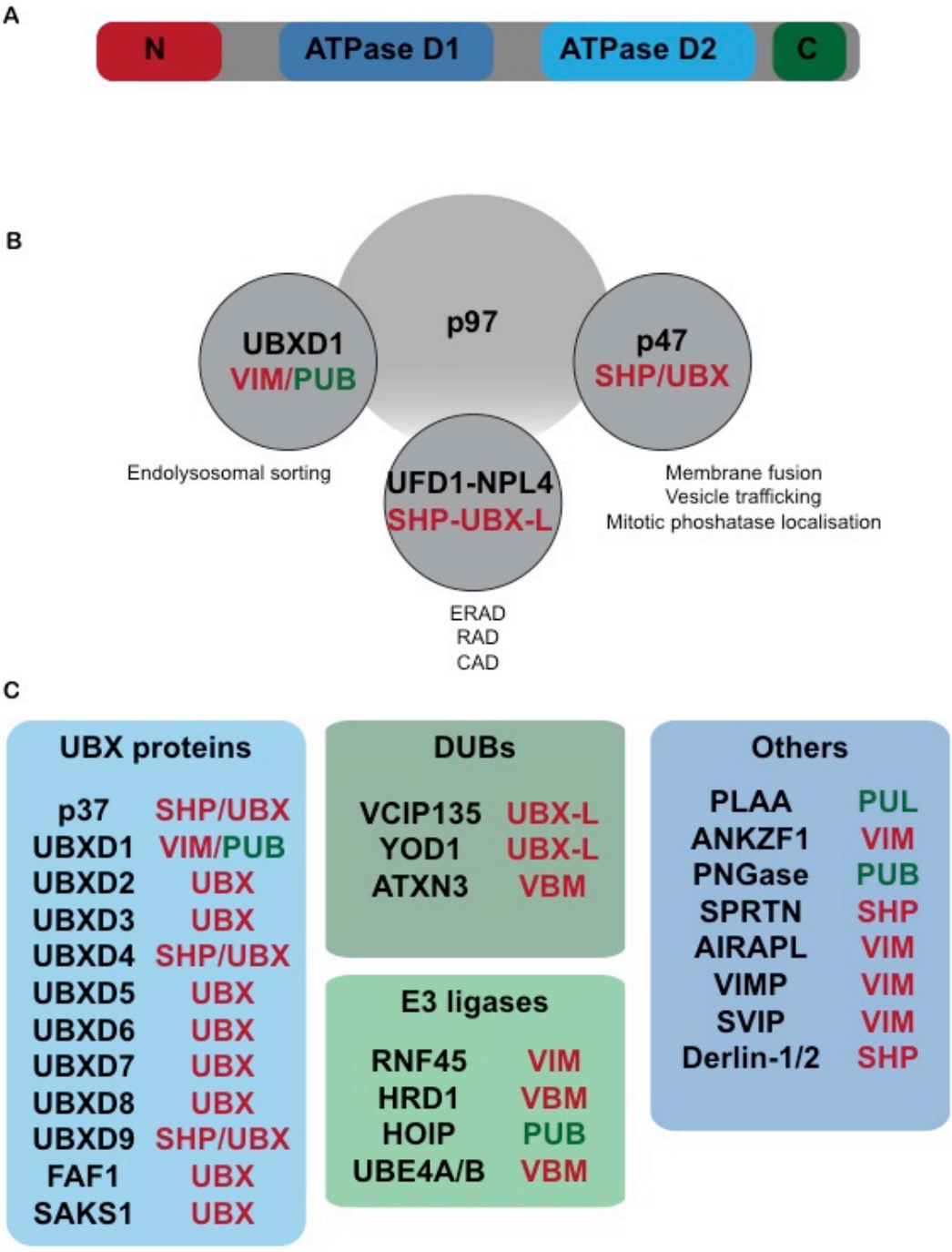


Figure 1-2. p97 and its cofactors. A: Schematic representation of the p97 protein. Indicated are the N- and C-terminal ends and the two ATPase domains D1 and D2. B: The three main p97 subcomplexes, $p97^{UBXD1}$, $p97^{UFD1\text{-}NPL4}$ and $p97^{p47}$ and their targeted cellular pathways. C: Summary of the known p97 cofactors (black) and their p97-interacting domains that either interact with the N terminus (red) or C terminus (green) of p97. Adapted from (Meyer and Weihl, 2014; Vaz et al., 2013).

1.3.2 p97 Inside The Nucleus

p97 has been shown to play important roles inside the nucleus (Vaz et al., 2013). It is associated with clearing the chromatin of unnecessary proteins to allow accurate mitosis, transcription, replication, cell division and also DNA damage repair.

p97 was initially identified in a screen (where it was named Cdc48) for cell division cycle (cdc) mutants in yeast (Moir et al., 1982). Yeast Cdc48 knock out leads to delayed G1/S transition and G2/M arrest. Moreover, it stimulates the degradation of ubiquitinated Far1p, a Cdc28-Cln inhibitor that needs to be degraded for G1/S transition (Fu et al., 2003). Additionally, Cdc48 removes the chromatin-bound transcription factor α2 in yeast to allow the switch in mating type (Wilcox and Laney, 2009).

Subsequently, metazoan p97, together with UFD1-NPL4, was firstly shown to extract the mitotic kinase Aurora B from chromatin (Sasagawa et al., 2012; Dobrynin et al., 2011; Ramadan et al., 2007), allowing accurate mitosis from *C. elegans* to humans.

In 2011, two groups reported, that p97 plays a role in DSB repair and is essential for orchestration of the DNA damage response (Meerang et al., 2011; Acs et al., 2011). p97 is important for regulating the ubiquitination signal at the site of DNA damage but also for the accurate recruitment of 53BP1, BRCA1 and RAD51 foci. These findings will be discussed more deeply in chapter 1.6.8.

1.3.3 p97's Role In Replication

In 2008, it was reported that accurate cell cycle progression relies on p97 in *C. elegans* and its loss leads to decreased replication efficacy (Mouysset et al., 2008).

In mammalian cells, p97 plays a strategic role in initiation, elongation and termination of replication (Ramadan et al., 2016).

For replication initiation, p97, together with its cofactor FAF1 (Fas associated factor 1), helps to extract the replication-licensing factor CDT1, which leads to appropriate replication fork firing (Franz et al., 2011; Raman et al., 2011; Franz et al., 2016). FAF1 has been further shown to be important for fork progression (Franz et al., 2016). Additionally, the p97 cofactor Spartan 1 (SPRTN) has been identified to play a major role in DNA replication (Davis et al., 2012; Ghosal et al., 2012; Mosbech et al., 2012; Lessel et al., 2014; Machida et al., 2012). SPRTN was shown to be important for translesion synthesis (TLS) during replication stress (Davis et al., 2012; Ghosal et al., 2012; Kim et al., 2013; Machida et al., 2012; Mosbech et al., 2012). It further helps to remove the replicative DNA Polδ, supports DNA Polη recruitment (Ghosal et al., 2012), and facilitates the removal of DNA Polη beyond the lesion (Davis et al., 2012; Mosbech et al., 2012) to regulate error-free TLS (Kim et al., 2013; Machida et al., 2012). It also enhances monoubiquitination of PCNA (proliferating cell nuclear antigen) by recruiting the E3 RAD18 (Centore et al., 2012). Moreover, biallelic and monogenic mutations in SPRTN were found to be the cause of Ruijs-Aalfs syndrome, a disease manifesting in progeroid features, genomic instability and early onset hepatocellular carcinoma (Lessel et al., 2014).

Finally, p97 helps to terminate replication by unloading ubiquitinated MCM7 (minichromosome maintenance protein 7) from DNA in a proteasome-independent manner (Maric et al., 2014; Moreno et al., 2014).

Additionally, p97 has been shown to be important in the orchestration of the Fanconi anemia repair pathway. This is further highlighted in chapter 1.5.5.

1.4 p97 Adaptors Connected To This Thesis

1.4.1 Ataxin-3 (ATXN3)

In 1994, Kawaguchi and colleagues identified a novel gene containing CAG repeats on chromosome 14q32.1 (Kawaguchi et al., 1994), that colocalises with the genetic locus for the neurodegenerative Machado-Joseph disease, also known as spinocerebellar ataxia type 3 (SCA3). It encodes ATXN3, a 198 amino acid DUB belonging to the MJD DUB family.

1.4.1.1 ATXN3 Structure And Activity

ATXN3 is an evolutionary conserved gene from fungi to humans. It contains 11 exons, with the CAG repeats being located in exon 10. Interestingly, different spliceoforms of exon 10 and 11 have been found (Ichikawa et al., 2001). Human ATXN3 encodes several different domains. The N-terminal part of ATXN3 encodes the Josephine domain (JD), with the cysteine at amino-acid position 14 being the active site of the DUB activity (see Fig 1.3). In the JD, two ubiquitin binding sites (UbS) are encoded. Moreover, ATXN3 contains three UIMs, two of them being located downstream of the JD and one downstream of the CAG repeats. ATXN3 interacts with p97 over a VBM that lies just upstream of the polyglutamine sequence.

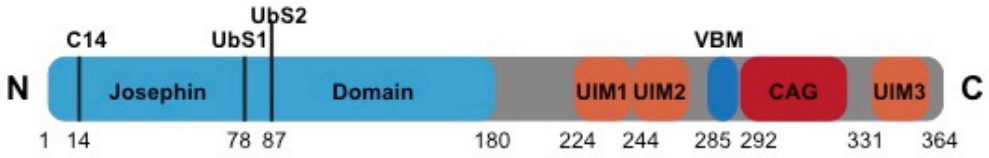


Figure 1-3. Schematic representation of ATXN3. Indicated is the Josephin Domain (JD) containing the active Cysteine C14, UbS1 and UbS2. On the C-terminal site are the three UIMs located as well as the p97-interacting motif (VBM) and the CAG repeats. The corresponding amino acid positions are indicated at the bottom.

ATXN3 has been shown to be an active endo-type DUB (Burnett et al., 2003; Donaldson et al., 2003; Doss-Pepe et al., 2003; Chai et al., 2004; Berke et al., 2005; Satoh et al., 2014). It trims polyubiquitin chains and has an affinity towards K48- but also K63-linked ubiquitin chains (Winborn et al., 2008b; Nicastro et al., 2010). Expanded (polyQ) ATXN3 retains DUB activity and binds both K48- and K63-linked ubiquitin chains, but also displays affinity for K27- and K29-linked ubiquitin chains (Durcan et al., 2011).

ATXN3 itself is also a target of ubiquitination, predominantly at K117. This PTM has been reported to enhance its activity (Todi et al., 2009). Furthermore, interaction with p97 enhances its DUB activity *in vitro* (Laco et al., 2012).

ATXN3 is a ubiquitously-expressed protein, localised in both the nucleus and cytoplasm. Nuclearisation increases upon heat shock or oxidative stress due to phosphorylation of ATXN3 at S111 by Plk1 (Polo-like kinase 1) (Reina et al., 2010). ATXN3, by its UbS2, interacts with RAD23 and mutation of UbS2 leads to accelerated proteasomal degradation of ATXN3 (Blount et al., 2014). It has been recently demonstrated that the ATXN3 disease variant (ATXN3-polyQ) displays increased interaction with the mammalian polynucleotide kinase 3'-phosphatase (PNKP). The physical interaction of PNKP with ATXN3-polyQ inhibits the PNKP

kinase activity, and consequently leads to accumulation of DNA breaks and activation of apoptosis (Gao et al., 2015; Chatterjee et al., 2015).

1.4.1.2 Machado-Joseph Disease (MJD)

ATXN3 is a member of the polyglutamine family as it encodes CAG repeats of variable length (encoding Glutamine = Q) in its C-terminal part. In healthy people, CAG repeats range from 13 to 36 repeats but, in SCA3 patients, are expanded to between 68 and 79 repeats (Kawaguchi et al., 1994; Maciel et al., 2001). MJD is the most common inherited ataxia in the world (Schols et al., 2004), inherited in an autosomal dominant manner and an inverse correlation between the number of CAG repeats and the age of disease onset is observed.

The first patient was described in 1972, and the disease was named after the first patient's family name, Machado (Nakano et al., 1972). A second patient, from a family called Joseph, was described in 1976 (Rosenberg et al., 1976), and the two patients were later found to be suffering from the same disease, hence the name Machado-Joseph disease (Coutinho and Andrade, 1978).

The expansion of the CAG repeats leads to the onset of disease at the age of 20 to 50 years which, in its most common form, manifests as spinocerebellar ataxia, progressive external ophthalmoplegia and pyramidal signs (Costa and Paulson, 2012). The mean survival time is around 21 years. It is a progressive neurodegenerative disease mostly affecting motor, but not sensory, neurons (Bettencourt and Lima, 2011).

1.4.1.3 ATXN3 And PolyQ ATXN3 Features

As discussed above, cells tightly control the turnover of proteins. If cells are overwhelmed by misfolded proteins, they transport them to a perinuclear

location near the microtubule-organisation center (MTOC), where they form aggresomes. This pathway has been shown to be dynein, microtubules and histone deacetylase 6 (HDAC6) dependent (Johnston et al., 1998, 2002; Garcia-Mata et al., 1999). ATXN3 is involved in the aggresome formation process, as it interacts with these three components, possibly binding polyubiquitinated misfolded proteins and guiding them to the MTOC for aggresome formation (Mazzucchelli et al., 2009; Burnett and Pittman, 2005).

PolyQ ATXN3 has a high propensity to misfold and aggregate inside the nucleus, which is considered to be the main cause of neurodegneration (Chai et al., 2002). Even though normal ATXN3 also forms aggregates, so called SDS-soluble fibrils, polyQ ATXN3 further amasses into SDS-insoluble aggregates (Ellisdon et al., 2006), and it sequesters its interaction partners into those aggregates (Yang et al., 2014). The DUB USP19 stabilises polyQ ATXN3 and overexpression of USP19 increases aggregate formation of polyQ ATXN3, indicating that PTMs are also involved in the aggregation of ATXN3 (He et al., 2016).

Some MJD patients show certain clinical features resembling Parkinson patients. Interestingly, ATXN3 interacts with and deubiquitinates the E3 ubiquitin ligase Parkin. Mutations in Parkin are linked to Parkinson's disease. This interaction depends on the UIM motifs and JD of ATXN3 but also on the ubiquitination status of Parkin. The polyQ ATXN3 shows stronger DUB activity towards Parkin, but cells expressing polyQ ATXN3 exhibit decreased Parkin stability mediated via the autophagy, but not proteasomal, pathway. Therefore, it can be speculated that the polyQ-induced accelerated degradation of Parkin may contribute to the pathogenesis of MJD patients and the Parkinson's disease-like features observed in some MJD patients (Durcan et al., 2011, 2012).

PolyQ ATXN3 was found to be in a complex with UBE4B and p97. Matsumoto et al. showed that ubiquitinated polyQ ATXN3 is further ubiquitinated by UBE4B, leading to the proteasomal degradation of polyQ ATXN3. Their results indicated that absence of UBE4B enhances polyQ ATXN3 aggregation (Matsumoto et al., 2004).

Functionally, ATXN3 plays a role in the UPS and protein homeostasis. It has been shown to interact with and regulate ubiquitin ligases, such as Parkin, and helps to deliver substrates to the proteasome with the help of the shuttle protein RAD23 (Durcan and Fon, 2011; Zhong and Pittman, 2006). By interacting with p97, ATXN3 is involved in shuttling proteins to the proteasome in ERAD (Boeddrich et al., 2006; Zhong and Pittman, 2006).

Overall, ATXN3 interacts with several different proteins but has mainly been shown to be involved in the regulation of aggresome formation and degradation. Other functions of ATXN3 are still poorly understood and elusive.

1.4.2 Yeast Ufd2 And Its Mammalian Orthologues UBE4A And UBE4B

In 1999, the ubiquitin fusion degradation protein 2 (Ufd2) in yeast was identified as the first E4-ubiquitin ligase (Koegl et al., 1999; Hatakeyama et al., 2001). Ufd2 contains a conserved C-terminal U-box that is structurally related to the RING domain from RING-type E3 ligases. Ufd2 is involved in ERAD by collaborating with p97/Cdc48. p97/Cdc48 interacts with proteins that are marked for ERAD. Subsequent interaction with Ufd2 leads to polyubiquitination of the substrate and interaction with the proteasome shuttle protein Rad23. This leads to the proteasomal degradation of the polyubiquitinated substrate (Richly et al., 2005; Baek et al., 2011). Ufd2 regulates mitosis by promoting degradation of the Mps1

(monopolar spindle 1) kinase together with the anaphase promoting complex (Liu et al., 2011).

Mammalian cells contain two homologues of Ufd2, UBE4A (UFD2b) and UBE4B (UFD2a). Little is known about their function. UBE4B has been shown to polyubiquitinate monoubiquitinated p53, which indicates that it possesses E4 ligase activity. p53 is monoubiquitinated by the E3 ligase Mdm2. While monoubiquitinated p53 is exported out of the nucleus, where it cannot function as a transcription factor anymore, elongation of those monoubiquitin signals by UBE4B targets p53 for proteasomal degradation. (Du et al., 2016; Wu et al., 2011a; Periz et al., 2015; Zhang et al., 2014a).

As mentioned above, UBE4B controls the stability of ATXN3 by regulating polyubiquitination of ATXN3 and inhibiting UBE4B function abolishes the proteasomal degradation of ATXN3 (Matsumoto et al., 2004).

High expression of UBE4B in hepatocellular carcinoma (HCC) in humans has been correlated with a poor prognosis. Meanwhile, depletion of UBE4B in HCC cells stops cell proliferation, migration and invasion and leads to an increased number of apoptotic events. This correlates with decreased expression of Bcl-2, a member of the Bcl-2 family of regulator proteins of cell death and an important anti-apoptotic protein, as well as increased expression of p53 (Zhang et al., 2016).

In contrast to HCC, UBE4A and UBE4B are speculated to serve as tumour suppressors in neuroblastoma in humans, as both genes are located in a common neuroblastoma deletion region (Carén et al., 2006). Furthermore, low expression of UBE4B in neuroblastoma has been associated with poor outcome and high risk tumour features for the patient (Woodfield et al., 2016).

1.5 DNA Damage Response

All the information a cell needs is conserved in its DNA, which is a macromolecule wound around histones to form a nucleosome. Nucleosomes together with RNA and various associated proteins form compact chromatin located inside the nucleus in eukaryotic cells. DNA is a fragile molecule and is constantly damaged via chemical (H_2O_2, formaldehydes) or physical (UV light, ionising radiation (IR)) sources. More than 100,000 various DNA damages happen per cell per day (Lindahl, 1993), including DNA deamination, oxidation, formation of abasic sites, pyrimidine dimers, DNA interstrand crosslinks (ICLs), DNA-protein crosslinks, single strand DNA breaks or DNA double strand breaks (DSBs). The cell has evolved sophisticated repair pathways, referred to as the DNA damage response (DDR), to resolve such DNA lesions in order to avoid mutations and possible cell death. Below, the main repair pathways are briefly discussed with the main focus being on the DSB repair and chromatin remodeling upon DSB induction.

1.5.1 Base Excision Repair (BER)

Cytosine can spontaneously undergo deamination, which converts it to uracil, a nucleotide not normally found in DNA. Furthermore, bases can be damaged by reactive oxygen species found in cells. BER is a specialised DNA repair pathway involved in detecting such damaged bases and removing them with specific DNA glycosylases, giving rise to an apurinic or apyrimidinic site. APEX1 (Apurinic/Apyrimidinic Endodeoxyribonuclease 1), a DNA lyase, cuts at the 5' side of the removed base and DNA Polβ eliminates the 5'-deoxyribosophosphate

residue and refills the gap. In a final step, the DNA LIG3-XRCC1 (Ligase 3 – X-ray repair cross complementing 1) seals the nick (Helleday et al., 2014).

1.5.2 Mismatch Repair (MMR)

MMR assesses mis-incorporated bases that have escaped the proofreading mechanism of the DNA polymerase and also deals with insertion/deletion loops (IDLs) that arise from heteroduplex formation of microsatellites during replication. The main aim of MMR is to degrade the error-containing part of the newly synthesised DNA, giving the DNA polymerase a second chance to duplicate in an error-free manner. Hence, the MMR machinery not only recognises mis-incorporated bases but also guides the repair to the newly synthesised DNA strand. In a first step, MutSα (MSH2 and MSH6) or MutSβ (MSH2 and MSH3) recognise the lesion at the replication fork. The DNA is then excised between the mismatch and a nearby nick by the endonuclease PMS2 and exonuclease 1 (EXO1), followed by the DNA Polδ that fills the gap, and ligation by LIG1.

Mutations in several MMR proteins are linked to hereditary non-polyp colon cancer and a high mutation rate in microsatellite sequences (Helleday et al., 2014; Jiricny, 2006).

1.5.3 Nucleotide Excision Repair (NER)

UV light can induce photolesions in the DNA, so called thymine dimers, and byproducts of cellular metabolism can lead to bulky lesions that distort the native DNA double helix. These lesions are recognised and repaired by the NER pathway. There are two sub-types of NER. One is transcription coupled NER (TC-NER), where RNA Pol II encounters a bulky lesion or transcriptional roadblocks. The stalled RNA Pol II complex needs to be removed before NER can function.

The second one is the more general, but slower, global genome NER (GG-NER), which examines the DNA for helix distortions.

GG-NER senses DNA distortions via XPC-RAD23 (Xeroderma pigmentosum protein C). UV-induced cyclobutane-pyrimidine dimers (CPDs), on the other hand, are poorly recognised by XPC due to their mild effect on the DNA helix. These lesions are recognised by the DDB1-DDB2 (DNA damage-binding protein 1-2) complex, which facilitates the binding of XPC. Binding of XPC then recruits the TFIIH (transcription initiation factor IIH) complex consisting of ten subunits including the two helicases XPB and XPD that unwind the DNA surrounding the lesion further. RPA (replication protein A) binds to the single-stranded DNA (ssDNA) on the undamaged site while XPA verifies the DNA damage by detecting chemically-altered nucleotides. Verification of damage is followed by the dual incision (both 5' and 3') by XPF-ERCC1 (Excision repair cross-complementing) and XPG, respectively, leading to the removal of around 30 nucleotides including the damaged DNA. Finally, the gap is filled in a way involving PCNA, RFC (replication factor C), different DNA polymerases (Polδ, ε or κ) as well as DNA LIG1 or XRCC1-LIG3. The choice of DNA polymerase and ligase mainly depends on the cell cycle stage of the repair, with Polε and LIG1 being mainly used in replicating cells, and Polδ or κ and XRCC1-LIG3 being preferred in non-replicating cells (Marteijn et al., 2014).

TC-NER, triggered by stalled RNA Pol II, leads to the recruitment of CSA and CSB (Cockayne syndrome A and B), which are necessary to further assemble the TC-NER machinery. This, in turn, will lead to the RNA Pol II backtracking, thus making the DNA lesion accessible to the NER repair proteins. Verification,

incision, excision and gap filling are then performed as described above in GG-NER (Marteijn et al., 2014).

p97 has been shown to play crucial roles in both GG- and TC-NER pathways. First, it has been shown that p97 removes RPB1, the largest subunit of RNA Pol II, from the RNA Pol II complex upon stalling and ubiquitination by the Cul3-RING ligase complex. This results in the degradation of RPB1 by the proteasome, indicating a tight relation between p97 and the proteasome to overcome UV lesions during transcription (Verma et al., 2011).

Second, p97 is involved in the turnover and regulation of two GG-NER DNA damage recognition subunits DDB2 and XPC. NER cannot be executed accurately if these two proteins are not extracted from chromatin by p97 ATPase in a controlled manner (Puumalainen et al., 2014).

Mutations in several of the XP genes are linked to the severe skin cancer-causing disease Xeroderma pigmentosum, while mutations in the CS proteins are linked to Cockayne syndrome.

1.5.4 DNA Double Strand Break Repair

The most rare naturally occurring DNA lesions are DNA double strand breaks (DSBs), but they are the most toxic ones. A single unrepaired DSB can lead to chromosomal aberrations, such as translocations or deletions, leading to loss of heterozygozity, tumorigenesis, senescence or apoptosis (Davis and Chen, 2013). DSBs can be induced by exogenous factors such as ionising radiation (IR), radiomimetic drugs or spontaneously due to metabolic processes and release of reactive oxygen species, class-switch recombination or collapsed DNA replication forks. DSBs are repaired by two main DSB repair pathways;

homologous recombination (HR) and canonical non-homologous end-joining (cNHEJ). Cells in G0, G1 or early S phase rely on the cNHEJ pathway, where the two ends are exposed to mild end-resection to create blunt ends followed by ligation. Hence, this pathway is error-prone. In later S or G2 phase, when sister chromatids are available, cells mostly use HR, a pathway that involves homology search and strand-invasion, and is considered to be error-free. Two additional pathways have been discovered that can also repair DSBs; the alternative NHEJ (aNHEJ) and single-strand annealing (SSA).

1.5.4.1 Canonical NHEJ (cNHEJ)

A freshly induced DSB is recognised within seconds by the KU70/KU80 heterodimer (Mari et al., 2006). KU70/80 interacts in a sequence-independent manner with DNA. Cells contain a vast amount of KU70/80 molecules (~500,000 molecules/cell). The heterodimer forms a ring-shaped structure fitting the DNA double helix in it, enabling KU70/80 to slide onto the DNA end. Once bound to the DSB ends, the Ku heterodimer protects the ends and serves as a recruitment platform to recruit further NHEJ factors, such as the DNA-PKcs kinase, X-ray cross complementing protein 4 (XRCC4), DNA LIG4, XRCC4-like factor (XLF) and Aprataxin-and-PNK-like factor (APLF) (Davis and Chen, 2013). Recently, PAXX (Paralog of XRCC4 and XLF) has been identified as an additional KU-interacting protein and a new player in the NHEJ pathway (Ochi et al., 2015). The DNA-PKcs kinase is one of the three DNA damage related members of the phosphatidylinositol-3 (PI-3) kinase-like kinase family (PIKK), the others being ataxia-telangiectasia mutated (ATM) and ATM and Rad3-related (ATR). Once the DNA-PKcs kinase is recruited over the KU70/80 complex, it becomes activated

and phosphorylates downstream proteins. This leads to recruitment and phosphorylation-dependent stabilisation of the core NHEJ complex, consisting of XRCC4, LIG4 and XLF (Davis and Chen, 2013). DSBs can have various damaged termini, such as abasic 5'-deoxyribose or a fragmented sugar such as 3'-phosphoglycolate. Hence, nucleases and phosphodiesterases need to be recruited that can process those ends. The nuclease Artemis, for instance, processes 3'-phosphoglycolate overhangs using ATP, creating 3'-hydroxyl ends. To do so, Artemis needs to be phosphorylated by DNA-PK to become an active endonuclease, being able to cleave various types of damaged DNA overhangs (Ma et al., 2002; Povirk et al., 2007).

Other nucleases found in NHEJ are WRN (Werner syndrome ATP-dependent helicase), APE1 and APE2 (Apurinic/apyrimidinic endonuclease 1 and 2) or APLF (Aprataxin-and-PNK-like factor). Aprataxin, TDP1 and TDP2 (Tyrosyl-DNA phosphodiesterase 1 and 2) are phosphodiesterases found to be involved in end-processing at DSB ends. Moreover, polynucleotide kinase/phosphatase (PNKP) is an additional important enzyme necessary for end processing, possessing 3'-phosphatase and 5'-kinase activity (Menon and Povirk, 2016). Subsequently, the DNA Polμ and λ are recruited to fill in the DNA gaps. The heterodimer XRCC4-LIG4, together with stimulating subunits such as XLF or APLF, is responsible for DNA ligation (Grundy et al., 2014; Yang et al., 2016; Davis and Chen, 2013).

1.5.4.2 Homologous Recombination (HR)

HR is considered an error free pathway for DSB repair. For a cell to be able to perform HR, it needs a sister chromatid available as a template. Therefore, cells only initiate HR in S or G2 of the cell cycle and suppress it in other phases. In

contrast to NHEJ, this pathway exhibits extensive 5' end resection that is initiated by the MRN complex, where the endonuclease activity of MRE11 (Meiotic recombination 11), promoted by CtIP (CtBP-interacting protein) and the ATPase activity of RAD50, is used to initiate 5' resection (Cannavo and Cejka, 2014). The more extensive end resection is then performed by EXO1 (exonuclease 1), a direct interaction partner of CtIP (Eid et al., 2010) or by the BLM helicase together with the DNA2 (DNA replication ATP-dependent helicase-like homolog 2) nuclease (Nimonkar et al., 2011) using 5'-3' exonuclease activity. The ssDNA-binding protein RPA is loaded onto the 3'ssDNA to protect it from degradation and secondary structure formation (Liu et al., 2014). BRCA2 (Breast cancer type 2 susceptibility protein), is itself recruited to the site of DSBs via its localiser PALB2 (partner and localizer of BRCA2) and BRCA1-BARD1 (BRCA1-associated RING domain protein 1) (Zhang et al., 2009), where it helps to stimulate the loading of RAD51 onto the ssDNA, replacing RPA. RAD51 promotes homology search with the help of RAD54 and strand invasion. This leads to D-loop formation and DNA synthesis, where, with the help of RAD54 and RAD54B, RAD51 is removed from the 3' end for priming (Mazin et al., 2010).

Different events are possible at this stage: the RTEL1 (regulator of telomere elongation helicase 1) helicase promotes synthesis-dependent strand annealing (SDSA) by D-loop displacement, a D-loop event that does not lead to crossing-over events. Here, the invaded strand only replicates the missing DNA sequence on the broken strand and then leaves the D-loop again (Barber et al., 2008).

The two sister chromatids can also form double Holliday junctions (dHJs). The BTR complex (BLM-TopoIIIα-RMI1-RMI2) decatenates dHJs leading to dissolution and formation of non-crossover products.

In cells lacking BLM (Bloom syndrome protein), a second dHJ-solving mechanism can be activated that relies on MUS81-EME1 (MMS and UV-sensitive protein 81 – essential meiotic endonuclease 1) and SLX1-SLX4 (synthetic lethal of unknown function protein 1 and 4), two heterodimeric endonucleases. This mechanism will lead to dHJs resolution leading to non-crossover and crossover formation and thus genomic instability (Matos and West, 2014).

1.5.4.3 Alternative NHEJ (aNHEJ) Or Microhomology-Mediated End Joining (MMEJ)

The most recently discovered DSB repair pathway is also the least understood and probably the most error-prone one. It is referred to as aNHEJ or MMEJ. It was initially thought to be executed in cells that lack important factors of the classical NHEJ, but has since been observed in cells with functional cNHEJ and HR (Truong et al., 2013) and it often leads to microhomologies and chromosome translocations. In the absence of the KU heterodimer, it uses poly(ADP-ribose)polymerase 1 (PARP1) for break sensing. PARP1 has been mainly implicated in the repair of single strand breaks, while in classical NHEJ it is outcompeted by the KU heterodimer. In aNHEJ, recruitment of PARP1 may tether the DNA ends, leading to recruitment of factors such as XRCC1, DNA LIG3 and the MRN complex (MRE11, RAD50, NBS1 (Nijmegen breakage syndrome protein 1)). aNHEJ depends on the annealing of microhomology, and thus requires some end resection. Hence, short stretches of ssDNA are created by MRN and CtIP followed by more extensive resection by EXO1 or BLM. For ligation, this pathway relays on Polδ, Polη and Polζ, before Polλ can perform gap fill-in synthesis. Furthermore, FEN1 (Flap endonuclease 1) might be needed for the removal of

DNA overhangs. The final ligation step is performed by either LIG3-XRCC1 or LIG1 (Frit et al., 2014). Recently, three groups showed that Polθ is a crucial promoter of MMEJ by binding pairs of resected ends, thus allowing for short homologous DNA sequences to form base pairs. Additionally, Polθ performs synthesis, which leads to the loss of the unpaired ends. Moreover, Polθ impairs HR by limiting RAD51 accumulation at resected ends (Mateos-Gomez et al., 2015; Ceccaldi et al., 2015; Kent et al., 2015).

1.5.4.4 Single Strand Annealing (SSA)

SSA is an alternative form of HR. It repairs DSBs by using two direct repeat sequences flanking the ends of the DSB. However, it will delete sequences between the repeats. SSA is generally observed more often in cells lacking BRCA2 or RAD51, which therefore fail to replace RPA on ssDNA (Stark et al., 2004). Therefore, after end-resection has been initiated as in HR, RAD52 binds the 3' ssDNA ends and initiates the strand annealing of the repeats, leading to overhanging flaps that are removed by XPF-ERCC1 (Al-Minawi et al., 2008) and ligation of the ends by LIG3 (Gottlich et al., 1998). Some understanding has been added by the publication by Ochs et al. They showed that 53BP1, generally considered a NHEJ-promoting protein, allows limited end-resection during S and G2 phase to initiate HR. Yet, if the amount of DSBs is too high, or the amount of 53BP1 availability is too low, the ends become unprotected and hyper-resected which can lead to HR-promoting RAD51 exhaustion and thus SSA-promoting RAD52 loading. Hence, 53BP1 plays a crucial role in the regulation of HR versus SSA pathway choice in S and G2 cells (Ochs et al., 2016).

However, the underlying mechanisms that distinguish aNHEJ and SSA are still poorly understood. Major differences to aNHEJ are the extensive end resection in SSA, the need of an extensive stretch of uninterrupted homology necessary for SSA, and that RAD52 appears dispensable for aNHEJ while PARP is unimportant for SSA (Bhargava et al., 2016).

1.5.5 FA Pathway To Repair Interstrand Crosslinks

The Fanconi anemia (FA) pathway is an essential repair pathway for dealing with interstrand crosslinks (ICLs), which are extremely toxic to cells if unrepaired. ICLs are of most danger to cells during replication and transcription, and, if left unrepaired, can lead to mutations but also chromosome missegregation and mitotic catastrophe (Lopez-Martinez et al., 2016). ICLs can be a by-product of IR in non-hybridised DNA regions such as replication forks, or transcription bubbles (Dextraze et al., 2010). Defects in the FA pathway sensitises cells to crosslinking agents such as mitomycin C, diepoxybutane or cisplatin, and can cause the autosomal recessive disease Fanconi anemia which is characterised by cancer predisposition, progressive bone marrow failure and multiple developmental abnormalities (Michl et al., 2016). 19 genes have been implicated in the FA pathway, making up the FA core complex (FANCA/B/C/E/F/G/L/M/T), the FANCD2/FANCI complex and the effector proteins (FANCD1/J/N/O/P/Q/R/S). They also collaborate with proteins from other repair pathways, such as HR or NER.

Incorporation of an ICL leads to replication stalling, as incoming replication forks cannot bypass the hooked DNA. Indeed, it has been suggested that FA is only performed if two forks meet the ICL from both sides (Zhang et al., 2015). BRCA1

helps to remove the replisome and the replication fork is protected by coating the ssDNA with RAD51. Upon detection of an ICL, the FA core complex, containing FANCL, an ubiquitin E3 ligase, and FANCT, an E2 enzyme, monoubiquitinates FANCD2/FANCI. This monoubiquitination happens only after FANCD2/FANCI is bound to the DNA via the Tower domain of FANCD2 (Liang et al., 2016). Moreover, the FANCD2/FANCI complex is phosphorylated at several sites by ATR. FANCD2/FANCI is then recruited to the site of the DNA lesion. This recruitment depends strongly on the ICL sensor UHRF1 that immediately recognises ICLs in cells and is recruited to the lesion site (Liang et al., 2015). SLX4/ERCC1-XPF assembles at the ICL site downstream of FANCD2/FANCI, leading to nucleolytic processing, including further nucleases such as MUS81-EME1. This unhooks the ICL so that the cell can perform translesion synthesis to bypass the lesion using the TLS polymerase REV1-polζ complex. The DSB created by the incision to remove the ICL is repaired by HR, including CtIP, the MRN complex, EXO1 and DNA2 for 5' end resection of the ends, RPA coating and BRCA2-mediated RAD51 loading onto the ssDNA. NER takes care to remove the unhooked ICL (Michl et al., 2016; Lopez-Martinez et al., 2016).

The $p97^{-SPRTN}$ complex facilitates the extraction and removal of FANCI and FANCD2 after the repair. SUMOylated FANCD2/FANCI are recognised and ubiquitinated by the SUMO-targeted ubiquitin ligase (STUbL) RNF4, which, in turn, allows the complex to be recognised by $p97^{SPRTN}$ (Gibbs-Seymour et al., 2015).

Additionally, it was recently suggested that p97 helps to dismantle the CMG helicase (consisting of Cdc45, MCM2-7 and GINS) from chromatin during ICL repair (Fullbright et al., 2016).

1.5.6 Chromatin Response To Orchestrate DSB Repair

Upon DSB induction, cells activate a vast set of proteins to control different mechanisms such as cell cycle arrest, damage repair and transcription silencing. The orchestration of the recruitment of different players of the DDR to the sites of damage has been subject of intensive studies in the last two decades.

The MRN complex recognises and binds DSB ends and recruits the ATM kinase and histone acetyltransferase TIP60 to sites of DNA damage. Phosphorylation of TIP60 by the c-Abl kinase triggers the activation of ATM, as acetylation of ATM by pTIP60 leads to autophosphorylation of ATM (Sun et al., 2005). ATM rapidly marks chromatin at sites of DSBs by phosphorylation of histone H2AX at Ser139 (γH2AX) in its C-terminal SQY motif (Rogakou et al., 1998). This signal is spread 0.5 to 2 megabases away from the break site in collaboration with MDC1 (mediator of DNA damage checkpoint protein 1). MDC1 recognises γH2AX via its phospho-binding BRCT (BRCA1 carboxyl terminus) domains and accumulates at the sites of damage (Stucki et al., 2005). MDC1 itself recruits ATM, enhancing the spreading of γH2AX further away from the initial damage site in a positive forward loop. MDC1 is also phosphorylated by ATM on its proline-serine-threonine (PST)-rich repeats (Jungmichel and Stucki, 2010). RNF8, an E3 ubiquitin ligase, recognises phosphorylated MDC1 via its forkhead-associated (FHA) domain. Once recruited to the site of DNA damage, RNF8, in complex with the E2 UBC13, poly-ubiquitinates histone H1 (Thorslund et al., 2015). RNF168, a second RING type E3 ligase, recognises ubiquitinated H1 via a UBD and thus gets recruited to the site of DNA damage (Pinato et al., 2009; Doil et al., 2009). Subsequently, RNF168 ubiquitinates H2A and H2AX on K13 and K15 (Mattiroli et al., 2012; Gatti et al., 2012), which further recruits RNF168. On one hand, it has

been shown, that both RNF8 and RNF168 can interact with UBC13 and thus promote the formation of K63-linked ubiquitin chains at the site of DNA damage (Doil et al., 2009). On the other hand, it has been recently shown, that RNF168 promotes the formation of atypical K27-linked ubiquitin chains (Gatti et al., 2015) and RNF8 promotes the formation of K48-linked ubiquitin chains at the site of DNA damage (Feng and Chen, 2012; Meerang et al., 2011; Ramadan, 2012). These initial ubiquitination events induced by RNF8 and RNF168 lead to the recruitment of downstream factors such as 53BP1, RIF1, PTIP, RAD18 or BRCA1. Accurate regulation of these proteins has direct impact on the repair pathway decision choice (Lukas et al., 2011).

Interestingly, during mitosis, cells suppress DSB repair. γH2AX and MDC1 are recruited to a DSB during mitosis, while downstream players, such as RNF8, RNF168 and 53BP1, are not. The laboratory of Daniel Durocher revealed that RNF8 cannot recognise phosphorylated MDC1 during mitosis due to phosphorylation of RNF8 by CDK1 on T198. This phosphorylation abolishes the interaction of RNF8 with phosphorylated MDC1 (Orthwein et al., 2014). A similar mechanism suppresses 53BP1 recruitment. In this case, the phosphorylation sites have been mapped to be in the UDR motif on T1609 (phosphorylated by CDK1) and S1618 (phosphorylated by PLK1) (Orthwein et al., 2014; Lee et al., 2014). If DSB repair is reactivated during mitosis, end-to-end chromosome fusions are observed, leading to dicentric chromosomes and aneuploidy. Once cells have reached G1, the phosphatase complex PP4C/R3β dephosphorylates 53BP1 to make it functional again for DSB recruitment (Lee et al., 2014). The phosphatase(s) for RNF8 have not yet been described in the literature.

Overall, DSB repair is highly regulated. The orchestrated recruitment of proteins and pathway choice depends on a highly organised PTM cascade in which ubiquitination has turned out to be fundamental. The main regulators of the ubiquitination at sites of DSBs are therefore discussed in more detail in the following chapter.

1.6 The Ubiquitination System In The Orchestration Of The DDR

1.6.1 RNF8

RNF8 is a RING E3 ubiquitin ligase that encodes a RING domain at its C-terminal part and a FHA domain at its N-terminal part. In 2007, several groups reported RNF8 as the first E3-ubiquitin ligase shown to be involved in the DNA damage response (Mailand et al., 2007; Huen et al., 2007; Kolas et al., 2007). Lack of RNF8 abolishes recruitment of BRCA1 and 53BP1 to the site of damage, thus making RNF8 an indispensable ligase for accurate repair and cell survival upon DSB induction. RNF8 is recruited to sites of DNA damage in an ATM-MDC1 phosphorylation-dependent manner (Fig 1.4). The FHA-domain of RNF8 recognises the phosphorylated PST repeats of MDC1. RNF8 collaborates with the E2-conjugating enzyme UBC13, an E2 that favours K63-linked chain formation (Hodge et al., 2016). In addition, different groups showed, by using linkage-specific antibodies, that RNF8 is also a ligase for building K48-linked ubiquitin chains at the site of DNA damage. These K48-linked chains target the substrate for proteasomal degradation, as was shown for KU80, where RNF8-induced poly-ubiquitination leads to removal and degradation of KU80 and, therefore, accurate NHEJ (Fig 1.4) (Feng and Chen, 2012; Meerang et al., 2011). Indeed, RNF8 can interact with E2 enzymes other than UBC13, such as UBCH8 or

UBCH5C, which prefer to create K48-linked ubiquitin chains (Lok et al., 2012; Mattiroli et al., 2012). Two point mutations have been found to directly affect the interaction of RNF8 with specific E2 enzymes.

The L451D RNF8 mutant showed reduced ability to stimulate UBC13 efficiently, thus impairing RNF8-mediated K63-linked chain formation. Hence, the recruitment of 53BP1 or BRCA1 in cells expressing this mutant is severely affected upon DSB induction (Hodge et al., 2016). Moreover, RNF8 mutants harboring the I405A point mutation do not interact with the E2 enzyme UBCH8. Interestingly, this mutant does not show a significant impact on the DDR (Lok et al., 2012). Together, these studies underline the importance of RNF8 as an E3 ligase for both K63- and K48-linked ubiquitin chains in the DDR.

RNF8 initially targets H1 for polyubiquitination with K63-linked ubiquitin chains (Thorslund et al., 2015), introducing the linker histone as a crucial target in the DDR (Fig 1.4). The initial studies about RNF8 all agreed that RNF8 could also target the core histones H2A and H2AX for ubiquitination (Mailand et al., 2007; Huen et al., 2007; Kolas et al., 2007). Additionally, *in vitro* it has been shown that RNF8 can ubiquitinate H2A(X) once it is monoubiquitinated by RNF168 (see below) (Mattiroli et al., 2012). Fluorescence recovery after photobleaching assays showed that RNF8 displays a very fast turnover rate at DSBs, which is much higher than that of RNF168 (Mok et al., 2014). RNF168 is also more abundant at the site of DNA damage, yet strictly depends on RNF8 for recruitment, which makes RNF8 the rate-limiting determinant in this cascade (Mok et al., 2014).

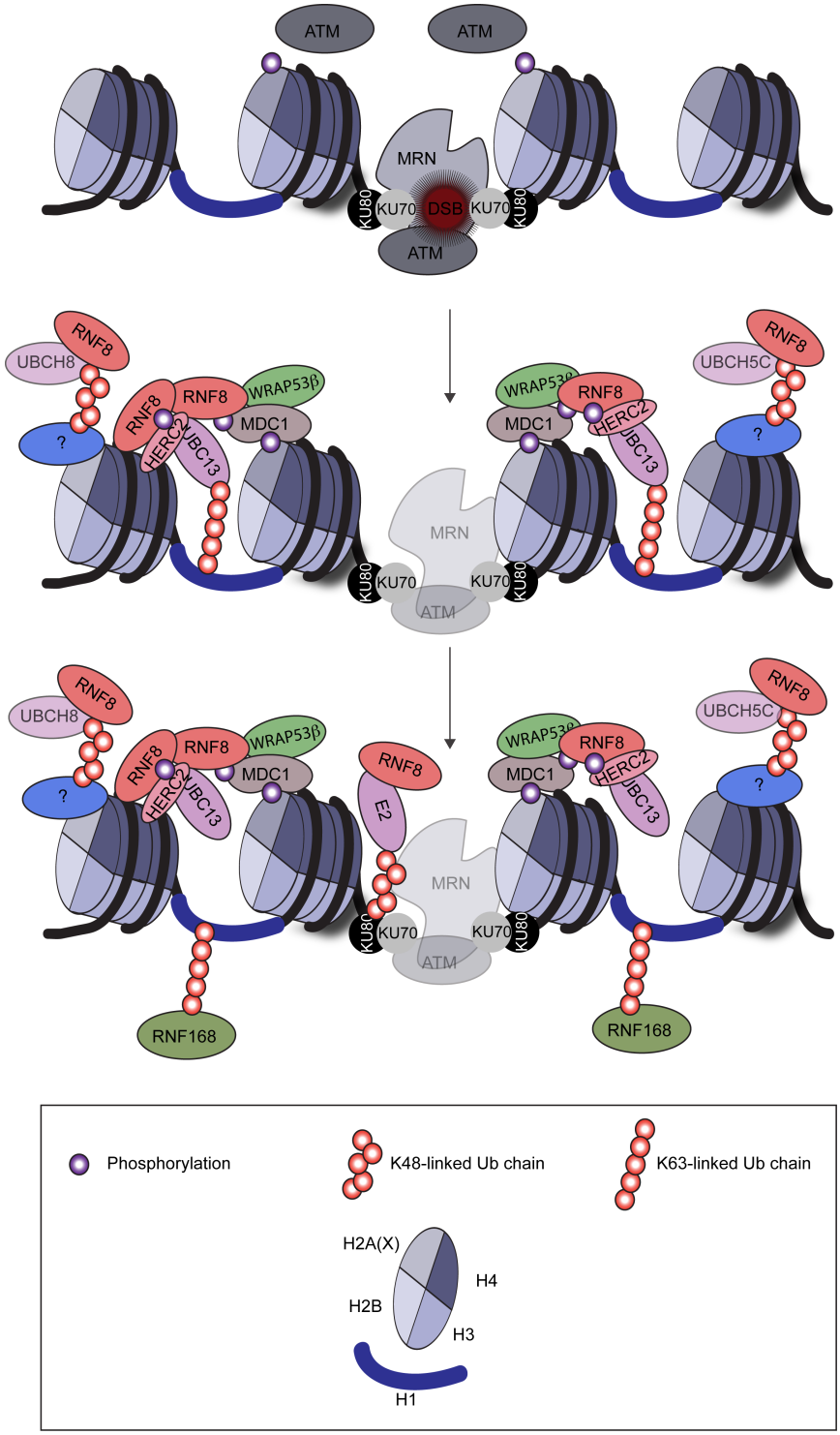


Figure 1-4. RNF8 induced ubiquitination at the site of DSBs. A DSB leads to the recruitment of the KU70/80 complex that binds the broken DNA ends. MRN and ATM initiate the phosphorylation by targeting H2AX. MDC1 recognises γH2AX and is itself phosphorylated by ATM. RNF8 recognises pMDC1 via its FHA domain and is recruited. RNF8 ubiquitinates H1 with K63-linked chains. The E3 ligase HERC2 is phosphorylated upon DSB induction and stabilises the RNF8-UBC13 interaction by interacting with the RNF8 FHA domain. RNF8 might ubiquitinate other proteins at the site of DNA damage with K48-linked chains by interacting with additional E2 conjugating enzymes. RNF168 recognises K63-linked ubiquitin chains on H1 and is recruited. Moreover, RNF8 targets KU80 with K48-linked ubiquitin chains that will lead to the unloading of KU80 from DNA.

RNF8 has an additional role in genome maintenance, which is to ensure accurate ATM activation. Together with the E3 ligase CHFR (Checkpoint with the Forkhead and Ring finger), RNF8 regulates the acetylation of H4K16 via MRG15, a common subunit of both the MOF and Tip60 acetyltransferase complexes. Hence, RNF8 and CHFR promote chromatin relaxation that facilitates ATM activation. Double knock out mice for RNF8 and CHFR are hypersensitive to IR and develop thymic lymphomas harboring chromosome translocations (Wu et al., 2011b). Moreover, RNF8 knock out mice accumulate DNA damage in neurons and display neuronal apoptosis that leads to neurodegeneration (Ouyang et al., 2015).

1.6.2 Stabilisation Of RNF8 And MDC1 Interaction

Even though recruitment of RNF8 mainly depends on MDC1 phosphorylation, at least two proteins have been reported to further stabilise this crucial interaction. The ubiquitin E3 ligase HERC2 (HECT domain and RCC1-like domain-containing protein 2) was shown to interact with RNF8 (Bekker-Jensen et al., 2010) and this interaction facilitates HERC2 recruitment to the site of DNA damage. HERC2 becomes phosphorylated at T4827 upon IR, which is recognised by the FHA of RNF8 (Fig 1.4). Subsequently, RNF8 forms homo-oligomers that bind both HERC2 and MDC1 via the FHA. Interestingly, HERC2 has no impact on MDC1 nor RNF8 recruitment to sites of damage, but cells lacking HERC2 fail to recruit 53BP1, RAP80, BRCA1 and RNF168 to DSBs. Therefore, HERC2 appears to stabilise the RNF8-UBC13 complex, thus avoiding interaction of RNF8 with other E2 enzymes (Bekker-Jensen et al., 2010).

The other protein responsible for accurate interaction of MDC1 with RNF8 is the scaffold protein WRAP53β which binds both proteins simultaneously. Lack of WRAP53β leads to less efficient HR and NHEJ (Henriksson et al., 2014; Rassoolzadeh et al., 2015).

JMJD1C (Jumonji domain-containing protein 1C), a demethylating enzyme, has been shown to demethylate MDC1. Lack of JMJD1C demethylase activity abrogates RNF8 recruitment. This leads to lesser ubiquitination at the site of DNA damage and, thus, impaired RAP80-BRCA1 recruitment. Conversely, RNF168 and 53BP1 recruitment appear unaffected by the absence of JMJD1C (Watanabe et al., 2013).

Overall, the interaction of MDC1 and RNF8 is crucial for the initiation of the ubiquitin signal at the sites of DNA damage, and cells have evolved different mechanisms that further regulate this interaction.

1.6.3 RNF168

In 2007, Stewart and colleagues reported a new human syndrome, called RIDDLE syndrome, characterised by radiosensitivity, immunodeficiency, dysmorphic features and learning difficulties. Cells from these patients were not able to form 53BP1 foci and displayed abnormal BRCA1 foci formation upon IR, but none of the known players upstream, such as RNF8 or MDC1, were affected in those cells (Stewart et al., 2007; Devgan et al., 2011). Only two years later it was discovered that RIDDLE syndrome is caused by biallelic mutations in RNF168. Several groups reported in 2009 that RNF168 is a new ubiquitin ligase in the DDR, which is recruited to the site of DNA damage in an RNF8-dependent manner. Furthermore, it amplifies local K63-linked ubiquitin chains targeting

H2A and H2AX. Like RNF8, RNF168 also collaborates with the E2 UBC13 and is responsible for efficient recruitment of 53BP1 and BRCA1 (Stewart et al., 2009; Doil et al., 2009; Pinato et al., 2009). *In vitro* analysis showed that RNF168 targets H2AK13/K15 in collaboration with UBCH5C (Mattiroli et al., 2012; Gatti et al., 2012). A specific point mutation, R57D, in RNF168 abolishes its ability to initiate the ubiquitination of H2A(X), even though the enzyme is still able to create ubiquitin chains (Mattiroli et al., 2012). RNF168 contains an N-terminal RING domain. Moreover, it contains three UBDs: a UMI and MIU next to the RING domain and a second MIU on the C-terminal side (Pinato et al., 2009, 2011). These domains are necessary for RNF168 recruitment to RNF8-induced K63-linked ubiquitin chains. A detailed study has shown that not only the UBDs but also short sequences adjacent to them (so called LR motifs; LRMs) are important for accurate target recognition and thus recruitment of RNF168 (Fig 1.5A). The N-terminal UBDs (UMI and MIU1) are flanked upstream by LRM1, while the C-terminal MIU2 is flanked downstream by LRM2. Together they have been grouped into UDMs (ubiquitin dependent DSB recruitment modules), where UDM1 (LRM1, UMI and MIU1) binds RNF8-generated K63-linked polyubiquitin chains on H1. UDM2 (LRM2, MIU2) is dispensable for this step, but it is important for the recognition of self-induced ubiquitination on the core histones H2A and H2AX. This leads to a positive feedback loop and more accumulation of RNF168 (Panier et al., 2012). By structure analysis, it was shown that RNF168 monoubiquitinates core histones H2A and H2AX on K13 and K15, while RNF8 is not able to. Hence, RNF8 needs RNF168 to monoubiquitinate those histones, in order for it to be capable of elongating H2A and H2AX monoubiquitination on K13 and K15 (Mattiroli et al., 2012). RNF168 has also been shown to catalyse

non-canonical K27-linked ubiquitin chains on histone H2A and H2AX (Gatti et al., 2015), which are essential for accurate recruitment of 53BP1 and BRCA1. Furthermore, synthetic K27-linked ubiquitin chains are recognised by RAP80, RNF168, RNF169 and 53BP1 (Gatti et al., 2015) (Fig 1.5C).

Interestingly, in the absence of RNF8, RNF168 chimeras encoding the γH2AX-recognising BRCT domain of MDC1 have been artificially targeted to chromatin. While this leads to the rescue of 53BP1 foci, BRCA1 foci formation and accurate ubiquitination is not restored (Hodge et al., 2016). This indicates that the correct interplay of the two E3 ligases at the site of DNA damage is important for the accurate recruitment of the factors needed for timely repair.

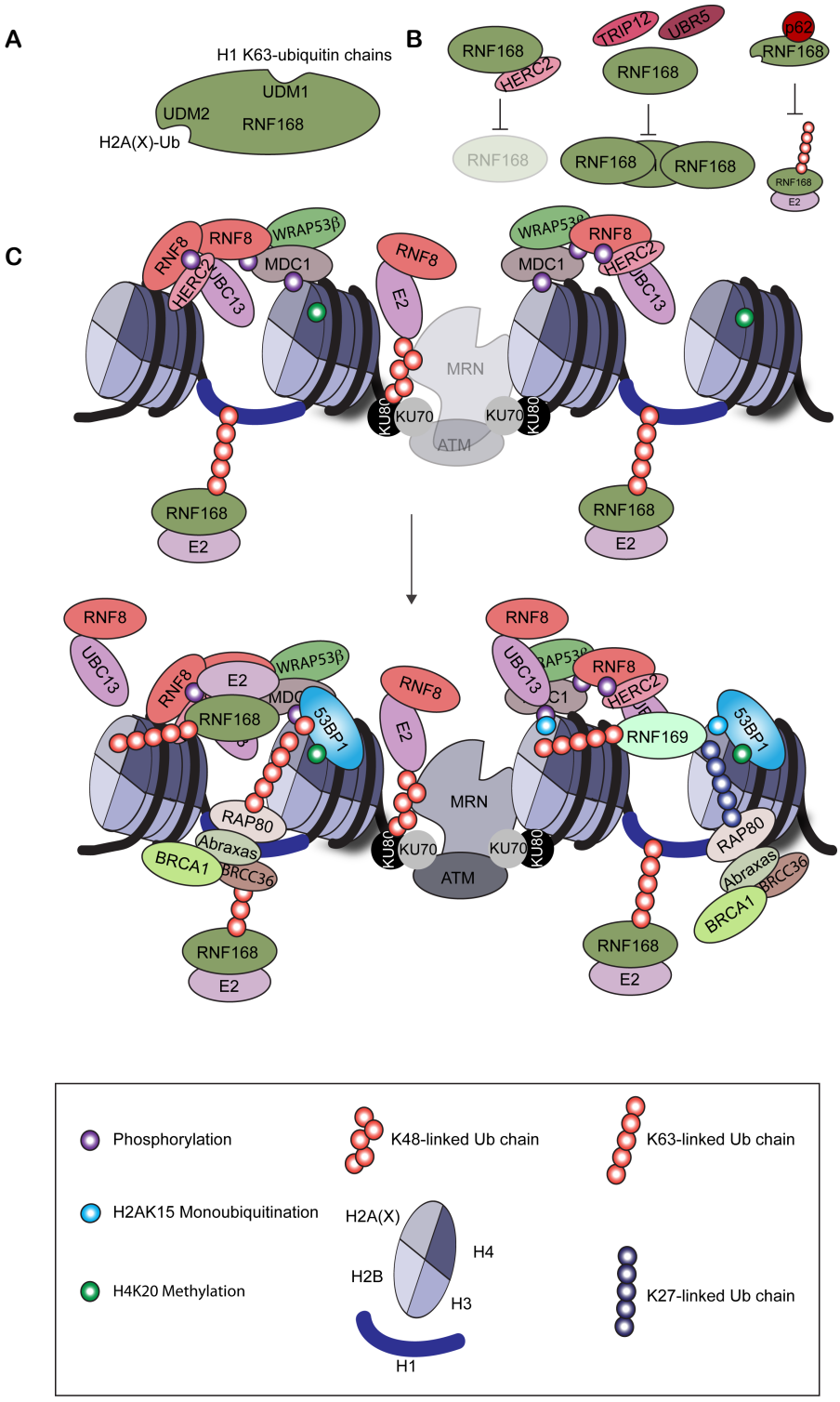


Figure 1-5. Regulation of RNF168 and its role at the site of DNA damage. A: Schematic representation of the two UDMs that recognise specific ubiquitination at the site of DNA damage. B: Regulation of the RNF168 pool by HERC2, TRIP12, UBR5 and p62. C: RNF168 is recruited to the site of DNA damage via its UDM1 and K63-linked ubiquitin chains on H1 induced by RNF8. There, RNF168 drives the ubiquitination at the site of DNA damage including targeting H2A(X)K13/K15, which signals for the recruitment 53BP1 and RAP80-BRCA1. RNF169 competes with RNF168 recruitment on ubiquitinated H2A(X)K13/K15 marks.

1.6.4 Regulation Of RNF168 Pool And Activity

Like RNF8, RNF168 interacts with the E3 ligase HERC2, but unlike RNF8 it does so in a DNA damage-independent manner. Absence of HERC2 leads to destabilisation of the RNF168 pool (Fig 1.5B) (Bekker-Jensen et al., 2010). An opposite regulation of the RNF168 pool is performed by the two HECT domain ubiquitin ligases TRIP12 and UBR5. Absence of these two ubiquitin ligases leads to hyper-accumulation of RNF168 at the site of DNA damage and massive spreading of ubiquitin, which leads to hyperaccumulation of 53BP1 and BRCA1 (Gudjonsson et al., 2012). Together, these data show that not only is the recruitment of the RNF168 to the site of DNA damage crucial but also that maintenance of its steady-state pool is tightly controlled by the cell.

RNF168 is also regulated by autophagy, an intracellular pathway that degrades and recycles cellular components in a proteasome-independent manner via the lysosome. In cells unable to perform autophagy, p62 accumulates inside the nucleus where it binds the MIU1 domain of, and thereby inhibits, RNF168 (Fig 1.5B). As a result, these cells are not able to ubiquitinate H2A anymore and fail to accumulate BRCA1, RAP80 or RAD51 (Wang et al., 2016a).

1.6.5 RNF169, A RNF168 Paralogue

RNF169 is a paralogue of RNF168 (Chen et al., 2012; Poulsen et al., 2012). Like RNF168, it has an N-terminal RING domain and potential UMI and MIU UBDs. RNF169 recognises RNF168-induced ubiquitinated H2A but does not recognise RNF8-induced H1 ubiquitination. Hence, RNF169 is recruited to the site of DNA damage in an RNF8-RNF168-dependent manner, but its presence is not necessary for the recruitment of RAD18, BRCA1 and 53BP1. Interestingly,

depletion of RNF169 leads to retention of 53BP1 at later time points (Poulsen et al., 2012). RNF169 does not have an impact on ubiquitination at the site of DNA damage but ectopic expression of RNF169 impairs the recruitment of 53BP1 and RAP80 in a noncatalytic manner. By competing with RNF8- and RNF168-induced ubiquitin signals for the recruitment of 53BP1 and RAP80, RNF169 suppresses NHEJ and stimulates repair via HR (Fig 1.5C) (Poulsen et al., 2012; Chen et al., 2012).

1.6.6 Dubs Involved In The Regulation Of The DDR

As described above, ubiquitination plays a crucial role in the organisation of the chromatin surrounding DSBs. As in all ubiquitin-dependent pathways, this process is reversible and highly regulated. In the recent years, several DUBs have been found to play a role in the DDR.

1.6.6.1 BRCC36

In 2003, several years before a role for RNF8 had been described in the DDR, Dong and colleagues isolated the BRCC holoenzyme, a complex containing BRCA1, BARD1, and the JAMM DUB BRCC36 (BRCA1-BRCA2-containing complex subunit 36) (Dong et al., 2003). The activity of the BRCA1-BARD1 E3 ubiquitin ligase is stimulated upon interaction with BRCC36, and lack of BRCC36 sensitises cells to IR (Shao et al., 2009) and affects the G2/M checkpoint. Moreover, RAP80 contains an Abraxas interaction domain, associating RAP80 with BRCA1 and BRCC36. Abraxas and BRCC36 interact via the coiled-coil domains of each protein (Wang and Elledge, 2007). Therefore, BRCC36 is recruited to DSBs via RAP80 where its DUB activity is necessary for counteracting RNF8-induced K63-linked ubiquitin chains on γH2AX (Sobhian et al., 2007; Cooper et al., 2009). A

failure to trim those K63-linked ubiquitin chains leads to increased 53BP1 recruitment (Shao et al., 2009) and thus reduced HR.

1.6.6.2 Members Of The USP Family

Many members of the USP family of DUBs have been shown to play a role in the organisation of ubiquitination on the chromatin surrounding a DSB.

USP3 counteracts RNF168 by removing the ubiquitin molecule from monoubiquitinated H2A and H2AX at K13/K15 upon DNA damage. As discussed above, these marks are specifically induced by RNF168, making USP3 a specific DUB against RNF168 (Sharma et al., 2014). Hence, lack of USP3 abrogates DSB repair as observed by prolonged γH2AX and ubiquitin foci (Nicassio et al., 2007).

USP7 deubiquitinates RNF168 and thus protects RNF168 from proteasomal degradation after UV treatment. Cells lacking USP7 show decreased H2A ubiquitination, total ubiquitination and BRCA1 recruitment. Interestingly, those cells are still able to normally recruit 53BP1 (Zhu et al., 2015).

USP16 interacts with HERC2 via its coiled-coil domain and the C-terminal HECT domain of HERC2. The absence of USP16 leads to an increased number of 53BP1 foci and retention of ubiquitination on H2A after IR. USP16 protein levels increase upon DNA damage induction in a HERC2-dependent manner. Therefore, after RNF168, it is the second DDR player whose pool is regulated by HERC2 (Zhang et al., 2014b). Furthermore, USP16 reverses the transcriptional silencing at DNA double strand breaks by deubiquitinating H2A on K119 (Shanbhag et al., 2010)

USP17L2/Dub3 directly deubiquitinates H2A and H2AX, counteracting RNF8 and RNF168. Therefore, Dub3 is another regulator of accurate 53BP1 and BRCA1

recruitment, with overexpression of Dub3 abrogating 53BP1 and BRCA1 foci formation (Delgado-Diaz et al., 2014).

Depletion of USP34 leads to compromised DNA repair and IR-induced hypersensitisation. USP34 is directly recruited to DSBs and MDC1 removal is delayed in cells lacking USP34. USP34 recruitment is dependent on RNF8, RNF168 and 53BP1 but not RAP80 or BRCA1. Interestingly, USP34 stabilises RNF168 upon IR. Ubiquitination of H2AX is reduced in cells lacking USP34, possibly due to reduced RNF168 levels. Therefore, the absence of USP34 leads to defective recruitment of BRCA1, 53BP1 and RAD18 to DSBs (Sy et al., 2013).

Three further USPs have been found to antagonise RNF8- and RNF168-induced ubiquitination at sites of DNA damage, namely USP26, USP29 and USP44. All three DUBs impair 53BP1 recruitment when individually overexpressed. Moreover, RAP80 recruitment and H2A monoubiquitination is also affected under these circumstances. Further investigation revealed that USP29 and USP44 play a role downstream of RNF8, not affecting RNF8 accumulation, but impairing RNF168 recruitment when overexpressed. This phenotype is due to the enzymatic activity of these DUBs as overexpression of an enzymatic dead version does not mimic this phenotype. While USP44 exclusively displays specificity for the RNF8-induced histone ubiquitination cascade, USP29 overexpression also affects p53 and MDM2, indicating additional roles for USP29 in the DDR (Mosbech et al., 2013).

USP51 is capable of binding H2A and H2B and to deubiquitinate H2A K13 and K15 *in vitro*. Furthermore, cells depleted for USP51 display increased spontaneous DNA damage foci formation and H2A K15 ubiquitination whereas RNF8 and RNF168 recruitment is not affected in these cells. On the other hand,

overexpression of this DUB abolishes 53BP1 and BRCA1 foci formation, indicating that USP51 is yet another DUB fine-tuning RNF8- and RNF168-induced ubiquitination in the DDR (Wang et al., 2016b).

1.6.6.3 Proteasome Associated DUB POH1/RPN11

Interestingly, the 19S proteasome-associated DUB POH1, a member of the JAMM DUB family, has been shown to play a role in 53BP1 and ubiquitin foci resolution. POH1 appears to counteract RNF8- and RNF168-induced ubiquitination and regulates JMJD2A (Jumonji domain-containing protein 2A) on the chromatin. On the other hand, absence of POH1 does not affect RAP80-BRCA1 recruitment, illustrating that the proteasome influences 53BP1 but not BRCA1 recruitment (Butler et al., 2012). Furthermore, POH1 displays K63-linkage specificity (Cooper et al., 2009).

1.6.6.4 OTUB1 And OTUB2

An interesting way of regulating the ubiquitination in the DDR is displayed by OTUB1. Although depletion of OTUB1 leads to persistence of ubiquitin and 53BP1 foci, this is not the result of losing its enzymatic activity (Nakada et al., 2010). X-ray crystallography showed that OTUB1 interacts with ubiquitin-charged UBC13 (UBC13~Ub). This interaction is allosterically regulated by free ubiquitin that also binds to OTUB1, thus increasing its affinity for UBC13~Ub. OTUB1 bound to UBC13 not only inhibits the E2 activity but it also disrupts heterodimerisation of UBC13 with UEV1A (ubiquitin-conjugating enzyme E2 variant 1A) (Juang et al., 2012; Wiener et al., 2012; Sato et al., 2012).

OTUB2 was found to fine-tune repair pathway choice as absence of OTUB2 leads to enhanced 53BP1 and RAP80 recruitment, while RPA and RAD51 foci

formation is suppressed, therefore favouring NHEJ pathway choice OTUB2 acts by fine-tuning the K63-linked ubiquitin chains initiated by RNF8 at the sites of DNA damage as well as acting on L3MBTL1 ubiquitination. Therefore, absence of OTUB2 promotes NHEJ-mediated DSB repair, and increases cellular sensitivity to camptothecin, a drug that induces DSBs in the context of replication (Kato et al., 2014).

1.6.7 Regulation Via SUMO-Dependent Ubiquitination

SUMOylation plays a role in the organisation of the DDR, as the recruitment of both 53BP1 and BRCA1 depends on the two SUMO E3 ligases PIAS1 (protein inhibitor of activated STAT 1) and PIAS4 (Morris et al., 2009; Galanty et al., 2009). PIAS4 SUMOylates HERC2 and RNF168 upon IR, and SUMOylation of HERC2 promotes its interaction with RNF8 (Danielsen et al., 2012). Furthermore, MDC1 is SUMOylated upon DNA damage, which is necessary for degradation of MDC1 which also results in the removal of 53BP1. RNF4, a SUMO-targeted E3-ubiquitin ligase (STUbL), recognises and ubiquitinates SUMOylated MDC1, tagging it for degradation. Inhibition of MDC1 SUMOylation, by mutating the SUMOylation site in MDC1, leads to a defect in the recruitment of CtIP, RPA and RAD51, and consequently impaired HR. Depleting 53BP1 in those cells rescues HR again, underlining how important accurate PTM regulation is for the balanced recruitment of the different DDR players (Luo et al., 2012; Yin et al., 2012). Moreover, RAP80 recruitment has been shown to depend on RNF4 (Guzzo et al., 2012). RAP80 recognises mixed chains consisting of SUMO and ubiquitin as it contains both UIMs and SIMs motifs.

RNF4 has also been shown to regulate the turnover of RPA. BRCA2 and RAD51 cannot properly replace RPA in cells lacking RNF4, thus impairing HR (Galanty et al., 2012). Interestingly, the removal of both MDC1 and RPA via RNF4 needs the proteasome, as the proteasome component PSMD4/RPN10 binds to MDC1 and RPA at the site of DNA damage in an RNF4- and RNF8-dependent manner.

The deSUMOylase SENP7 (sentrin-specific protease) has been reported to be needed for the removal of SUMO2/3 from KAP1 (KRAB-associated protein 1), regulating chromatin relaxation upon DNA damage, which is necessary for HR repair (Garvin et al., 2013).

Likewise, SENP6 has been reported to regulate RPA SUMOylation and HR repair. SENP6 keeps RPA70 hypoSUMOylated during the S-phase, whereas upon replication stress, SENP6 does not protect RPA70 anymore, allowing it to be SUMOylated. This SUMOylation promotes RAD51 loading and thus HR (Dou et al., 2010).

1.6.8 p97 Dependent Processes At The Site Of DNA Damage

p97 has been shown to play a crucial role in the regulation of the DDR upon DSB induction (Meerang et al., 2011; Acs et al., 2011). Cells depleted of p97 display inefficient repair by both HR and NHEJ (Meerang et al., 2011). p97 is directly recruited to the site of DNA damage in an UFD1-NPL4-dependent manner. Once recruited to the chromatin, it needs its ATPase activity for regulation as an ATPase-dead mutant (EQ mutant) fails to stimulate accurate DSB repair. Recruitment of p97 is RNF8-dependent but upstream of RNF168, 53BP1 and BRCA1. Abolishing the activity of p97 leads to hyperaccumulation of K48-linked ubiquitin chains at the site of DNA damage. The production of those K48-linked

ubiquitin chains appears to be RNF8, but not RNF168, dependent. The absence of p97 leads to decreased 53BP1 and BRCA1 foci formation and defective RAD51 localisation after IR (Meerang et al., 2011). Therefore, p97 is needed for accurate DSB repair for removing substrates from the site of DNA damage that are marked with K48-linked ubiquitin chains and thus orchestrating accurate recruitment of important DSB players, including BRCA1 and 53BP1.

One of the p97 substrates has been identified to be the polycomb protein L3MBTL1 (Acs et al., 2011). L3MBTL1 usually binds H4K20me2 in non-damaged cells and thus prevents 53BP1 binding. After induction of DNA damage, L3MBTL1 is ubiquitinated and extracted from the chromatin by p97. This process enables recruitment of 53BP1 to H4K20me2 and 53BP1 IR-induced foci formation (Fig 1.6).

It has been shown that Cdc48 (p97 in yeast) binds to SUMOylated Rad52. Upon interaction with Rad52, Cdc48 disrupts the Rad51-Rad52 complex and removes them from the chromatin, thus controlling the recombination rates by indirectly controlling the Rad51 recombinase (Bergink et al., 2013).

An additional role for p97 in the DDR is exemplified by the findings that p97 interacts with RNF4 to target pS824-SUMO-KAP1 for degradation during S/G2 phase (Kuo et al., 2016). This KAP1 degradation is of importance to recruit BRCA1 and RAD51 for HR. It has been shown that UFD1, the cofactor of p97, interacts with SUMO via a SIM motif (Nie et al., 2012).

These examples may only scratch the surface of the action of p97 in the DDR. Being able to interact with a large set of cofactors, it is expected that p97 regulates a much more broad spectrum of proteins in the DDR.

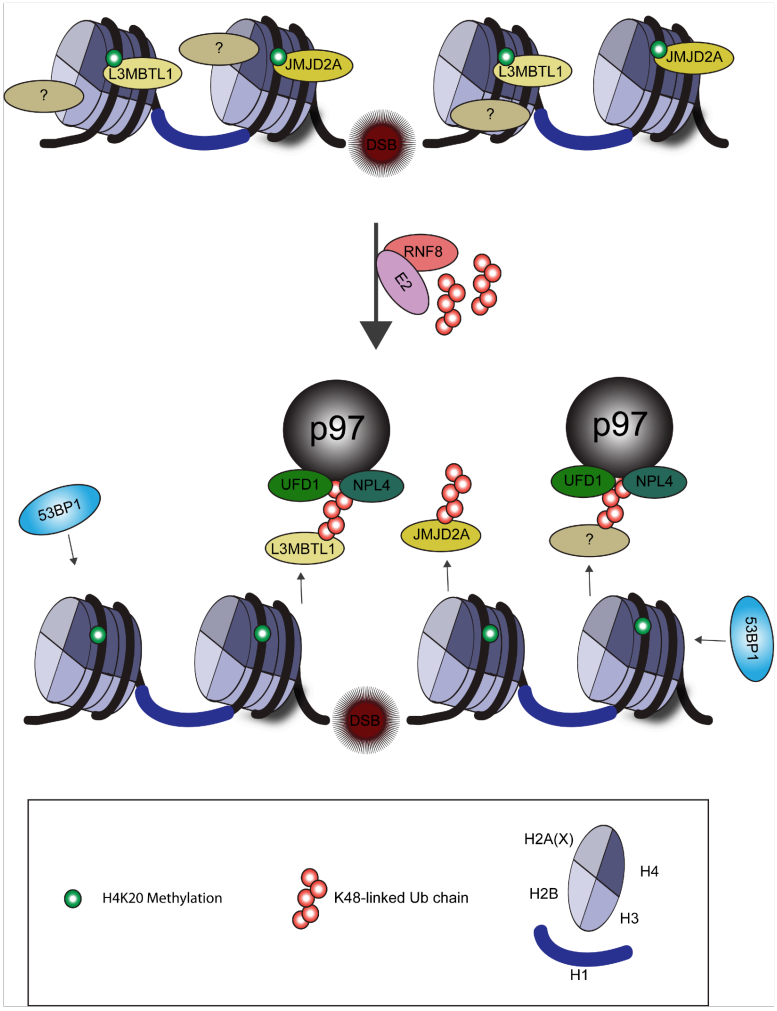


Figure 1-6. p97 orchestrates the removal of proteins from the site of DNA damage. Methylated H4K20 is bound by chromatin-binding proteins such as L3MBTL1 or JMJD2A in unstressed cells. Upon DSB induction, those proteins are K48-Ub tagged by RNF8. p97$^{UFD1-NPL4}$ is recruited to the site of DNA damage and is involved in the removal of K48-tagged proteins such as L3MBTL1. This results in the H4K20 methylation being available for 53BP1 recruitment.

1.6.9 Events Downstream Of RNF8 And RNF168

1.6.9.1 Regulation Of 53BP1

53BP1 is a large protein, consisting of more than 2000 amino acids. On the N-terminal half, it encodes 28 S/TQ sites that are phosphorylated upon DNA damage by the ATM and ATR kinases. Phosphorylation of those sites leads to interaction with RIF1 and PTIP, important for 53BP1's ability to block end-resection at the broken DNA ends and coordinate NHEJ. The S/TQ sites are followed by a oligomerisation region, the tandem Tudor domains, the ubiquitin-dependent recruitment (UDR) motif, a nuclear localisation signal (NLS) and at its very C terminal part, it encodes a pair of BRCT domains (Zimmermann and de Lange, 2014).

Functionally, in 2004, it was reported that Crb2, the yeast orthologue of mammalian 53BP1, requires methylation of histone H4K20 for recruitment to the site of DNA damage (Sanders et al., 2004). By crystallography, this finding was further supported for Crb2 but also 53BP1 in 2006. Botuyan and colleagues showed that the two orthologues interact with H4K20me2 via their tandem Tudor domains (Botuyan et al., 2006). In non-damaged cells, most of H4K20 exists in dimethylated form and is bound by the polycomb protein L3MBTL1 and JMJD2A (Fig 1.6). Upon DNA damage, both L3MBTL1 and JMJD2A are removed from the chromatin around the sites of DNA damage. L3MBTL1 removal is both RNF8- and RNF168-dependent. These two ligases ubiquitinate L3MBTL1, which is then recognised and extracted by p97 (Acs et al., 2011). JMJD2A was reported to be ubiquitinated in an RNF8-dependent manner that leads to its proteasomal degradation (Fig 1.6) (Mallette et al., 2012). Additionally, MBTD1 (MBT domain-

containing protein 1), a stable subunit of the TIP60/NuA4 acetyltransferase complex, recognises H4K20me2 via its malignant brain tumour (MBT) domain. Upon DSB induction, MBTD1 competes with 53BP1 for binding to those sites and then recruits TIP60. Subsequently, TIP60 acetylates H2AK15 blocking that site for RNF168-induced ubiquitination, suppressing downstream NHEJ component recruitment and promoting HR (Jacquet et al., 2016). Overall, H4K20me2 is a crucial site that is tightly regulated upon DSB induction to accurately recruit 53BP1 and protect the broken DNA ends from end resection.

In addition to the H4K20me2 signature, 53BP1 also recognises RNF168-induced H2AK15 monoubiquitination via its UDR motif (Fradet-Turcotte et al., 2013). This has been further demonstrated by a cryomicroscopy structure of a 53BP1 fragment bound to H4K20me2 and H2AK15ub (Wilson et al., 2016). RNF168 depletion abolishes recruitment and retention of 53BP1 at the sites of DNA damage. Bohgaki and colleagues showed that RNF168 interacts with and ubiquitinates 53BP1 with K63-linked chains on K1268 in an MDC1- and RNF8-independent manner. This ubiquitination step is crucial for initial 53BP1 foci formation (Bohgaki et al., 2013). Controversially, Hu and colleagues found that most of the nuclear 53BP1 protein pool is degraded upon DSB induction in an RNF8- and RNF168-dependent manner and that only 53BP1 located at the site of damage is protected from this degradation wave, leading to foci formation at the site of damage (Hu et al., 2014)

1.6.9.2 BRCA1-RAP80 Complex

BRCA1 is a 1863 amino acid protein, containing a RING domain on its N-terminal part, followed by two NLS motifs. On the C-terminal part, it carries the coiled-coil

and BRCT domains. The different domains enable the protein to interact with different proteins.

BARD1 interacts with BRCA1 via the RING domain of BRCA1. Together they form a functional E3 ubiquitin ligase (Xia et al., 2003). It has been shown that the BRCA1-BARD1 complex ubiquitinates H2A on its C-terminal tail on K127 and K129 in a nucleosome-specific context (Kalb et al., 2014). Therefore, BRCA1-BARD1 targets different lysines on H2A than RNF8 and RNF168.

The BRCA1-A complex consists of RAP80, Abraxas, BRCC36, BRCC45 and MERIT40 (Mediator of RAP80 interactions and targeting subunit of 40 kDa). BRCA1 interacts with Abraxas via its BRCT domain upon phosphorylation of Abraxas on Ser406, which bridges BRCA1 to RAP80. RAP80 contains a tandem UIM that recognises DNA damage-dependent K63-linked ubiquitin chains on H2A initiated by RNF8 (Sato et al., 2009; Wu et al., 2009). Therefore, Abraxas and RAP80 are responsible for the recruitment of BRCA1 to the site of DNA damage (Kim et al., 2007; Wang et al., 2007; Sobhian et al., 2007). Binding of Abraxas to BRCA1 excludes other BRCA1 interaction partners such as BRCA1-associated C terminal helicase (BACH1) and CtIP from the complex (Wang et al., 2007).

Functionally, RAP80 inhibits excessive BRCA1-dependent DNA end-resection and thus avoids hyper-recombination (Coleman and Greenberg, 2011; Hu et al., 2011). Hence, BRCA1 is not interacting with RAP80 during end-resection as the presence of RAP80 leads to inhibition of MRE11-CtIP-dependent end-resection and HR (Coleman and Greenberg, 2011). Therefore, the RAP80-BRCA1 complex is an NHEJ promoter, while the BRCA1-C complex, consisting of BRCA1, CtIP and the MRN complex is a HR promoter.

1.6.10 Regulation Of DSB Repair And Pathway Choice

Cells strictly regulate the utilisation of NHEJ and HR. It has been observed, that lack of BRCA1 shifts cells towards a mutagenic NHEJ pathway during the S-phase, leading to embryonic lethality, chromosomal abnormalities and tumourigenesis. In cells lacking both BRCA1 and 53BP1, these phenotypes can be relieved (Bouwman et al., 2010; Bunting et al., 2010; Cao et al., 2009), indicating that 53BP1 and BRCA1 have opposing roles in the response to DSBs.

Neither 53BP1 nor BRCA1 have cell cycle-dependent expression levels, so how does the cell suppress HR during G1? 53BP1 interacts with several proteins that help it to block 5' end resection during G1. One of them is RIF1 (Rap1 interacting factor 1), that was first shown in yeast to be of importance for the maintenance of telomere length (Hardy et al., 1992). In 2013, it was shown that, in the mammalian system, RIF1 interacts with 53BP1 via the phosphorylated S/TQ domain of 53BP1 upon DNA damage (Zimmermann et al.; Di Virgilio et al., 2013; Chapman et al., 2013; Escribano-Díaz et al., 2013; Feng et al., 2013). 53BP1-RIF1 suppresses the recruitment of BRCA1 to the site of DNA damage (Escribano-Diaz et al., 2013), thus promoting NHEJ and preventing HR. During S phase, CDK1 is active and phosphorylates CtIP on T847. This activates the BRCA1-CtIP complex that is then able to remove 53BP1 from the ends and initiate end resection for HR (Escribano-Diaz et al., 2013).

Additionally, PTIP is a second 53BP1-interacting protein shown to help prevent unscheduled 5' end-resection in G1 cells. Similar to RIF1, it interacts with phosphorylated 53BP1 via its BRCT domains with the eight most N-terminal S/TQ phosphorylation sites of 53BP1 (Callen et al., 2013).

Thirdly, the NHEJ-driving nuclease Artemis has been shown to interact with PTIP (Wang et al., 2014), shedding further light on how 53BP1 prevents end-resection. Artemis interacts with the BRCT2 of PTIP and needs its nuclease activity to protect cells from 5' end-resection (Wang et al., 2014).

On the other hand, BRCA1 interacts with BRCA2, another important player for end resection and HR, over PALB2. Durocher and colleagues have observed that during G1, BRCA1 cannot interact with PALB2 (Orthwein et al., 2015). KEAP, a substrate adaptor for a CUL3-RING ubiquitin ligase (CRL3), binds PALB2 via its KELCH domain, and acts as a BRCA1-PALB2 interaction inhibitor by ubiquitinating PALB2 on K25 and K30. During S and G2 phases, PALB2K25/K30 ubiquitination is reversed by the DUB USP11. USP11 itself is very unstable during G1, and even more so upon IR during G1, where it is phosphorylated in an ATM-dependent manner and degraded by the proteasome. Thus, the cell cycle tightly regulates the recruitment of BRCA1-PALB2-BRCA2 (Orthwein et al., 2015).

Cells need to strictly regulate when to initiate excessive 5' end-resection and initiate HR. Recent advances have improved the understanding of the cellular regulation. An improved understanding of the mechanisms will lead to the development of better treatment for cancer.

1.7 Genomic Instability And Cancer

Mutations in genes can lead to genomic instability and ultimately to severe diseases such as cancer, neurodegeneration and accelerated ageing. Cancer is a very heterogeneous disease but it shares the following hallmarks that have been summarised by Hanahan and Weinberg in 2000 and expanded in 2011: 1) Cell

death resistance 2) sustaining proliferative signaling, 3) evading growth suppressors, 4) activating invasion and metastasis, 5) enabling replicative immortality, 6) inducing angiogenesis, 7) deregulating cellular energetics and 8) avoiding immune destruction (Hanahan and Weinberg, 2000, 2011). Tumour-promoting inflammation, genome instability and mutations are the characteristics without which none of the 8 hallmarks can be achieved. (Hanahan and Weinberg, 2011).

It is therefore not surprising that most human tumours display genomic instability, which is due to aberrant behavior of the DDR. For instance, loss-of-function mutations in MSH2 and MLH1, MMR genes, are associated with hereditary non-polyposis colorectal cancer (HNPCC), manifesting in microsatellite instability (Jiricny, 2006). Inherited defects in HR proteins, such as BRCA1, BRCA2, PALB2 or ATM, underlie many familial breast, ovarian and pancreatic cancers. Moreover, several loss-of-function mutations in several DDR proteins are linked to rare syndromes including Werner syndrome, Fanconi anaemia, Bloom's syndrome, ataxia telangiectasia (ATM) and Ruijs-Aalfs syndrome.

1.7.1 The Components Of DDR As Druggable Targets

In summary, defects in the DDR lead to genomic instability associated with accelerated ageing, neurodegeneration, and cancer. So far, the DDR has been best explored as a potential avenue for cancer therapy. In cancer therapy, induction of DNA damage, either by radio- or chemotherapy, has been one of the major tools for cancer therapy. Radiotherapy is responsible for approximately 40% of all cures (O'Connor, 2015). 1 Gy of IR generates around 1000 single strand breaks

and 35 DSBs in a cell. On the other hand, acute and chronic tissue toxicity in patients receiving radiotherapy is a limiting factor for the dose delivery with this therapy.

A different, yet successful, approach used in cancer therapy is the concept of synthetic lethality, where a defect in one protein is compatible with cell viability but combined with a second defect leads to cell death. The best example of exploiting synthetic lethality is in the treatment of BRCA1- or BRCA2-mutated cancers, where the inhibition of PARP1 leads to synthetic lethality. Unfortunately, during applications using olaparib, a PARP1 inhibitor, it has emerged that patients tend to develop drug resistance due to further mutations in the BRCA2 gene, restoring its function (Lord et al., 2015).

Hence, using DDR inhibitors in combination with radiotherapy to sensitise the cancer cells is a tempting application of synthetic lethality. A more detailed understanding of the DDR will help to develop new strategies to treat cancer more efficiently (O'Connor, 2015).

DUBs, similar to protein kinases, can be inhibited by small molecules. For instance, as USP7 controls p53 stability, several specific inhibitors against USP7 have been developed for cancer therapy. Other DUBs have also emerged as promising druggable targets for cancer therapy due their involvement in apoptosis or other cancer-related processes. They have not yet been approved for clinical trials but preclinical studies have shown promising results. For instance, P5091, an inhibitor of USP7 and USP47, induces apoptosis of multiple myeloma cells that are resistant to the proteasome inhibitor bortezomib (Chauhan et al., 2012; Weinstock et al., 2012).

1.7.2 Targeting The UPS

Another important target in cancer therapy is the UPS. The proteasome inhibitor bortezomib (Velcade) was the first approved anti-cancer drug that targets components of the UPS. Bortezomib is a potent therapeutic for multiple myeloma and mantle cell lymphoma. Increased numbers of chromosomes (polyploidy), one of the main characteristics of the majority of cancers, leads to increased number of proteins in cancer cells. It is roughly estimated that 90% of human solid tumor cells carry more than two copies of at least one chromosome (Weaver and Cleveland, 2006). Thus cancer cells are under constant proteotoxic stress. In addition, the high genetic mutation rates in cancer cells leads to an additional increase in proteotoxic stress, as many of the mutated genes will be translated into aberrant proteins that are not functional due to their inappropriate folding. Unfortunately, the effect of bortezomib in treatment of solid tumours is not as efficient as in B-cell tumours. One of the reasons is that solid tumours need much higher levels of the inhibitor and longer exposure to achieve cell death when compared to multiple myeloma (Deshaies, 2014).

For similar reasons to the proteaseome, p97 is also an appealing target for cancer treatment. p97 is involved in many subcellular protein quality control processes, which may explain why cancer cells heavily rely on it and loss of p97 is much more cytotoxic to cancer cells than normal cells. Furthermore, high expression of p97 in cancer cells correlates with a bad patient prognosis (Vekaria et al., 2016), and many malignant cells actually display moderate to strong nuclear and cytoplasmic staining (http://www.proteinatlas.org/ENSG00000165280-VCP/cancer). Therefore, screens for specific inhibitors of p97 ATPase activity have been performed

(Deshaies, 2014). In 2015, a potential p97 inhibitor, that is orally bioavailable, has been validated *in vitro* and on xenograft models (Anderson et al., 2015).

1.8 Aim Of The Thesis

Understanding the fundamental changes that occur at the site of IR-induced DSBs is essential for the further development of better strategies and the identification of new druggable targets for cancer treatment in relation to radiotherapy. p97 has emerged as an essential player in the context of the IR-induced DDR. Our laboratory aims to further investigate the role of p97, its cofactors and the UPS in the repair of IR-induced DSBs. Therefore, the aim of this thesis was to gain further understanding of three p97 cofactors after IR.

As part of a collaboration with the Shiloh laboratory, we investigated two novel E3/4-ubiquitin ligases at sites of DNA damage and their role in DSB repair.

In the second part of this thesis, and as an independent project, we investigated how the deubiqutinating enzyme ATXN3 regulates the IR-induced DDR. One of the main goals of our laboratory is to identify new druggable targets that radiosensitise cells. Thus, I believe that my thesis significantly contributes to the mission of the Ramadan laboratory, as it identifies three enzymes (UBE4A, UBE4B and ATXN3), whose inactivation leads to IR-induced hypersensitivity.

2 MATERIALS AND METHODS

2.1 Buffers:

The following buffers were made in the laboratory. Chemicals used to make up buffers were all obtained from Sigma unless indicated otherwise.

2.1.1 10x Phosphate Buffered Saline (PBS)

For 1 L, the following was dissolved in 800 ml ddH_2O:

- 18.1 g $Na_2HPO_4 \bullet 2H_2O$
- 80 g NaCl
- 2 g KCl
- 2.4 g KH_2PO_4

pH was adjusted to 7.4 with HCl and the mix filled up to 1 L with ddH_2O

The 10x PBS was diluted 1:10 for working concentration (137 mM NaCl, 12 mM Phosphate, 2.7 mM KCl, pH 7.4)

2.1.2 10x TBS (Tris-buffered saline)

For 1 L, the following was dissolved in 900 ml ddH_2O:

- 88 g NaCl
- 24 g Tris base

pH was adjusted to 7.6 with HCl and filled up to 1 L with ddH_2O.

The 10x TBS was diluted 1:10 for working concentration (20 mM Tris, 150 mM NaCl)

For 1x TBS-Tween, Tween-20 (Sigma) was added to 1x TBS to a final concentration of 0.1%.

2.1.3 10x Tris/Glycine Buffer

For 1 L the following was dissolved in ddH_2O:

- 30 g Tris base
- 144 g Glycine

The 10x Tris/Glycine buffer was used to make 1x running and transfer buffer for Western blots.

2.1.4 1x Running Buffer For Western Blots

10x Tris/Glycine buffer was diluted to 1x with ddH_2O and SDS was supplemented to a final concentration of 0.1%.

2.1.5 1x Transfer Buffer For Western Blots

10x Tris/Glycine buffer was diluted to 1x with ddH_2O, 20% Methanol and 0.025% SDS.

2.1.6 5x Laemmli Buffer (LB)

- Bromophenol blue (SLS; 0.25%)
- Glycerol (Fisher Scientific; 50%)
- SDS (10%)
- Tris-HCl (0.25 M, pH 6.8)

5x LB buffer was diluted 1:5 for working concentration (50 mM Tris-HCl pH 6.8, 2% SDS, 10% Glycerol, 15% β-mercaptoethanol, 0.05% bromophenol blue)

2.2 Mammalian Cell Culture

2.2.1 Human Cell Lines

The human osteosarcoma cell line U-2 OS (U2OS), human embryonic kidney 293T (HEK293T) and HeLa cells were purchased from ATCC (American Type Culture Collection).

2.2.2 Maintenance Of Human Cell Lines

U2OS, HeLa and HEK293T cells were cultured in Dulbecco's Modified Eagle's Medium (DMEM, Gibco) supplemented with 10% Fetal Bovine Serum (FBS, Sigma) and 1x Penicillin/Streptomycin (Pen/Strep; Gibco). They were incubated at 37°C in 5% CO_2 in a humidified air incubator. When reaching 80-90% confluency, cells were split. In short, they were washed once with 1x PBS, trypsinised with 1x trypsin (0.05%) in autoclaved 1x PBS and re-seeded 1:5 (U2OS) or 1:10 (HEK293T, HeLa). Cells were used until passage 25.

To freeze cells, they were trypsinised off the plates, centrifuged at 500 rcf, washed once with 1x PBS, centrifuged again and resuspended in freezing medium (45% DMEM, 45% FBS, 10% DMSO (Sigma)). Aliquots of 1 ml were frozen down using cell freezing container (CoolCell) at -80°C for 24 hrs before they were transferred to liquid nitrogen.

Freshly thawed cells were tested for Mycoplasma using PlasmoTest (InvivoGen) according to the manufacture's instructions.

2.3 Manipulating Human Cells

2.3.1 siRNA Transfections

8-12x10^5 cells were seeded in a 6-well plate or an according number for different sized plates, and the next day were transfected with indicated siRNA using Lipofectamine RNAiMAX (Invitrogen). For this, the volume of DMEM in the wells was reduced to 1 ml. The desired amount of siRNA was diluted in 100 µl OptiMEM (Gibco). Working concentrations of the different siRNA sequences is summarised in Table 1. 2 µl of RNAiMAX was diluted in 100 µl OptiMEM and left at room temperature (RT) for 5 min. Then, siRNA and RNAiMAX were mixed together and left at RT for 15 min before being added drop wise to the cells. Depletion was performed over 72 hours before cells were further used and depletion efficiency was assessed by Western blot. The list of siRNA sequences is given in Table 1.

Gene	Sequence	Working Concentration	Reference
siLuc (Control)	CGUACGCGGAAUACUUCGA	varies	Microsynth AG
siAtaxin-3_6	GGACAGAGUUCACAUCCAU	20 nM	ON-Target Dharmacon
siAtaxin-3_7	ACAGGAAGGUUAUUCUAUA	20 nM	ON-Target Dharmacon
siAtaxin-3_8	GCAGGGCUAUUCAGCUAAG	20 nM	ON-Target Dharmacon
siRNF8	GGACAAUUAUGGACAACAA	100 nM	Microsynth (Mailand et al., 2007)
siRNF168	GGCGAAGAGCGAUGGAAGA	100 nM	Microsynth (Doil et al., 2009)
siUBE4A_1	GAUAAUAGCGUGUCAGAGA	100 nM	Shiloh lab
siUBE4A_2	GCAGAUAACCUGGGUGAUU	100 nM	Shiloh lab
siUBE4B_1	CCUAGUUGCCGUCGCUAUA	100 nM	Shiloh lab
siUBE4B_4	GUGUGAAUGCAACGAUGGA	100 nM	Shiloh lab
sip97_2	AAGUAGGGUAUGAUGACAUUG	20 nM	Qiagen
sip97_5	CGGGAGAGGCGCGCGCCAU	20 nM	5' UTR
sip97_6	AAGAUGGAUCUCAUUGACCUA	20 nM	Qiagen
sip97_7	AACAGCCAUUCUCAAACAGAA	20 nM	Qiagen

Table 1 Summary of siRNA sequences

2.3.2 Plasmid transfection

HEK293T cells were seeded in 10 or 15 cm cell culture plates and allowed to reach 50% confluency. DNA as well as 25x PEI was diluted in 1x PBS, mixed together and vortexed 3x 3 seconds at medium intensity (See Table 2 for protocol). The mixture was left at RT for 15 minutes while DMEM on cells was exchanged for DMEM without FBS and Pen/Strep. 4 hours after transfection, medium was exchanged for complete media.

Dish size	DMEM	DNA	1x PBS	25x PEI	1x PBS
10 cm	5 ml	5 µg	250 µl	10 µl	240 µl
15 cm	10 ml	10 µg	500 µl	20 µl	480 µl

Table 2 Plasmid transfection using PEI

2.3.3 Cycloheximide Chases, Proteasome Inhibitor And p97 Inhibitor

Cells were seeded in dishes of interest. If desired, protein depletions were performed. At the time of interest, translational elongation and thus protein biosynthesis was inhibited by adding 50-100 µg/ml cycloheximide (Sigma) to the cells for the indicated times. Proteasome inhibitor MG132 (Sigma) was used at a final concentration of 10 µM for the indicated time. The allosteric p97 inhibitor NMS-873 (Sigma) was used at 10 µg/ml for at least 2 hrs. After the treatments, cells were collected and processed for protein analysis (Chapter 2.4).

2.4 Analysis Of Proteins

2.4.1 Preparation Of Cell Lysates

Cell pellets were lysed using radioimmunoprecipitation assay (RIPA) buffer (25 mM Tris HCl, pH 7.4, 150 mM NaCl, 0.1% SDS, 0.5% sodium deoxycholate, 1% Triton X-100) for whole cell extracts (WCEs). Lysis buffer was freshly supplemented with all inhibitors to inhibit proteases, phosphatases and deubiquitination enzymes (Table 3). Cell lysates were rotated at 10 rpm on a tube rotator (Stuart) for 20 min at 4°C before being sonicated using the Bioruptor (Diagenode) at high intensity for 30 sec on, 30 sec off to shread the DNA. Lysate was then centrifuged at 21000 rcf for 15 min at 4°C and supernatant was collected for further analysis.

If specific subcellular fractions were required for the experiment, cells were fractionated as described in (Méndez and Stillman, 2000). In short, cytoplasmic fraction was isolated by resuspending cells using buffer A (10 mM HEPES, 10 mM KCl, 1.5 mM $MgCl_2$, 0.34 M Sucrose, 10% Glycerol) supplemented with inhibitors (Table 3). 0.1% Triton X-100 was freshly added and cells were rotated at 10 rpm for 20 min at 4°C. Cells were then centrifuged at 1300 rcf for 4 min at 4°C. The supernatant containing the cytoplasmic proteins was collected. The pellet containing the nuclei was washed 2x with buffer A without Trition X-100 and centrifuged as mentioned. Nuclei were then lysed using lysis buffer (150 mM NaCl, 1.5 mM EDTA, 50 mM Tris HCl, pH 7.4) including inhibitors for 20 min while rotating at 10 rpm at 4°C. Lysate was centrifuged at 1500 rcf for 4 min and supernatant containing nuclear proteins was collected. DNA in the pellet was then washed 1x with Benzonase buffer (20 mM Tris HCl, pH 8.0, 20 mM NaCl, 2 mM $MgCl_2$) and digested using Benzonase buffer containing 500 U/ml of Benzonase while rotating at 10 rpm for 30 min at RT. Samples were then centrifuged at full speed for 20 min at 4°C and supernatant was pooled with the nuclear protein-containing supernatant to obtain nuclear lysates.

Protein concentrations were measured using the RC DC Protein Assay kit from BioRad.

Name of Compound	Working Concentration	Inhibitor Type
Leupeptin	10 µg / ml	Protease Inhibitor
Pepstatin	10 µg / ml	Protease Inhibitor
Chymostatin	10 µg / ml	Protease Inhibitor
PMSF	1 mM	Protease Inhibitor
Aproptinin	10 µg / ml	Protease Inhibitor
NEM	20 mM	DUB inhibitor
Sodium Fluoride	20 mM	Phosphatase Inhibitor
Sodium Orhovanadate	2.5 mM	Phosphatase Inhibitor
Sodium Pyrophosphate	4 mM	Phosphatase Inhibitor

Table 3 List of inhibitors

2.4.2 SDS-Polyacrylamide Gel Electrophoresis (PAGE)

Homemade gels of a specific percentage or gradient 5-18% gels were casted using the mini-PROTEAN tetra hand cast system from BioRad. The protocol for preparation of running and stacking gels is given in Table 4. Protein samples were loaded in a range of 10 – 30 µg diluted in 1x LB. The volume of the samples was adjusted to 30 µl using ddH_2O. Samples were boiled at 95°C for 5 min in a heat block (Labnet) and spun down with a tabletop centrifuge for a few seconds prior to loading. 2 µl of precision plus protein standards (BioRad) was used to indicate protein size. Electrophoresis was performed by applying 10 mA per gel for stacking and 20 mA for separation of bands in 1x running buffer (Chapter 2.1.4).

Ingredient	Stacking Gel (1.5 ml)	Running Gel (10%; 12 ml)
ddH_2O	1.22 ml	4.93 ml
4x Buffer*	0.5 ml	3.00 ml
30% Acrylamide	0.27 ml	4.00 ml
10% APS	10 µl	60 µl
TEMED	2 µl	8 µl
* 4x Stacking buffer: 0.5 M Tris base, 0.4% SDS, pH 6.8		
* 4x Running Buffer: 1.5 M Tris base, 0.4% SDS, pH 8.8		

Table 4 Protocol for running and stacking gels

2.4.3 Western Blotting

PVDF membranes (BioRad) were activated by incubation in 100% methanol for 10 sec and equilibrated in 1x transfer buffer (Chapter 2.1.5) while shaking for 5 min. Sponges, 3MM paper and gels were also equilibrated in transfer buffer and then assembled into the transfer cassettes and apparatus. Transfer tanks were filled with ice-cold transfer buffer and supplemented with a cooling unit. Transfer was performed at 100 V for 75 min.

Membranes were washed with 1x TBST (0.1%) and blocked for 1 hr with 5% milk in 1x TBST (0.1%) at RT. Antibodies were diluted in 5% BSA in 1x TBST (0.1%) and membranes were incubated over night at 4°C while rolling (Stuart). The next day, membranes were washed 3x 10 min with 1x TBST (0.1%) at RT before incubation with HRP-conjugated secondary antibodies diluted in 2.5% milk in 1x TBST (0.1%) for 1 h at RT. Membranes were washed again 3x 10 min with 1x TBST (0.1%) at RT before activation using Clarity Western ECL (BioRad) for 5 min. Signal detection was performed using the ChemiDoc MP system (BioRad). The list of antibodies used for western blotting is shown in Table 5.

Non-commercial antibodies were all produced in the laboratory of Raimundo Freire, Unidad de Investigacion, Tenerife, Spain. K48- and K63-linked ubiquitin chains were obtained from Enzo.

Protein	**Working Dilution**	**Source**
Vinculin	1:1000	Abcam
Ataxin-3	1:1000	Non-commercial
RNF8	1:1000	Non-commercial
RNF168	1:6000	Non-commercial
Ku80	1:1000	Abcam
Ku70	1:1000	Sigma
Flag	1:5000	Sigma
GFP	1:10'000	Abcam
Myc	1:5000	Cell Signaling
p97	1:1000	Non-commercial
Proteasomal subunit α6	1:1000	Enzo
UBE4A	1:1000	Santa Cruz
UBE4B	1:1000	Abcam
K48-linked Ub chains	1:10,000	Genetech
K63-linked Ub chains	1:10'000	Genetech
PCNA	1:1000	Abcam
αTubulin	1:2000	Abcam
Mouse-HRP	1:50'000	Sigma
Rabbit-HRP	1:50'000	Sigma

Table 5 List of antibodies used for Western blotting

2.5 DNA Damage Induction

2.5.1 Preparation Of Cells For And Performance Of UV-A Laser Damage Induction

During the time of this thesis, two different systems of UV-A laser were used. For the UBE4A and UBE4B part (Chapter 3), the MMI CellCut Plus was used. The 355 nm laser source was connected to an Olympus IX71 and focused through a 40x objective. Settings used on that instrument were as follows: Velocity: 50%, Focus: 47.2%, Power: 55.1%. Cells were seeded onto 10 mm cover glasses No.1 (VWR) and pre-sensitised to UV-A laser exposure by supplementing the media with 10 µM BrdU 24 hrs prior to the experiment. Cover glasses were transferred to LabTek chambers for the duration of laser exposure and allowed to recover for the indicated times in the incubator.

For the ATXN3 part (Chapter 4-6), cells were lasered using the in-house built UV laser system. It contains a UVA (355 nm) light source that is focused through a slit aperture, leading to a laser line width of ~400 nm. The source releases the light in pulses, and each pulse lasts about 5 ns and can irradiate several cells as the slit focuses the light to a line. The pulses are added manually by pressing a button for each pulse. The energy of the light can be measured at the source and filters (OD1, OD2) on the light path allows for further adjustment of the energy. The laser is connected to a Nikon TE2000 and optimised for use with a 10x objective. The stage is moved in between each pulse by an adjustable width. For this system, cells were seeded onto 10 mm No. 1 cover glasses (VWR) and protein depletion was performed as mentioned in chapter 2.3.1. To sensitise cells, 10 µg/ml Hoechst 33258 (Sigma) was added to the media 30 min prior to lasering. Cover slips were then transferred into in-house made glass-bottom

dishes containing complete media. Laser pulses were released onto the cells, applying 300 mV initial energy, using an OD1 filter, leading to a final 30 mV source energy. Between each pulse, the stage holding the dish was moved 25 µm. For recovery, cover glasses were transferred into 12-well plates containing complete media and stored back into the incubator.

2.5.2 Ionising Radiation (IR)

Cells were exposed to the indicated Gray (Gy) of IR using a ^{137}Caesium source (Gamma-Service Medical GmbH) at a dose rate of 1.3 Gy/min. Cells were left to recover in the incubator for indicated time.

2.6 Colony Forming Assay

HeLa cells were seeded at appropriate concentrations and the next day, cells were transfected as described in chapter 2.3.1. After two days of siRNA treatment the cells were trypsinised and cells were seeded against different dose of IR (0, 1, 2, 4 Gy) for each condition (see Table 6). After 6-8 hrs of recovery the cells were exposed to a different dose of IR and incubated for 8 days to form colonies. At the end of the 8th day, the colonies (around 50 cells per colony) were fixed and stained with crystal violet solution (Sigma) for 20 min. The staining solution was washed with normal water under the running tap and plates were left to air dry. The number of formed colonies was counted manually.

	0 Gy (1x)	1 Gy (1.666x)	2 Gy (2x)	4 Gy (5.333x)
siLuc	150	250	300	800
sip97	10,000	16,660	20,000	53,330
siATXN3_6	800	1,328	1,600	4,264
siATXN3_7	800	1,328	1,600	4,264

Table 6 Number of HeLa cells seeded for colony forming assay

2.7 Immunofluorescence (IF)

Cells were seeded onto 10 mm No. 1 cover glasses (VWR). At the desired time point, cover glasses were transferred to 12-well plates (Greiner) and washed once with 1x PBS. Cells were then either pre-extracted (25 mM HEPES pH 7.4, 50 mM NaCl, 1 mM EDTA, 3 mM $MgCl_2$, 300 mM Sucrose, 0.5% Triton X-100, Inhibitors) for 5 min on ice followed by two washes with 1x PBS or instantly fixed with 4% formaldehyde in 1x PBS for 20 min at RT. Cells were then permeabilised using 0.5% Triton X-100 in 1x PBS for 5 min at RT and blocked with 5% BSA in 1x PBS over night at 4°C. The next day, cells were washed once with 1x PBS. Cover glasses were then transferred to a wet chamber, where 20 µl drops of antibody dilutions were dropped onto parafilm, with the cells facing towards the antibody dilutions. Antibodies were diluted in 2.5% BSA in 1x PBS at specific dilutions (see Table 7). Each antibody was incubated separately for 1 hr at RT. In between each antibody, cover glasses were transferred back into the 12-well plates and cells were washed three times with 1x PBS. After the last antibody incubation, cells were incubated with 1x PBS containing DAPI (1 µg/ml) for 20 min at RT and washed once again with 1x PBS. Cover glasses were then dipped into ddH_2O, dried on a tissue and mounted onto microscope slides (Thermo Scientific) with FluoroMount-G hard mounting medium (Interchim).

Antibody	Dilution	Source
yH2AX (Mouse)	1:500	Millipore
yH2AX (Rabbit)	1:500	Novus Biologicals
53BP1	1:500	Santa Cruz
Ataxin-3	1:100	Non-commercial
RNF8	1:200	Non-commercial
RNF168	1:1000	Non-commercial
p97	1:200	Proteintech
BRCA1	1:500	Santa Cruz
K48-linked Ub chains	1:1000	Genetech
K63-linked Ub chains	1:1000	Genetech
FK2 total ubiquitin	1:500	Biomol
Alexa Fluor 488 donkey anti-mouse	1:500	Invitrogen
Alexa Fluor 488 donkey anti-rabbit	1:500	Invitrogen
Alexa Fluor 594 donkey anti-mouse	1:500	Invitrogen
Alexa Fluor 594 donkey anti-rabbit	1:500	Invitrogen
Dylight 488 goat anti-human	1:100	Jackson Immuno Research Laboratories

Table 7 List of antibodies used for immunofluorescence

2.7.1 Immunofluorescence Microscopy And Image Quantifications

Images of the immunolabelled cells were taken using a Nikon 90i epifluorescent microscope equipped with a Nikon DS-Qi1Mc digital microscope camera. Images were captured using a 60x objective and images were exported as tifs. Image analysis was performed using ImageJ. For laser line analysis, intensity at the site of DNA damage was analysed by circling the γH2AX signal and measuring the intensity of the protein of interest at this area. From the same nucleus, a measurement of the background signal was also taken and subtracted from the

intensity of the damage area. All measurements were normalised to a specific time point in siLuc treated cells to compare between the different experiments.

2.8 Protein Co-Immunoprecipitations (Co-IPs)

HEK293T cells were transfected with the plasmids of interest as described in chapter 2.3.2. After treatment of interest, cells were collected by trypsinisation. Cells were centrifuged at 700 rcf for 5 min at 4°C and pellets were washed twice with 1x PBS by repeating the centrifugation step. Cells were lysed using IP lysis buffer (50 mM Tris HCl pH 7.4, 150 mM NaCl, 1 mM EDTA, 0.5-1% Triton X-100, Inhibitors) for 20 min at 4°C, while rotating the tubes at 15 rpm. Lysates were centrifuged at 21,000 rcf for 15 min at 4°C and the supernatant was removed and stored on ice. The pellets were washed once with Benzonase buffer (2 mM $MgCl_2$, 50 mM Tris HCl pH 8.0, 20 mM NaCl, Inhibitors) and centrifuged at 700 rcf for 5 min at 4°C. Next, pellets were incubated in Benzonase buffer containing Benzonase (500 U/ml) at 4°C for 1 hr or until the pellets were digested, while rotating at 15 rpm. Meanwhile, beads of interest were prepared by washing the desired amount of beads three times with their specific washing buffer (see Table 8). Digested pellets were spun down again at 21'000 rcf and supernatant was collected and added to the IP lysates. 10% of lysate was kept as input and 90% of lysate was loaded onto beads and capturing was performed according to instructions of the manufacture (see Table 8) at 4°C rotating at 15 rpm. Beads and lysates were centrifuged at 50 rcf and supernatant was removed. Beads were washed 3-5x with the indicated washing buffer and centrifugation at 50 rcf. Proteins were eluted by addition of 2x LB and boiling for 5-10 min at 95°C. Elutions were analysed by Western blotting.

Bead	Washing Buffer	Capturing	Source
GFP	150 mM NaCl 50 mM Tris HCl pH 7.4	1 h	Chromotek
Flag	150 mM NaCl 50 mM Tris HCl pH 7.4	2 h	Sigma
Strep-Tactin Sepharose	150 mM NaCl 50 mM Tris HCl pH 8	2-4 h	IBA

Table 8 IP beads used and their washing buffers

2.9 Stable Isotope Labeling With Amino Acids In Cell Culture (SILAC) Mass Spectrometry

HEK293T Flip/In cells were used to mildly express the p97 ATPase-deficient substrate-trapping mutant $E^{578}Q$ (EQ) (Meerang et al., 2011) tagged at the N-terminus with myc and Strep. The EQ mutant was used in Mass Spectrometry experiments to stabilise transient interactions between p97 and p97-substrates.

When not for SILAC experiment, cells were maintained in DMEM supplemented with 10% FCS, 1% pen/strep, 10 µg/ml Blasticidin and 50 µg/ml Hygromycin.

For triplex-SILAC labelling, three cultures of cells were grown in parallel in DMEM media containing three different isotopes of arginine and lysine: R0K0 ("light"), R6K4 ("medium") or R10K8 ("heavy"), respectively, dialysed FCS MWCO 10 kDa (Dundee Cell) and appropriate antibiotics. Cells were grown until a cell number of approx. $8x10^8$ was reached.

Cells were then exposed to the desired amount of IR and allowed to recover for the necessary time in the incubator. Cells were collected and fractionated as described in chapter 2.4.1. Co-IP was performed as described in section 5.7 using Strep-Tactin Sepharose. Elution was performed with 2.5 mM biotin in three sequential extractions that were pooled at the end.

Trypsin in-solution digestion was performed to each IP elute. Mass spectrometry analysis was performed by the group of Benedikt Kessler, Target Discovery Institute, Oxford.

The set of MS/MS raw data was searched against a UniProt/SwissProt database using Proteome Discoverer. The parameters for data search included standard peptide filtering for SILAC experiments

SILAC ratios representing particular protein enrichments in p97 complexes at times 30 min and at time 8h after IR were calculated by Proteome Discoverer software (Thermo) comparing peptides from each particular protein at the given time point, with peptides of the same time point without irradiation.

2.10 Plasmid Manipulation And Cloning

Plasmids used and/or generated during this study are summarised in Table 9.

Plasmid Name	Source
pFLAG-6A-ATX3Q_22(Wt)	AddGene
pFLAG-6A-ATX3Q_22-C14A	AddGene
pFLAG-6A-ATX3Q_22-UIM*	AddGene
pFLAG-6A-ATX3Q_80 (polyQ)	AddGene
pFLAG-6A-ATX3Q_22-VIM*	Mutagenesis
pFLAG-6A-ATX3Q_22 UbS1	Mutagenesis
pFLAG-6A-ATX3Q_22 UbS2	Mutagenesis
pcDNA5/FRT/TO nEGFP ATXN3Q_22 (Wt)	Sub-Cloning
pcDNA 3.1 myc-strep-p97	Our laboratory
pcDNA4/TO FLAG RNF8	Our laboratory
pcDNA 3.1 Flag RNF168	Our laboratory
pcDNA 3.1 Flag-KU80	Our laboratory

Table 9 List of plasmids used

2.10.1 Transformation Of Bacteria

DH5α competent *Escherichia coli* aliquots, stored at -80°C, were thawed slowly on ice. 1 µg of plasmid was mixed with 50 µl of bacteria slurry and incubated for 30 min on ice. Heat-shock was applied by incubating the bacteria/DNA mixture in a 42°C water bath for 90 s before being instantly re-transferred onto ice for an additional 2 min. Transformed bacteria were then shaken at 37°C at 250 rpm in a bacteria shaker (New Brunswick Scientific) for 1 hr. Transformed and recovered bacteria were then plated onto agar plates (Sigma) containing the necessary antibiotics and were allowed to form colonies over night at 37°C in a bacterial incubator (Binder). Single colonies were picked for further amplification in 5 ml of LB (Luria-Broth, Sigma) medium, containing antibiotics, shaking at 250 rpm in a bacteria shaker over night.

2.10.2 Mini/Maxiprep Plasmid Purification

Plasmid purification was performed according to the instructions of the manufacturer (QIAGEN). In short, after overnight amplification, bacteria were centrifuged down at 4000 rcf for 10 min at RT, resuspended in 250 µl Buffer P1 (50 mM Tris HCl, pH 8.0, 10 mM EDTA, RNase A, 100 µg/ml final concentration,) and transferred into a 1.5 ml eppendorf tube. Bacteria were then lysed by adding 250 µl buffer P2 (200 mM NaOH, 1% SDS) and gentle mixing by tube inversion for 5 min at RT, followed by neutralisation by addition of buffer N3 (4.2 M Gu-HCl, 0.9 M potassium acetate, pH 4.8) again by gently mixing the solutions. Genomic DNA and cell debris were then pelleted by centrifugation at 17,900 rcf for 10 min and the supernatant was loaded onto a QIAprep spin column. DNA was bound to the membrane by centrifugation for 1 min and the columns were

washed with 750 µl PE buffer (10 mM Tris HCl, pH 7.5, 80% ethanol) and centrifugation. After an additional drying centrifugation step, DNA was eluted by using 30-50 µl EB buffer (10 mM Tis HCl, pH 8.5) incubating for 1-10 min followed by centrifugation for 1 min at 17,900 rcf. Purity and amount of eluted DNA was assessed using Nanodrop 1000 (Thermoscientific) and plasmids were stored at -20°C. Sequencing was performed to exclude the possibility of spontaneous mutation of the encoded gene during amplification.

For purification of larger amounts of DNA, a MaxiPrep kit from QIAGEN was used following the instructions of the manufacturer. In short, 200 ml of over night bacteria culture was pelleted and resuspended in 10 ml P1, followed by lysis with 10 ml P2 and neutralisation with buffer P3 (3 M potassium acetate, pH 5.5). Lysates were centrifuged at 6000 rcf for 15 min at RT and supernatant was loaded onto a QIAGEN-tip 500, pre-equilibrated with 10 ml QBT buffer (750 mM NaCl, 50 mM MOPS, pH 7.0, 15% ispropanol, 0.15% Triton X-100) and allowed to drain before being washed 2x with 30 ml buffer QC (1 M NaCl, 50 mM MOPS, pH 7.0, 15% isopropanol). DNA was eluted in 15 ml of high-salt buffer QF (1.25 M NaCl, 50 mM Tris HCl, pH 8.5, 15% isopropanol) and precipitated with 10.5 ml 100% isopropanol and centrifugation at 6000 rcf for 20 min at 4°C. Supernatant was removed and DNA was washed with 70% ethanol followed by another centrifugation at 6000 rcf for 20 min at 4°C. DNA was air-dried and resuspended in 200-1000 µl TE buffer (10 mM Tris HCl, pH 8, 1 mM EDTA). Plasmid quality was assessed as for minipreps.

2.10.3 Site-Directed Mutagenesis

A list of primers can be found in Table 11. The following mix was set up for site-directed mutagenesis:

Primer Fw:	1 µl [10 µM]
Primer Rv:	1 µl [10 µM]
10x PFX Buffer:	2.5 µl
Polymerase PFX:	0.25 µl
Template:	2 µl [10 ng/µl]
ddH_2O:	18.25 µl
Total:	25 µl

PCR settings:

1)	95°C	4 min
2)	95°C	30 sec
3)	Tm_{Primer} - 4°C	30 sec
4)	68°C	6 min
5)	68°C	10 min
6)	4°C	∞

Steps 2-4 were repeated for 25 cycles.

PCR templates were Dpn1 digested: 0.5 µl Dpn1 per 25 µl reaction at 37°C for 1 h

After digestion, the PCR products were transformed into DH5α and plated on agar plates and incubated overnight at 37°C. Single colonies were picked the following day, amplified in 5 ml LB media for 16 h at 37°C shaking. The plasmids were purified using MiniPrep and sent for sequencing (Source Bioscience).

2.10.4 Sub-Cloning

The ATXN3 WT construct was subcloned into pcDNA5/FRT/TO nEGFP (Invitrogen). Therefore, the ATXN3 cDNA was amplified using forward and reverse primers containing a BamH1 (Fw) or Xho1 (Rv) restriction sites, respectively.

Mix set-up:

Fw primer [10 µM]	2 µl
Rv primer [10 µM]	2 µl
Polymerase PFX (Invitrogen; 2.5 kU/ml)	0.4 µl
10x PFX buffer	5 µl
Flag-ATXN3 plasmid [130 ng/µl]	0.8 µl
ddH_2O	40.6 µl
Total	50 µl

PCR settings:

1)	95°C	4 min
2)	95°C	30 sec
3)	Tm_{Primer} - 4°C	30 sec
4)	68°C	90 sec
5)	68°C	10 min
6)	4°C	∞

Steps 2-4 were repeated for 35 cycles.

PCR products were run on an 0.8% agarose gel (Ladder: 1kb NEB) to clean up the reaction mix. Insert bands were cut out and purified using the QIAquick Gel Extraction kit (QIAGEN). In short, the excised gel containing the insert of interest was weighed on a scale. The agarose was dissolved by addition of 3x the volume of solubilisation buffer and incubation at 50°C for 10 min. Afterwards, 1 volume of isopropanol was added. The resulting mixture was added into a provided 2 ml collection tube and centrifuged for 1 min at 18000 rcf. The DNA bound to the silica membrane was washed with 750 µl of wash buffer, followed by two centrifugation steps. DNA was eluted with 50 µl elution buffer (10 mM TrisHcl pH 8.5) and quantified using Nanodrop.

An over-night double digestion was performed at 37°C:

	Insert	pcDNA5/FRT/TO nEGFP
DNA	20 µl (5 µg)	6.2 µl [4 µg/µl]
CutSMART 10x buffer	3 µl	3 µl
BamH1 (NEB; 20 kU/ml)	1 µl	1 µl

Xho1 (NEB; 20 kU/ml)	1 µl	1 µl
ddH_2O	5 µl	18.8 µl
Total	30 µl	30 µl

Table 10 Set-up of over-night double digestion of insert and plasmid for sub-cloning of ATXN3

The following day, the products were again run on an 0.8% agarose gel and bands of interest were cut out and purified with the QIAquick Gel Extraction kit (QIAGEN). A ligation reaction was set up as follows and incubated for 1 hr at 37°C:

pcDNA5/FRT/TO nEGFP	10 µl [90 ng/µl]
Digested insert	5 µl [175 ng/µl]
T4 10x buffer	2 µl
T4 ligase (NEB; 400 kU/ml)	1 µl
ddH_2O	2 µl
Total	20 µl

Ligation products were transformed into DH5α competent *E. Coli* as described in section 2.10.1 and plated on agar plates. Single colonies were amplified and plasmids were purified. Correct subcloning was verified by sequencing.

Primer Name	Sequence	Tm [°C]
ATX3_SIM_162IFVVK_AFAAK_Fw	CGCAATCTGGCAGATCACCCTTAGCGGCAAATGCAGAA TAACCTTCCTGTTGTAATTGA	67
ATX3_SIM_162IFVVK_AFAAK_Rv	TCAATTACAACAGGAAGGTTATTCTGCATTTGCCGCTA AGGGTGATCTGCCAGATTGCG	67
ATXN3_STOP1_185aa_FW	TTTGGTCGATGCATCTATTGGACCCTAATCATCTGC	59
ATXN3_STOP1_185aa_RV	GCAGATGATTAGGGTCCAATAGATGCATCGACCAAA	59
ATXN3_STOP2_290aa_FW	TGCTTTTGCTGCTGTTTTTAAAAGTAGGCTTCTCGTCTC	59
ATXN3_STOP2_290aa_RV	GAGACGAGAAGCCTACTTTTAAAAACAGCAGCAAAAGC A	59
ATXN3_UBS2W87A_FW	GCAATGCCTTGAAAGTTGCGGGTTTAGAACTAA TCCTGTC	61
ATXN3_UBS2W87A_RV	GACAGGATTAGTTCTAAACCCGCAACTTTCAAGGCATT GC	61
ATXN3_UBS1IQ78AQ_FW	GACAGTGGTTTTTTCTCTGCTCAGGTTATAAGCAATGC CTTG	61
ATXN3_UBS1IQ78AQ_RV	CAAGGCATTGCTTATAACCTGAGCAGAGAAAAAACCAC TGTC	61
ATXN3_UBS1AQ78AA_FW	GACAGTGGTTTTTTCTCTGCTGCGGTTATAAGCAATGC CTTG	62
ATXN3_UBS1AQ78AA_RV	CAAGGCATTGCTTATAACCGCAGCAGAGAAAAAACCAC TGTC	62
ATXN3_VBMRKRR285AKAR_FW	AAAGTAGGCTTCTCGTGCCTTCGCAAGCTCTTCTGAAG TAAGATTTGTACCTGAT	66
ATXN3_VBMRKRR285AKAR_RV	ATCAGGTACAAATCTTACTTCAGAAGAGCTTGCGAAGG CACGAGAAGCCTACTTT	66
ATXN3_VBMAKAR285AAAA_FW	CTTCAGAAGAGCTTGCGGCGGCAGCAGAAGCCTACTTT GAAAAAC	66
ATXN3_VBMAKAR285AAAA_RV	GTTTTTCAAAGTAGGCTTCTGCTGCCGCCGCAAGCTCTT CTGAAG	66
ATX3_NFlag3_fw	ATATGGATCCATGGAGTCCATCTTCCACGAG	56
ATX3_NFlag3_rv	ATATCTCGAGTTATTTTTTTCCTTCTGTTTTCAAATCAT TTCTG	56

Table 11 List of primers

2.11 Statistical Analysis

Statistical analysis was performed using the GraphPad Prism software. Unpaired *t*-test was performed unless mentioned otherwise. P values refer to: < 0.0001***, < 0.001** < 0.05*, > 0.05 ns.

3 RESULTS 1: UBE4A AND UBE4B: TWO NOVEL E3-UBIQUITIN LIGASES IN DSB REPAIR

The laboratory of Yosef Shiloh, Tel Aviv University, has performed a functional screen in search of novel DDR players. One of their hits was UBE4B (Ufd2a), the human orthologue of the yeast ubiquitin E3/E4 ligase Ufd2 (see Chapter 1.4.2). UBE4B, as well as its orthologue UBE4A (Ufd2b) are poorly characterised proteins in the mammalian system. Nevertheless, both proteins have been suggested to be tumor suppressors in neuroblastomas (Caren et al., 2006). Therefore, even though only UBE4B was identified in the screen, they decided to investigate both orthologues for a possible role in the DDR.

Experiments performed by the Shiloh laboratory (personal communication) revealed, that cells depleted for UBE4A or UBE4B were hypersensitive to the IR mimicking drug Neocarzinostatin (NCS), which was a first indication that these two orthologues play a role in the repair of DSBs. Additional experiments showed that both proteins are important for accurate 53BP1 foci formation and resolution, further underlining their involvement in the repair of DSBs. UBE4A depleted cells displayed an increased number of unresolved 53BP1 foci 24 hrs post IR exposure, indicating that those cells have a defect in DSB repair. UBE4B depleted cells exhibited increased numbers of 53BP1 IRIFs at 4 and 8 hrs of recovery compared to control cells but at 24 hrs of recovery they managed to resolve the 53BP1 foci. Analysing the efficiency of the two main DSB repair pathways, HR and NHEJ, by GFP-reporter assays revealed that absence of either ubiquitin ligase negatively affected both repair pathways. Finally, both proteins were found physically at the site of DNA damage, as visualised by

immunofluorescence experiments. Overall, their data strongly imply that both UBE4A and UBE4B are new players involved in DSB repair. Considering the different 53BP1 kinetics displayed by either depletion, it appears that the two orthologues play different roles in the DDR. As the two proteins are putative ubiquitin E3/E4 ligases, it was intriguing to hypothesise that they are involved in the regulation of ubiquitination at sites of DNA damage.

UBE4A and UBE4B are cofactors of p97 (Chapter 1.3.2) and p97 plays an essential role in DSB repair (Meerang et al., 2011). Therefore, we did a collaborative project with the Shiloh group, with the ultimate goal being to better understand how the p97 system regulates ubiquitination at sites of DNA damage.

3.1 UBE4A Helps To Maintain K63-Linked Ubiquitin Chains

DSB repair is a highly regulated process and ubiquitination plays an essential role in its orchestration. As the yeast homolog of UBE4A, Ufd2, is the prototype of an ubiquitin E4 enzyme, it is an interesting hypothesis that UBE4A could be a new ubiquitin E3/E4 enzyme in the DDR, thus actively affecting the ubiquitination at the site of DSBs. To test this idea, we decided to investigate the ubiquitination pattern at the site of UV-A (355 nm) micro-beam irradiation ("laser technique") induced DNA damage in great detail by analysing the pattern of both K48- and K63-linked ubiquitin chains by immunofluorescence (IF). To this end, specific linkage antibodies were used (Meerang et al., 2011; Newton et al., 2008). To verify their specificity, Western blot analysis was performed, detecting pure, commercially-available ubiquitin chains that are either K48- or K63-linked (Fig 3.1A). Indeed, the antibodies detect specifically their target.

U2OS cells, depleted for either UBE4A or p97, were fixed either 15 min or 2 hrs after laser damage induction. p97 depletion served as a positive control, as it has been shown previously that its depletion leads to hyperaccumulation of ubiquitination at the sites of DNA damage (Meerang et al., 2011). Depletion efficiency was assessed by Western blotting, and a representative blot is shown in Fig 3.1B.

Quantification of the signal intensity of the K63-ubiquitin specific antibody at the site of DNA damage (as indicated by γH2AX) showed that absence of UBE4A at either of the analysed time points resulted in strong reduction of K63-linked ubiquitin chains (Fig 3.2A and C). Specifically, after 15 min of recovery, the intensity was reduced by approximately 50% compared to control depleted cells (siLuc). While control cells displayed an overall increase of around 40% in signal intensity at the 2 hrs compared to 15 min time point, UBE4A depleted cells did not exhibit an increase in signal intensity over time, but remained approximately the same as at 15 min of recovery.

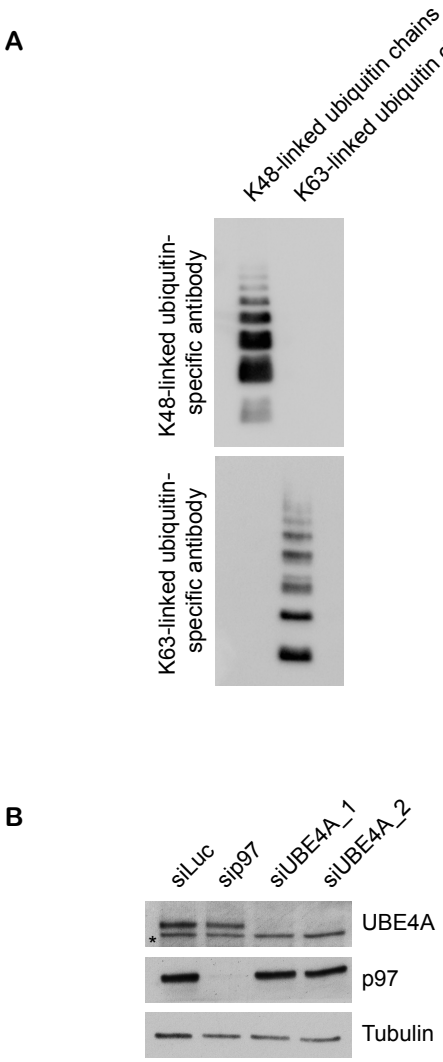


Figure 3-1. Representative control Western blots. A: Specificity of K48- and K63-ubiquitin linkage antibodies. 10 µg of indicated ubiquitin chains was loaded on a SDS-gel and blotted. Linkage specific antibodies were used, detecting only their linkage specific chain type. B: Representative blot depicting siRNA mediated depletion efficiency for the indicated proteins after 72 hrs of depletion. Asterisk indicates an unspecific band detected by the UBE4A antibody.

In stark contrast, p97 depleted cells displayed a strong increase in K63-linked ubiquitin chain signal intensity at both time points (Fig 3.2A and C). At the early time point, those cells displayed an increase of around 160% compared to siLuc transfected cells. At the 2 hrs time point, the K63 signal slightly decreased by around 10%, which represented a 60% increase compared to the control cells at the same time point.

To exclude the possibility of an off-target effect of using a single UBE4A siRNA sequence, K63-ubiquitin signal intensity was analysed at the 2 hrs time point with a second siRNA sequence targeting UBE4A (siUBE4A_1). The initial sequence (siUBE4A_2) also reduced K63-linked ubiquitin chains strongly compared to control cells in these additional experiments. The second siRNA sequence yielded an average signal intensity reduction of 35%, supporting the initial results (Fig 3.2B).

Overall, analysis of the K63-linked ubiquitin chain signal showed that UBE4A is involved in the stabilisation and fine-tuning of this chain linkage type at the site of DSBs. Absence of UBE4A leads to a reduced intensity of K63-ubiquitin signal at the early time point and while this signal still increases until the 2 hrs time point in control cells, UBE4A depleted cells display an unchanged intensity at the later time point.

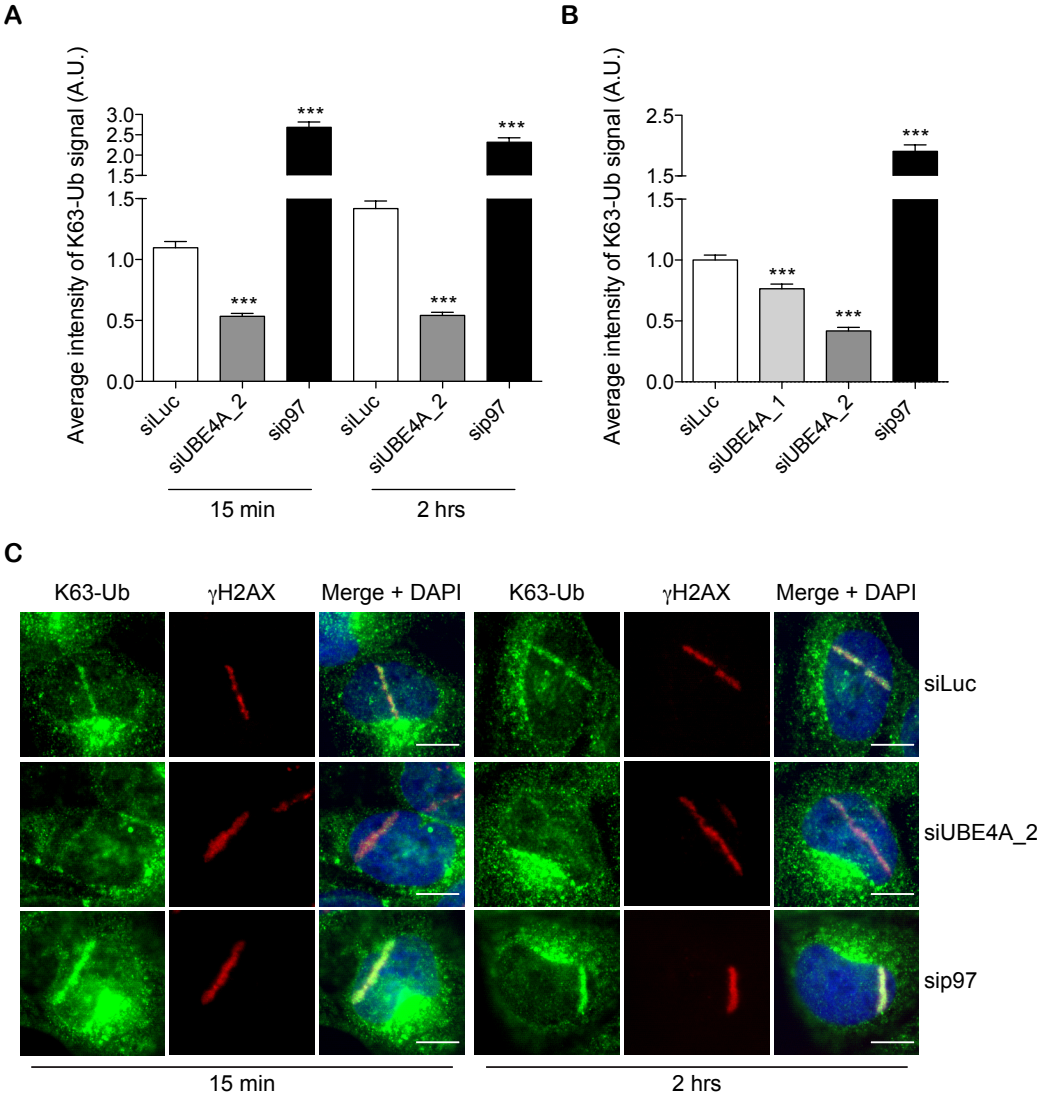


Figure 3-2. UBE4A helps to maintain K63-linked ubiquitin chains at the site of DNA damage. U2OS cells were depleted for indicated proteins for 72 hrs prior to UV-A laser damage induction. Cells were allowed to recover for the indicated time before K63-linked ubiquitin chains were detected using a specific K63-Ub antibody. Signal intensity was quantified at the site of DNA damage (γH2AX). A: Quantification results of the siUBE4A_2 sequence at both 15 min and 2 hrs of recovery. B: Same as A but including a second siUBE4A sequence. Only the 2 hrs time point was analysed with this sequence. C: Representative images for A for each condition. Statistics: unpaired *t*-test; P value < 0.0001*; mean + SEM; n = 3, > 100 laser lines were analysed per experiment and condition; Scale bar: 10 µm.**

3.2 UBE4A Regulates K48-Linked Ubiquitin Chains At Sites Of DSBs

In contrast to the K63-ubiquitin signal, which persists with similar intensity for a long period of time after DNA damage, the K48-ubiquitin signal rapidly vanishes from sites of DNA damage (Ramadan, 2012).

Analysing the laser samples immunolabelled for K48-linked ubiquitin chain signal showed indeed, that the K48-ubiquitin signal is rapidly formed after DNA damage (15 min after DNA damage induction), and almost completely abolished after 2 hrs of recovery time. Specifically, in siLuc control cells, the signal was reduced by about 80% at the 2 hrs when compared to 15 min. (Fig 3.3A and C). Depletion of UBE4A reduced the initial K48-ubiquitin chain signal by approximately 50% compared to siLuc treated cells. Similarly, after 2 hrs of recovery, UBE4A depleted cells displayed reduced K48-linked ubiquitin signal of approximately 50% compared to control cells at the same time point.

As expected, depletion of p97 yielded a hyperaccumulation of the K48-linked ubiquitin chain signal (Fig 3.3A and C). At the 15 min time point, the average intensity was about 200% increased compared to control cells. Although the average signal intensity decreased at the 2 hrs time point by about 50%, the average signal intensity was still increased by about 500% compared to control cells.

To gain further confidence, the experiments were partially repeated using the additional UBE4A siRNA sequence (siUBE4A_1) and were analysed at 15 min of recovery time after DNA damage (Fig 3.3B). Indeed, while the initial siUBE4A sequence, siUBE4A_2, reproducibly reduced the K48-Ub signal by around 50% compared to control cells, depletion with the second sequence yielded a reduction of K48-linked ubiquitin chain signal of about 35%.

Together, these results indicate that UBE4A regulates formation of K48-ubiquitin signal at sites of DNA damage.

Overall, our data demonstrate that UBE4A is a novel and important player in the DDR for proper formation and maintenance of both K63-ubiquitin chain signaling and K48-ubiquitin chain degradation pathways at the sites of DNA damage. UBE4A is mandatory for full formation of both K48- and K63-linked ubiquitin chains at early and late time points during DNA damage repair, supporting the hypothesis that UBE4A is a new ubiquitin ligase in the DNA damage response.

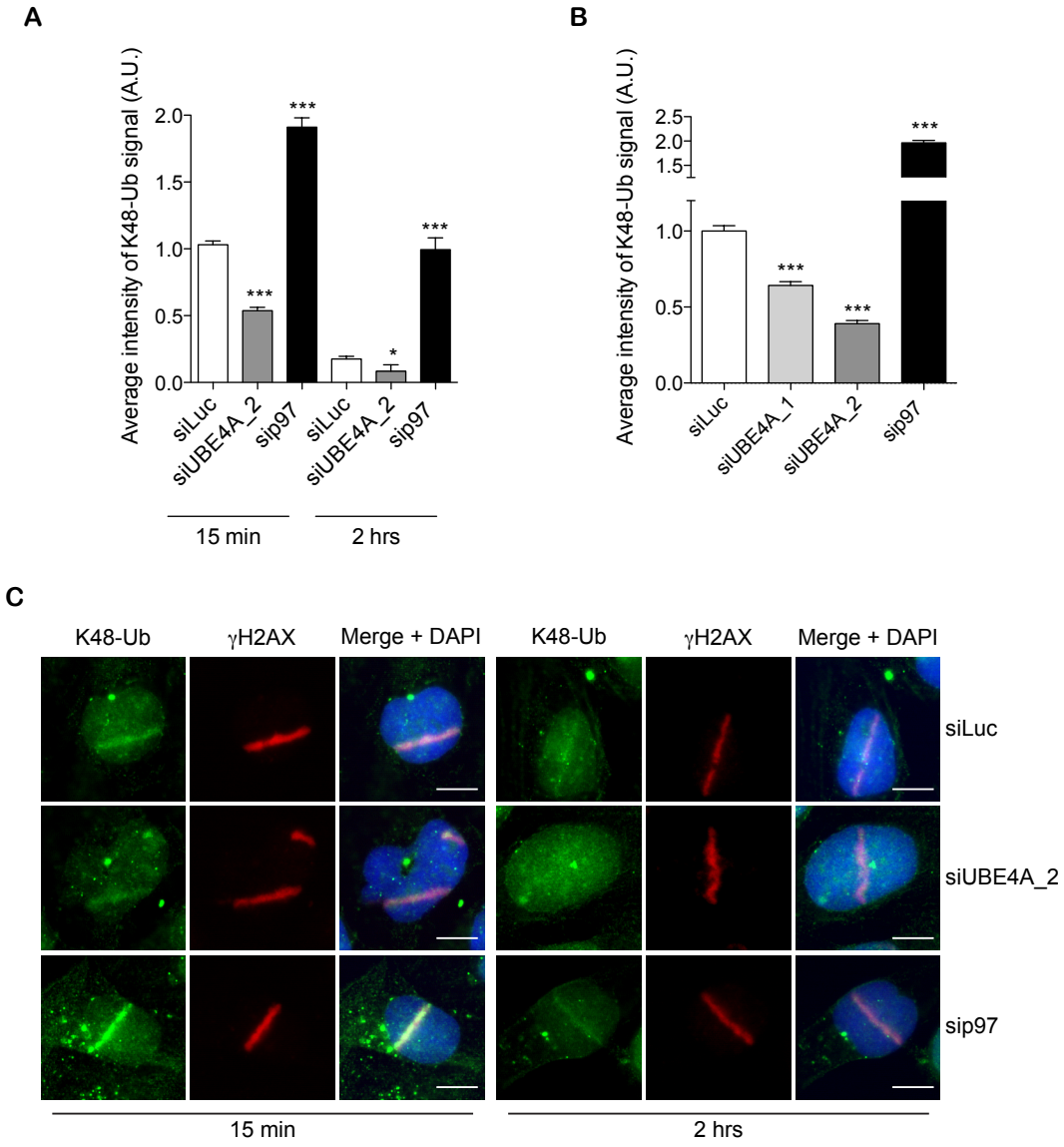


Figure 3-3. UBE4A helps to maintain K48-linked ubiquitin chains at the site of DNA damage. U2OS cells were depleted of the indicated proteins for 72 hrs prior to UV-A laser damage induction. Cells were allowed to recover for the stated time before K48-linked ubiquitin chains were detected using a specific K48-Ub antibody and signal intensity was quantified at the site of DNA damage (γH2AX). A: Quantification results of the siUBE4A_2 sequence at both 15 min and 2 hrs of recovery. B: Same as A but including a second siUBE4A sequence. Only the 15 min time point was quantified with this sequence. C: Representative images for A for each condition. Statistics: unpaired *t*-test; P value < 0.0001*, < 0.05*; mean + SEM; n = 3, > 100 laser lines were analysed per experiment and condition. Scale bar: 10 µm.**

3.3 UBE4B Helps To Fine-Tune The K48- And K63- Linked Ubiquitin Chains At The Site Of DNA Damage

Having observed that UBE4A plays such a strong role in the regulation of the ubiquitin signaling at the site of DNA damage, we were curious to understand if depletion of UBE4B displayed a similar behaviour.

Two different siRNAs were used against UBE4B (siUBE4B and siUBE4B_4). Again, p97 depletion served as a control for this set of experiments. Depletion efficiency was assessed by Western blotting, and a representative blot is depicted in Fig 3.4.

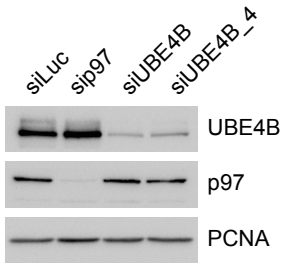


Figure 3-4. Representative Western blot for p97 and UBE4B depletion efficiency in U2OS cells. Cells were depleted for the indicated proteins for 72 hrs and then harvested. Western blotting was performed using the indicated antibodies. PCNA serves as a loading control.

3.4 Absence Of UBE4B Leads To Prolonged K48-Linked Ubiquitination

UBE4B depleted cells were left to recover 15 min or 2 hrs after UV-A irradiation and K48-linked ubiquitin chains were detected with the linkage specific antibody. Intensity of K48-ubiquitin was quantified at the site of DNA damage, as indicated by γH2AX signal. In contrast to UBE4A depletion, analysis of the 15 min time point in cells depleted for UBE4B did not reveal a difference in signal intensity compared to control depleted (siLuc) cells (Fig 3.5A and B). Even more strikingly, while the ubiquitin signal in siLuc transfected cells decreased by about 80% after 2 hrs of recovery, cells depleted for UBE4B with two different siRNA sequences displayed a much milder signal reduction of about 30% on average, representing a significant increase of K48-linked ubiquitin chains at the 2 hrs time point compared to control cells.

Depletion of p97 increased the initial signal by approximately 100% compared to siLuc transfected cells. After 2 hrs of recovery, the K48-linked ubiquitin chain signal intensity dropped by around 50%, which manifested in a signal increase of 500% compared to control cells, but which was similar to UBE4B depleted cells.

In summary, no effect on the K48-linked ubiquitin pattern could be observed 15 min after UV-A laser damage induction in cells lacking UBE4B. Interestingly, absence of UBE4B resulted in decreased removal of the K48-linked ubiquitin chains from the site of DSBs, which resembled the pattern of p97-depleted cells to a certain extent, especially at the 2 hrs time point.

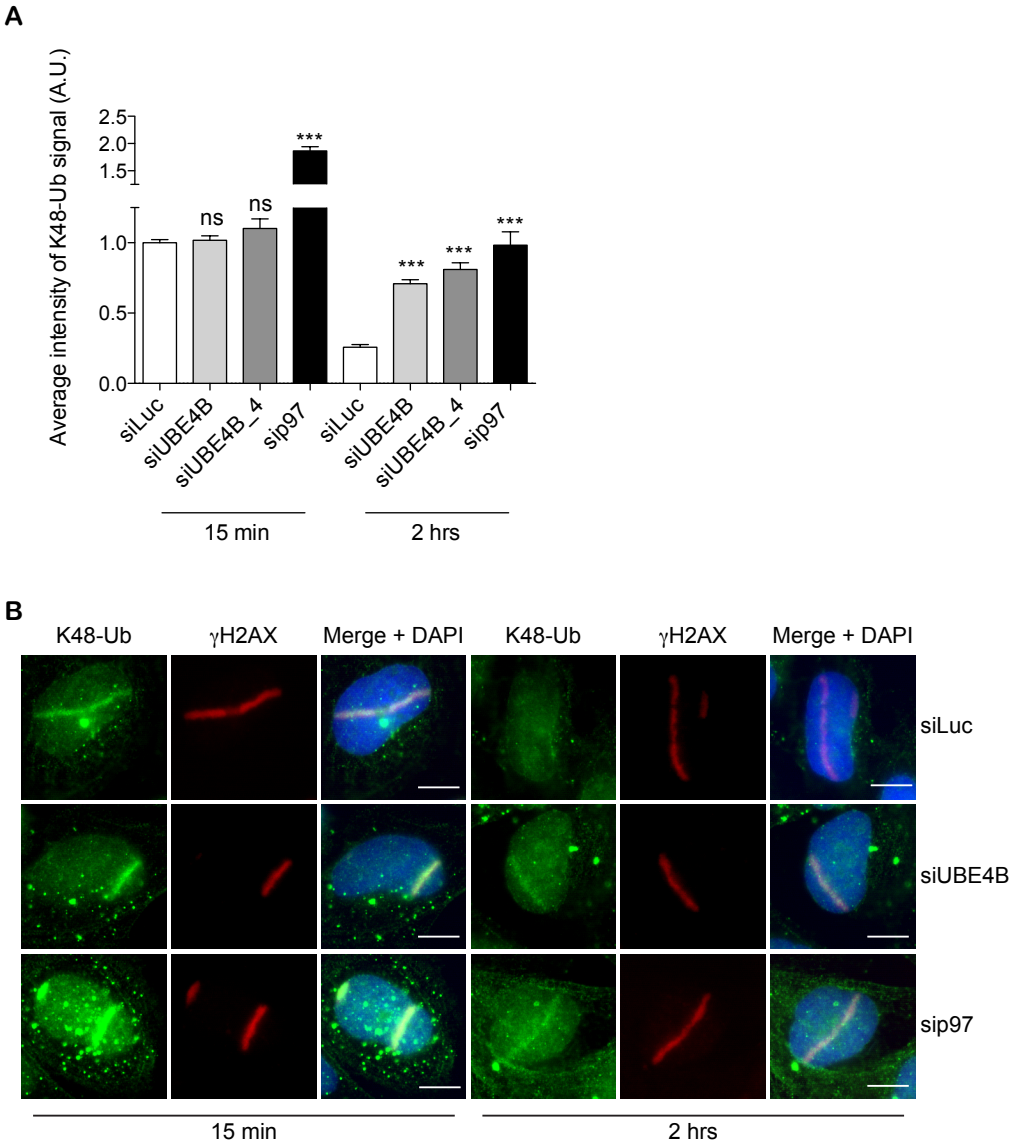


Figure 3-5. UBE4B is involved in the turnover of K48-linked chains ubiquitinated proteins at later time point after damage induction. U2OS cells were depleted for indicated proteins for 72 hrs prior to UV-A laser damage induction. Cells were allowed to recover for the indicated time before K48-linked ubiquitin chains were detected using a specific K48-Ub antibody and signal intensity was quantified at the site of DNA damage (γH2AX). A: Quantification results of the K48-Ub signal intensity after 15 min and 2 hrs of recovery. B: Representative images for A. Statistics: unpaired *t*-test; P value < 0.0001*, > 0.05 ns; mean + SEM; n = 3, > 100 laser lines were analysed per experiment and condition. Scale bar: 10 µm.**

3.5 UBE4B Helps To Maintain The K63-Linked Ubiquitin Chains At The Site Of DNA Damage

Cells depleted for UBE4B and exposed to UV-A laser DNA damage were also analysed for K63-ubiquitin chain formation at both 15 min and 2 hrs of recovery time. Two different siRNA sequences against UBE4B or p97 were used. Signal intensity was analysed at the site of DNA damage, as indicated by γH2AX.

As depicted in Fig 3.6A and 3.6B, control depleted cells (siLuc) exhibited a moderate K63-ubiquitin signal at 15 min of recovery, which increased by about 40% after 2 hrs recovery. In contrast, UBE4B depleted cells displayed a 10-40% reduction in signal intensity after 15 min of recovery compared to siLuc-transfected cells. A similar percentage of reduction could be observed in UBE4B depleted cells after 2 hrs of recovery compared to control cells, yet the K63-ubiquitin chain formation also increased over time in UBE4B depleted cells. Notably, the reduction of K63-ubiquitin chain signal in the UBE4B depletion varies from 10-40% while depletion efficacy of the differend siRNA sequences is very similar. This could be due to an off-target effect by either of the two siRNA sequences used for this study. To further investigate this observation, the best would be to reproduce these results in a knock-out cell line using CRISPR CAS9 technology. p97 depleted cells displayed the expected hyperaccumulation of K63-linked ubiquitin chain signal intensity at both time points analysed.

Overall, UBE4B affects the two different ubiquitin linkages in a different manner. K48-linked ubiquitin initially displayed a normal pattern in cells lacking UBE4B, but the reduction of signal intensity over time was significantly lower compared to control cells. In contrast, K63-linked ubiquitination was negatively affected in

UBE4B depleted cells. At both time points a reduction in signal intensity was observed compared to control cells.

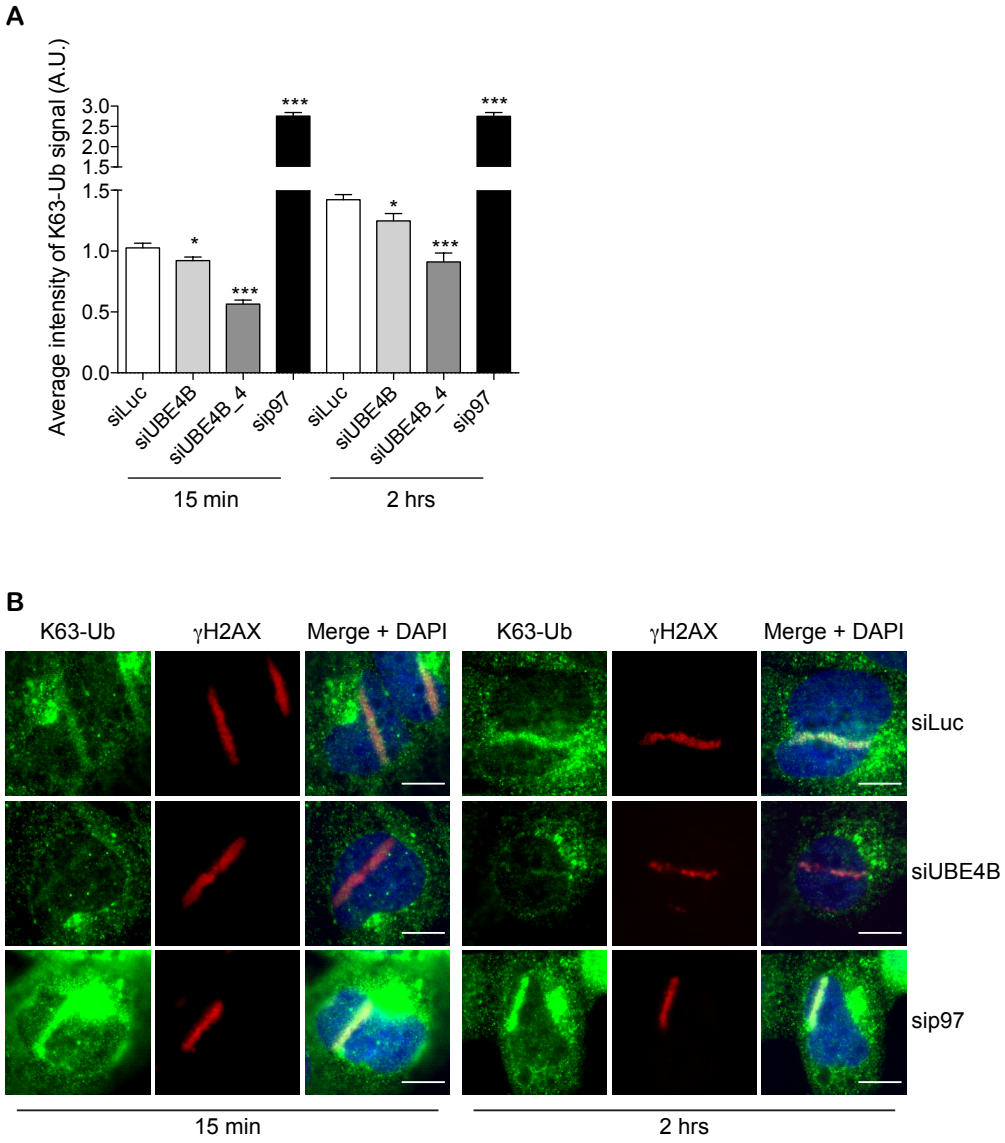


Figure 3-6. UBE4B helps to maintain the K63-linked ubiquitin signal at the site of DNA damage. U2OS cells were depleted using siRNAs against the indicated proteins for 72 hrs prior to UV-A laser damage induction. Cells were allowed to recover for either 15 min or 2 hrs before being stained for K63-linked ubiquitin chains and γH2AX. A: Quantification of the K63-Ub signal at the site of DNA damage (γH2AX) normalised to siLuc 15 min. B: Representative images for the conditions in A. Statistics: unpaired *t*-test; P value < 0.0001*, < 0.05*; mean + SEM; n = 3, > 100 laser lines were analysed per experiment and condition. Scale bar: 10 µm.**

3.6 Discussion

Ufd2 is a cofactor of p97 and the founder protein of the new group of E4-ubiquitin enzymes. Its main role lies in the cytoplasmic ubiquitin-proteasome degradation system, where it polyubiquitinates substrates and shuttles them to the proteasome for degradation in collaboration with Rad23 and p97 (Koegl et al., 1999; Richly et al., 2005). UBE4A and UBE4B are the mammalian homologues of yeast Ufd2. UBE4A and UBE4B are poorly characterised proteins. The laboratory of Yosef Shiloh has shown that both UBE4A and UBE4B interact with p97 (personal communication). Moreover, they found that both proteins are new players in the DDR, as absence of either of them sensitises cells to the radiomimetic drug NCS and both proteins are recruited to the site of DNA damage.

Our results support such findings, as absence of UBE4A abolishes both K48- and K63-linked ubiquitin chains at sites of DNA damage (Fig 3.2 and 3.3). Diminished ubiquitination at sites of DNA damage in UBE4A depleted cells was observed at early and late recovery time points. This could lead to severe defects in the ubiquitin-dependent protein cascade, such as that of 53BP1 and BRCA1-RAP80 in the context of K63-linked ubiquitin chains. On the other hand, little is still known about the role of K48-linked ubiquitin chains at the site of DNA damage. In general, this ubiquitin mark is a signal to target proteins for proteasomal degradation. Chromatin-bound proteins such as L3MBTL1 or JMJD2A have been shown to be marked by ubiquitin for degradation at the sites of DSBs (Acs et al., 2011; Mallette et al., 2012). The removal of these two histone-binding proteins from chromatin by p97 is essential for recruitment of 53BP1 at sites of DNA damage. Thus, it seems that reduced K48-linked ubiquitination could lead to

inefficient removal of such proteins, and consequently defective recruitment of some essential DDR proteins like 53BP1 and BRCA1.

Based on our results at this moment, we cannot address if UBE4A acts as an E3- or E4-ubiquitin ligase at the site of DSB. Nevertheless, it is exciting to speculate that the classical E3-ubiquitin ligases RNF8 and RNF168 get support from UBE4A. Thus, UBE4A would serve as a fine-tuner of the ubiquitination signal initiated by canonical E3-ubiquitin ligases. Additionally, our results indicate that UBE4A contributes to both ubiquitin linkages, namely K63 and K48. As an UBE4A orthologue in yeast, Ufd2, creates K48-linked ubiquitin chains, it could be speculated that UBE4A acts in a similar way. Therefore, the reduced K63-ubiquitin signal in UBE4A-depleted cells could result from inefficient recruitment of RNF8 and RNF168 due to the fact that the initial chromatin clearance is not performed accurately in a UBE4A/K48-ubiqutin signaling dependent manner. Further *in vitro* investigation is needed to answer those questions.

UBE4B, an orthologue of UBE4A, displayed increased 53BP1 foci at 4 and 8 hrs of recovery but normal foci resolution at 24 hrs of recovery. This 53BP1 dynamics already implied that UBE4B may have a different role than UBE4A. Indeed, our ubiquitination analysis at the site of DNA damage yielded very different results in cells depleted for UBE4A when compared to UBE4B depleted cells. Our analysis of K48-linked ubiquitin at the site of DSB shows that cells depleted for UBE4B have a slower reduction of this specific linkage over time up to 2 hrs of recovery (Fig 3.5). It is exciting to speculate that UBE4B might, in collaboration with p97, be involved in further ubiquitination of proteins marked for degradation at the site of DNA damage, and thus contributes to their extraction

from chromatin in a p97-dependent manner. Hence, the absence of UBE4B would slow down the removal of those proteins. This could lead to defects in the recruitment of other proteins resulting in the observed decrease of K63-linked ubiquitination in UBE4B-depleted cells (Fig 3.6). At both time points that we have analysed, we observed a similar reduction of K63 ubiquitin signal, which could also imply that UBE4B helps fine-tune K63-linked ubiquitin chains. More research needs to be invested to fully understand the mechanism of this new enzyme at the site of DNA damage.

Overall, our collaborative work with the Shiloh laboratory has led to the discovery of two new ubiquitin ligases involved in the repair of DSBs.

4 RESULTS 2: ATXN3 IS A NEW PLAYER IN THE DNA DAMAGE RESPONSE

p97 has been shown to play an important role in the repair of IR-induced DSBs (Meerang et al., 2011; Acs et al., 2011). However, little is known about the mechanistic role of p97, its cofactors, and substrates in DSB repair. Although p97 is known to interact with about 30 different cofactors (Chapter 1.3.1), only the UFD1-NPL4 heterodimer cofactor complex has so far been shown to be involved in orchestrating the function of p97 in DSB repair. The UFD1-NPL4 heterodimer facilitates p97 recruitment to sites of DNA damage. In addition, only one protein, L3MBTL1, has been identified as a p97 substrate in the DSB repair (Acs et al., 2011). However, the phenotype, namely reduced 53BP1, RAD51 and BRCA1 recruitment at sites of IR-induced DNA damage, observed upon p97 depletion indicates that p97 plays a much wider role in the response to DSBs (Meerang et al., 2011).

In order to gain a deeper understanding of the role of p97 in the IR-induced DNA damage response, and in order to identify p97 substrates and possible cofactors other than UFD1-NPL4 involved in DSB repair, our laboratory performed a SILAC based mass-spectrometry (MS) experiment to study the p97-interactome upon IR. The system set-up allowed for the quantitative comparison of the p97-interactome in HEK293T cells before and after IR. An early (30 min) and late (8 hrs) time point of recovery were chosen to be analysed after exposure to 10 Gy of IR. Moreover, the cells were fractionated in cytosolic, nuclear and chromatin fractions prior to p97 pull-downs and MS analysis. As expected, different known ERAD-related p97 cofactors were found in the p97-interactome in the

cytoplasmic fraction before DSB induction, such as UBXD8, UBXD9 or AMFR. The p97 cofactors UFD1 and NPL4 were also found inside the nucleus to interact with p97 and they displayed a slight increase in interaction upon exposure to IR. Moreover, more ubiquitin was found in the complex of p97 upon exposure to IR, which served as a good control as they have been shown to be important for the role of p97 in CAD upon DNA damage (Meerang et al., 2011). After IR exposure, p97 was itself found more inside the nucleus (data not shown).

Interestingly, ATXN3, a known p97 cofactor involved in protein homeostasis in the cytoplasm, has emerged as one of the most prominent proteins whose interaction with p97 after IR is significantly increased inside the nucleus, but not in the cytoplasm (Fig 4.1). As the increased interaction of p97 and ATXN3 after IR occurred exclusively inside the nucleus, we hypothesised that ATXN3 has a possible role in the regulation of the DDR after IR as a part of the p97 system.

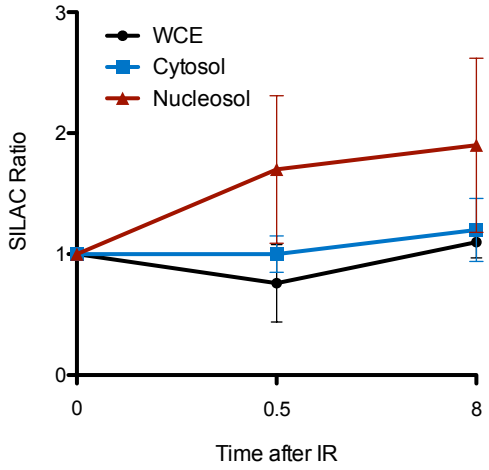


Figure 4-1. p97 shows increased interaction with ATXN3 inside the nucleus upon IR. SILAC ratio of p97 interacting proteins located either in the cytosol or nucleosol were analysed either in untreated (0) or cells exposed to 10 Gy IR and allowed to recover 30 min (0.5) or 8 hrs. n= 3 independent experiments. Mean ± SD. Unpublished data produced by Dr Ignacio Torrecilla.

4.1 ATXN3 Depletion Hypersensitises Cells To IR

It has been previously shown that inactivation of p97 hypersensitises human cells (U2OS) to IR (Meerang et al., 2011). The observation that ATXN3 increases interaction with p97 after IR indicated that ATXN3 might be a new cofactor for p97 in the DDR. Hence, absence of ATXN3 should also affect survival of cells exposed to IR. To test this hypothesis clonogenic assays were performed in HeLa cells depleted for ATXN3 by siRNA. p97 depleted cells were used as a positive control. The cells were exposed to increasing amounts of IR and allowed to recover and grow for 8 days. Then, the cell colonies were counted. As is shown in Fig 4.2A, control depleted cells (siLuc) displayed a decreased survival with increasing dose of IR, leading to 40% survival after 4 Gy of IR. However, ATXN3 depleted cells were more sensitive to IR, with 2 Gy leading to an overall survival of 50% and only around 15% survival after 4 Gy of IR. The survival of ATXN3 depleted cells was similar to p97 depleted cells. The depletion efficiency of the different siRNAs used in HeLa cells was confirmed by Western blotting (Fig 4.2B). Both siRNAs against p97 and ATXN3 showed very efficient depletion. Interestingly, it could be observed that p97 depletion also affected the ATXN3 protein pool, a phenotype that was observed in different cell lines throughout this study.

Overall, the results of this experiment suggest that ATXN3 protects cells from IR, strengthening the idea that ATXN3 is an, as yet, uncharacterised player of the DDR.

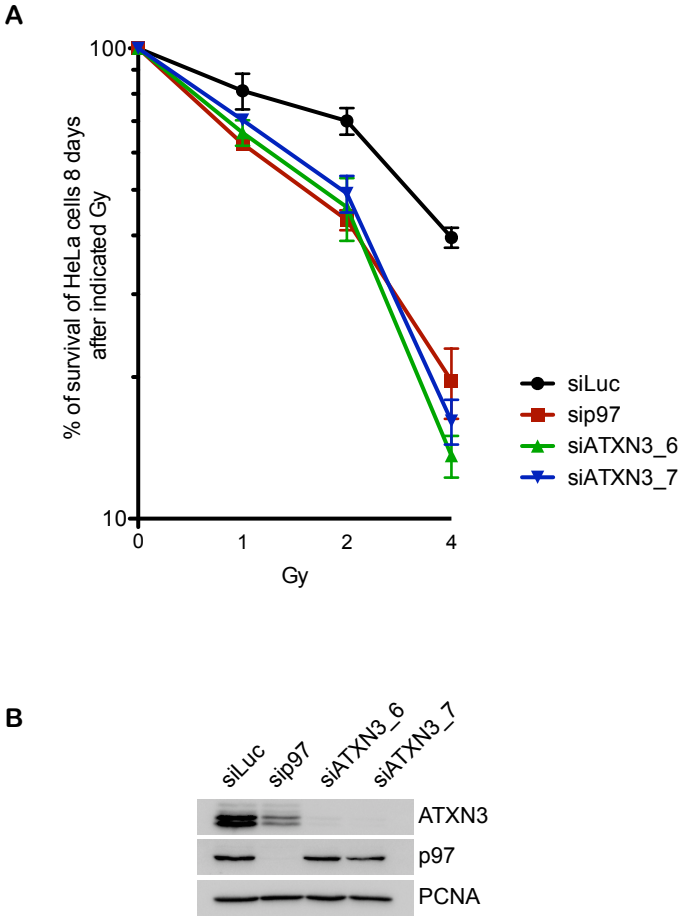


Figure 4-2. ATXN3 protects HeLa cells from IR induced DSBs. A: HeLa cells were transfected with indicated siRNA, irradiated with indicated amount of Gy and allowed to form colonies for 8 days before the number of colonies was counted. n = 3, each performed in triplicates; B: Depletion efficacy for HeLa cells for indicated proteins was assessed by Western blot. Representative blot depicted. Clonogenics assay performed by Dr Abhay Singh. Mean ± SEM.

4.2 ATXN3 Is Recruited To Sites Of DNA Damage

The results so far indicate that ATXN3 forms a complex with p97 and plays an important role in protecting cells from IR. Many DDR players relocalise to the site of DNA damage upon DSB induction, which can be visualised by IF. To test if ATXN3 has a role directly at the site of DNA damage, a local and defined region of DNA damage was induced in living U2OS cells by using UV-A laser lines. ATXN3 recruitment to sites of DNA damage was monitored in fixed cells using a non-comercial antibody against endogenous ATXN3. As shown in Fig 4.3, endogenous ATXN3 was recruited to sites of DNA damage as early as 1 min after induction of DNA damage and the intensity increases over time while its recruitment vanished 5 hrs after UV-A irradiation. Endogenous ATXN3 recruitment was only detectable using our non-commercial antibody raised against full length ATXN3.

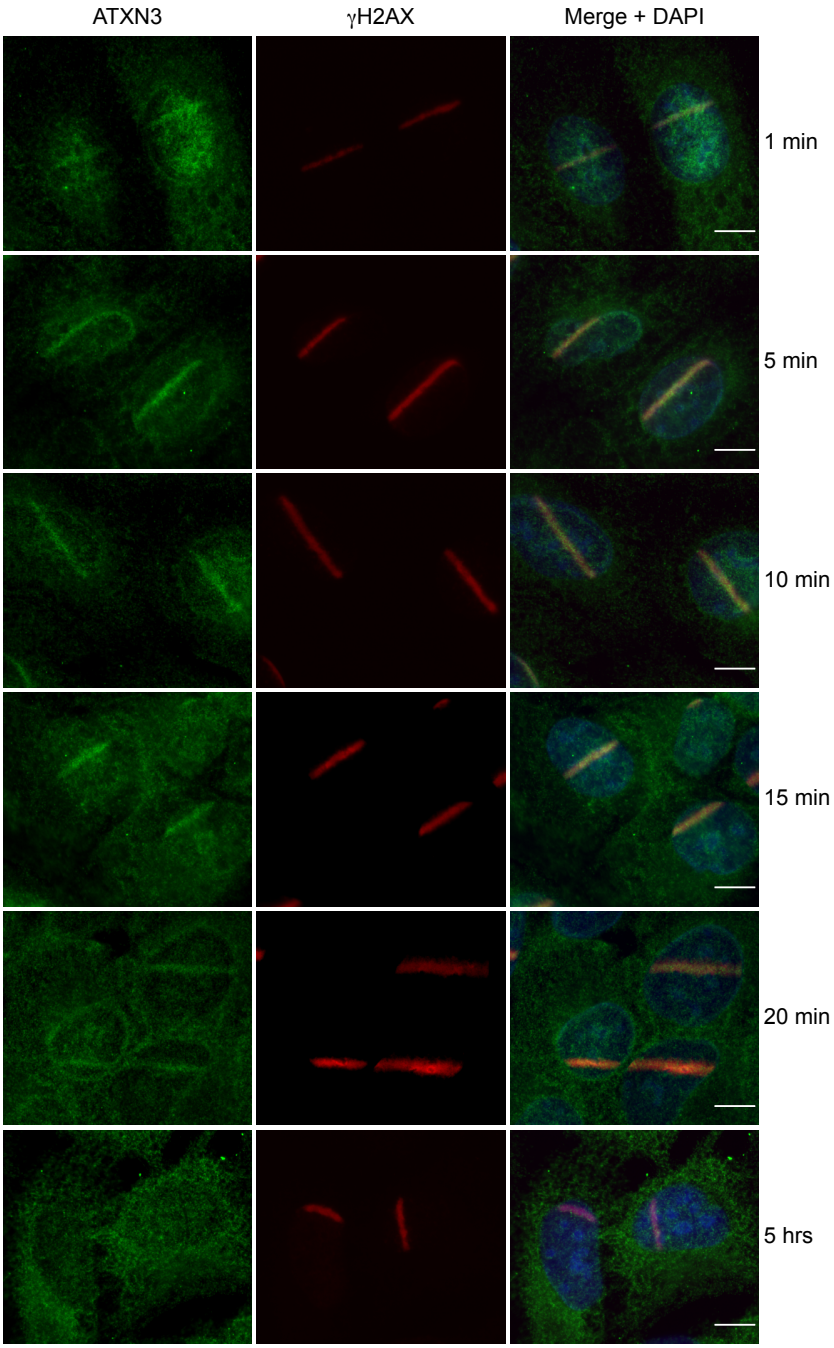


Figure 4-3. Endogenous ATXN3 is instantly recruited to sites of DNA damage. U2OS cells were exposed to UV-A laser damage, allowed to recover for the indicated time, fixed and stained using a non-commercial ATXN3 antibody. ATXN3 signal can be detected at sites of DNA damage (indicated by γH2AX) from as early as 1 min of recovery and increases in intensity over time. 5 hrs after DNA damage, the majority of ATXN3 vanished from sites of DNA damage. Scale bar: 10 µm.

To verify that the antibody we have created is specific, U2OS cells were either transfected with siATXN3 (sequence 7) or siLuc for 72 hrs before UV-A irradiation, and the recruitment of endogenous ATXN3 was monitored. Shortly, the cells were allowed to recover for 5 min after induction of UV-A laser damage, then cells were fixed and stained with the non-commercial ATXN3 antibody. As shown in Fig 4.4, ATXN3 depletion leads to a strong reduction of the nuclear staining with the non-commercial ATXN3 antibody compared to siLuc treated cells. Also, no positive signal for ATXN3 could be detected at sites of UV-A irradiation (as indicated by γH2AX) in ATXN3-depleted cells. Thus, these experiments directly demonstrate the specificity of our antibody and that ATXN3 is indeed recruited to sites of DNA damage. Altogether, our results suggest that ATXN3 is physically present at sites of DNA damage, and thus it is very likely directly involved in DSB repair after IR.

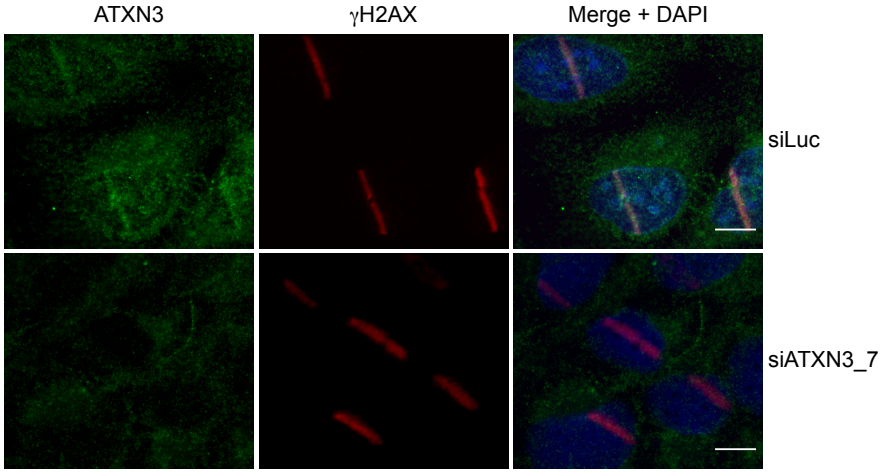


Figure 4-4. Non-commercial ATXN3 antibody recognises ATXN3 specifically. U2OS cells were either mock depleted (siLuc) or ATXN3 depleted for 72 hrs, UV-A laser lines were inflicted and cells were allowed to recover for 5 min and immunostained with the non-commercial ATXN3 antibody. While siLuc treated cells showed a positive signal for ATXN3 at sites of DNA damage, siATXN3_7 depleted cells displayed a complete abolishment of staining, supporting specificity of our non-commercial ATXN3 antibody. Scale bar: 10 μm.

4.3 Absence Of ATXN3 Delays Initial 53BP1 Recruitment And Leads To Impaired 53BP1 Foci Resolution

γH2AX and 53BP1 ionising radiation-induced foci (IRIF) formation and colocalisation is a widely accepted marker for DSBs. As discussed in chapter 1.5.9.1, the recruitment of 53BP1 to sites of DSB depends on posttranslational modifications on histones. 53BP1 recognises ubiquitinated H2AK15/K13 via its UDR motif and, via its Tudor domain, binds to methylated H4K20. As the H2AK15 ubiquitination is RNF8- and RNF168-dependent, defects in the ubiquitination pathway of the DDR leads to abnormal recruitment of 53BP1, which can be analysed by monitoring 53BP1 foci formation and dissolution. Moreover, unresolved DSBs will lead to prolonged persistence of 53BP1 and γH2AX foci. Therefore, to understand if ATXN3 was involved in DSB repair, a 53BP1 IRIF kinetics experiment was performed. U2OS cells were depleted for either ATXN3 or p97 for 72 hrs. The depletion efficiency for the sequences used in U2OS were assessed by Western blotting (Fig 4.5), showing that both p97 and ATXN3 were efficiently depleted at the time of the experiment. Similar to the blotting results in HeLa cells, depletion of p97 by siRNA in U2OS cells also slightly affected the protein stability of ATXN3 (Fig 4.5, compare lane 1 and 2).

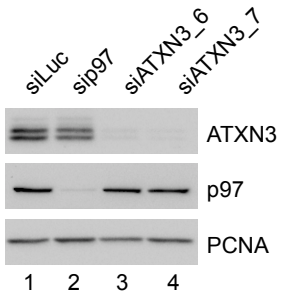


Figure 4-5. ATXN3 and p97 are efficiently knocked down in U2OS. Cells were transfected with indicated siRNAs for 72 hrs. Depletion efficiency was assessed by Western blotting using non-commercial ATXN3 or p97 antibody. PCNA serves as a loading control.

Cells were then exposed to 2 Gy of IR and collected at different time points, fixed and stained for 53BP1 and γH2AX. The percentage of cells with more than five 53BP1 foci per nucleus was assessed for each time point. As depicted in Fig 4.6, 15 min after IR, ATXN3 and siLuc depleted cells exhibited the same amount of IR-induced γH2AX foci. Surprisingly, in contrast to γH2AX, the formation of 53BP1 foci was significantly reduced in both ATXN3 and p97 depleted cells compared to control cells 15 min after IR (Fig 4.6A). While the formation of 53BP1 foci was significantly delayed in p97 depleted cells, reaching a maximum at 8 hrs with around 65% positive nuclei, ATXN3 depleted cells peaked at 1 hr of recovery, similar to siLuc treated cells. 8 hrs and especially 24 hrs after IR, control cells were able to almost completely resolve both γH2AX and 53BP1 foci, strongly suggesting IR-induced DSBs were efficiently repaired. In stark contrast to control cells, γH2AX and 53BP1 foci in ATXN3 depleted and p97 depleted cells persisted even 24 hrs after IR (Fig 4.6A and B). These results suggest that inactivation of ATXN3 strongly reduces DSB repair kinetics, visualised as persistence of γH2AX and 53BP1 foci after IR.

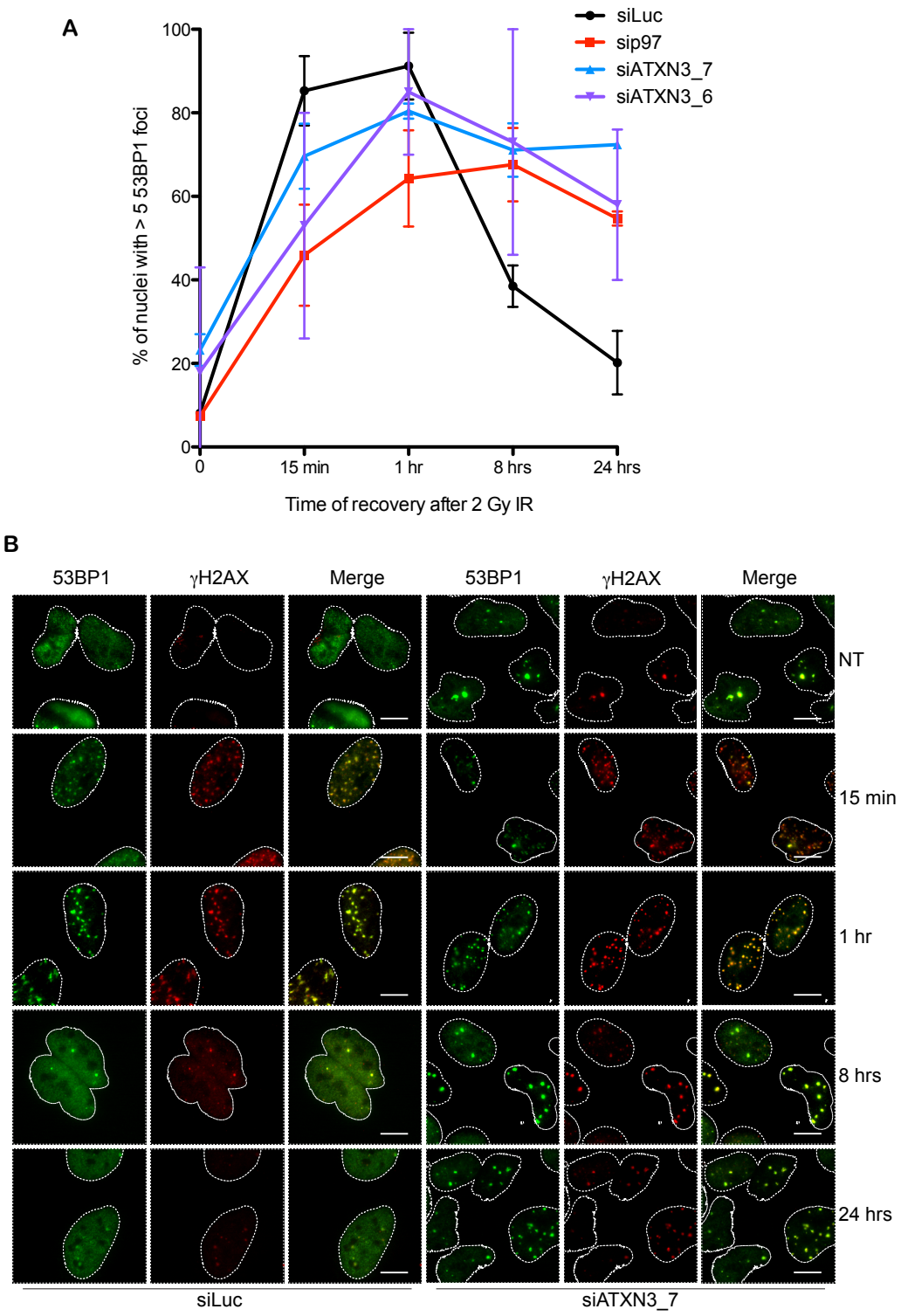


Figure 4-6. Depletion of p97 or ATXN3 affects the repair of DSB indicated by delayed initial formation of 53BP1 foci and retention of them at later time points. A: U2OS cells were depleted with indicated siRNAs for 72 hrs before exposure to 2 Gy of IR. Cells were allowed to recover for the indicated time points before being fixed and immunostained for 53BP1 and γH2AX. The percentage of cells with more than five 53BP1 foci per nucleus were scored for the different depletions and different time points. B: representative images for either siLuc or siATXN3_7 depleted cells showing 53BP1 and γH2AX foci. Mean ± SD; n = 3; > 100 nuclei were analysed per condition and per experiment; Scale bar: 10 µm. Data produced together with Dr Abhay Singh.

To further analyse whether the initial defect in 53BP1 recruitment after IR in ATXN3 depleted cells is observable with another source of DNA damage, we induced UV-A laser micro-irradiation and monitored 53BP1 signal intensity at sites of DNA damage, visualised by γH2AX. U2OS cells were transfected with siLuc, siATXN3_7, siATXN3_8, sip97, siRNF8 or siRNF168 for 72 hrs. Depletion efficiency for the different siRNAs was assessed by Western blot and, as depicted in Fig 4.7, all the sequences resulted in good depletion efficiencies. RNF8 and RNF168 depletions served as positive controls, as the absence of either protein is known to interfere with 53BP1 recruitment (Fradet-Turcotte et al., 2013). The cells were fixed at early (30 min) and late (5 hrs) time points after induction of DNA damage, and stained for 53BP1 and γH2AX. The average signal intensity of 53BP1 at each time point was analysed at sites of DNA damage (γH2AX). As depicted in Fig 4.8A and B, ATXN3 depletion resulted in lower 53BP1 intensity at the early time point compared to control cells. The average reduction was about 35%. The lower 53BP1 intensity at sites of DNA damage was also observed in p97, RNF8 and RNF168 depleted cells. At the late time point, ATXN3 depleted cells had similar average signal intensity to control cells, which was about twice as much compared to the initial time point, while p97, RNF8 and RNF168 depleted cells displayed significantly reduced intensity of 53BP1 signal.

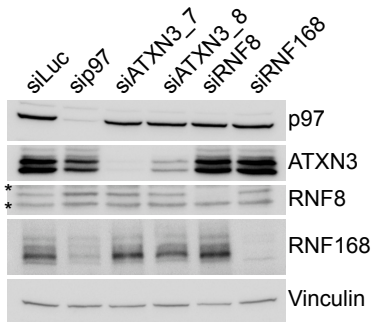


Figure 4-7. Efficiency of siRNA depletion. U2OS cells were transfected with the inidcated siRNA sequences for 72 hrs and depletion efficiency was assessed by Western blotting using specific antibodies. Vinculin serves as a loading control. Asterisks indicate two off-target bands detected by the RNF8 antibody.

Overall, our analysis of 53BP1 revealed that inactivation of ATXN3 interferes with initial 53BP1 recruitment at sites of DNA damage, either induced by IR or UV-A laser. Specifically, cells lacking ATXN3 display initial recruitment problems for 53BP1, similar to p97, RNF8 and RNF168 depleted cells. However, in contrast to p97, RNF8 and RNF168 depleted cells, ATXN3-depleted cells manage to overcome this initial defect in 53BP1 recruitment at intermediate time points and reach a 53BP1 recruitment efficiency similar to control cells (siLuc) at sites of DNA damage. While control cells are able to perform accurate DSB repair and resolve the 53BP1 IRIF foci after 8 hrs, ATXN3 depleted cells display much higher numbers of 53BP1 foci at late time points, up to 24 hrs, that colocalise with γH2AX, indicating unrepaired DNA damage.

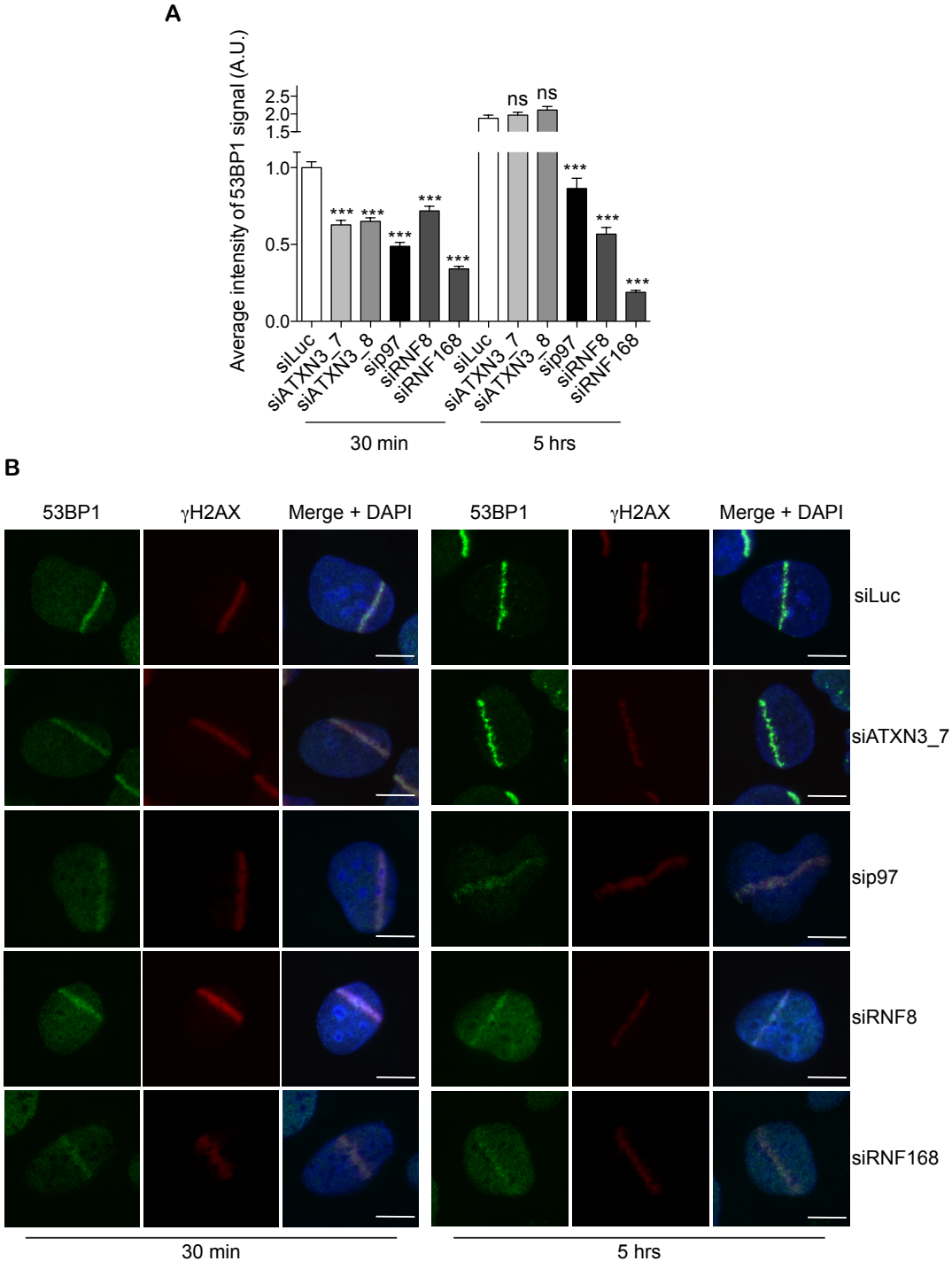


Figure 4-8. 53BP1 recruitment to sites of DNA damage is affected upon ATXN3 depletion at 30 min but not 5 hrs of recovery. A: U2OS cells were depleted with indicated siRNA for 72 hrs before UV-A micro-irradiation. Cells were allowed to recover for the indicated time points. Average signal intensity of 53BP1 at the site of DNA damage, normalised to siLuc 30 min. B: Representative images for the different conditions of A. Statistics: unpaired *t*-test; P value < 0.0001*, > 0.05 ns; mean + SEM; n = 3, > 100 laser lines were analysed per experiment and condition. Scale bar: 10 µm.**

4.4 ATXN3 Is Necessary For Accurate Ubiquitination At DSBs

ATXN3 is known to be an active DUB that is capable of cleaving K48- and K63-linked ubiquitin chains (Nicastro et al., 2010; Winborn et al., 2008a). Both of these ubiquitin chain linkages have been implicated in the orchestration of DSB repair (Meerang et al., 2011; Ramadan, 2012; Feng and Chen, 2012). As ATXN3 is physically present at sites of DNA damage and its inactivation leads to initially diminished 53BP1 foci recruitment, we hypothesised that ATXN3 might regulate the ubiquitination status at sites of DNA damage. Therefore, ubiquitination at DSBs was assessed using an established antibody (FK2) that recognises mono- and polyubiquitinated proteins. U2OS cells were either mock depleted (siLuc) or ATXN3 depleted, irradiated with 2 Gy, and left to recover for 15 min or 24 hrs (Fig 4.9). The number of FK2 foci per nucleus were counted at the different time points. Strikingly, the average number of FK2 foci per nucleus was significantly higher in ATXN3 depleted cells compared to control cells, indicating that inactivation of ATXN3 causes hyperubiquitination at sites of IR-foci.

Additionally, the ubiquitination intensity was also assessed after UV-A laser micro-irradiation. U2OS cells were depleted for ATXN3 or p97 for 72 hrs and fixed at early (30min) or late (5 hrs) recovery time points after laser stripe induction before staining for total ubiquitin with the FK2 antibody. Analysis of the different conditions revealed a significant increase of ubiquitin signal in ATXN3 depleted cells compared to control cells at both early and late time points (Fig 4.10A and B). As previously shown, the ubiquitin accumulation in p97 depleted cells was hugely increased (Meerang et al., 2011) and served as a positive control in these experiments.

Overall, the results suggest that inactivation of ATXN3 causes hyper-accumulation of ubiquitinated substrates at sites of DNA damage either after IR or UV-A laser, which is in agreement with the role of p97 at sites of DNA damage.

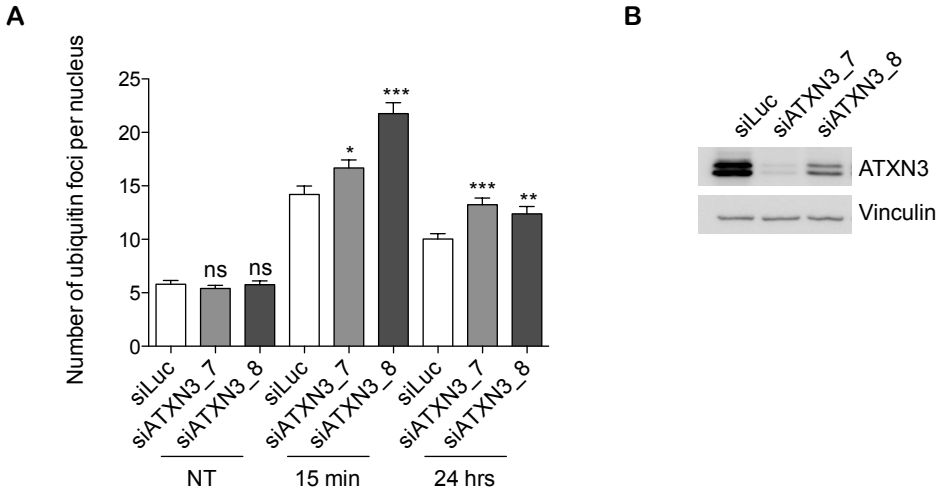


Figure 4-9. ATXN3 regulates ubiquitination at the site of DSB. U2OS cells were depleted with indicated siRNA for 72 hrs. Cells were irradiated with 2 Gy and allowed to recover for the inidcated time before being immunolabelled for total ubiquitin (FK2 antibody). A: Number of ubiquitin foci per nucelus were counted. B: Representative WB. Statistics: unpaired *t*-test; P value < 0.0001*, < 0.001** < 0.05*, > 0.05 ns; mean + SEM; n = 2, > 100 laser lines were analysed per experiment and condition.**

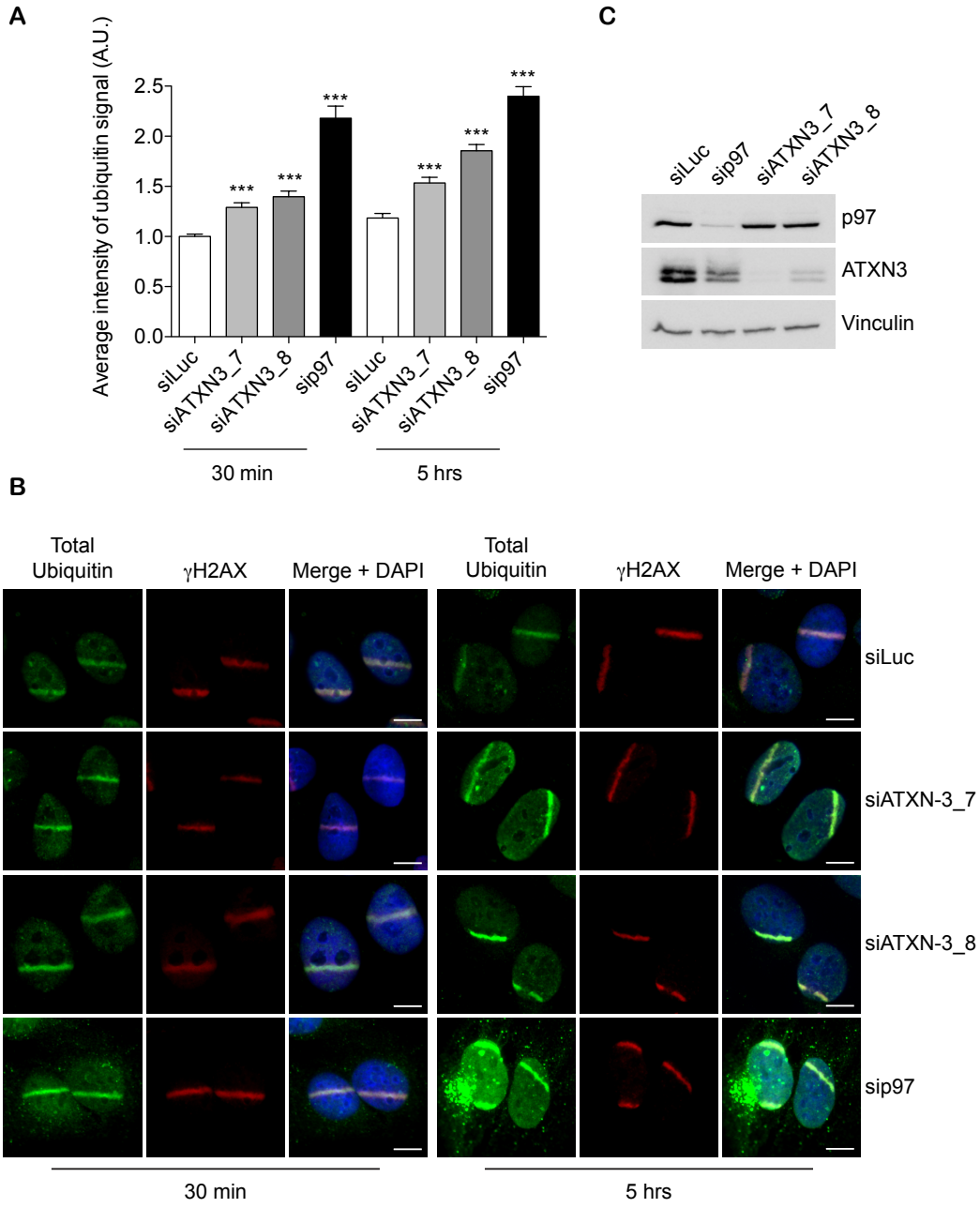


Figure 4-10. ATXN3 depletion leads to increased ubiquitination at the site of DNA damage. A: U2OS cells were depleted with indicated siRNAs for 72 hrs. UV-A laser micro-irradiation was performed and cells were allowed to recover for the indicated time before fixation and immunostaining with the antibody for total ubiquitin (FK2) and γH2AX. Total ubiquitin intensity at the site of DNA damage (γH2AX) was quantified and normalised to siLuc 30 min B: Representative images immunostained for total ubiquitin and γH2AX for each time point and condition of A. C: Representative WB. Statistics: unpaired *t*-test; P value < 0.0001*; mean + SEM; n = 3, > 100 laser lines were analysed per experiment and condition. Scale bar: 10 µm.**

4.5 Absence Of ATXN3 Leads To Increased BRCA1 Retention At A Later Time Point After DNA Damage Induction

ATXN3 appears to be involved in the regulation of the ubiquitination at the site of DNA damage (Fig 4.9 and 4.10), as well as 53BP1 recruitment (Fig 4.6 and 4.8). Ubiquitination is crucial for the regulation of the DDR at DSBs. Lack of RNF8 and RNF168 not only affects recruitment of 53BP1 but also the recruitment of the tumor suppressor protein BRCA1 via its adaptor protein RAP80, which relies on K63-linked ubiquitination (Kim et al., 2007; Sobhian et al., 2007; Wang et al., 2007). Therefore, it was of interest to understand if ATXN3 also regulates BRCA1 at the site of DNA damage. To this end, UV-A laser micro-irradiation was performed in control (siLuc) or ATXN3 depleted U2OS cells that were allowed to recover for either 30 min or 5 hrs after damage induction. Then, the cells were fixed and stained for BRCA1 and γH2AX. As a positive control for defects in BRCA1 recruitment, cells were also depleted for RNF8, RNF168 or p97. Signal intensity was quantified at sites of UV-A laser-induced DNA damage. Interestingly, the analysis revealed that BRCA1 recruitment was not affected in ATXN3 depleted cells at the early time point (Fig 4.11A and B). At the late time point, ATXN3 depletion led to significant hyperaccumulation of BRCA1 at sites of DNA damage compared to control (siLuc) cells. As expected, cells depleted for RNF8, RNF168 or p97 showed a significant decrease in BRCA1 intensity at both time points, early and late, after UV-A laser exposure. Therefore, we concluded that ATXN3 is regulating the ubiquitination at the site of DNA damage, which does not affect initial BRCA1 recruitment but results in BRCA1 hyperaccumulation during recovery after DNA damage.

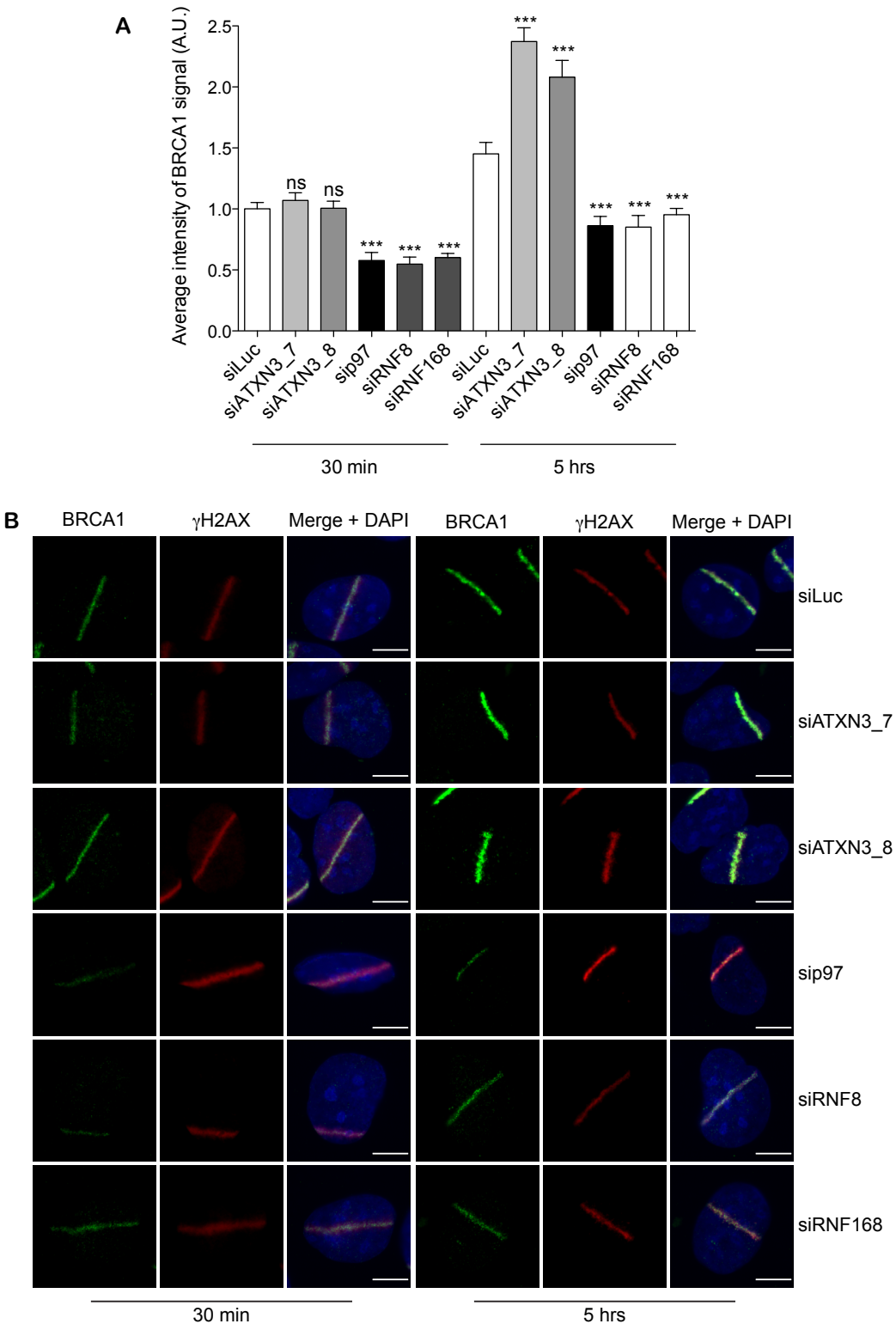


Figure 4-11. ATXN3 depletion leads to BRCA1 hyperaccumulation at the site of DNA damage at the later time point. A: U2OS cells were transfected with indicated siRNAs for 72 hrs before UV-A laser experiments were performed. After indicated recovery time cells were fixed and immunostained with γH2AX and BRCA1 antibodies. Intensity of BRCA1 signal at the site of DNA damage was quantified and normalised to siLuc 30 min. B: Representative images for each time point and condition of A. For representative WB refer to Fig 4.7. Statistics: unpaired *t*-test; P value < 0.0001*, > 0.05 ns; mean + SEM; n = 3, > 100 laser lines were analysed per experiment and condition. Scale bar: 10 µM.**

Together, these data additionally support that ATXN3 is a new player in the regulation of the DNA damage response, which suppresses hyperaccumulation of the ubiquitin signal at sites of DNA damage, thus affecting regulation of the downstream proteins 53BP1 and BRCA1.

4.6 Discussion

The orchestration of the DDR has emerged to be a well-organised interplay of different PTMs such as methylation, phosphorylation, ubiquitination and SUMOylation. p97 is a crucial factor in the ubiquitin-proteasome degradation system, and has emerged in the recent years as a fundamental player in nearly all cellular pathways including the DDR (Meyer et al., 2012; Vaz et al., 2013; Ramadan et al., 2016). Being equipped with a large set of cofactors, it can adapt to a variety of substrates located in different cellular structures. However, ubiquitin is the main commander of p97 function (Ye, 2006). It has been shown that $p97^{UFD1\text{-}NPL4}$ plays a fundamental role in the preparation of chromatin at a DSB for the recruitment of important DSB repair proteins, such as 53BP1 and BRCA1 (Meerang et al., 2011; Acs et al., 2011). However, a deeper mechanistic understanding of how p97 and its cofactors are involved in the repair of DSBs is still elusive. To gain a deeper understanding of the role of p97 and its cofactors in the response of IR, our laboratory has performed a SILAC-based mass spectrometry screen. Surprisingly, one of the major hits inside the nucleus that increased its interaction with p97 after IR exposure was ATXN3 (Fig 4.1). ATXN3 is a DUB that has been mainly implicated to play a role in protein homeostasis in collaboration with p97 inside the cytosol (Durcan and Fon, 2011; Reina et al., 2010; Boeddrich et al., 2006). Yet, our initial data strongly supports that ATXN3

is an active player located at sites of DNA damage (Fig 4.3) protecting cells from IR-induced DNA damage (Fig 4.2). Moreover, our results strongly support that ATXN3 suppresses hyperubiquitination at the site of DNA damage. Absence of ATXN3 leads to increased ubiquitination at sites of DSBs (Fig 4.9 and Fig 4.10). Interestingly, this hyperaccumulation negatively influences the recruitment of 53BP1 soon after induction of DNA damage (Fig 4.6 and Fig 4.8). This indicates that the absence of ATXN3 somehow leads to aberrant ubiquitination that, at least initially, slows down the recruitment of 53BP1. However, and as expected, this hyperubiquitination leads to increased accumulation of BRCA1 (Fig 4.11) and persistence of 53BP1 at later time points (Fig 4.6). Several DUBs have so far been shown to play a role in the DDR. Different members of the USP family were shown to counteract RNF8 and RNF168 signaling by removing ubiquitin from H2A and H2AX K15, such as USP3 (Sharma et al., 2014) or USP17L3/Dub3 (Delgado-Diaz et al., 2014).

Together, ATXN3 appears to be a novel DUB in the DDR and gaining deeper understanding of its action at the site of DNA damage will be covered in the following two chapters.

5 RESULTS 3: ATXN3 PHYSICALLY INTERACTS WITH CRUCIAL DDR FACTORS

5.1.1 ATXN3 Forms A Complex With Important Players Of The DDR In Unchallenged Cells

ATXN3, as a cofactor of p97, has been shown to interact with p97 and other p97-interacting proteins, such as E3-ligases Parkin, the proteasome shuttle protein RAD23 or UBE4B (Durcan et al., 2011; Zhong and Pittman, 2006; Boeddrich et al., 2006). To gain a further understanding of how ATXN3 regulates the DNA damage response and to investigate a possible physical association between ATXN3 and main components of the DDR, we set out to investigate whether ATXN3 physically interacts with the components of the DDR *in vivo*. To this end, Flag-tagged ATXN3 wild type (purchased from Addgene) was overexpressed in HEK293T cells for 36 hrs and co-immunoprecipitation (co-IP) was performed over Flag antibody-coated beads under native conditions. The focus was to identify possible DDR proteins related to the ubiquitin system and DSB repair pathway. Excitingly, besides its known interaction partner p97, serving as a positive control, the Western blot analysis of ATXN3 co-IP elutions revealed interaction partners such as the two main E3-ubiquitin ligases in DSB repair, RNF8 and RNF168, and the essential factor for IR-induced NHEJ repair, the KU complex (Fig 5.1). On the other hand, 53BP1 was not found to co-elute with ATXN3. Interestingly, the proteasomal subunit α6 was also found in the complex with ATXN3, indicating that the ATXN3 complex associated with DDR components is also linked to the proteasome.

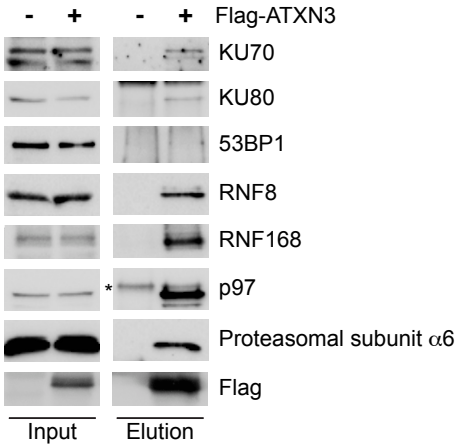


Figure 5-1. ATXN3 interacts with important players of the DDR. HEK293T cells were transfected with Flag-ATXN3 or were empty transfected for 36 hrs before being harvested. Lysates were immunoprecipitated over Flag beads under native conditions and the elutions were analysed by Western blotting using indicated antibodies. Flag-ATXN3 interacts with KU70, KU80, RNF8, RNF168, p97 and the proteasomal subunit α6. Asterisk indicates an unspecific IgG band.

In order to further verify these new ATXN3 interaction partners, reciprocal co-IPs were performed. To this end, HEK293T cells were transiently transfected with GFP-ATXN3 and either Flag-RNF8, Flag-RNF168 or Flag-KU80 for 36 hrs before native co-IPs over Flag beads were performed. As shown in Fig 5.2, the isolates showed that GFP-ATXN3 was co-precipitated with all three proteins, supporting that those proteins are interacting partners of the ATXN3 complex.

As an additional test for the specificity of the interaction, HEK293T cells were depleted for either RNF8 or RNF168 before performing co-IPs. To avoid the possibility that RNF8 or RNF168 interact with the Flag-tag unspecifically, a plasmid containing a Flag-GFP empty construct was used as a negative control. In short, HEK293T cells were depleted for RNF8 or RNF168 24 hrs prior to overexpression of Flag-ATXN3 or Flag-GFP for an additional 36 hrs.

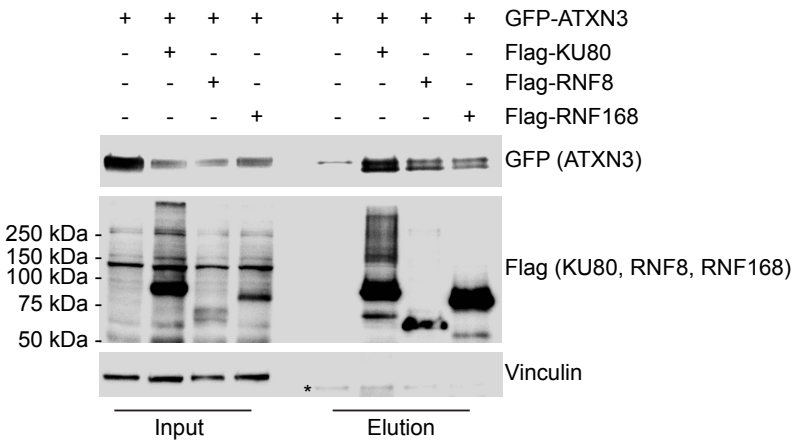


Figure 5-2. ATXN3 is pulled down over RNF8, RNF168 and KU80 reciprocally. HEK293T cells were cotransfected with GFP-ATXN3 and one of the Flag-tagged proteins of interest for 36hrs. Co-IP was performed over Flag beads and elutions were analysed for presence of GFP-ATXN3. GFP-ATXN3 co-eluted with Flag-KU80, RNF8 and RNF168. Asterisk indicates a non-specific band.

Cells were then collected and lysed to perform co-IPs over Flag beads. Inputs and elutions were blotted for either RNF8 or RNF168 to check the specificity of the detected bands. Both RNF8 (Fig 5.3, lane 3) and RNF168 (Fig 5.3, lane 4) showed specific depletion in the inputs with those antibodies. Blotting the elutions showed that the band for RNF8 (Fig 5.3, lane 3) and RNF168 (Fig 5.3, lane 4) depletion was reduced to the background level pulled down over the Flag-GFP construct. Together, this data further confirms that the detected interaction of ATXN3 and RNF8 and RNF168, respectively, is specific.

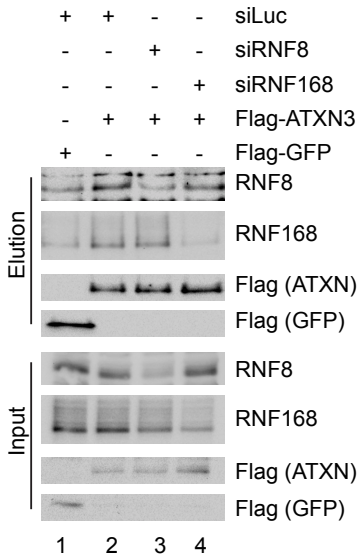


Figure 5-3. ATXN3 interacts specifically with RNF8 and RNF168. HEK293T cells were depleted for either RNF8 or RNF168 using siRNA 24 hrs prior to overexpression of Flag-ATXN3 or Flag-GFP for additional 36 hrs. Co-IPs were performed over Flag beads and inputs and elutions were analysed for RNF8 and RNF168 by Western blot. Inputs showed decreased band detection in the depleted cells using indicated antibodies, verifying depletion. Elutions showed specific binding of the two ligases in Flag-ATXN3 co-IPs.

5.2 ATXN3 Interaction With RNF168 Changes Upon DSB Induction

Having established the interaction of ATXN3 with DDR players such as RNF8, RNF168 or KU80, we were interested to understand how ATXN3 interacts with them upon IR treatment. To test this, HEK293T cells were transfected with Flag-ATXN3 for 36 hrs. One set of transfected cells was exposed to 10 Gy IR and allowed to recover for 30 min before cells were lysed and native co-IPs were performed over Flag beads. The inputs and elutions were blotted for RNF8, RNF168, KU80, p97 and the proteasomal subunit α6. Analysing the inputs, it was observable that RNF168 displayed a reduced smearing pattern after IR (Fig 5.4; Input, lane 3), while the pattern of other factors did not change upon IR. This indicates that RNF168 undergoes PTM changes upon IR, an observation previously reported by others (Sy et al., 2013). Analysis of the elutions showed that all tested proteins, except RNF168, were still interacting with ATXN3 similarly after IR as prior to IR. Interestingly, RNF168 showed a reduced interaction with ATXN3 post-IR (Fig 5.4; Elution, lane 3), specifically also losing the smearing bands corresponding to modified versions of RNF168. This indicates that ATXN3 interacts with the DDR factors both before and after IR, but in the case of RNF168, the interaction appears to be dependent on the modified forms of RNF168 (smear on top of the main band), which disappear upon IR, leading to a reduced interaction with ATXN3.

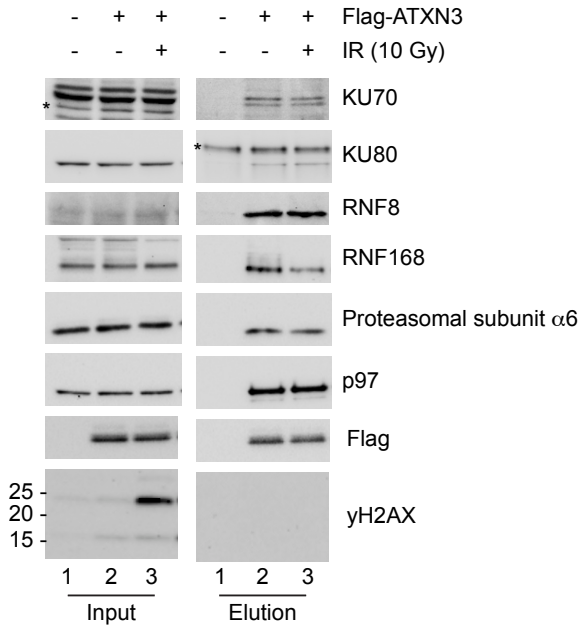


Figure 5-4. ATXN3 interactions with the tested proteins do not change upon IR except for RNF168. HEK293T cells were transfected with Flag-ATXN3 for 36 hrs and either lysed without treatment or 30 min after exposure to 10 Gy IR. Blotting for the indicated proteins did not reveal a changed interaction pattern before and after IR except for RNF168. RNF168 displayed a reduced PTM pattern in the input and the elution. Also, the main band of RNF168 was reduced in the elution upon IR but not in the input indicating that the interaction of RNF168 with ATXN3 depends on the PTMs of RNF168.

5.3 Interaction With RNF168, RNF8 And KU80 Is Mediated Over The Josephin Domain Of ATXN3

5.3.1 Creation Of Different ATXN3 Mutants

ATXN3 contains different domains that enable it to interact with other proteins (Fig 5.5). These include the UIMs, the VBM, the UbS1 and UbS2, the CAG repeats or the catalytic domain. To gain further understanding of how ATXN3 interacts with the DDR proteins found in complex, different plasmids encoding mutated versions of ATXN3 were obtained from Addgene or, in the case of the VBM, UbS1, and UbS2 mutants, produced by site-directed mutagenesis. Overall, Flag-tagged versions of the enzymatic dead (C14A), ubiquitin binding motif dead (UIM*),

p97-interacting motif dead (VBM*), ubiquitin binding site 1 mutated (UbS1*) and the expanded CAG (polyQ, 80 repeats) ATXN3 were gathered for interaction studies. ATXN UbS2* was excluded for interaction studies due to the observed strong instability of the protein inside cells (Fig 5.6A), which was also reported earlier (Blount et al., 2014).

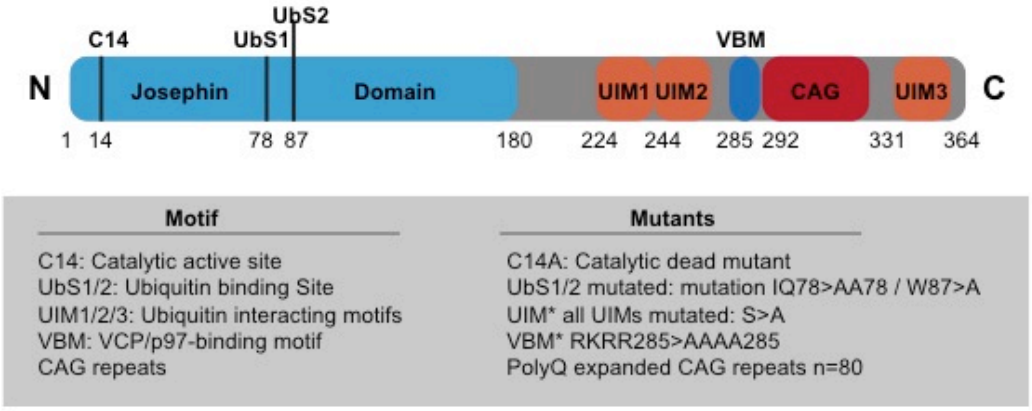


Figure 5-5. Schematic depiction of ATXN3. N-terminal, it harbors the Josephin domain (JD) with the catalytic site C14 indicated. The JD locates two ubiquitin binding sites (UbS1 and UbS2). Two UIMs are located between the JD and the p97-interacting motif (VBM), which is located before the CAG repeats. On the C-terminal end the third UIM is located. Different mutants, as described in the grey, were produced by site-directed mutagenesis or purchased from Addgene.

HEK293T cells were transiently transfected and allowed to express the different ATXN3 constructs for 36 hrs prior to collection and co-IP over Flag-beads. As the different constructs were expressed with different efficiency, 1% of each elution was blotted against Flag to normalise the capturing efficiency for the ATXN3 constructs (Fig 5.6A). ATXN3 UbS2* was eluted very inefficiently and was therefore excluded for further studies (Fig 5.6A).

Western blots were then performed with the normalised elutions as well as with inputs. Immunoblotting for the DDR proteins of interest was performed and analysed for loss in the elutions of the different mutants (Fig 5.6B). The

interaction with the proteins was compared to their interaction with ATXN3 WT. As expected, ATXN3 VBM* was unable to interact with p97, while ATXN3 VBM* interaction with other tested proteins was not affected. We concluded that the interaction of ATXN3 with RNF8, RNF168, KU80 and the proteasomal subunit α6 was not orchestrated over p97. Importantly, the inability of ATXN3 VBM* to interact with p97 showed that the overexpressed ATXN3 constructs are not forming a complex with endogenous wild type ATXN3. Thus, this approach demonstrates that it is unnecessary to deplete the endogenous ATXN3 protein prior to overexpression of mutant ATXN3 constructs.

While the comparison of ATXN3 WT with PolyQ, UbS1* or C14A did not reveal any defect in the interaction with the tested proteins, ATXN3 UIM* reproducibly reduced the interaction with RNF168. This indicates that ATXN3 needs its UIMs to stabilise the interaction with RNF168. Hence, ATXN3 appears to interact with a ubiquitinated version of RNF168, which is consistent with the reduced interaction after IR shown in Fig 5.4.

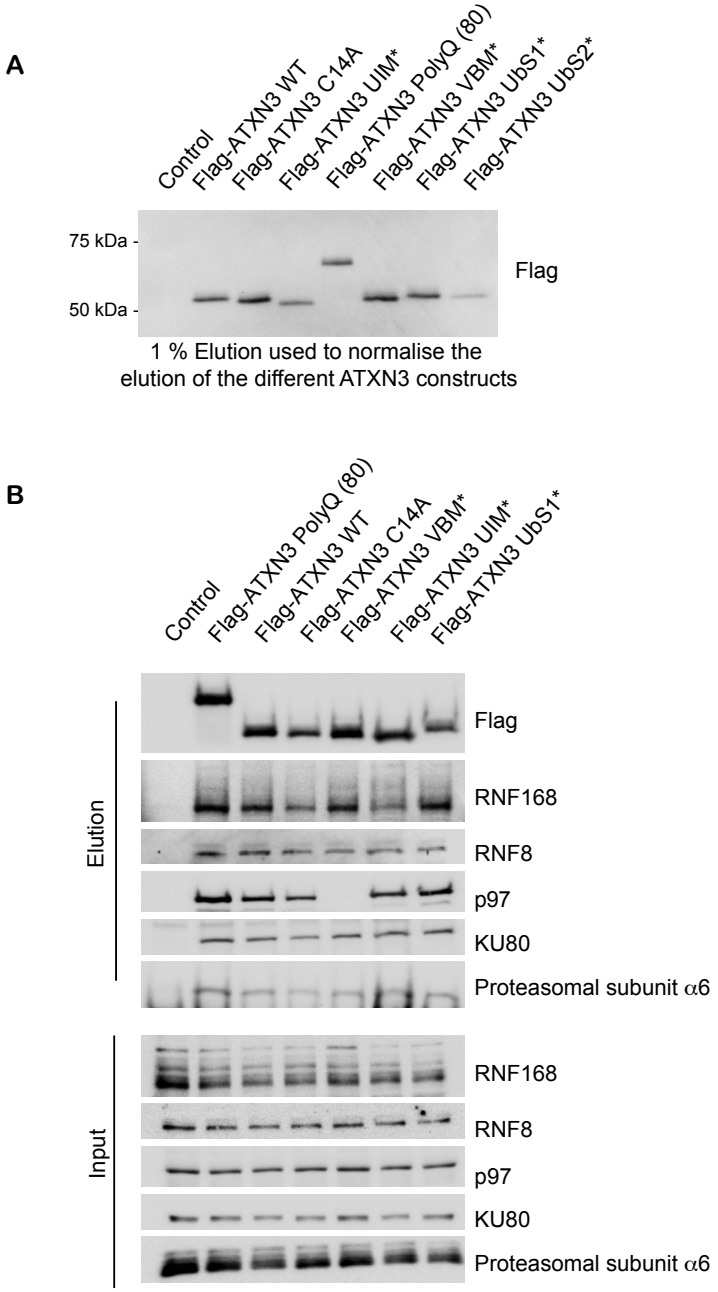


Figure 5-6. Different mutant constructs of ATXN3 do not abolish the interaction with the proteins of interest except for ATXN3 UIM* and RNF168. HEK293T cells were allowed to overexpress the indicated ATXN3 construct for 36 hrs before native co-IPs over Flag beads were performed. A: 1% of the elutions was blotted for Flag to normalise the elutions. B: Representative Western blot depicting the blotting for the proteins of interest from co-IPs over the different Flag-ATXN3 mutants. ATXN3 VBM* abolishes interaction with p97 completely. ATXN3 UIM* displays reduced interaction with RNF168. All the other tested ATXN3 mutants do not display reproducible changes in interaction with the different proteins of interest.

5.3.2 Mutation Of Putative SIM Does Not Abolish Interaction With The DDR Proteins

As none of the above-mentioned ATXN3 mutations, except ATXN3 UIM* and its interaction with RNF168, abolished the interaction with the tested proteins, sequence analysis of ATXN3 was performed to search for possible other protein-protein interacting motifs. The sequence analysis using GPS-SUMO revealed one putative SUMO interacting motif (SIM) located in the JD of ATXN3, with a medium score of 60.9. The putative SIM in ATXN3 consists of the amino acid sequence IFVVK starting at the amino acid position 162. Primers were designed to mutate this motif from IFVVK to AFAAK leading to the ATXN3 SIM* construct. As the UIM* mutant reduced the interaction with RNF168 in previous experiments, the SIM was also mutated in the ATXN3 UIM* mutant, leading to ATXN3 UIM* SIM* double mutant (Fig 5.7)

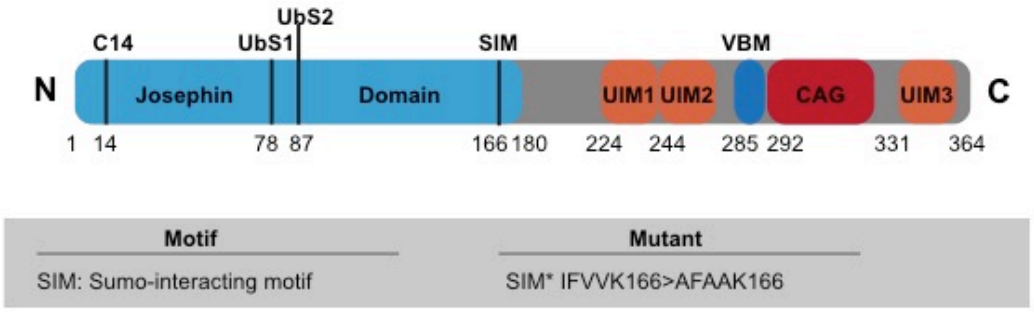


Figure 5-7. Creation of SIM mutant ATXN3 SIM*. The putative SIM IFVVK, located at the C-terminal end of the JD, was mutated to AFAAK by site-directed mutagenesis.

These constructs were transfected into HEK293T cells for 36 hrs and co-IPs were performed. The interaction with the proteins was analysed by Western blotting (Fig 5.8). Elution analysis for 1% of the Flag-tagged constructs revealed a strong instability for the SIM mutated proteins and thus, very low capturing efficiency

(Fig 5.8A). Therefore, elutions were normalised before loading for immunoblotting against the different proteins of interest (Fig 5.8B). Comparing the normalised elutions showed that abolishing the SIM led to an increased interaction with RNF8, RNF168 and KU80, but did not affect the interaction with p97. Nevertheless, the UIM* SIM* ATXN3 mutant showed a decreased interaction with RNF168 compared to the SIM* mutant alone, with levels similar to the ATXN3 WT construct.

Overall, the data indicates that the putative SIM has a negative impact on the interaction of ATXN3 with the three tested DDR proteins. Therefore, loss of the SIM motif has a trapping effect on RNF8, RNF168 and KU80. As SIMs non-covalently bind SUMOylated conjugates, this result suggests that SUMOylation on RNF8, RNF168 and KU80 might regulate their accessibility to and processivity by ATXN3.

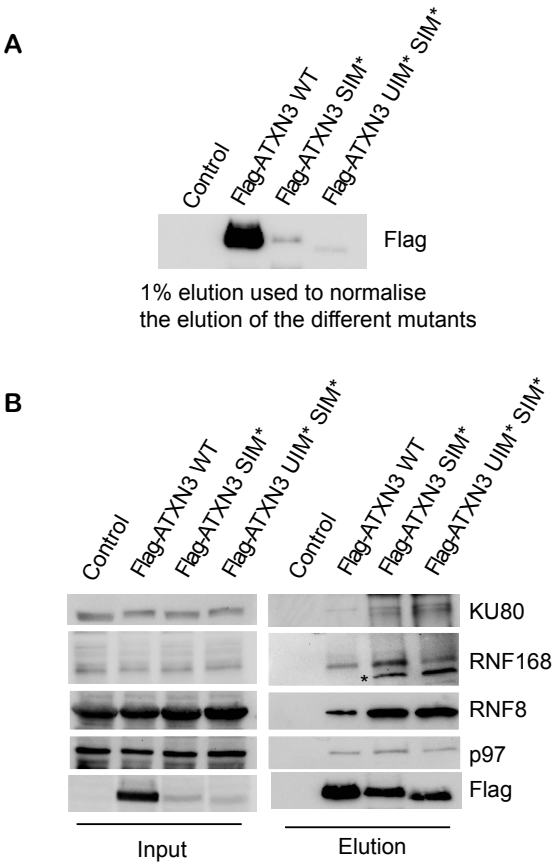


Figure 5-8. Mutating the putative SIM in ATXN3 does not abolish interaction with RNF8, RNF168 nor KU80. HEK293T cells were allowed to express the transfected ATXN3 constructs for 36 hrs prior to harvesting and co-IP over Flag beads. A: 1% of each elution was loaded and blotted for Flag to normalise capturing efficiency as the ATXN3 SIM* and ATXN UIM* SIM* appeared very instable. B: Interaction with p97 was not affected upon mutating the SIM. The two different SIM* mutants had a trapping effect on RNF8, RNF168 and KU80 as opposed to abolishing the interaction.

5.3.3 Interaction Of ATXN3 With The DDR Proteins Is Facilitated Over The Josephin Domain

In order to map the interaction of ATXN3 with the proteins of interest, fragment constructs of ATXN3 were produced by introducing stop codons either after the catalytic domain (F1) or before the polyQ tract (F2) (Fig 5.9). These constructs were expressed in HEK293T cells for 36 hrs and the lysates were captured over Flag beads.

Immunoblotting of the elutions revealed that losing the C-terminal part of the protein did not abolish the interaction of ATXN3 with tested DDR proteins (Fig 5.10). For all three proteins it was observed that the interaction with the fragmented version even increased compared to the wild type ATXN3 protein. Both fragments led to abolishment of interaction with p97. Together, this data strongly indicates that ATXN3 interacts with the proteins over its JD and that it needs its C-terminal part to process the proteins as loss of the C-terminal part exhibited a trapping phenotype.

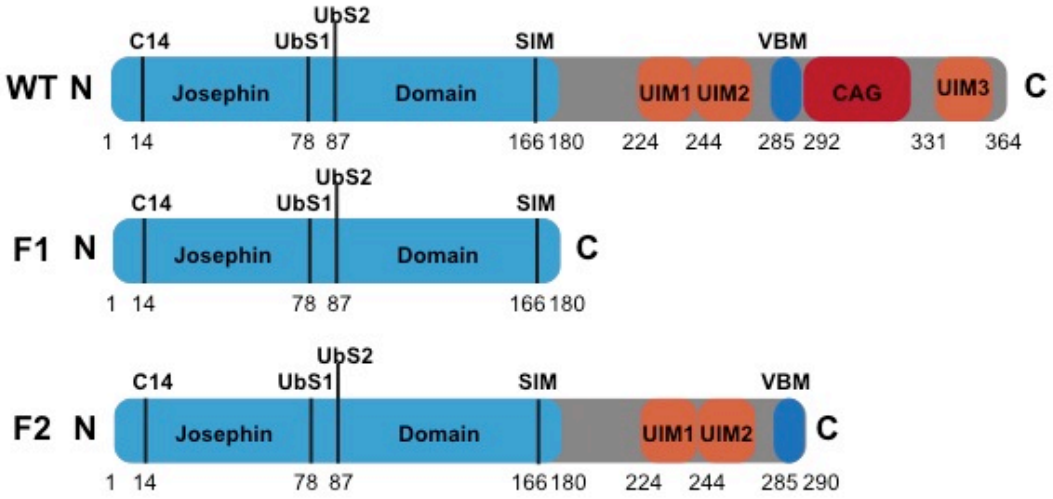


Figure 5-9. Schematic representation of the different fragments produced. Stop codons were introduced after the Josephin domain leading to fragment F1 or before the polyQ tract, leading to fragment F2.

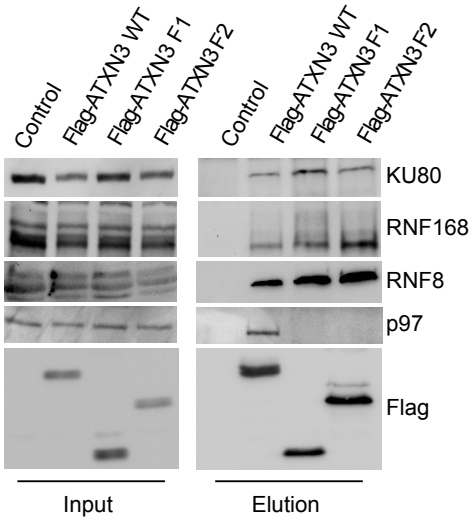


Figure 5-10. Interaction with RNF8, RNF168 and KU80 is facilitated over the N-terminal Josephine domain. The ATXN3 constructs containing early stop codons and wild type ATXN3 were overexpressed transiently in HEK293T cells for 36 hrs prior to lysing and co-IP over Flag beads. Inputs and elutions were analysed for the indicated proteins. Both shortened fragments abolished the interaction with p97. Interaction with KU80, RNF8 and RNF168 was not abolished but increased upon fragmentation of ATXN3. Therefore, the main interaction of ATXN3 with those proteins depends on the Josephine Domain but the C-terminal part of the protein is needed to further process the interaction partners as absence of the C-terminal part traps the interacting proteins.

5.4 Discussion

The chromatin surrounding a DSB is reorganised upon damage induction in a highly organised manner to help recruit repair proteins accurately in time and space (Schwertman et al., 2016). Ubiquitination is an important PTM used by cells to achieve this and our initial data with ATXN3 has revealed that it affects the formation of ubiquitination and regulation of BRCA1 and 53BP1 (see chapter 4). Searching for interaction partners of ATXN3 revealed that it interacts with the two DDR ubiquitin ligases RNF8 and RNF168 and moreover with KU70/80 and the proteasomal subunit α6 as well as p97 (Fig 5.1). Further, our data shows that this complex is formed independently of p97 (Fig 5.6). By creating and using different mutants of ATXN3, we have been able to show that the interaction with RNF168 depends on the PTMs of RNF168 and on the UIMs of ATXN3, although

absence of the UIMs does not completely abolish interaction with RNF168 (Fig 5.6). In general, it appears that the interaction is dependent on the JD of ATXN3, as the expression of ATXN3 C-terminal truncated variant did not abolish complex formation with ATXN3 but rather had a trapping effect on the interactions (Fig 5.10). Nevertheless, creating an N-terminal mutant that lacks the JD domain should answer this question. However, similar observations have been made by other groups for the interaction with Parkin, where both the JD of ATXN3 but also the PTMs of Parkin are responsible for complex formation (Durcan et al., 2011).

Both RNF8 and RNF168 display a high turnover at the site of DNA damage (Mok et al., 2014). Having observed that ATXN3 is necessary to regulate ubiquitination at the site of DNA damage and as well as recruitment of 53BP1 and BRCA1, it was interesting to speculate that ATXN3 might be involved in the regulation of these ligases at the sites of DNA damage. Being in a complex both before and after IR with RNF8 and RNF168, but also with the segregase p97, the question arose if ATXN3 might regulate the turnover of the ligases directly at the site of DNA damage. Therefore, analysing the assembly and disassembly efficiency of those proteins was of further interest to us.

6 RESULTS 4: ATXN3 REGULATES BOTH RNF8 AND RNF168 AT SITES OF DNA DAMAGE

The data from chapter 5 shows that ATXN3 forms a physical complex with RNF8 and RNF168, two crucial E3-ubiquitin ligases in the DDR. Depletion of ATXN3 leads to increased ubiquitination at sites of DNA damage (Fig 4.9 and 4.10, Chapter 4.4) and ATXN3 itself is directly recruited to sites of DNA damage (Fig 4.3, Chapter 4.2). As ATXN3 is a DUB whose inactivation leads to increased total ubiquitin signal at sites of DNA damage, we hypothesised that ATXN3 regulates the E3-ubiquitin ligase activity of RNF8 and RNF168 at sites of DNA damage, possibly in collaboration with p97. To test this hypothesis, U2OS cells were depleted for ATXN3 or p97 for 72 hrs by siRNA transfection. DNA damage was induced by UV-A laser micro-irradiation and the recruitment/disassembly efficiency of these two ubiquitin ligases was studied. An early (30 min) and late time point (5 hrs) were selected to investigate the recruitment/disassembly efficiency of RNF8 and RNF168 by signal intensity analysis, as described earlier.

6.1 RNF8 Hyperaccumulates At Sites Of DNA Damage Upon ATXN3 Depletion

As the RNF8 antibody used for the following experiments is a non-commercial antibody, the specificity of the RNF8 antibody for IF signal was first verified by comparing siLuc depleted cells with siRNF8 depleted cells. To this end, U2OS cells were transfected for 72 hrs with either siRNA before UV-A laser damage was induced and detection of RNF8 was analysed by IF (Fig 6.1). Indeed, 30 min after induction of DNA damage, in siLuc treated cells RNF8 was observed at the

site of DNA damage, as indicated by γH2AX and RNF8 signal merge but not in RNF8 depleted cells. This experiment confirmed the specificity of the non-commercial RNF8 antibody.

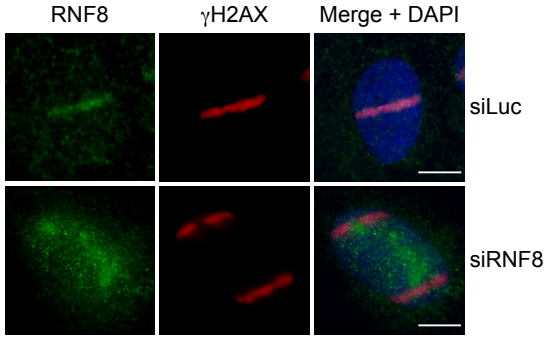


Figure 6-1. Non-commercial RNF8 antibody recognises RNF8 at sites of DNA damage specifically. U2OS cells were control depleted (siLUC) or RNF8 depleted and micro-irradiated with UV-A laser, fixed and stained with γH2AX and non-commercial RNF8 antibody. Indeed, while siLuc revealed a specific staining with RNF8 antibody at the site of DNA damage, siRNF8 depleted cells did not display any specific staining.

To assess if ATXN3 regulates RNF8 recruitment or disassembly, U2OS cells were treated with siLuc, siATXN3 or sip97 for 72 hrs prior to UV-A laser experiments. Cells were allowed to recover for the indicated time and immunostained for RNF8 and γH2AX. RNF8 fluorescence intensity was analysed and quantified for each condition as depicted in Fig 6.2.

At the early time point (Fig 6.2, 30 min), RNF8 signal intensity was significantly higher by 40-60% using two different siRNAs against ATXN3 compared to siLuc treated cells. In p97 depleted cells, this effect was even stronger, with cells having four-fold higher RNF8 signal intensity on average compared to control cells. Hence, ATXN3 depletion leads to hyperaccumulation of RNF8 at an early recovery time point after DNA damage, a phenotype that is intensified in p97 depleted cells.

The hyperaccumulation was still observable at the late time point (Fig 6.2, 5 hrs), where the average RNF8 signal intensity in ATXN3 depleted cells was 20-30% higher compared to control cells at the same recovery time. Depletion of p97 led to roughly twice as much RNF8 hyperaccumulation at the late time point compared to control cells.

Overall, Fig 6.2 shows that p97 is highly important for the accurate turnover of RNF8 at the site of DSB, and the absence of p97 leads to hyperaccumulation of RNF8 at sites of DNA damage at both recovery times tested in our experiments after DNA damage induction. Although not as severely as p97, the absence of ATXN3 also significantly affects the turnover of RNF8, leading to increased RNF8 at sites of DNA damage. Altogether, these data indicate that p97 and its cofactor ATXN3 regulate the turnover of RNF8 at sites of DNA damage.

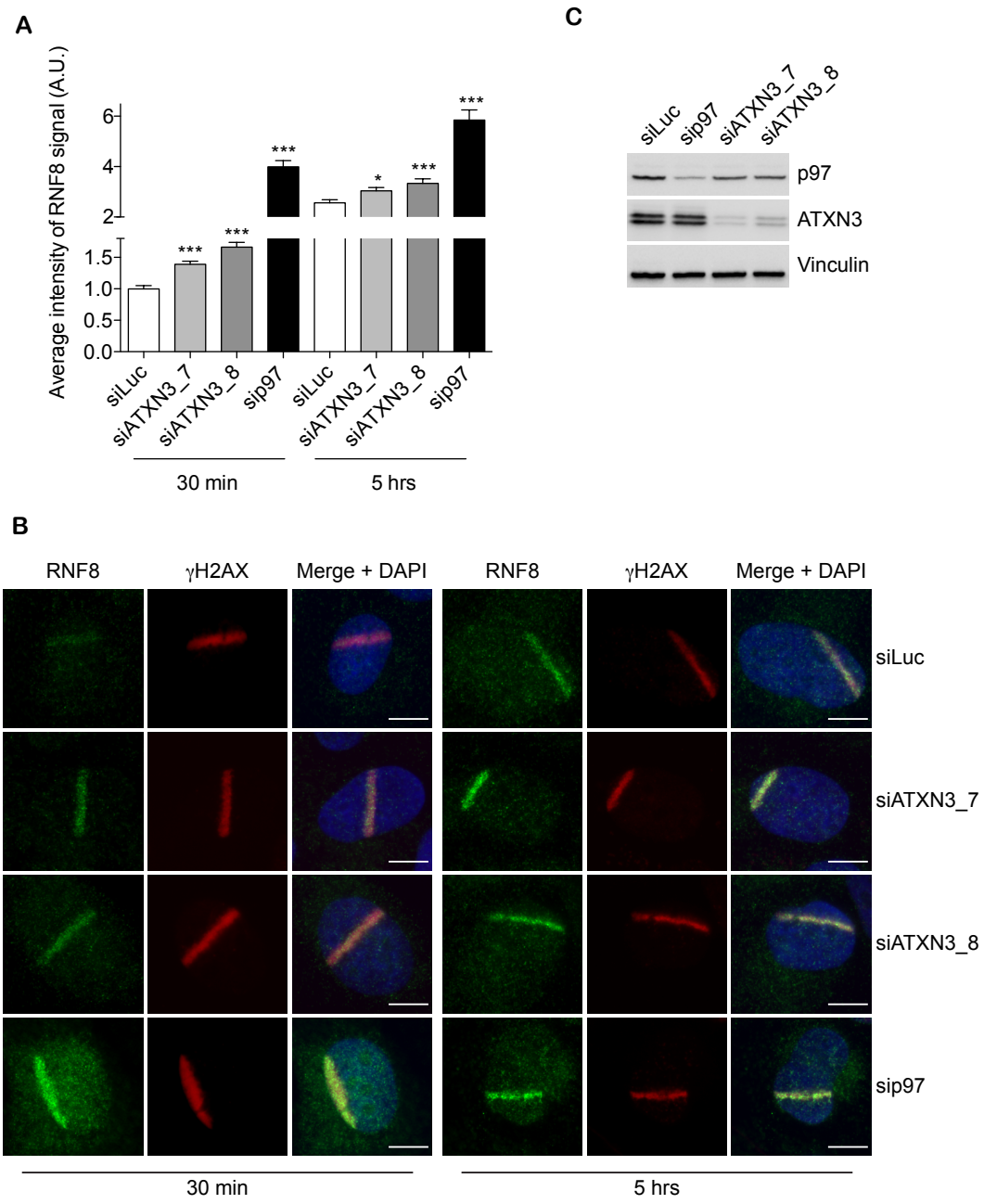


Figure 6-2. ATXN3 or p97 depletion leads to hyperaccumulation of RNF8 at the site of DNA damage. A: U2OS cells were depleted for the indicated proteins for 72 hours before recruitment of endogenous RNF8 to the site of UV-A laser induced DNA damage was assessed by immunofluorescence at the indicated recovery time points. RNF8 signal intensity was quantified at the site of DNA damage (γH2AX) and normalised to siLuc 30 min. B: Representative images for each condition of A. C: Representative WB. Statistics: unpaired *t*-test; P value < 0.0001*, < 0.05*; mean + SEM; n =3, > 100 laser lines were analysed per experiment and condition. Scale bar = 10 µm.**

6.2 ATXN3 Fine-Tunes RNF168 Recruitment

In order to test the recruitment of RNF168 to sites of DNA damage, our non-commercial antibody against RNF168 was tested for signal specificity at sites of DNA damage. U2OS cells were treated with siRNF168 or siLuc for 72 hrs prior to UV-A laser damage induction. After 30 min of recovery, the cells were fixed and immunostained using the non-commercial RNF168 antibody. Indeed, as shown in Fig 6.3, it could be observed that the antibody nicely recognises RNF168 at sites of DNA damage (γH2AX) in siLuc treated cells, which was not observable in siRNF168 treated cells. This demonstrates the specificity of our antibody to target RNF168 for IF.

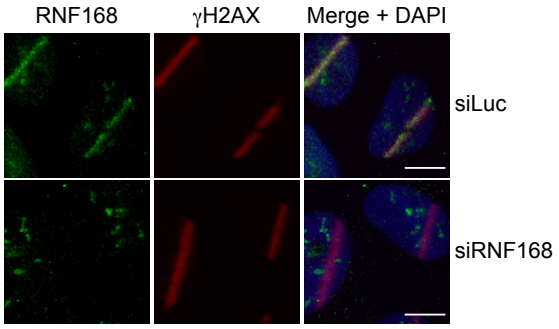


Figure 6-3. The non-commercial RNF168 antibody recognises RNF168 specifically at the site of DNA damage by IF. RNF168 was siRNA-depleted in U2OS cells, before being irradiated with UV-A laser and left to recover for 30 min, fixed and stained with indicated antibodies. Depletion of RNF168 specifically abolishes the recognised signal.

Having assessed the specificity of the antibody against RNF168, we sought to address whether ATXN3 is involved in the regulation of RNF168 at the site of DNA damage. To this end, U2OS cells were depleted for ATXN3 and p97 as well as for RNF8 as RNF8 is needed for the recruitment of RNF168 to the site of DNA damage and served as a control in these experiments (Doil et al., 2009; Pinato et

al., 2009; Stewart et al., 2009). The same recovery times as for RNF8 analysis were used.

After 30 min of recovery, RNF168 intensity quantification revealed that absence of ATXN3 leads to 30–40% reduced RNF168 recruitment compared to control cells (Fig 6.4, 30 min). This decrease was not as strong as depletion of RNF8, which abolished RNF168 intensity by around 70%. Surprisingly, p97 led to stark reduction (around 90%) of RNF168 recruitment.

Interestingly, in marked contrast to the early time point, ATXN3 depletion resulted in a 30-40% hyperaccumulated RNF168 fluorescence intensity at sites of DNA damage after 5 hrs of recovery compared to siLuc-transfected cells (Fig 6.4, 5 hrs).

Therefore, we concluded that ATXN3 is responsible for the accurate fine-tuning of RNF168 and absence of ATXN3 initially delays or slows down the recruitment of RNF168 but over time leads to hyperaccumulation of the ligase. As expected, RNF8 depleted cells displayed a severe defect in RNF168 recruitment. Analysing p97 depleted cells at the later time point revealed that there was almost no RNF168 recruited. Most of the cells displayed no detectable RNF168 at the sites of DNA damage, resulting in an overall 80% decreased RNF168 recruitment.

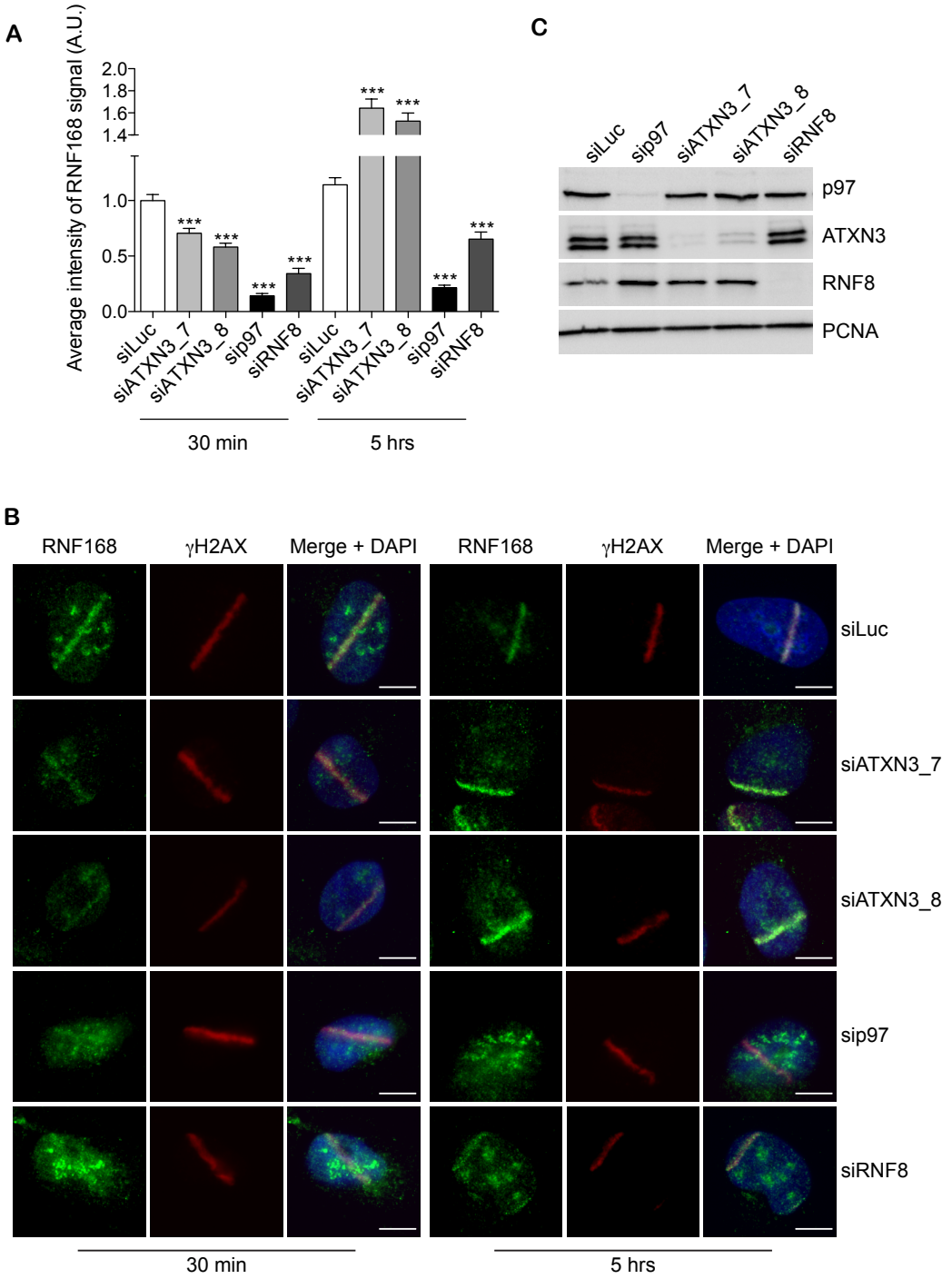


Figure 6-4. ATXN3 fine-tunes RNF168 turnover at the sites of DNA damage. A: U2OS cells were depleted for the indicated proteins for 72 hrs before DNA damage was induced with a UV-A laser. Cells were fixed at the indicated time points of recovery and stained for RNF168 and γH2AX. Signal intensity of the RNF168 at γH2AX positive areas was measured and normalised to siLuc 30 min recovery. B: Representative images for the different conditions analysed in A. C: Representative WB. Statistics: unpaired *t*-test; P value < 0.0001*; mean + SEM; n = 3, > 100 laser lines were analysed per experiment and condition. Scale bar = 10 µm.**

6.3 p97 Regulates RNF168 Homeostasis In Undamaged Cells

The observation that RNF168 recruitment was almost completely abolished upon p97 depletion was very striking as the effects were even stronger than in siRNF8 depleted cells. Different reasons were possible for this finding. It could be that RNF8, which is hyperaccumulated in p97 depleted cells, leads to space limitations resulting in exclusion of RNF168. On the other hand, the reduced RNF168 recruitment could result from reduced RNF168 availability. As for each experiment, depletion of the different proteins was analysed by Western blotting, the second hypothesis could be easily addressed. Surprisingly, a huge decrease of the total RNF168 protein level was observed in p97-depleted samples (Fig 4.7, Chapter 4.3). As all the experiments were performed using a single, published (Meerang et al., 2011) p97 siRNA sequence (sip97_7), this could be triggered by an off-target effect of the sequence on RNF168. Therefore, U2OS and HEK293T cells were transfected with four different sip97 sequences to exclude the possibility of an off-target effect. RNF168 was depleted as a positive control. Cells were harvested 72 hrs post transfection and lysates were analysed by Western blotting. As shown in Fig 6.5A, the different siRNAs sequences efficiently depleted the p97 protein, albeit to different extents. siRNA depletion of p97 with all tested sequences strongly reduced RNF168 protein levels. In the case for sip97_2 and sip97_7, the reduction was similar to the siRNF168 treated cells.

In order to analyse if the observed decreased pool of RNF168 was due to an accelerated turnover of RNF168 in the absence of p97, a cycloheximide (CHX) chase experiment was performed in the presence of a selective allosteric p97 inhibitor (NMS-873). For this experiment HeLa cells were used. In contrast to

siRNA depletion over 3 days, the usage of the chemical p97 inhibitor (NMS-873) allowed us to investigate the immediate effect of p97 inactivation on RNF168 protein stability. The cells were treated with NMS-873 2 hrs prior to the chase experiments. Cells were harvested after NMS-873 treatment or after addition of cyclohexamide for 4 and 8 hrs. RNF168 protein level was analysed by Western blotting. Indeed, it could be observed that in control (DMSO) cells (Fig 6.5B, lanes 1–3), RNF168 is slightly instable upon CHX chase, especially the modified forms of RNF168 (smear on top of the main band). Addition of the p97 inhibitor accelerated RNF168 degradation tremendously, as even the main band of RNF168 was severely reduced in those cells upon CHX chase (Fig 6.5B, lanes 4–6). On the other hand, addition of MG132, a proteasome inhibitor, stabilised RNF168 completely in the NMS-873-treated cells (Fig 6.5B, lanes 7-9), indicating that the observed RNF168 instability after p97 inhibition is due to accelerated proteasomal degradation.

Together, these data strongly suggests that the RNF168 pool in unchallenged cells, independently of cell line, steadily depends on p97. Instability observed upon loss of p97 is due to accelerated proteasomal degradation.

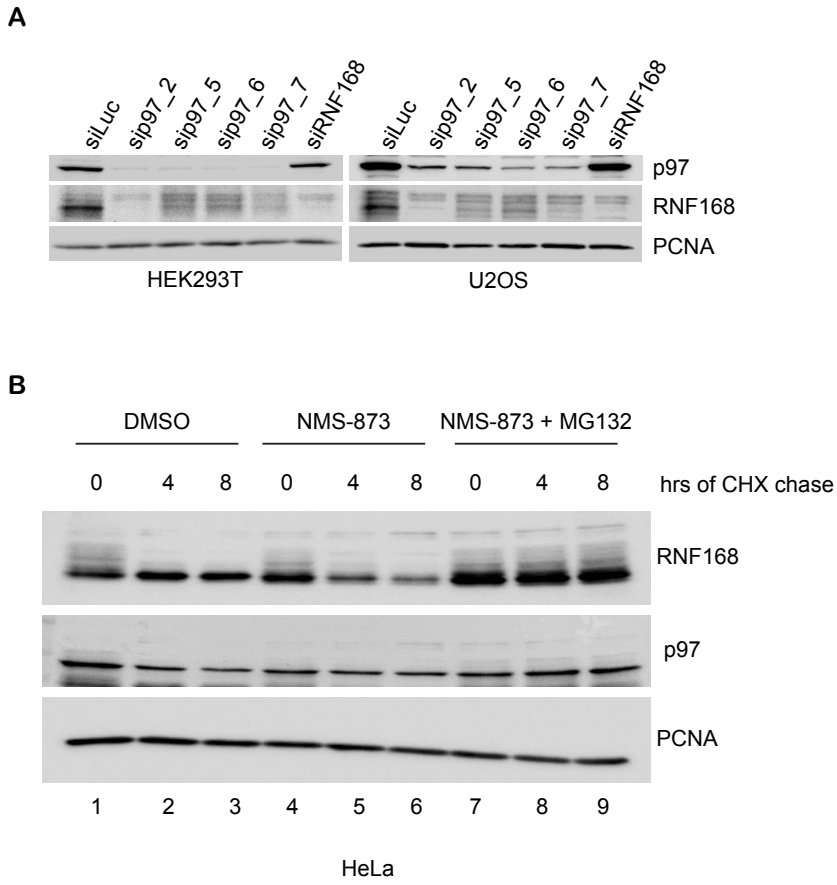


Figure 6-5. p97 stabilises RNF168 in unchallenged mammalian cells. A: p97 was depleted for 72 hrs in U2OS or HEK293T cells using four different siRNA sequences targeting p97. Cells were lysed and protein levels were analysed by Western blotting for the indicated proteins. siRNF168 serves as a control. B: p97 was inhibited in HeLa cells by using the allosteric inhibitor NMS-873 (10 μM) 2 hrs prior to CHX chase ± proteasom inhibitor MG132 (10 μM). Tranlsation of new proteins was then inhibited by addition of CHX (100 μg/ml) and cells were collected at the indicated time points. Protein levels of RNF168 was analysed by Western blotting. Data for B by Dr Abhay Singh.

6.3.1 ATXN3 depletion does not affect p97 recruitment to sites of DNA damage

p97 interacts with numerous cofactors that govern p97 specificity towards its substrates and cellular locations (Chapter 1.3.1). Without the help of its cofactors, p97 is not able to perform its specific tasks inside the cell. It has been shown that p97 recruitment to sites of DNA damage depends on its main cofactor complex UFD1-NPL4 (Meerang et al., 2011). ATXN3 is a p97 cofactor whose interaction with p97 is mediated via its VBM, located in close proximity to the CAG repeats (Fig 5.6) (Boeddrich et al., 2006). ATXN3 is rapidly recruited to sites of DNA damage (Fig 4.3, Chapter 4.2), where it regulates RNF8 and RNF168

recruitment (Fig 6.2 and Fig 6.4). As p97 is also involved in RNF8 regulation (Fig 6.2), it is possible that ATXN3 targets p97 to RNF8 by bringing it into proximity with RNF8. To test this hypothesis, p97 recruitment to UV-A laser damage lines was analysed in cells depleted for ATXN3. RNF8 depleted cells were used as a control, as it has been shown that loss of RNF8 leads to decreased p97 recruitment, albeit not completely (Meerang et al., 2011). The cells were allowed to recover 20 min after UV-A laser micro-irradiation, and p97 recruitment at sites of DNA damage was analysed by IF. As previously reported, RNF8-depletion significantly reduced the average p97 signal intensity at sites of DNA damage compared to control cells (Fig 6.6). However, depletion of ATXN3 did not affect p97 recruitment. Hence, ATXN3 seems not to be involved in targeting p97 to the damaged area at the tested time point.

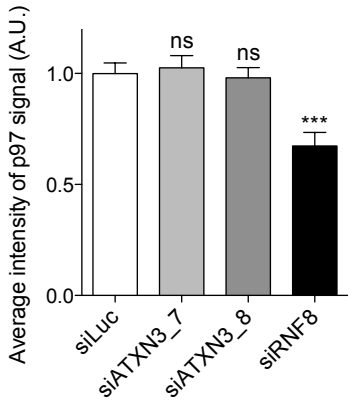


Figure 6-6. ATXN3 depletion does not affect p97 recruitment at sites of DNA damage. U2OS cells were depleted with the indicated siRNAs for 72 hrs. UV-A laser micro-irradiation was induced and cells were fixed after 20 min of recovery and immunostained for p97. Signal intensity analysis of the p97 signal is summarised in the blot. RNF8 served as a positive control that partially affects p97. Statistics: unpaired *t*-test; P value < 0.0001*, > 0.05 ns; mean + SEM; n = 3, > 100 laser lines were analysed per experiment and condition. Scale bar = 10 μm**

6.4 ATXN3 Recruitment To Sites Of DNA Damage Depends On p97

We have observed that ATXN3 is rapidly recruited to the sites of DNA damage (Fig 4.3), but it is not responsible for recruitment of p97 (Fig 6.6). This suggests that p97 acts downstream of RNF8 but upstream of ATXN3 at sites of DNA damage. To investigate how ATXN3 is recruited to sites of DNA damage, p97, RNF8 or RNF168 were depleted in U2OS cells before UV-A laser micro-irradiation. The cells were allowed to recover for 10 min before being fixed and analysed for recruitment of endogenous ATXN3 by IF (Fig 6.7A). Quantification of those laser lines revealed that neither RNF8 nor RNF168 affected the recruitment of ATXN3 to sites of damage at the tested time point. On the other hand, p97 depletion resulted in a slight but significant decrease in ATXN3 recruitment at 10 min after DNA damage. This indicated that ATXN3 recruitment, to a certain extent, depends on p97, but not on the classical

RNF8/RNF168 ubiquitin signaling cascade. To further verify the above result, the experiment was repeated using the specific allosteric p97 inhibitor NMS-873 at 10 μM for 2 hrs prior to the UV-A laser experiments (Fig 6.7B). After 10 min of recovery, the cells were fixed and stained for endogenous ATXN3. Quantification of the signal intensity at the site of DNA damage showed a significant reduction of ATXN3 recruitment in cells where p97 was allosterically inhibited. Together, these data showed that p97 is partially responsible for ATXN3 recruitment. The current results also indicate that there must be additional mechanism(s), which regulates ATXN3 recruitment to sites of DNA damage, independently of p97. Moreover, as p97 recruitment partially depends on RNF8, which does not apply for ATXN3, it is interesting to speculate that there are two different recruitment pathways for p97, with the one involving ATXN3 being independent of RNF8.

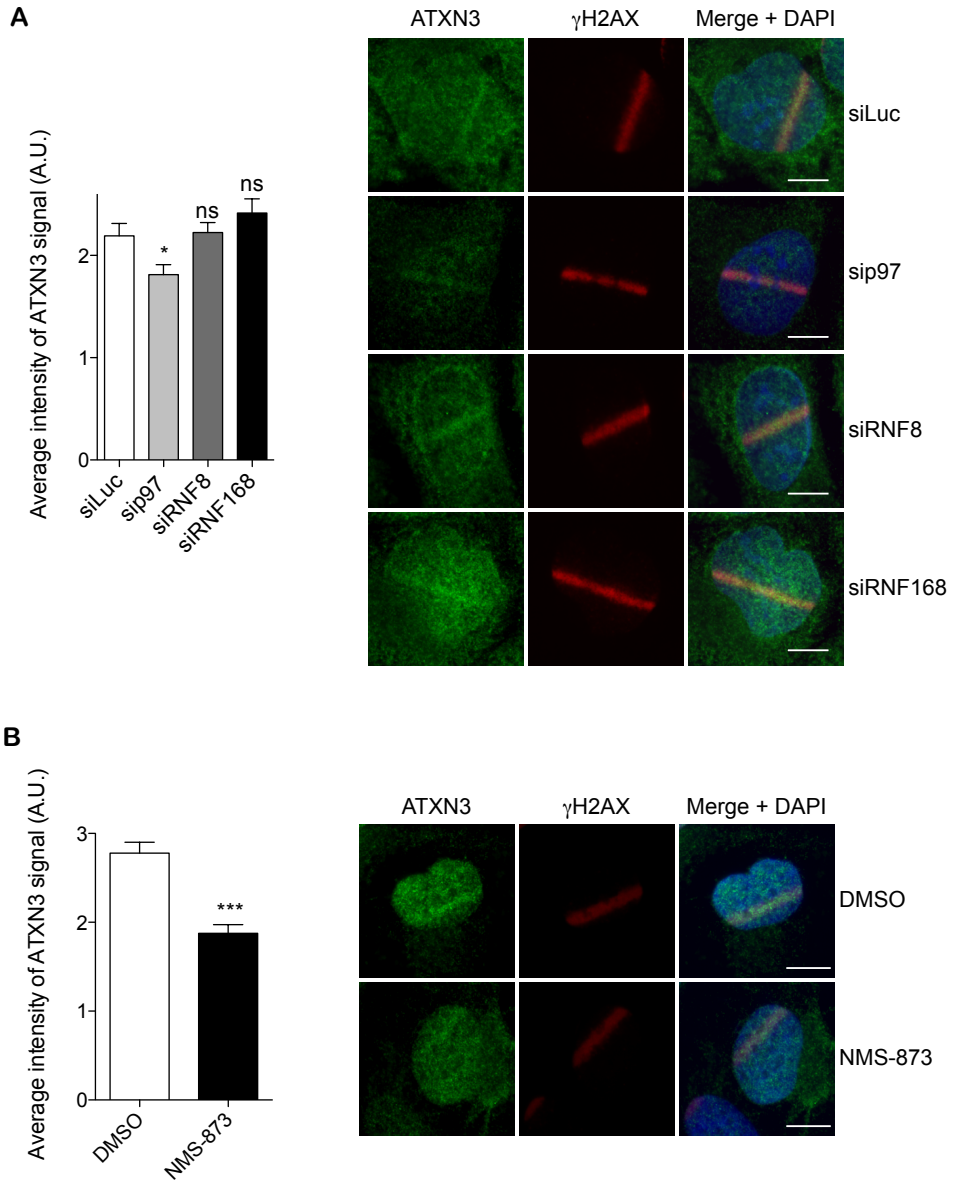


Figure 6-7. ATXN3 recruitment to the site of DNA damage depends partially on p97. A: U2OS cells were transfected with the indicated siRNAs for 72 hrs. UV-A laser damage was induced and the cells were allowed to recover for 10 min before fixation and immunostaining for endogenous ATXN3. Quantification of the ATXN3 signal at the site of DNA damage (γH2AX) is summarised in the blot next to the representative images. B: The allosteric p97 inhibitor NMS-873 (10 µM) or DMSO (control) was added to U2OS cells 2 hrs prior to UV-A laser experiments. Cells were left to recover 10 min before fixation and immunostaining. ATXN3 signal intensity was quantified at the sites of DNA damage (γH2AX) and normalised to DMSO treatment. Statistics: unpaired *t*-test; P value < 0.0001*, < 0.05*, > 0.05 ns; Mean + SEM; n = 2; > 100 lines per condition were analysed. Scale bar: 10 µm**

6.5 ATXN3 Forms A Physical Complex With p97$^{UFD1\text{-}NPL4}$

The p97 hexameric protein is capable of interacting with several cofactors simultaneously (Chapter 1.2.1). However, p97 interaction with its core cofactors, UFD1-NPL4 heterodimer, p47 and UBXD1, is mutually exclusive (Chapter 1.2.1). UFD1-NPL4 has been shown to be important for recruitment of p97 to sites of DNA damage (Meerang et al., 2011). However, ATXN3 is not needed to recruit p97 to sites of DNA damage, while p97 helps to recruit ATXN3 to the site of DNA damage. Therefore, it is possible that ATXN3 is part of the p97$^{UFD1\text{-}NPL4}$ complex and not an exclusive cofactor. To test this hypothesis, co-IPs were performed either over ectopically-expressed Strep-p97 or GFP-ATXN3 in HEK293T cells, co-overexpressing Myc-UFD1 for 36 hrs. Co-IPs were either performed using Streptavidin beads or GFP traps and for each condition a negative control was used to avoid the possibility that Myc-UFD1 binds to the beads unspecifically (Fig 6.8). The elutions were analysed first for p97, which was eluted in both co-IPs. The shift in size of the Strep-p97 in the elution (Fig 6.8, lane 3) is due to the tag of p97, which makes it run slightly higher in the SDS-PAGE. Blotting the elutions for UFD1 with a Myc-specific antibody revealed that UFD1 was eluted strongly in both co-IPs. Even though there was less p97 in the GFP-ATXN3 elution, there was more Myc-UFD1 eluted. This might be due to the fact that p97 can interact with many different cofactors and only some contain UFD1-NPL4, while ATXN3 might exclusively interact with p97$^{UFD1\text{-}NPL4}$.

Overall, this experiment shows that ATXN3 is part of a p97$^{UFD1\text{-}NPL4}$ complex. This is further supported by the finding that ATXN3 recruitment to sites of DNA damage is at least partially dependent on p97.

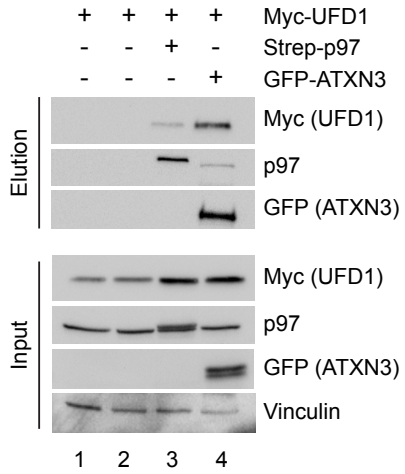


Figure 6-8. ATXN3 is part of the p97$^{UFD1-NPL4}$ complex. HEK293T cells were co-transfected with plasmids expressing Myc-UFD1 and either Strep-p97 or GFP-ATXN3 for 36 hrs before being collected. Co-IPs were performed over either Strep-Tactin Sepharose or GFP traps. Lane one is the loading of the negative control for the Strep-Tactin sepharose co-IP and lane 2 is the negative control for the GFP trap co-IP. UFD1 is pulled down over both p97 and ATXN3 (lane 3 and 4).

6.6 Discussion

The turnover of proteins at the site of DSB is a highly regulated process. Proteins bound to chromatin need to be removed to make space for other proteins. Hence, over- and underaccumulation of proteins will affect the efficiency of DSB repair. Our analysis of RNF8 recruitment shows that absence of either p97 or ATXN3 triggers a hyperaccumulation of this E3 ligase at the site of DNA damage early after DNA damage. In contrast, RNF168 displays initially reduced recruitment to the site of DNA damage upon ATXN3 depletion, but hyperaccumulates at the later time point. Thus, it appears that ATXN3 not only interacts with the ubiquitin ligases but is also involved in the accurate assembly and disassembly of these two main E3-ubiquitin ligases in the DDR. It has been suggested that RNF8 displays a much faster turnover at the site of DNA damage than RNF168, and also that lesser RNF8 is found at a DSB compared to RNF168 (Mok et al., 2014). As

the protein turnover must be tightly regulated at sites of DSBs, our data implies that ATXN3, possibly together with p97, is involved in this regulation. In addition, Dr Abhay Singh, a postdoctoral fellow in our laboratory, discovered that ATXN3 helps to stabilise RNF8 and RNF168 in unstressed cells. Specifically, CHX chase experiments have revealed that, in ATXN3 depleted conditions, the degradation rate of RNF8 and RNF168 is accelerated compared to control cells (Fig 6.9A and B). This suggests ATXN3 has an impact on the ligases even before DNA damage is induced.

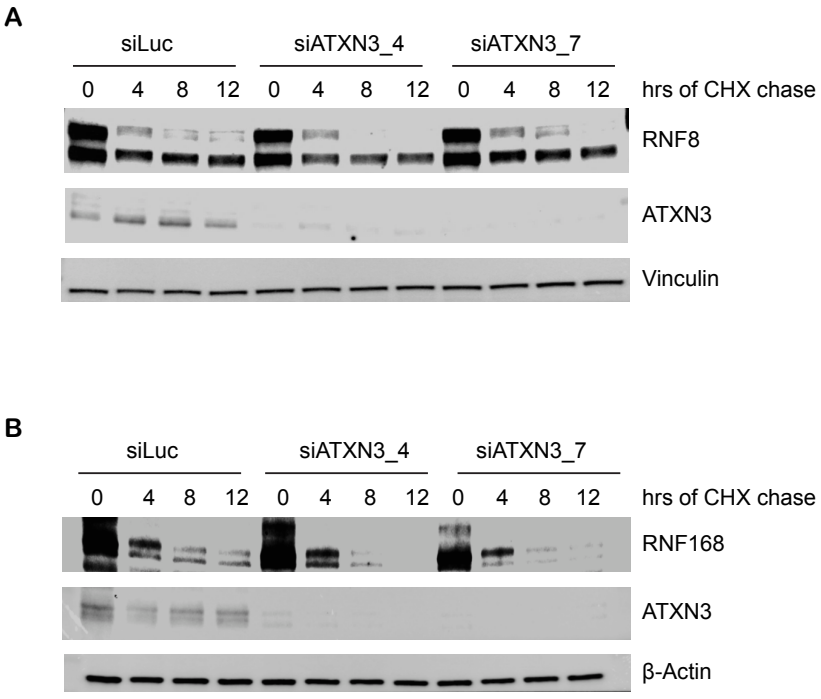


Figure 6-9. ATXN3 is involved in stabilising RNF8 and RNF168 in unstressed cells. A: HEK293 cells were depleted for ATXN3 with two different siRNA sequences for 72 hrs. Protein synthesis was then inhibited by addition of CHX (50 μm) for the indicated time and cells were collected at indicated time points. Turnover of RNF8 was visualised by Western blotting. B: Same as A but blotting for RNF168. Data by Dr Abhay Singh.

To our astonishment, absence of p97 nearly abolishes the complete pool of RNF168 in unstressed cells. This effect is neither cell line nor siRNA sequence specific but can be rescued by inhibition of the proteasome. Our experiments do

not address the molecular details of how p97 is involved in the regulation of RNF168 but strongly demonstrate that p97 is essential for RNF168 stability.

Recruitment of p97 depends on both RNF8 and its core adaptor heterodimer UFD1-NPL4. ATXN3 does not seem to be involved in the recruitment of p97 to the sites of DSBs, whereas the absence of p97 leads to slightly reduced recruitment of ATXN3 to the site of DNA damage. It is therefore not surprising that ATXN3 appears to be in a complex with $p97^{UFD1\text{-}NPL4}$. Yet, there must exist an additional signaling pathway involved in the recruitment of ATXN3 to the site of DNA damage as only a small proportion of ATXN3 is recruited over p97, and ATXN3 recruitment is completely independent of the RNF8/RNF168 ubiquitin cascade. ATXN3 is interacting with both components of the KU heterodimer. The KU complex is one of the first players that recognises and binds a DSB within seconds (Mari et al., 2006). One appealing possibility is that ATXN3 is recruited to the sites of DNA damage via the KU complex or possibly other PTMs like SUMOylation or even parylation.

Together, these results show that ATXN3, possibly in tight collaboration with p97, regulates the turnover of the ubiquitin ligases RNF8 and RNF168 at the site of DNA damage.

7 DISCUSSION

7.1 UBE4A And UBE4B Fine-Tune Ubiquitination At The Site Of DNA Damage

Ubiquitination has emerged as one of the major PTMs that the cell uses to organise its subcellular processes. Ubiquitination, initially discovered as a signature for proteasomal degradation in the late 1970s, has since turned out to be involved in virtually all cellular processes such as the innate immune response, vesicular trafficking, mitosis, cell division, DNA replication and the DNA damage response. Ubiquitination is a highly organised, dynamic and reversible process, involving hundreds of enzymes for both the addition and removal of ubiquitin to and from substrates (Amerik and Hochstrasser, 2004). A major function of ubiquitination lies in the protein homeostasis by the UPS. In this context, the ubiquitin-dependent AAA ATPase p97 plays a crucial role. Initially recognised as a fundamental player of ERAD (Xia et al., 2016), p97 soon turned out to be involved in many more processes, including membrane fusion, vesicle trafficking or endolysosomal sorting (Meyer and Weihl, 2014). p97 also works on the chromatin in collaboration with its core adaptor heterodimer UFD1-NPL4 complex and additional cofactors, facilitating cell cycle progression, replication, mitosis and transcription (Vaz et al., 2013). Recently, p97 has been implicated as a major regulator of the DDR (Acs et al., 2011; Meerang et al., 2011; Bergink et al., 2013; Kuo et al., 2016).

Induction of a DSB leads to excessive changes on the chromatin surrounding the lesion, most of which are induced by PTMs. This ensures the orchestrated recruitment of DSB mediator and repair proteins and the appropriate choice of

repair pathway, culminating in the repair of the lesion and resetting of the chromatin once repair is finished (Schwertman et al., 2016). Around a decade ago, K63-linked ubiquitin chains orchestrated by RNF8 were discovered as crucial regulators of the DDR (Huen et al., 2007; Kolas et al., 2007; Mailand et al., 2007). Its absence abolishes the recruitment of well-established DSB repair proteins such as BRCA1 and 53BP1. A few years later, RNF168 entered the picture (Doil et al., 2009; Pinato et al., 2009; Stewart et al., 2009), further underlying the importance of ubiquitin in the regulation of DSB repair. However, understanding the exact impact of these ligases has taken time and is still ongoing. Recently, in 2015, it was demonstrated that RNF8 targets mainly histone H1 for K63-linked polyubiquitination, thus recruiting RNF168 over the linker histone (Thorslund et al., 2015) to initiate ubiquitination on the core histones H2A and H2AX on K13 and K15 (Mattiroli et al., 2012; Thorslund et al., 2015). The different types of ubiquitin chain linkages add further complexity to the ubiquitin field, as it is still a burden to accurately analyse the linkages by common molecular biology tools *in vivo*. Historically, K63-linked ubiquitin chains have been implicated at the site of DNA damage, induced by the ligases via the E2-ubiquitin conjugating enzyme UBC13. These chains can be recognised by specific UBDs and help to recruit proteins. It has recently been shown that K48-linked chains (Meerang et al., 2011; Feng and Chen, 2012) and even non-canonical K27-linked ubiquitin chains are formed at the site of DNA damage (Gatti et al., 2015). While the K27-linked chains are formed by RNF168 (Gatti et al., 2015), the K48-linked chains might be formed by RNF8 via its interactions with the E2 UBCH8 or UBCH5C (Lok et al., 2012; Feng and Chen, 2012; Mattiroli et al., 2012). KU80, for instance, has been shown to be poly-ubiquitinated by

RNF8, targeting it for proteasomal degradation (Feng and Chen, 2012). Additional ligases have been implicated at the site of DNA damage, such as HERC2 (Bekker-Jensen et al., 2010), RNF169 (Chen et al., 2012; Poulsen et al., 2012) and RNF138 (Ismail et al., 2015), indicating that ubiquitination at the site of DNA damage is a highly complex system which will still need dedicated investigation to fully comprehend.

Our work, in collaboration with the laboratory of Yosef Shiloh, now introduces two additional ubiquitin ligases into the ubiquitin-dependent regulation of DNA damage. UBE4A and UBE4B are two cofactors of p97 and appear to play a role in the initial stage of the DDR as absence of either ligase negatively affects both major DSB repair pathways, HR and NHEJ. Taking advantage of linkage-specific antibodies has helped us to understand the different roles they play.

UBE4A could be the first ubiquitin E4 enzyme to be identified in the DDR. Firstly, its yeast homologue Ufd2 is the classical E4 enzyme, whose E4 activity has been shown to elongate existing short ubiquitin chains initiated by the E3 Ufd4 both *in vivo* and *in vitro* (Hoppe, 2005; Koegl et al., 1999). *In vitro* reactions with an E1, E2 and E3 yields short ubiquitin chains on the UFD substrate Ubi-GST, but upon addition of Ufd2, these chains are multiubiquitinated. *In vivo*, knock-out of Ufd2 leads to inefficient multiubiquitination of the short-lived substrate Ubi-Proβgal, demonstrating the importance of Ufd2 in accurate ubiquitination for protein turnover (Koegl et al., 1999). Secondly, we have observed that both K48- and K63-linked ubiquitin chains are markedly reduced upon UBE4A depletion at the sites of DNA damage. It would be of interest to investigate if UBE4A can act as an E4 together with either of the E3 ligases implicated at the sites of DNA damage. Consistent with the reduction in K48- and K63-linked ubiquitin at the site of DNA

damage, the number of 53BP1 foci upon NCS treatment is increased after 24 hrs of recovery, which are almost completely dissolved in control cells. The reduced ubiquitination could lead to severely impaired DSB repair efficiency in cells depleted of UBE4A making UBE4A an important fine-tuner at sites of DSBs (Fig 7.1).

UBE4B, an orthologue of UBE4A, and the second mammalian homologue of the yeast Ufd2, showed similar results for K63-linked ubiquitin chains as UBE4A. Absence of UBE4B negatively affects the accumulation of K63-linked ubiquitin chains at both tested time points. This could be due to intrinsic E3 or E4 activity of the UBE4B enzyme itself. However, in the case of K48-linked ubiquitin chains, depletion of UBE4B delayed the removal of these linkage-specific chains. This could indicate that UBE4B is involved in the removal of proteins targeted for degradation from the site of DNA damage. The Shiloh group has shown that UBE4B physically interacts with p97 (personal communication) and it is therefore interesting to speculate that UBE4B might be forming a complex with p97, targeting it to the K48-conjugated substrates, which it could further polyubiquitinate, allowing p97 to segregate the substrate and hand it over to the proteasome. In line with this idea is the observation that UBE4B depletion resulted in higher numbers of 53BP1 foci at 4 and 8 hrs post-IR exposure compared to control cells (personal communication with the Shiloh lab). Hence, 53BP1 could be one of the targets of the possible $p97^{UBE4B}$ complex. Moreover, it would be interesting to understand if other proteins also display slowed-down disassembly kinetics in this background.

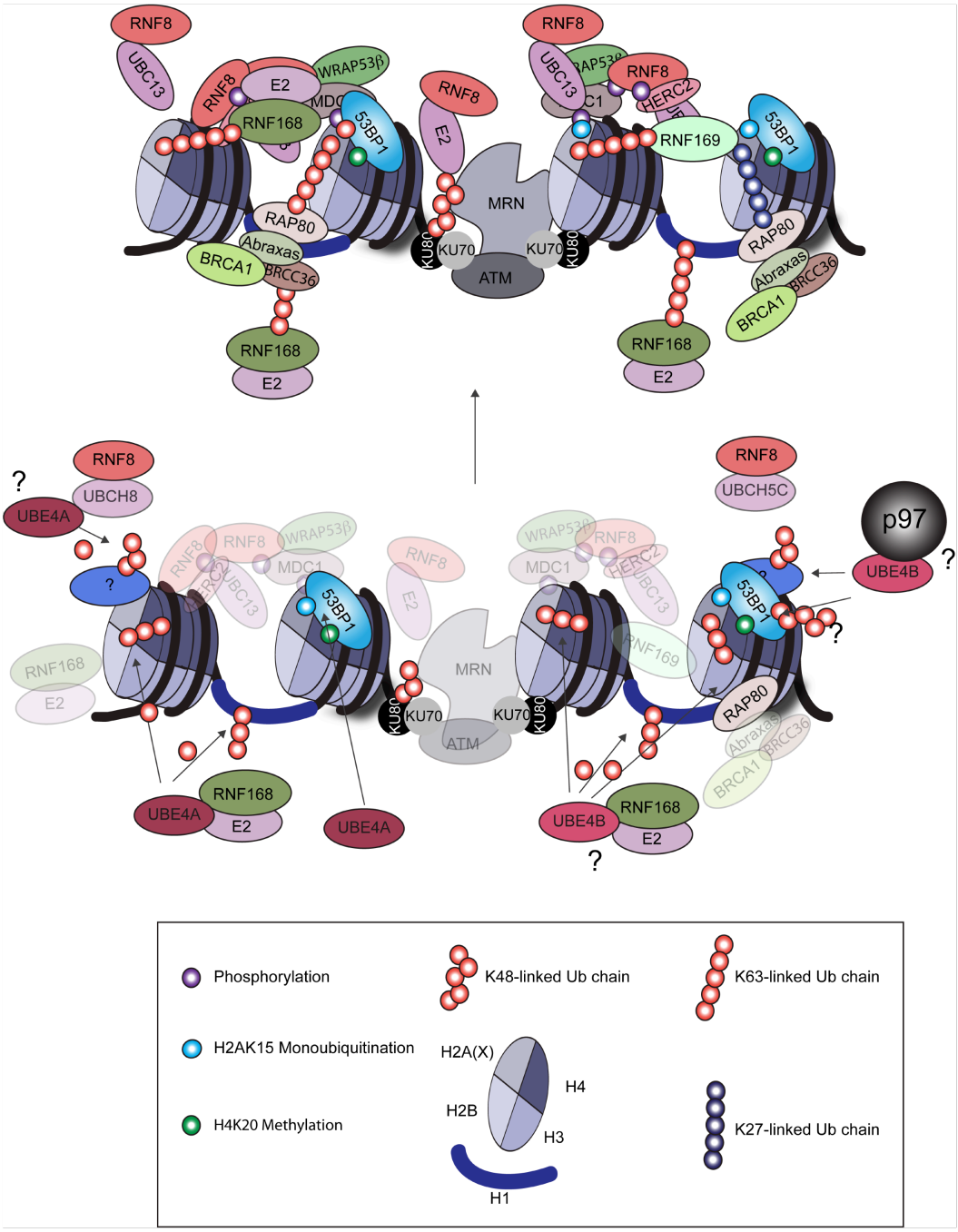


Figure 7-1. UBE4A and UBE4B are important new players in the maintenance of ubiquitination at the site of DNA damage. UBE4A could be a ubiquitin E4 enzyme at the site of DNA damage, supporting ligases in creating accurate ubiquitination at the site of DNA damage. Both K63- and K48-linked ubiquitin chains are affected in the absence of UBE4A and 53BP1 foci are not dissolved after 24 hrs of recovery from NCS treatment. UBE4B may be involved in the maintenance of K63-linked ubiquitin chains. Additionally, it may, in collaboration with p97, ubiquitinate substrate proteins with K48-linked ubiquitin chains, tagging them for removal via p97.

53BP1 has been shown to undergo a strong ubiquitination wave upon DNA damage that removes most of the 53BP1 and leads to its degradation, with only the 53BP1 close to the damaged area remaining (Hu et al., 2014). Hence, in a second wave, 53BP1 might again be ubiquitinated, possibly by RNF8, similar to KU80 (Feng and Chen, 2012), to be resolved after DSB repair has been performed (Fig 7.1).

7.2 ATXN3, A New DUB Involved In The Fine-Tuning Of DSB Repair

While ubiquitin ligases are required to create ubiquitin chains, DUBs are necessary to remove ubiquitin moieties or whole chains and are therefore important components of the ubiquitination cycle. DUBs have also been shown to be essential for the regulation of the DDR. Many of them have been shown to target H2A or H2AX K13/K15 ubiquitination induced by RNF8 and RNF168, such as USP3 (Sharma et al., 2014; Nicassio et al., 2007), USP17L2 (Delgado-Diaz et al., 2014) or USP51 (Wang et al., 2016b). The number of DUBs involved in the regulation of the core histone ubiquitination indicates that deubiquitination is a tightly regulated process, with different DUBs possibly performing similar roles.

Ubiquitin ligases are able to not only ubiquitinate substrates but also themselves and this can have a role in regulating ligase activity (de Bie and Ciechanover, 2011). RNF168 has been shown to be ubiquitinated in *trans* by TRIP12 and UBR5, which regulates the RNF168 pool in undamaged cells (Gudjonsson et al., 2012). Depletion of TRIP12 and UBR5 leads to an increased RNF168 pool and upon DNA damage, DSBs are hyperubiquitinated and increased BRCA1 and 53BP1 recruitment can be observed due to the hyperavailability of RNF168. Interestingly, several cancers have been reported to harbour aberrations of

TRIP12 and UBR5, suggesting that increased ubiquitination at the sites of DSBs is genotoxic, albeit the underlying mechanisms are not understood (Gudjonsson et al., 2012). Added control of RNF168 activity in unstressed cells is provided by the ubiquitin ligase HERC2 (Bekker-Jensen et al., 2010). Moreover, USP34 stabilises RNF168 by removing K48-linked ubiquitin chains from the ligase, both in unstressed and irradiated cells (Sy et al., 2013). Together, the data presented here show that the E3 ubiquitin ligase RNF168 is tightly controlled under physiological conditions and that its aberrant control affects DDR efficiency. Yet, no such regulator has been found for RNF8. HERC2 does impact RNF8 efficiency at the site of DNA damage by stabilising its interaction with UBC13 but no regulatory effect on the RNF8 pool or turnover has been reported in connection with HERC2 (Bekker-Jensen et al., 2010).

The ligases undergo rapid turnover at the site of DNA damage (Mok et al., 2014) with RNF8 displaying much faster turnover rates than RNF168. But how this turnover is regulated is still unclear. Our findings that ATXN3, a well-established cofactor of p97, and p97 itself strongly promote the disassembly of RNF8 at the site of DNA damage has shed light on the regulation of this essential E3 ligase in the DDR. In unstressed cells, we have observed that ATXN3 helps to stabilise RNF8. By CHX chase experiments we could observe an increased instability of the ligase in ATXN3 depleted cells. However, at the sites of DSBs, we have observed hyperaccumulation of RNF8 in both ATXN3 or p97 depleted cells. Hence, p97, partially supported by ATXN3, could help to segregate RNF8 away from the chromatin and thus regulate accurate turnover of the ligase (Fig 7.2). Additionally, ATXN3 affects assembly and disassembly of RNF168. As our data indicates that the interaction of RNF168 and ATXN3 depends on ubiquitination

of RNF168, it is possible that ATXN3 initially performs a protective role towards RNF168 by deubiquitinating it at the site of DNA damage, which could shield it from removal and degradation. As RNF168 has been shown to be involved in the redistribution of 53BP1 upon DSB induction (Bohgaki et al., 2013), the observed absence of RNF168 at the initial time point could explain the delayed 53BP1 foci formation shown in our kinetics analysis. In contrast to this initial role, at later time points of repair, ATXN3 could be involved in helping to remove RNF168 and RNF8 by targeting p97 to these two E3 ligases (Fig 7.2). Unfortunately, our existing data does not answer if p97 is involved in removing RNF168 from the site of DNA damage, as depletion or chemical inhibition of p97 eradicates the existing pool of RNF168 in cells (Fig 7.3).

RNF168 has been shown to play an important role in the formation of K63-linked ubiquitin chains. Our results support a model where RNF168 is neglectable for the formation of K48- and K63-linked ubiquitin chains. Firstly, depletion of p97 strongly affects stability of RNF168 to such an extent that we were unable to detect RNF168 recruitment to UV-A laser stripes. Moreover, Western blot analysis revealed that the reduction of RNF168 was as strong as in RNF168-depleted cells. These results show that p97 is indispensable for the maintenance of the RNF168 pool under physiological conditions. Secondly, in cells depleted for p97, we observe hyperaccumulation of both K48- and K63-linked chains, indicating that both chains are still excessively formed in the absence of p97 and hence RNF168. Absence of p97 leads to hyperaccumulation of RNF8. Therefore, our results strongly support a model where RNF8 is capable of forming both K48- and K63- linked chains while RNF168 is responsible for forming additional chains, such as the K27-linked ubiquitin chains as recently

demonstrated (Gatti et al., 2015). In p97 depleted cells, even though hyperubiquitination is occurring, both BRCA1 and 53BP1 recruitment is severely affected. It would be of interest to understand if the recruitment defects of these two mediator proteins induced by p97 depletion could be rescued by overexpressing RNF168 in those cells.

ATXN3 has been identified at sites of DNA damage in a DUB screen performed by the Jackson laboratory in 2014 (Nishi et al., 2014). While they observed direct recruitment of ATXN3 to the site of DNA damage, they did not observe a defect in repair efficiency in ATXN3-depleted cells after treatment with phleomycin, as assessed by neutral comet assay. Thus, ATXN3 did not draw much attention in the DDR field and was left unaddressed. However, in contrast to the DUB screen performed in the Jackson lab, we identified ATXN3 as an essential component in DDR and DSB repair after IR. The easiest explanation as to why we were able to identify ATXN3 as a novel DDR factor is that we used IR as the source of DNA damage, coupled to three sensitive assays. First, colony forming assay, second, analysis of 53BP1/y-H2AX foci, and third, mass-spectrometry on nuclear fractions. However, to further prove a direct role of ATXN3 in DSB repair we have to directly analyse DSB repair of the whole genome after IR in ATXN3-depleted cells by pulsed-field gel electrophoresis.

It has been shown that ATXN3 is regulated by UBE4B-mediated ubiquitination, followed by degradation (Matsumoto et al., 2004). Both UBE4B and ATXN3 are new players at the site of DNA damage. Therefore, it would be interesting to test the possibility that UBE4B is a regulator of ATXN3 at the site of DNA damage, interconnecting the data presented in this thesis.

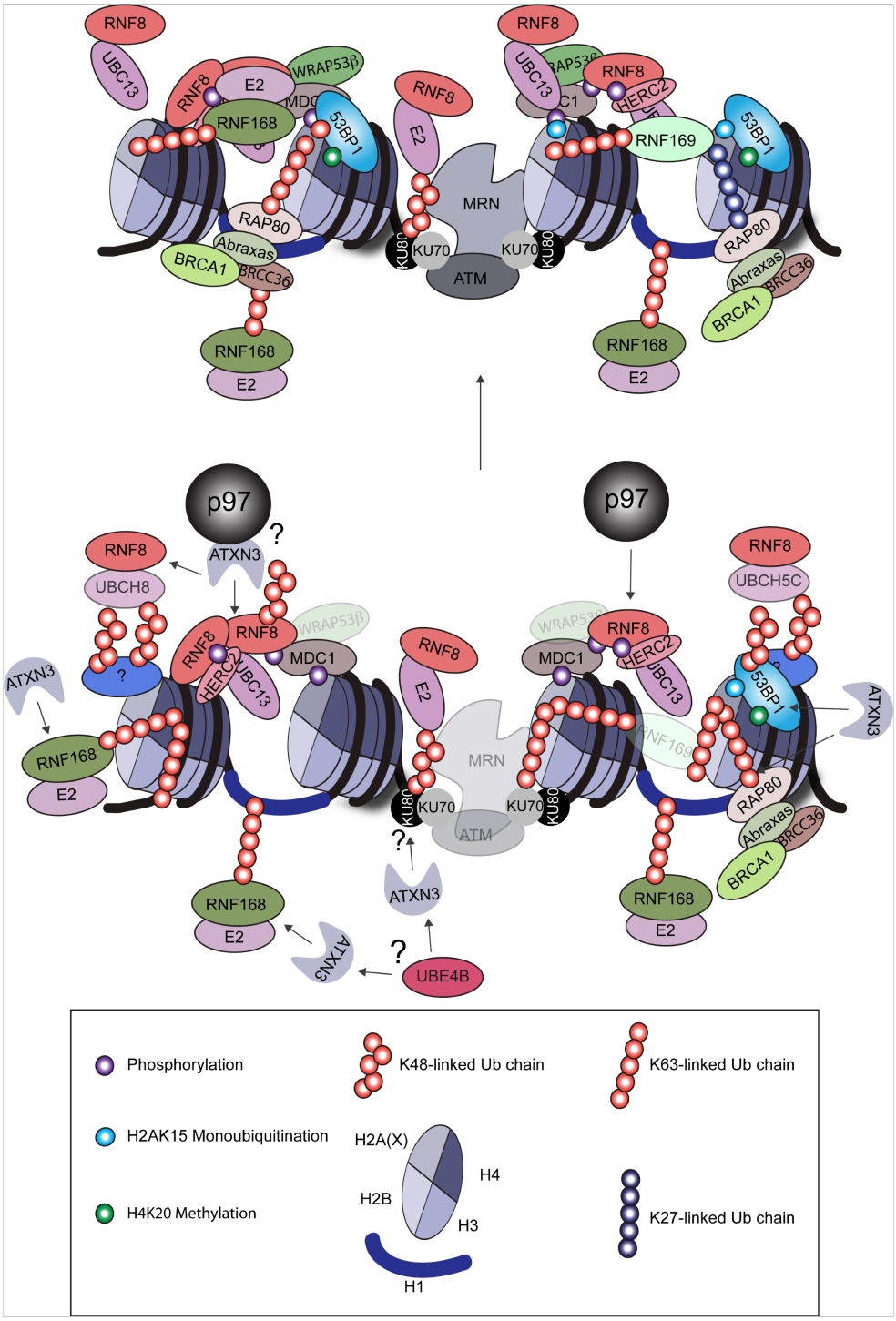


Figure 7-2. ATXN3 is a fine-tuner of RNF8 and RNF168 turnover at the site of DNA damage. Absence of ATXN3 or p97 leads to hyperaccumulation of RNF8 at the site of DNA damage. Therefore, ATXN3 could, possibly as a cofactor of p97, regulate the turnover of RNF8 at the site of DNA damage. Additionally, ATXN3 also leads to hyperaccumulation of RNF168 over time at the site of DNA damage. ATXN3 is therefore regulating the ubiquitination status at the site of DNA damage and the assembly and disassembly of the important DSB mediator proteins 53BP1 and BRCA1. As ATXN3 also interacts with the KU complex, it is possible that ATXN3 also regulates the turnover of this complex at the site of DNA damage. UBE4B could be a regulator of ATXN3 at the site of DNA damage.

Overall, our ongoing research suggests a model where ATXN3 plays a dual role. On one hand, in unstressed cells, ATXN3 appears to protect RNF8 and RNF168 from premature degradation by removing K48-ubiquitin from these two E3 ligases, and thus protecting them from premature proteasomal degradation. ATXN3 interacts with the two ligases in both untreated and irradiated cells, and this interaction strongly depends on the Josephine domain of ATXN3. This suggests that ATXN3 works as a DUB on the two enzymes, which is further supported by the CHX chase experiments. On the other hand, upon DSB induction, ATXN3 has a regulatory role in the turnover of those ligases at sites of DNA damage, possibly in collaboration with p97.

7.3 ATXN3 As A Possible Druggable Target For Cancer Therapy

Cancer is one of the major challenges of our society as around 40% of all people will be diagnosed with it during their lives (Siegel et al., 2016). Cancer is usually treated by chemotherapy, radiotherapy, surgery or combinations of any of the three treatments. Radiotherapy is the most commonly used means of treatment, with around 50% of the patients in the UK receiving this treatment. Thus, understanding the DDR to DSBs, especially those induced by IR, will help in the development of specific drugs that can be used to sensitise cancer cells to radiotherapy. Our findings on ATXN3 support such a notion. Depletion of ATXN3 strongly sensitises cells to IR. On the other hand, we have not observed any effect on cell growth or increased cell death in ATXN3 depleted cells in different cell lines. So far, our findings indicate that ATXN3-inactivation causes cell death only after IR. Thus, we anticipate that targeting ATXN3 will be an excellent approach for a two-hit cancer therapy based on IR and chemical inhibition of ATXN3

deubiquitinating activity. Our findings with ATXN3 should strongly encourage further investigation and possible screening for specific ATXN3 inhibitors. To this day, no such inhibitor is available. DUBs are considered interesting targets for treatment as, being cysteine proteases, they are easily druggable, which makes them more appealing than E3 ligases. The active site cysteines of DUBs are generally reactive to electrophiles and compounds containing α,β-unsaturated ketones have been successfully tested to inhibit cellular DUBs (D'Arcy et al., 2015).

7.4 Future Work

For almost ten years, researchers have been focusing on ubiquitination in the field of DSB repair. Yet, recent publications show that we are still far from understanding the exact mechanisms and impact of this PTM at sites of DNA damage. Future work might focus on the different ubiquitin linkages found at DSBs using high throughput tools such as mass spectrometry. High throughput screens will further identify proteins, such as DUBs and ligases, which are involved in the regulation and recognition of ubiquitination at sites of DNA damage. Moreover, further investigation into the nature of UBDs will help to understand how proteins can be specifically recruited and recognise their targets selectively.

REFERENCES

Acs, K., M.S. Luijsterburg, L. Ackermann, F.A. Salomons, T. Hoppe, and N.P. Dantuma. 2011. The AAA-ATPase VCP/p97 promotes 53BP1 recruitment by removing L3MBTL1 from DNA double-strand breaks. *Nat. Struct. Mol. Biol.* 18:1345–1350. doi:10.1038/nsmb.2188.

Al-Minawi, A.Z., N. Saleh-Gohari, and T. Helleday. 2008. The ERCC1/XPF endonuclease is required for efficient single-strand annealing and gene conversion in mammalian cells. *Nucleic Acids Res.* 36:1–9. doi:10.1093/nar/gkm888.

Amerik, A.Y., and M. Hochstrasser. 2004. Mechanism and function of deubiquitinating enzymes. *Biochim. Biophys. Acta - Mol. Cell Res.* 1695:189–207. doi:10.1016/j.bbamcr.2004.10.003.

Anderson, D.J., R. Le Moigne, S. Djakovic, B. Kumar, J. Rice, S. Wong, J. Wang, B. Yao, E. Valle, S. Kiss von Soly, A. Madriaga, F. Soriano, M.K. Menon, Z.Y. Wu, M. Kampmann, Y. Chen, J.S. Weissman, B.T. Aftab, F.M. Yakes, L. Shawver, H.J. Zhou, D. Wustrow, and M. Rolfe. 2015. Targeting the AAA ATPase p97 as an Approach to Treat Cancer through Disruption of Protein Homeostasis. *Cancer Cell*. 28:653–665. doi:10.1016/j.ccell.2015.10.002.

Arif, S., A. Rehman, Y.A. Kristariyanto, S. Choi, K. Labib, K. Hofmann, Y. Kulathu, S. Arif, A. Rehman, Y.A. Kristariyanto, S. Choi, P.J. Nkosi, and S. Weidlich. 2016. Short Article MINDY-1 Is a Member of an Evolutionarily Conserved and Structurally Distinct New Family of Deubiquitinating Enzymes Short Article MINDY-1 Is a Member of an Evolutionarily Conserved and Structurally Distinct New Family of Deubiquitinating Enz. *Mol. Cell*. 63:1–10. doi:10.1016/j.molcel.2016.05.009.

Baek, G.H., I. Kim, and H. Rao. 2011. The Cdc48 ATPase modulates the interaction between two proteolytic factors Ufd2 and Rad23. *Proc. Natl. Acad. Sci. U. S. A.* 108:13558–13563. doi:10.1073/pnas.1104051108.

Barber, L.J., J.L. Youds, J.D. Ward, M.J. McIlwraith, N.J. O'Neil, M.I.R. Petalcorin, J.S. Martin, S.J. Collis, S.B. Cantor, M. Auclair, H. Tissenbaum, S.C. West, A.M. Rose, and S.J. Boulton. 2008. RTEL1 maintains genomic stability by suppressing homologous recombination. *Cell*. 135:261–271.

doi:10.1016/j.cell.2008.08.016.

Bekker-Jensen, S., J. Rendtlew Danielsen, K. Fugger, I. Gromova, A. Nerstedt, C. Lukas, J. Bartek, J. Lukas, and N. Mailand. 2010. HERC2 coordinates ubiquitin-dependent assembly of DNA repair factors on damaged chromosomes. *Nat. Cell Biol.* 12:12–80. doi:10.1038/ncb2008.

Bergink, S., T. Ammon, M. Kern, L. Schermelleh, H. Leonhardt, and S. Jentsch. 2013. Role of Cdc48/p97 as a SUMO-targeted segregase curbing Rad51-Rad52 interaction. *Nat Cell Biol*. 15:526–532. doi:10.1038/ncb2729.

Berke, S.J.S., Y. Chai, G.L. Marrs, H. Wen, and H.L. Paulson. 2005. Defining the role of ubiquitin-interacting motifs in the polyglutamine disease protein, ataxin-3. *J. Biol. Chem.* 280:32026–32034. doi:10.1074/jbc.M506084200.

Bettencourt, C., and M. Lima. 2011. Machado-Joseph Disease: from first descriptions to new perspectives. *Orphanet J. Rare Dis.* 6:35. doi:10.1186/1750-1172-6-35.

Bhargava, R., D.O. Onyango, and J.M. Stark. 2016. Regulation of Single-Strand Annealing and its Role in Genome Maintenance. *Trends Genet.* 32:566–575. doi:10.1016/j.tig.2016.06.007.

Bhattacharyya, S., H. Yu, C. Mim, and A. Matouschek. 2014. Regulated protein turnover: snapshots of the proteasome in action. *Nat. Rev. Mol. Cell Biol.* 15:122–133. doi:10.1038/nrm3741.

de Bie, P., and a Ciechanover. 2011. Ubiquitination of E3 ligases: self-regulation of the ubiquitin system via proteolytic and non-proteolytic mechanisms. *Cell Death Differ.* 18:1393–1402. doi:10.1038/cdd.2011.16.

Biel, M., V. Wascholowski, and A. Giannis. 2004. A fatal affair: The ubiquitinylation of proteins. *Angew. Chemie - Int. Ed.* 43:6414–6416. doi:10.1002/anie.200462346.

Blount, J.R., W.-L. Tsou, G. Ristic, A.A. Burr, M. Ouyang, H. Galante, K.M. Scaglione, and S. V Todi. 2014. Ubiquitin-binding site 2 of ataxin-3 prevents its proteasomal degradation by interacting with Rad23. *Nat. Commun.* 5:4638. doi:10.1038/ncomms5638.

Boeddrich, A., S. Gaumer, A. Haacke, N. Tzvetkov, M. Albrecht, B.O. Evert, E.C. Muller, R. Lurz, P. Breuer, N. Schugardt, S. Plassmann, K. Xu, J.M. Warrick, J. Suopanki, U. Wullner, R. Frank, U.F. Hartl, N.M. Bonini, and E.E. Wanker.

2006. An arginine/lysine-rich motif is crucial for VCP/p97-mediated modulation of ataxin-3 fibrillogenesis. *EMBO J.* 25:1547–1558. doi:10.1038/sj.emboj.7601043.

Bohgaki, M., T. Bohgaki, S. El Ghamrasni, T. Srikumar, G. Maire, S. Panier, A. Fradet-Turcotte, G.S. Stewart, B. Raught, A. Hakem, and R. Hakem. 2013. RNF168 ubiquitylates 53BP1 and controls its response to DNA double-strand breaks. *Proc. Natl. Acad. Sci. U. S. A.* 110:20982–20987. doi:10.1073/pnas.1320302111.

Botuyan, M.V., J. Lee, I.M. Ward, J.-E. Kim, J.R. Thompson, J. Chen, and G. Mer. 2006. Structural basis for the methylation state-specific recognition of histone H4-K20 by 53BP1 and Crb2 in DNA repair. *Cell*. 127:1361–1373. doi:10.1016/j.cell.2006.10.043.

Bouwman, P., A. Aly, J.M. Escandell, M. Pieterse, J. Bartkova, H. van der Gulden, S. Hiddingh, M. Thanasoula, A. Kulkarni, Q. Yang, B.G. Haffty, J. Tommiska, C. Blomqvist, R. Drapkin, D.J. Adams, H. Nevanlinna, J. Bartek, M. Tarsounas, S. Ganesan, and J. Jonkers. 2010. 53BP1 loss rescues BRCA1 deficiency and is associated with triple-negative and BRCA-mutated breast cancers. *Nat. Struct. Mol. Biol.* 17:688–695. doi:10.1038/nsmb.1831.

Buchberger, A., H. Schindelin, and P. H??nzelmann. 2015. Control of p97 function by cofactor binding. *FEBS Lett.* 589:2578–2589. doi:10.1016/j.febslet.2015.08.028.

Bunting, S.F., E. Callen, N. Wong, H.-T. Chen, F. Polato, A. Gunn, A. Bothmer, N. Feldhahn, O. Fernandez-Capetillo, L. Cao, X. Xu, C.-X. Deng, T. Finkel, M. Nussenzweig, J.M. Stark, and A. Nussenzweig. 2010. 53BP1 inhibits homologous recombination in Brca1-deficient cells by blocking resection of DNA breaks. *Cell*. 141:243–254. doi:10.1016/j.cell.2010.03.012.

Burnett, B., F. Li, and R.N. Pittman. 2003. The polyglutamine neurodegenerative protein ataxin-3 binds polyubiquitylated proteins and has ubiquitin protease activity. *Hum. Mol. Genet.* 12:3195–3205. doi:10.1093/hmg/ddg344.

Burnett, B.G., and R.N. Pittman. 2005. The polyglutamine neurodegenerative protein ataxin 3 regulates aggresome formation. *Proc. Natl. Acad. Sci. U. S. A.* 102:4330–4335. doi:10.1073/pnas.0407252102.

Butler, L.R., R.M. Densham, J. Jia, A.J. Garvin, H.R. Stone, V. Shah, D. Weekes, F. Festy, J. Beesley, and J.R. Morris. 2012. The proteasomal de-ubiquitinating enzyme POH1 promotes the double-strand DNA break response. *EMBO J.* 31:3918–3934. doi:10.1038/emboj.2012.232.

Callen, E., M. Di Virgilio, M.J. Kruhlak, M. Nieto-Soler, N. Wong, H.T. Chen, R.B. Faryabi, F. Polato, M. Santos, L.M. Starnes, D.R. Wesemann, J.E. Lee, A. Tubbs, B.P. Sleckman, J.A. Daniel, K. Ge, F.W. Alt, O. Fernandez-Capetillo, M.C. Nussenzweig, and A. Nussenzweig. 2013. 53BP1 mediates productive and mutagenic DNA repair through distinct phosphoprotein interactions. *Cell*. 153:1266–1280. doi:10.1016/j.cell.2013.05.023.

Cannavo, E., and P. Cejka. 2014. Sae2 promotes dsDNA endonuclease activity within Mre11-Rad50-Xrs2 to resect DNA breaks. *Nature*. 514:122–125. doi:10.1038/nature13771.

Cao, L., X. Xu, S.F. Bunting, J. Liu, R.-H. Wang, L.L. Cao, J.J. Wu, T.-N. Peng, J. Chen, A. Nussenzweig, C.-X. Deng, and T. Finkel. 2009. A selective requirement for 53BP1 in the biological response to genomic instability induced by Brca1 deficiency. *Mol. Cell*. 35:534–541. doi:10.1016/j.molcel.2009.06.037.

Caren, H., A. Holmstrand, R.-M. Sjoberg, and T. Martinsson. 2006. The two human homologues of yeast UFD2 ubiquitination factor, UBE4A and UBE4B, are located in common neuroblastoma deletion regions and are subject to mutations in tumours. *Eur. J. Cancer*. 42:381–387. doi:10.1016/j.ejca.2005.09.030.

Carén, H., A. Holmstrand, R.M. Sjöberg, and T. Martinsson. 2006. The two human homologues of yeast UFD2 ubiquitination factor, UBE4A and UBE4B, are located in common neuroblastoma deletion regions and are subject to mutations in tumours. *Eur. J. Cancer*. 42:381–387. doi:10.1016/j.ejca.2005.09.030.

Ceccaldi, R., J.C. Liu, R. Amunugama, I. Hajdu, B. Primack, M.I.R. Petalcorin, K.W. O'Connor, P.A. Konstantinopoulos, S.J. Elledge, S.J. Boulton, T. Yusufzai, and A.D. D'Andrea. 2015. Homologous-recombination-deficient tumours are dependent on Polθ-mediated repair. *Nature*. 518:258–62. doi:10.1038/nature14184.

Centore, R.C., S.A. Yazinski, A. Tse, and L. Zou. 2012. Spartan/C1orf124, a reader

of PCNA ubiquitylation and a regulator of UV-induced DNA damage response. *Mol. Cell*. 46:625–635. doi:10.1016/j.molcel.2012.05.020.

Chai, Y., S.S. Berke, R.E. Cohen, and H.L. Paulson. 2004. Poly-ubiquitin binding by the polyglutamine disease protein ataxin-3 links its normal function to protein surveillance pathways. *J. Biol. Chem.* 279:3605–3611. doi:10.1074/jbc.M310939200.

Chai, Y., J. Shao, V.M. Miller, A. Williams, and H.L. Paulson. 2002. Live-cell imaging reveals divergent intracellular dynamics of polyglutamine disease proteins and supports a sequestration model of pathogenesis. *Proc. Natl. Acad. Sci. U. S. A.* 99:9310–9315. doi:10.1073/pnas.152101299.

Chapman, J.R., P. Barral, J.-B. Vannier, V. Borel, M. Steger, A. Tomas-Loba, A.A. Sartori, I.R. Adams, F.D. Batista, and S.J. Boulton. 2013. RIF1 is essential for 53BP1-dependent nonhomologous end joining and suppression of DNA double-strand break resection. *Mol. Cell*. 49:858–871. doi:10.1016/j.molcel.2013.01.002.

Chatterjee, A., S. Saha, A. Chakraborty, A. Silva-Fernandes, S.M. Mandal, A. Neves-Carvalho, Y. Liu, R.K. Pandita, M.L. Hegde, P.M. Hegde, I. Boldogh, T. Ashizawa, A.H. Koeppen, T.K. Pandita, P. Maciel, P.S. Sarkar, and T.K. Hazra. 2015. The role of the mammalian DNA end-processing enzyme polynucleotide kinase 3'-phosphatase in spinocerebellar ataxia type 3 pathogenesis. *PLoS Genet.* 11:e1004749. doi:10.1371/journal.pgen.1004749.

Chauhan, D., Z. Tian, B. Nicholson, K.G.S. Kumar, B. Zhou, R. Carrasco, J.L. McDermott, C.A. Leach, M. Fulcinniti, M.P. Kodrasov, J. Weinstock, W.D. Kingsbury, T. Hideshima, P.K. Shah, S. Minvielle, M. Altun, B.M. Kessler, R. Orlowski, P. Richardson, N. Munshi, and K.C. Anderson. 2012. A small molecule inhibitor of ubiquitin-specific protease-7 induces apoptosis in multiple myeloma cells and overcomes bortezomib resistance. *Cancer Cell*. 22:345–358. doi:10.1016/j.ccr.2012.08.007.

Chen, J., W. Feng, J. Jiang, Y. Deng, and M.S.Y. Huen. 2012. Ring finger protein RNF169 antagonizes the ubiquitin-dependent signaling cascade at sites of DNA damage. *J. Biol. Chem.* 287:27715–27722. doi:10.1074/jbc.M112.373530.

Chen, Z.J., and L.J. Sun. 2009. Nonproteolytic Functions of Ubiquitin in Cell Signaling. *Mol. Cell*. 33:275–286. doi:10.1016/j.molcel.2009.01.014.

Ciechanover, A. 2015. The unravelling of the ubiquitin system. *Nat. Rev. Mol. Cell Biol.* 16:322–324. doi:10.1038/nrm3982.

Coleman, K.A., and R.A. Greenberg. 2011. The BRCA1-RAP80 complex regulates DNA repair mechanism utilization by restricting end resection. *J. Biol. Chem.* 286:13669–13680. doi:10.1074/jbc.M110.213728.

Cooper, E.M., C. Cutcliffe, T.Z. Kristiansen, A. Pandey, C.M. Pickart, and R.E. Cohen. 2009. K63-specific deubiquitination by two JAMM/MPN+ complexes: BRISC-associated Brcc36 and proteasomal Poh1. *EMBO J.* 28:621–631. doi:10.1038/emboj.2009.27.

Costa, M. do C., and H.L. Paulson. 2012. Toward understanding Machado-Joseph disease. *Prog. Neurobiol.* 97:239–257. doi:10.1016/j.pneurobio.2011.11.006.

Coutinho, P., and C. Andrade. 1978. Autosomal dominant system degeneration in Portuguese families of the Azores Islands. A new genetic disorder involving cerebellar, pyramidal, extrapyramidal and spinal cord motor functions. *Neurology*. 28:703–709.

D'Arcy, P., X. Wang, and S. Linder. 2015. Deubiquitinase inhibition as a cancer therapeutic strategy. *Pharmacol. Ther.* 147:32–54. doi:10.1016/j.pharmthera.2014.11.002.

Danielsen, J.R., L.K. Povlsen, B.H. Villumsen, W. Streicher, J. Nilsson, M. Wikstrom, S. Bekker-Jensen, and N. Mailand. 2012. DNA damage-inducible SUMOylation of HERC2 promotes RNF8 binding via a novel SUMO-binding Zinc finger. *J. Cell Biol.* 197:179–187. doi:10.1083/jcb.201106152.

Davis, A.J., and D.J. Chen. 2013. DNA double strand break repair via non-homologous end-joining. *Transl. Cancer Res.* 2:130–143. doi:10.3978/j.issn.2218-676X.2013.04.02.

Davis, E.J., C. Lachaud, P. Appleton, T.J. Macartney, I. Nathke, and J. Rouse. 2012. DVC1 (C1orf124) recruits the p97 protein segregase to sites of DNA damage. *Nat. Struct. Mol. Biol.* 19:1093–1100. doi:10.1038/nsmb.2394.

Delgado-Diaz, M.R., Y. Martin, A. Berg, R. Freire, and V.A.J. Smits. 2014. Dub3 controls DNA damage signalling by direct deubiquitination of H2AX. *Mol. Oncol.* 8:884–893. doi:10.1016/j.molonc.2014.03.003.

Deshaies, R.J. 2014. Proteotoxic crisis, the ubiquitin-proteasome system, and cancer therapy. *BMC Biol.* 12:94. doi:10.1186/s12915-014-0094-0.

Devgan, S.S., O. Sanal, C. Doil, K. Nakamura, S.A. Nahas, K. Pettijohn, J. Bartek, C. Lukas, J. Lukas, and R.A. Gatti. 2011. Homozygous deficiency of ubiquitin-ligase ring-finger protein RNF168 mimics the radiosensitivity syndrome of ataxia-telangiectasia. *Cell Death Differ.* 18:1500–1506. doi:10.1038/cdd.2011.18.

Dextraze, M.-E., T. Gantchev, S. Girouard, and D. Hunting. 2010. DNA interstrand cross-links induced by ionizing radiation: An unsung lesion. *Mutat. Res. Mutat. Res.* 704:101–107. doi:10.1016/j.mrrev.2009.12.007.

Dikic, I., S. Wakatsuki, and K.J. Walters. 2009. Ubiquitin-binding domains - from structures to functions. *Nat. Rev. Mol. Cell Biol.* 10:659–671. doi:10.1038/nrm2767.

Dobrynin, G., O. Popp, T. Romer, S. Bremer, M.H.A. Schmitz, D.W. Gerlich, and H. Meyer. 2011. Cdc48/p97-Ufd1-Npl4 antagonizes Aurora B during chromosome segregation in HeLa cells. *J. Cell Sci.* 124:1571–1580. doi:10.1242/jcs.069500.

Doil, C., N. Mailand, S. Bekker-Jensen, P. Menard, D.H. Larsen, R. Pepperkok, J. Ellenberg, S. Panier, D. Durocher, J. Bartek, J. Lukas, and C. Lukas. 2009. RNF168 binds and amplifies ubiquitin conjugates on damaged chromosomes to allow accumulation of repair proteins. *Cell*. 136:435–446. doi:10.1016/j.cell.2008.12.041.

Donaldson, K.M., W. Li, K.A. Ching, S. Batalov, C.-C. Tsai, and C.A.P. Joazeiro. 2003. Ubiquitin-mediated sequestration of normal cellular proteins into polyglutamine aggregates. *Proc. Natl. Acad. Sci. U. S. A.* 100:8892–8897. doi:10.1073/pnas.1530212100.

Dong, Y., M.-A. Hakimi, X. Chen, E. Kumaraswamy, N.S. Cooch, A.K. Godwin, and R. Shiekhattar. 2003. Regulation of BRCC, a holoenzyme complex containing BRCA1 and BRCA2, by a signalosome-like subunit and its role in DNA repair. *Mol. Cell*. 12:1087–1099.

Doss-Pepe, E.W., E.S. Stenroos, W.G. Johnson, and K. Madura. 2003. Ataxin-3 interactions with rad23 and valosin-containing protein and its associations with ubiquitin chains and the proteasome are consistent with a role in

ubiquitin-mediated proteolysis. *Mol. Cell. Biol.* 23:6469–6483. doi:10.1128/MCB.23.18.6469-6483.2003.

Dou, H., C. Huang, M. Singh, P.B. Carpenter, and E.T.H. Yeh. 2010. Regulation of DNA repair through deSUMOylation and SUMOylation of replication protein A complex. *Mol. Cell*. 39:333–345. doi:10.1016/j.molcel.2010.07.021.

Du, C., H. Wu, and R.P. Leng. 2016. UBE4B targets phosphorylated p53 at serines 15 and 392 for degradation. *Oncotarget*. 7:2823–2836. doi:10.18632/oncotarget.6555.

Durcan, T.M., and E.A. Fon. 2011. Mutant ataxin-3 promotes the autophagic degradation of parkin. *Autophagy*. 7:233–234. doi:10.4161/auto.7.2.14224.

Durcan, T.M., M. Kontogiannea, N. Bedard, S.S. Wing, and E.A. Fon. 2012. Ataxin-3 deubiquitination is coupled to parkin ubiquitination via E2 ubiquitin-conjugating enzyme. *J. Biol. Chem.* 287:531–541. doi:10.1074/jbc.M111.288449.

Durcan, T.M., M. Kontogiannea, T. Thorarinsdottir, L. Fallon, A.J. Williams, A. Djarmati, T. Fantaneanu, H.L. Paulson, and E.A. Fon. 2011. The Machado-Joseph disease-associated mutant form of ataxin-3 regulates parkin ubiquitination and stability. *Hum. Mol. Genet.* 20:141–154. doi:10.1093/hmg/ddq452.

Eid, W., M. Steger, M. El-Shemerly, L.P. Ferretti, J. Pena-Diaz, C. Konig, E. Valtorta, A.A. Sartori, and S. Ferrari. 2010. DNA end resection by CtIP and exonuclease 1 prevents genomic instability. *EMBO Rep.* 11:962–968. doi:10.1038/embor.2010.157.

Ellisdon, A.M., B. Thomas, and S.P. Bottomley. 2006. The two-stage pathway of ataxin-3 fibrillogenesis involves a polyglutamine-independent step. *J. Biol. Chem.* 281:16888–16896. doi:10.1074/jbc.M601470200.

Esaki, M., and T. Ogura. 2010. ATP-bound form of the D1 AAA domain inhibits an essential function of Cdc48p/p97. *Biochem. Cell Biol.* 88:109–117. doi:10.1139/o09-116.

Escribano-Diaz, C., A. Orthwein, A. Fradet-Turcotte, M. Xing, J.T.F. Young, J. Tkac, M.A. Cook, A.P. Rosebrock, M. Munro, M.D. Canny, D. Xu, and D. Durocher. 2013. A cell cycle-dependent regulatory circuit composed of 53BP1-RIF1 and BRCA1-CtIP controls DNA repair pathway choice. *Mol. Cell*. 49:872–883.

doi:10.1016/j.molcel.2013.01.001.

Escribano-Díaz, C., A. Orthwein, A. Fradet-Turcotte, M. Xing, J.T.F. Young, J. Tkáč, M.A. Cook, A.P. Rosebrock, M. Munro, M.D. Canny, D. Xu, and D. Durocher. 2013. A Cell Cycle-Dependent Regulatory Circuit Composed of 53BP1-RIF1 and BRCA1-CtIP Controls DNA Repair Pathway Choice. *Mol. Cell*. 49:872–883. doi:10.1016/j.molcel.2013.01.001.

Feng, L., and J. Chen. 2012. The E3 ligase RNF8 regulates KU80 removal and NHEJ repair. *Nat. Struct. Mol. Biol.* 19:201–206. doi:10.1038/nsmb.2211.

Feng, L., K.W. Fong, J. Wang, W. Wang, and J. Chen. 2013. RIF1 counteracts BRCA1-mediated end resection during DNA repair. *J. Biol. Chem.* 288:11135–11143. doi:10.1074/jbc.M113.457440.

Finley, D. 2009. Recognition and processing of ubiquitin-protein conjugates by the proteasome. *Annu. Rev. Biochem.* 78:477–513. doi:10.1146/annurev.biochem.78.081507.101607.

Fradet-Turcotte, A., M.D. Canny, C. Escribano-Díaz, A. Orthwein, C.C.Y. Leung, H. Huang, M.-C. Landry, J. Kitevski-LeBlanc, S.M. Noordermeer, F. Sicheri, D. Durocher, F.S.& D.D. Amélie Fradet-Turcotte, Marella D. Canny, Cristina Escribano-Díaz, Alexandre Orthwein, Charles C. Y. Leung, Hao Huang, Marie-Claude Landry, Julianne Kitevski-LeBlanc, Sylvie M. Noordermeer, A. Fradet-Turcotte, M.D. Canny, C. Escribano-Díaz, A. Orthwein, C.C.Y. Leung, H. Huang, M.-C. Landry, J. Kitevski-LeBlanc, S.M. Noordermeer, F. Sicheri, and D. Durocher. 2013. 53BP1 is a reader of the DNA-damage-induced H2A Lys 15 ubiquitin mark. *Nature*. 499:50–4. doi:10.1038/nature12318.

Franz, A., M. Orth, P.A. Pirson, R. Sonneville, J.J. Blow, A. Gartner, O. Stemmann, and T. Hoppe. 2011. CDC-48/p97 coordinates CDT-1 degradation with GINS chromatin dissociation to ensure faithful DNA replication. *Mol. Cell*. 44:85–96. doi:10.1016/j.molcel.2011.08.028.

Franz, A., P.A. Pirson, D. Pilger, S. Halder, D. Achuthankutty, H. Kashkar, K. Ramadan, and T. Hoppe. 2016. Chromatin-associated degradation is defined by UBXN-3/FAF1 to safeguard DNA replication fork progression. *Nat. Commun.* 7:10612. doi:10.1038/ncomms10612.

Frit, P., N. Barboule, Y. Yuan, D. Gomez, and P. Calsou. 2014. Alternative end-joining pathway(s): bricolage at DNA breaks. *DNA Repair (Amst).* 17:81–97.

doi:10.1016/j.dnarep.2014.02.007.

Fu, X., C. Ng, D. Feng, and C. Liang. 2003. Cdc48p is required for the cell cycle commitment point at Start via degradation of the G1-CDK inhibitor Far1p. *J. Cell Biol.* 163:21–26. doi:10.1083/jcb.200307025.

Fullbright, G., H.B. Rycenga, J.D. Gruber, and D.T. Long. 2016. p97 Promotes a Conserved Mechanism of Helicase Unloading During DNA Crosslink Repair. *Mol. Cell. Biol.* doi:10.1128/MCB.00434-16.

Galanty, Y., R. Belotserkovskaya, J. Coates, and S.P. Jackson. 2012. RNF4, a SUMO-targeted ubiquitin E3 ligase, promotes DNA double-strand break repair. *Genes Dev.* 26:1179–1195. doi:10.1101/gad.188284.112.

Galanty, Y., R. Belotserkovskaya, J. Coates, S. Polo, K.M. Miller, and S.P. Jackson. 2009. Mammalian SUMO E3-ligases PIAS1 and PIAS4 promote responses to DNA double-strand breaks. *Nature*. 462:935–939. doi:10.1038/nature08657.

Gao, R., Y. Liu, A. Silva-Fernandes, X. Fang, A. Paulucci-Holthauzen, A. Chatterjee, H.L. Zhang, T. Matsuura, S. Choudhary, T. Ashizawa, A.H. Koeppen, P. Maciel, T.K. Hazra, and P.S. Sarkar. 2015. Inactivation of PNKP by mutant ATXN3 triggers apoptosis by activating the DNA damage-response pathway in SCA3. *PLoS Genet.* 11:e1004834. doi:10.1371/journal.pgen.1004834.

Garcia-Mata, R., Z. Bebok, E.J. Sorscher, and E.S. Sztul. 1999. Characterization and dynamics of aggresome formation by a cytosolic GFP-chimera. *J. Cell Biol.* 146:1239–1254.

Garvin, A.J., R.M. Densham, S.A. Blair-Reid, K.M. Pratt, H.R. Stone, D. Weekes, K.J. Lawrence, and J.R. Morris. 2013. The deSUMOylase SENP7 promotes chromatin relaxation for homologous recombination DNA repair. *EMBO Rep.* 14:975–983. doi:10.1038/embor.2013.141.

Gatti, M., S. Pinato, A. Maiolica, F. Rocchio, M.G. Prato, R. Aebersold, and L. Penengo. 2015. RNF168 promotes noncanonical K27 ubiquitination to signal DNA damage. *Cell Rep.* 10:226–238. doi:10.1016/j.celrep.2014.12.021.

Gatti, M., S. Pinato, E. Maspero, P. Soffientini, S. Polo, and L. Penengo. 2012. A novel ubiquitin mark at the N-terminal tail of histone H2As targeted by RNF168 ubiquitin ligase. *Cell Cycle*. 11:2538–2544. doi:10.4161/cc.20919.

Ghosal, G., J.W.-C. Leung, B.C. Nair, K.-W. Fong, and J. Chen. 2012. Proliferating cell nuclear antigen (PCNA)-binding protein C1orf124 is a regulator of translesion synthesis. *J. Biol. Chem.* 287:34225–34233. doi:10.1074/jbc.M112.400135.

Gibbs-Seymour, I., Y. Oka, E. Rajendra, B.T. Weinert, L.A. Passmore, K.J. Patel, J. V Olsen, C. Choudhary, S. Bekker-Jensen, and N. Mailand. 2015. Ubiquitin-SUMO circuitry controls activated fanconi anemia ID complex dosage in response to DNA damage. *Mol. Cell*. 57:150–164. doi:10.1016/j.molcel.2014.12.001.

Gottlich, B., S. Reichenberger, E. Feldmann, and P. Pfeiffer. 1998. Rejoining of DNA double-strand breaks in vitro by single-strand annealing. *Eur. J. Biochem.* 258:387–395.

Grabbe, C., K. Husnjak, and I. Dikic. 2011. The spatial and temporal organization of ubiquitin networks. *Nat. Rev. Mol. Cell Biol.* 12:295–307. doi:10.1038/nrm3099.

Grundy, G.J., H.A. Moulding, K.W. Caldecott, and S.L. Rulten. 2014. One ring to bring them all--the role of Ku in mammalian non-homologous end joining. *DNA Repair (Amst).* 17:30–38. doi:10.1016/j.dnarep.2014.02.019.

Gudjonsson, T., M. Altmeyer, V. Savic, L. Toledo, C. Dinant, M. Gr??fte, J. Bartkova, M. Poulsen, Y. Oka, S. Bekker-Jensen, N. Mailand, B. Neumann, J.K. Heriche, R. Shearer, D. Saunders, J. Bartek, J. Lukas, and C. Lukas. 2012. TRIP12 and UBR5 suppress spreading of chromatin ubiquitylation at damaged chromosomes. *Cell*. 150:697–709. doi:10.1016/j.cell.2012.06.039.

Guzzo, C.M., C.E. Berndsen, J. Zhu, V. Gupta, A. Datta, R.A. Greenberg, C. Wolberger, and M.J. Matunis. 2012. RNF4-dependent hybrid SUMO-ubiquitin chains are signals for RAP80 and thereby mediate the recruitment of BRCA1 to sites of DNA damage. *Sci. Signal.* 5:ra88. doi:10.1126/scisignal.2003485.

H??nzelmann, P., A. Buchberger, and H. Schindelin. 2011. Hierarchical binding of cofactors to the AAA ATPase p97. *Structure*. 19:833–843. doi:10.1016/j.str.2011.03.018.

Hanahan, D., and R.A. Weinberg. 2000. The hallmarks of cancer. *Cell*. 100:57–70.

Hanahan, D., and R.A. Weinberg. 2011. Hallmarks of cancer: the next generation. *Cell*. 144:646–674. doi:10.1016/j.cell.2011.02.013.

Hanna, J., N.A. Hathaway, Y. Tone, B. Crosas, S. Elsasser, D. Kirkpatrick, D.S. Leggett, S.P. Gygi, R.W. King, and D. Finley. 2006. Deubiquitinating Enzyme Ubp6 Functions Noncatalytically to Delay Proteasomal Degradation. *Cell*. 127:99–111. doi:10.1016/j.cell.2006.07.038.

Hardy, C.F.J., L. Sussel, and D. Shore. 1992. A RAP1-interacting protein involved in transcriptional silencing and telomere length regulation. *Genes Dev.* 6:801–814. doi:10.1101/gad.6.5.801.

Hatakeyama, S., M. Yada, M. Matsumoto, N. Ishida, and K.I. Nakayama. 2001. U box proteins as a new family of ubiquitin-protein ligases. *J. Biol. Chem.* 276:33111–33120. doi:10.1074/jbc.M102755200.

He, W.-T., X.-M. Zheng, Y.-H. Zhang, Y.-G. Gao, A.-X. Song, F.G. van der Goot, and H.-Y. Hu. 2016. Cytoplasmic Ubiquitin-Specific Protease 19 (USP19) Modulates Aggregation of Polyglutamine-Expanded Ataxin-3 and Huntingtin through the HSP90 Chaperone. *PLoS One*. 11:e0147515. doi:10.1371/journal.pone.0147515.

Helleday, T., S. Eshtad, and S. Nik-Zainal. 2014. Mechanisms underlying mutational signatures in human cancers. *Nat. Rev. Genet.* 15:585–598. doi:10.1038/nrg3729.

Henriksson, S., H. Rassoolzadeh, E. Hedstrom, C. Coucoravas, A. Julner, M. Goldstein, G. Imreh, B. Zhivotovsky, M.B. Kastan, T. Helleday, and M. Farnebo. 2014. The scaffold protein WRAP53beta orchestrates the ubiquitin response critical for DNA double-strand break repair. *Genes Dev.* 28:2726–2738. doi:10.1101/gad.246546.114.

Hershko, A., H. Heller, S. Elias, and A. Ciechanover. 1983. Components of Ubiquitin-Protein Ligase System. *J. Biol. Chem.* 258:8206–8214.

Hodge, C.D., I.H. Ismail, R.A. Edwards, G.L. Hura, A.T. Xiao, J.A. Tainer, M.J. Hendzel, and J.N.M. Glover. 2016. RNF8 E3 Ubiquitin Ligase Stimulates Ubc13 E2 Conjugating Activity That Is Essential for DNA Double Strand Break Signaling and BRCA1 Tumor Suppressor Recruitment. *J. Biol. Chem.* 291:9396–9410. doi:10.1074/jbc.M116.715698.

Hoppe, T. 2005. Multiubiquitylation by E4 enzymes: “One size” doesn’t fit all. *Trends Biochem. Sci.* 30:183–187. doi:10.1016/j.tibs.2005.02.004.

Hu, M., P. Li, L. Song, P.D. Jeffrey, T.A. Chenova, K.D. Wilkinson, R.E. Cohen, and Y.

Shi. 2005. Structure and mechanisms of the proteasome-associated deubiquitinating enzyme USP14. *EMBO J.* 24:3747–56. doi:10.1038/sj.emboj.7600832.

Hu, Y., R. Scully, B. Sobhian, A. Xie, E. Shestakova, and D.M. Livingston. 2011. RAP80-directed tuning of BRCA1 homologous recombination function at ionizing radiation-induced nuclear foci. *Genes Dev.* 25:685–700. doi:10.1101/gad.2011011.

Hu, Y., C. Wang, K. Huang, F. Xia, J.D. Parvin, and N. Mondal. 2014. Regulation of 53BP1 protein stability by RNF8 and RNF168 is important for efficient DNA double-strand break repair. *PLoS One*. 9:e110522. doi:10.1371/journal.pone.0110522.

Huen, M.S.Y., R. Grant, I. Manke, K. Minn, X. Yu, M.B. Yaffe, and J. Chen. 2007. RNF8 transduces the DNA-damage signal via histone ubiquitylation and checkpoint protein assembly. *Cell*. 131:901–914. doi:10.1016/j.cell.2007.09.041.

Ichikawa, Y., J. Goto, M. Hattori, A. Toyoda, K. Ishii, S.Y. Jeong, H. Hashida, N. Masuda, K. Ogata, F. Kasai, M. Hirai, P. Maciel, G.A. Rouleau, Y. Sakaki, and I. Kanazawa. 2001. The genomic structure and expression of MJD, the Machado-Joseph disease gene. *J. Hum. Genet.* 46:413–422. doi:10.1007/s100380170060.

Imai, Y., M. Soda, S. Hatakeyama, T. Akagi, T. Hashikawa, K.I. Nakayama, and R. Takahashi. 2002. CHIP is associated with Parkin, a gene responsible for familial Parkinson's Disease, and enhances its ubiquitin ligase activity. *Mol. Cell*. 10:55–67. doi:10.1016/S1097-2765(02)00583-X.

Ismail, I.H., J.-P. Gagné, M.-M. Genois, H. Strickfaden, D. McDonald, Z. Xu, G.G. Poirier, J.-Y. Masson, and M.J. Hendzel. 2015. The RNF138 E3 ligase displaces Ku to promote DNA end resection and regulate DNA repair pathway choice. *Nat. Cell Biol.* 17:1446–57. doi:10.1038/ncb3259.

Jacquet, K., A. Fradet-Turcotte, N. Avvakumov, J.-P. Lambert, C. Roques, R.K. Pandita, E. Paquet, P. Herst, A.-C. Gingras, T.K. Pandita, G. Legube, Y. Doyon, D. Durocher, and J. Cote. 2016. The TIP60 Complex Regulates Bivalent Chromatin Recognition by 53BP1 through Direct H4K20me Binding and H2AK15 Acetylation. *Mol. Cell*. 62:409–421.

doi:10.1016/j.molcel.2016.03.031.

Jiricny, J. 2006. The multifaceted mismatch-repair system. *Nat. Rev. Mol. Cell Biol.* 7:335–346. doi:10.1038/nrm1907.

Johnson, J.O., J. Mandrioli, M. Benatar, Y. Abramzon, V.M. Van Deerlin, J.Q. Trojanowski, J.R. Gibbs, M. Brunetti, S. Gronka, J. Wuu, J. Ding, L. McCluskey, M. Martinez-Lage, D. Falcone, D.G. Hernandez, S. Arepalli, S. Chong, J.C. Schymick, J. Rothstein, F. Landi, Y.-D. Wang, A. Calvo, G. Mora, M. Sabatelli, M.R. Monsurro, S. Battistini, F. Salvi, R. Spataro, P. Sola, G. Borghero, G. Galassi, S.W. Scholz, J.P. Taylor, G. Restagno, A. Chio, and B.J. Traynor. 2010. Exome sequencing reveals VCP mutations as a cause of familial ALS. *Neuron*. 68:857–864. doi:10.1016/j.neuron.2010.11.036.

Johnston, J.A., M.E. Illing, and R.R. Kopito. 2002. Cytoplasmic dynein/dynactin mediates the assembly of aggresomes. *Cell Motil. Cytoskeleton*. 53:26–38. doi:10.1002/cm.10057.

Johnston, J.A., C.L. Ward, and R.R. Kopito. 1998. Aggresomes: a cellular response to misfolded proteins. *J. Cell Biol.* 143:1883–1898.

Juang, Y.C., M.C. Landry, M. Sanches, V. Vittal, C.C.Y. Leung, D.F. Ceccarelli, A.R.F. Mateo, J.N. Pruneda, D.Y.L. Mao, R.K. Szilard, S. Orlicky, M. Munro, P.S. Brzovic, R.E. Klevit, F. Sicheri, and D. Durocher. 2012. OTUB1 Co-opts Lys48-Linked Ubiquitin Recognition to Suppress E2 Enzyme Function. *Mol. Cell*. 45:384–397. doi:10.1016/j.molcel.2012.01.011.

Jungmichel, S., and M. Stucki. 2010. MDC1: The art of keeping things in focus. *Chromosoma*. 119:337–349. doi:10.1007/s00412-010-0266-9.

Kalb, R., D.L. Mallery, C. Larkin, J.T.J. Huang, and K. Hiom. 2014. BRCA1 is a histone-H2A-specific ubiquitin ligase. *Cell Rep.* 8:999–1005. doi:10.1016/j.celrep.2014.07.025.

Kato, K., K. Nakajima, A. Ui, Y. Muto-Terao, H. Ogiwara, and S. Nakada. 2014. Fine-tuning of DNA damage-dependent ubiquitination by OTUB2 supports the DNA repair pathway choice. *Mol. Cell*. 53:617–630. doi:10.1016/j.molcel.2014.01.030.

Kawaguchi, Y., T. Okamoto, M. Taniwaki, M. Aizawa, M. Inoue, S. Katayama, H. Kawakami, S. Nakamura, M. Nishimura, and I. Akiguchi. 1994. CAG expansions in a novel gene for Machado-Joseph disease at chromosome

14q32.1. *Nat. Genet.* 8:221–228. doi:10.1038/ng1194-221.

Kent, T., G. Chandramouly, S.M. McDevitt, A.Y. Ozdemir, and R.T. Pomerantz. 2015. Mechanism of microhomology-mediated end-joining promoted by human DNA polymerase theta. *Nat Struct Mol Biol*. 22:230–237. doi:10.1038/nsmb.2961.

Kevei, É., and T. Hoppe. 2014. Ubiquitin sets the timer: impacts on aging and longevity. *Nat. Publ. Gr.* 21:290–292. doi:10.1038/nsmb.2806.

Kim, H., J. Chen, and X. Yu. 2007. Ubiquitin-binding protein RAP80 mediates BRCA1-dependent DNA damage response. *Science*. 316:1202–1205. doi:10.1126/science.1139621.

Kim, M.S., Y. Machida, A.A. Vashisht, J.A. Wohlschlegel, Y.-P. Pang, and Y.J. Machida. 2013. Regulation of error-prone translesion synthesis by Spartan/C1orf124. *Nucleic Acids Res.* 41:1661–1668. doi:10.1093/nar/gks1267.

Kimonis, V.E., M.J. Kovach, B. Waggoner, S. Leal, A. Salam, L. Rimer, K. Davis, R. Khardori, and D. Gelber. 2000. Clinical and molecular studies in a unique family with autosomal dominant limb-girdle muscular dystrophy and Paget disease of bone. *Genet. Med.* 2:232–241. doi:10.1097/00125817-200007000-00006.

Koegl, M., T. Hoppe, S. Schlenker, H.D. Ulrich, T.U. Mayer, and S. Jentsch. 1999. A Novel Ubiquitination Factor, E4, Is Involved in Multiubiquitin Chain Assembly. *Cell*. 96:635–644. doi:10.1016/S0092-8674(00)80574-7.

Kolas, N.K., J.R. Chapman, S. Nakada, J. Ylanko, R. Chahwan, F.D. Sweeney, S. Panier, M. Mendez, J. Wildenhain, T.M. Thomson, L. Pelletier, S.P. Jackson, and D. Durocher. 2007. Orchestration of the DNA-damage response by the RNF8 ubiquitin ligase. *Science*. 318:1637–1640. doi:10.1126/science.1150034.

Komander, D., and M. Rape. 2012. The Ubiquitin Code. *Annu. Rev. Biochem.* 81:203–229. doi:10.1146/annurev-biochem-060310-170328.

Kondo, H., C. Rabouille, R. Newman, T.P. Levine, D. Pappin, P. Freemont, and G. Warren. 1997. p47 is a cofactor for p97-mediated membrane fusion. *Nature*. 388:75–78. doi:10.1038/40411.

Koulich, E., X. Li, and G.N. DeMartino. 2008. Relative structural and functional

roles of multiple deubiquitylating proteins associated with mammalian 26S proteasome. *Mol. Biol. Cell*. 19:1072–1082. doi:10.1091/mbc.E07-10-1040.

Kravtsova-Ivantsiv, Y., T. Sommer, and A. Ciechanover. 2013. The Lysine48-Based polyubiquitin chain proteasomal signal: Not a single child anymore. *Angew. Chemie - Int. Ed.* 52:192–198. doi:10.1002/anie.201205656.

Kuo, C.-Y., X. Li, J.M. Stark, H.-M. Shih, and D.K. Ann. 2016. RNF4 regulates DNA double-strand break repair in a cell cycle-dependent manner. *Cell Cycle*. 15:787–798. doi:10.1080/15384101.2016.1138184.

Laco, M.N., L. Cortes, S.M. Travis, H.L. Paulson, and A.C. Rego. 2012. Valosin-containing protein (VCP/p97) is an activator of wild-type ataxin-3. *PLoS One*. 7:e43563. doi:10.1371/journal.pone.0043563.

Lee, D.-H., S.S. Acharya, M. Kwon, P. Drane, Y. Guan, G. Adelmant, P. Kalev, J. Shah, D. Pellman, J.A. Marto, and D. Chowdhury. 2014. Dephosphorylation enables the recruitment of 53BP1 to double-strand DNA breaks. *Mol. Cell*. 54:512–525. doi:10.1016/j.molcel.2014.03.020.

Lessel, D., B. Vaz, S. Halder, P.J. Lockhart, I. Marinovic-Terzic, J. Lopez-Mosqueda, M. Philipp, J.C.H. Sim, K.R. Smith, J. Oehler, E. Cabrera, R. Freire, K. Pope, A. Nahid, F. Norris, R.J. Leventer, M.B. Delatycki, G. Barbi, S. von Ameln, J. Högel, M. Degoricija, R. Fertig, M.D. Burkhalter, K. Hofmann, H. Thiele, J. Altmüller, G. Nürnberg, P. Nürnberg, M. Bahlo, G.M. Martin, C.M. Aalfs, J. Oshima, J. Terzic, D.J. Amor, I. Dikic, K. Ramadan, and C. Kubisch. 2014. Mutations in SPRTN cause early onset hepatocellular carcinoma, genomic instability and progeroid features. *Nat. Genet.* 46:1239–44. doi:10.1038/ng.3103.

Liang, C.-C., Z. Li, D. Lopez-Martinez, W. V Nicholson, C. Venien-Bryan, and M.A. Cohn. 2016. The FANCD2-FANCI complex is recruited to DNA interstrand crosslinks before monoubiquitination of FANCD2. *Nat. Commun.* 7:12124. doi:10.1038/ncomms12124.

Liang, C.-C., B. Zhan, Y. Yoshikawa, W. Haas, S.P. Gygi, and M.A. Cohn. 2015. UHRF1 is a sensor for DNA interstrand crosslinks and recruits FANCD2 to initiate the Fanconi anemia pathway. *Cell Rep.* 10:1947–1956. doi:10.1016/j.celrep.2015.02.053.

Lindahl, T. 1993. Instability and decay of the primary structure of DNA. *Nature*. 363:709–715. doi:10.1038/362709a0.

Liu, C., D. van Dyk, V. Choe, J. Yan, S. Majumder, M. Costanzo, X. Bao, C. Boone, K. Huo, M. Winey, H. Fisk, B. Andrews, and H. Rao. 2011. Ubiquitin ligase Ufd2 is required for efficient degradation of Mps1 kinase. *J. Biol. Chem.* 286:43660–43667. doi:10.1074/jbc.M111.286229.

Liu, C., S. Srihari, K.A.L. Cao, G. Chenevix-Trench, P.T. Simpson, M.A. Ragan, and K.K. Khanna. 2014. A fine-scale dissection of the DNA double-strand break repair machinery and its implications for breast cancer therapy. *Nucleic Acids Res.* 42:6106–6127. doi:10.1093/nar/gku284.

Lok, G.T.-M., S.M.-H. Sy, S.-S. Dong, Y.-P. Ching, S.W. Tsao, T.M. Thomson, and M.S.Y. Huen. 2012. Differential regulation of RNF8-mediated Lys48- and Lys63-based poly-ubiquitylation. *Nucleic Acids Res.* 40:196–205. doi:10.1093/nar/gkr655.

Lopez-Martinez, D., C.-C. Liang, and M.A. Cohn. 2016. Cellular response to DNA interstrand crosslinks: the Fanconi anemia pathway. *Cell. Mol. Life Sci.* 73:3097–3114. doi:10.1007/s00018-016-2218-x.

Lord, C.J., A.N.J. Tutt, and A. Ashworth. 2015. Synthetic lethality and cancer therapy: lessons learned from the development of PARP inhibitors. *Annu. Rev. Med.* 66:455–470. doi:10.1146/annurev-med-050913-022545.

Lukas, J., C. Lukas, and J. Bartek. 2011. More than just a focus: The chromatin response to DNA damage and its role in genome integrity maintenance. *Nat. Cell Biol.* 13:1161–1169. doi:10.1038/ncb2344.

Luo, K., H. Zhang, L. Wang, J. Yuan, and Z. Lou. 2012. Sumoylation of MDC1 is important for proper DNA damage response. *EMBO J.* 31:3008–3019. doi:10.1038/emboj.2012.158.

Ma, Y., U. Pannicke, K. Schwarz, and M.R. Lieber. 2002. Hairpin opening and overhang processing by an Artemis/DNA-dependent protein kinase complex in nonhomologous end joining and V(D)J recombination. *Cell*. 108:781–794. doi:10.1016/S0092-8674(02)00671-2.

Machida, Y., M.S. Kim, and Y.J. Machida. 2012. Spartan/C1orf124 is important to prevent UV-induced mutagenesis. *Cell Cycle*. 11:3395–3402. doi:10.4161/cc.21694.

Maciel, P., M.C. Costa, A. Ferro, M. Rousseau, C.S. Santos, C. Gaspar, J. Barros, G.A. Rouleau, P. Coutinho, and J. Sequeiros. 2001. Improvement in the molecular

diagnosis of Machado-Joseph disease. *Arch. Neurol.* 58:1821–1827.

Mailand, N., S. Bekker-Jensen, H. Faustrup, F. Melander, J. Bartek, C. Lukas, and J. Lukas. 2007. RNF8 ubiquitylates histones at DNA double-strand breaks and promotes assembly of repair proteins. *Cell*. 131:887–900. doi:10.1016/j.cell.2007.09.040.

Mallette, F.A., F. Mattiroli, G. Cui, L.C. Young, M.J. Hendzel, G. Mer, T.K. Sixma, and S. Richard. 2012. RNF8- and RNF168-dependent degradation of KDM4A/JMJD2A triggers 53BP1 recruitment to DNA damage sites. *EMBO J.* 31:1865–1878. doi:10.1038/emboj.2012.47.

Mari, P.-O., B.I. Florea, S.P. Persengiev, N.S. Verkaik, H.T. Bruggenwirth, M. Modesti, G. Giglia-Mari, K. Bezstarosti, J.A.A. Demmers, T.M. Luider, A.B. Houtsmuller, and D.C. van Gent. 2006. Dynamic assembly of end-joining complexes requires interaction between Ku70/80 and XRCC4. *Proc. Natl. Acad. Sci. U. S. A.* 103:18597–18602. doi:10.1073/pnas.0609061103.

Maric, M., T. Maculins, G. De Piccoli, and K. Labib. 2014. Cdc48 and a ubiquitin ligase drive disassembly of the CMG helicase at the end of DNA replication. *Science*. 346:1253596. doi:10.1126/science.1253596.

Marteijn, J. a, H. Lans, W. Vermeulen, and J.H.J. Hoeijmakers. 2014. Understanding nucleotide excision repair and its roles in cancer and ageing. *Nat. Rev. Mol. Cell Biol.* 15:465–81. doi:10.1038/nrm3822.

Mateos-Gomez, P.A., F. Gong, N. Nair, K.M. Miller, E. Lazzerini-Denchi, and A. Sfeir. 2015. Mammalian polymerase θ promotes alternative NHEJ and suppresses recombination. *Nature*. 518:254–7. doi:10.1038/nature14157.

Matos, J., and S.C. West. 2014. Holliday junction resolution: regulation in space and time. *DNA Repair (Amst).* 19:176–181. doi:10.1016/j.dnarep.2014.03.013.

Matsumoto, M., M. Yada, S. Hatakeyama, H. Ishimoto, T. Tanimura, S. Tsuji, A. Kakizuka, M. Kitagawa, and K.I. Nakayama. 2004. Molecular clearance of ataxin-3 is regulated by a mammalian E4. *EMBO J.* 23:659–669. doi:10.1038/sj.emboj.7600081.

Mattiroli, F., J.H.A. Vissers, W.J. van Dijk, P. Ikpa, E. Citterio, W. Vermeulen, J.A. Marteijn, and T.K. Sixma. 2012. RNF168 ubiquitinates K13-15 on H2A/H2AX to drive DNA damage signaling. *Cell*. 150:1182–1195.

doi:10.1016/j.cell.2012.08.005.

Mazin, A. V, O.M. Mazina, D. V Bugreev, and M.J. Rossi. 2010. Rad54, the motor of homologous recombination. *DNA Repair (Amst).* 9:286–302. doi:10.1016/j.dnarep.2009.12.006.

Mazzucchelli, S., A. De Palma, M. Riva, A. D'Urzo, C. Pozzi, V. Pastori, F. Comelli, P. Fusi, M. Vanoni, P. Tortora, P. Mauri, and M.E. Regonesi. 2009. Proteomic and biochemical analyses unveil tight interaction of ataxin-3 with tubulin. *Int. J. Biochem. Cell Biol.* 41:2485–2492. doi:10.1016/j.biocel.2009.08.003.

Meerang, M., D. Ritz, S. Paliwal, Z. Garajova, M. Bosshard, N. Mailand, P. Janscak, U. Hübscher, H. Meyer, and K. Ramadan. 2011. The ubiquitin-selective segregase VCP/p97 orchestrates the response to DNA double-strand breaks. *Nat. Cell Biol.* 13:1376–1382. doi:10.1038/ncb2367.

Méndez, J., and B. Stillman. 2000. Chromatin association of human origin recognition complex, cdc6, and minichromosome maintenance proteins during the cell cycle: assembly of prereplication complexes in late mitosis. *Mol. Cell. Biol.* 20:8602–12. doi:10.1128/MCB.20.22.8602-8612.2000.Updated.

Menon, V., and L.F. Povirk. 2016. End-processing nucleases and phosphodiesterases: An elite supporting cast for the non-homologous end joining pathway of DNA double-strand break repair. *DNA Repair (Amst).* 43:57–68. doi:10.1016/j.dnarep.2016.05.011.

Meray, R.K., and P.T. Lansbury. 2007. Reversible Monoubiquitination Regulates the Parkinson Disease-associated Ubiquitin Hydrolase UCH-L1. *J. Biol. Chem.* . 282:10567–10575. doi:10.1074/jbc.M611153200.

Meyer, H., M. Bug, and S. Bremer. 2012. Emerging functions of the VCP/p97 AAA-ATPase in the ubiquitin system. *Nat. Cell Biol.* 14:117–123. doi:10.1038/ncb2407.

Meyer, H., and C.C. Weihl. 2014. The VCP/p97 system at a glance: connecting cellular function to disease pathogenesis. *J. Cell Sci.* 127:3877–83. doi:10.1242/jcs.093831.

Michl, J., J. Zimmer, and M. Tarsounas. 2016. Interplay between Fanconi anemia and homologous recombination pathways in genome integrity. *EMBO J.* 35:909–923. doi:10.15252/embj.201693860.

Moir, D., S.E. Stewart, B.C. Osmond, and D. Botstein. 1982. Cold-sensitive cell-division-cycle mutants of yeast: isolation, properties, and pseudoreversion studies. *Genetics*. 100:547–563.

Mok, M.T.S., A.S.L. Cheng, and B.R. Henderson. 2014. The ubiquitin ligases RNF8 and RNF168 display rapid but distinct dynamics at DNA repair foci in living cells. *Int. J. Biochem. Cell Biol.* 57:27–34. doi:10.1016/j.biocel.2014.09.027.

Moreno, S.P., R. Bailey, N. Campion, S. Herron, and A. Gambus. 2014. Polyubiquitylation drives replisome disassembly at the termination of DNA replication. *Science*. 346:477–481. doi:10.1126/science.1253585.

Morris, J.R., C. Boutell, M. Keppler, R. Densham, D. Weekes, A. Alamshah, L. Butler, Y. Galanty, L. Pangon, T. Kiuchi, T. Ng, and E. Solomon. 2009. The SUMO modification pathway is involved in the BRCA1 response to genotoxic stress. *Nature*. 462:886–890. doi:10.1038/nature08593.

Mosbech, A., I. Gibbs-Seymour, K. Kagias, T. Thorslund, P. Beli, L. Povlsen, S.V. Nielsen, S. Smedegaard, G. Sedgwick, C. Lukas, R. Hartmann-Petersen, J. Lukas, C. Choudhary, R. Pocock, S. Bekker-Jensen, and N. Mailand. 2012. DVC1 (C1orf124) is a DNA damage-targeting p97 adaptor that promotes ubiquitin-dependent responses to replication blocks. *Nat. Struct. Mol. Biol.* 19:1084–1092. doi:10.1038/nsmb.2395.

Mosbech, A., C. Lukas, S. Bekker-Jensen, and N. Mailand. 2013. The deubiquitylating enzyme USP44 counteracts the DNA double-strand break response mediated by the RNF8 and RNF168 ubiquitin ligases. *J. Biol. Chem.* 288:16579–16587. doi:10.1074/jbc.M113.459917.

Mouysset, J., A. Deichsel, S. Moser, C. Hoege, A.A. Hyman, A. Gartner, and T. Hoppe. 2008. Cell cycle progression requires the CDC-48UFD-1/NPL-4 complex for efficient DNA replication. *Proc. Natl. Acad. Sci. U. S. A.* 105:12879–12884. doi:10.1073/pnas.0805944105.

Nakada, S., I. Tai, S. Panier, A. Al-Hakim, S.-I. Iemura, Y.-C. Juang, L. O'Donnell, A. Kumakubo, M. Munro, F. Sicheri, A.-C. Gingras, T. Natsume, T. Suda, and D. Durocher. 2010. Non-canonical inhibition of DNA damage-dependent ubiquitination by OTUB1. *Nature*. 466:941–946. doi:10.1038/nature09297.

Nakano, K.K., D.M. Dawson, and A. Spence. 1972. Machado disease. A hereditary ataxia in Portuguese emigrants to Massachusetts. *Neurology*. 22:49–55.

Newton, K., M.L. Matsumoto, I.E. Wertz, D.S. Kirkpatrick, J.R. Lill, J. Tan, D. Dugger, N. Gordon, S.S. Sidhu, F.A. Fellouse, L. Komuves, D.M. French, R.E. Ferrando, C. Lam, D. Compaan, C. Yu, I. Bosanac, S.G. Hymowitz, R.F. Kelley, and V.M. Dixit. 2008. Ubiquitin Chain Editing Revealed by Polyubiquitin Linkage-Specific Antibodies. *Cell*. 134:668–678. doi:10.1016/j.cell.2008.07.039.

Nicassio, F., N. Corrado, J.H.A. Vissers, L.B. Areces, S. Bergink, J.A. Marteijn, B. Geverts, A.B. Houtsmuller, W. Vermeulen, P.P. Di Fiore, and E. Citterio. 2007. Human USP3 is a chromatin modifier required for S phase progression and genome stability. *Curr. Biol.* 17:1972–1977. doi:10.1016/j.cub.2007.10.034.

Nicastro, G., S. V Todi, E. Karaca, A.M.J.J. Bonvin, H.L. Paulson, and A. Pastore. 2010. Understanding the role of the Josephin domain in the PolyUb binding and cleavage properties of ataxin-3. *PLoS One*. 5:e12430. doi:10.1371/journal.pone.0012430.

Nie, M., A. Aslanian, J. Prudden, J. Heideker, A.A. Vashisht, J.A. Wohlschlegel, J.R. Yates, and M.N. Boddy. 2012. Dual recruitment of Cdc48 (p97)-Ufd1-Npl4 ubiquitin-selective segregase by small ubiquitin-like modifier protein (SUMO) and ubiquitin in SUMO-targeted ubiquitin ligase-mediated genome stability functions. *J. Biol. Chem.* 287:29610–29619. doi:10.1074/jbc.M112.379768.

Nimonkar, A. V, J. Genschel, E. Kinoshita, P. Polaczek, J.L. Campbell, C. Wyman, P. Modrich, and S.C. Kowalczykowski. 2011. BLM-DNA2-RPA-MRN and EXO1-BLM-RPA-MRN constitute two DNA end resection machineries for human DNA break repair. *Genes Dev.* 25:350–362. doi:10.1101/gad.2003811.

Nishi, R., P. Wijnhoven, C. le Sage, J. Tjeertes, Y. Galanty, J. V Forment, M.J. Clague, S. Urbé, and S.P. Jackson. 2014. Systematic characterization of deubiquitylating enzymes for roles in maintaining genome integrity. *Nat. Cell Biol.* 16:1016–26, 1–8. doi:10.1038/ncb3028.

O'Connor, M.J. 2015. Targeting the DNA Damage Response in Cancer. *Mol. Cell*. 60:547–560. doi:10.1016/j.molcel.2015.10.040.

Ochi, T., A.N. Blackford, J. Coates, S. Jhujh, S. Mehmood, N. Tamura, J. Travers, Q. Wu, V.M. Draviam, C. V Robinson, T.L. Blundell, and S.P. Jackson. 2015. DNA repair. PAXX, a paralog of XRCC4 and XLF, interacts with Ku to promote DNA double-strand break repair. *Science (80-.).* 347:185–188.

doi:10.1126/science.1261971.

Ochs, F., K. Somyajit, M. Altmeyer, M.-B. Rask, J. Lukas, and C. Lukas. 2016. 53BP1 fosters fidelity of homology-directed DNA repair. *Nat. Struct. Mol. Biol.* 23:714–21. doi:10.1038/nsmb.3251.

Orthwein, A., A. Fradet-Turcotte, S.M. Noordermeer, M.D. Canny, C.M. Brun, J. Strecker, C. Escribano-Diaz, and D. Durocher. 2014. Mitosis inhibits DNA double-strand break repair to guard against telomere fusions. *Science*. 344:189–193. doi:10.1126/science.1248024.

Orthwein, A., S.M. Noordermeer, M.D. Wilson, S. Landry, R.I. Enchev, A. Sherker, M. Munro, J. Pinder, J. Salsman, G. Dellaire, B. Xia, M. Peter, and D. Durocher. 2015. A mechanism for the suppression of homologous recombination in G1 cells. *Nature*. 528:422–426. doi:10.1038/nature16142.

Ouyang, S., Y. Song, Y. Tian, Y. Chen, X. Yu, and D. Wang. 2015. RNF8 deficiency results in neurodegeneration in mice. *Neurobiol. Aging*. 36:2850–2860. doi:10.1016/j.neurobiolaging.2015.07.010.

Panier, S., Y. Ichijima, A. Fradet-Turcotte, C.C.Y. Leung, L. Kaustov, C.H. Arrowsmith, and D. Durocher. 2012. Tandem Protein Interaction Modules Organize the Ubiquitin-Dependent Response to DNA Double-Strand Breaks. *Mol. Cell*. 47:383–395. doi:10.1016/j.molcel.2012.05.045.

Periz, G., J. Lu, T. Zhang, M.W. Kankel, A.M. Jablonski, R. Kalb, A. McCampbell, and J. Wang. 2015. Regulation of protein quality control by UBE4B and LSD1 through p53-mediated transcription. *PLoS Biol.* 13:e1002114. doi:10.1371/journal.pbio.1002114.

Pinato, S., M. Gatti, C. Scandiuzzi, S. Confalonieri, and L. Penengo. 2011. UMI, a novel RNF168 ubiquitin binding domain involved in the DNA damage signaling pathway. *Mol. Cell. Biol.* 31:118–126. doi:10.1128/MCB.00818-10.

Pinato, S., C. Scandiuzzi, N. Arnaudo, E. Citterio, G. Gaudino, and L. Penengo. 2009. RNF168, a new RING finger, MIU-containing protein that modifies chromatin by ubiquitination of histones H2A and H2AX. *BMC Mol. Biol.* 10:55. doi:10.1186/1471-2199-10-55.

Poulsen, M., C. Lukas, J. Lukas, S. Bekker-Jensen, and N. Mailand. 2012. Human RNF169 is a negative regulator of the ubiquitin-dependent response to DNA double-strand breaks. *J. Cell Biol.* 197:189–199.

doi:10.1083/jcb.201109100.

Povirk, L.F., T. Zhou, R. Zhou, M.J. Cowan, and S.M. Yannone. 2007. Processing of 3'-phosphoglycolate-terminated DNA double strand breaks by artemis nuclease. *J. Biol. Chem.* 282:3547–3558. doi:10.1074/jbc.M607745200.

Puumalainen, M.-R., D. Lessel, P. Ruthemann, N. Kaczmarek, K. Bachmann, K. Ramadan, and H. Naegeli. 2014. Chromatin retention of DNA damage sensors DDB2 and XPC through loss of p97 segregase causes genotoxicity. *Nat. Commun.* 5:3695. doi:10.1038/ncomms4695.

Ramadan, K. 2012. p97/VCP- and Lys48-linked polyubiquitination form a new signaling pathway in DNA damage response. *Cell Cycle*. 11:1062–1069. doi:10.4161/cc.11.6.19446.

Ramadan, K., R. Bruderer, F.M. Spiga, O. Popp, T. Baur, M. Gotta, and H.H. Meyer. 2007. Cdc48/p97 promotes reformation of the nucleus by extracting the kinase Aurora B from chromatin. *Nature*. 450:1258–1262. doi:10.1038/nature06388.

Ramadan, K., S. Halder, K. Wiseman, and B. Vaz. 2016. Strategic role of the ubiquitin-dependent segregase p97 (VCP or Cdc48) in DNA replication. *Chromosoma*. doi:10.1007/s00412-016-0587-4.

Raman, M., C.G. Havens, J.C. Walter, and J.W. Harper. 2011. A Genome-wide Screen Identifies p97 as an Essential Regulator of DNA Damage-Dependent CDT1 Destruction. *Mol. Cell*. 44:72–84. doi:10.1016/j.molcel.2011.06.036.

Rassoolzadeh, H., C. Coucoravas, and M. Farnebo. 2015. The proximity ligation assay reveals that at DNA double-strand breaks WRAP53beta associates with gammaH2AX and controls interactions between RNF8 and MDC1. *Nucleus*. 6:417–424. doi:10.1080/19491034.2015.1106675.

Reina, C.P., X. Zhong, and R.N. Pittman. 2010. Proteotoxic stress increases nuclear localization of ataxin-3. *Hum. Mol. Genet.* 19:235–249. doi:10.1093/hmg/ddp482.

Richly, H., M. Rape, S. Braun, S. Rumpf, C. Hoege, and S. Jentsch. 2005. A series of ubiquitin binding factors connects CDC48/p97 to substrate multiubiquitylation and proteasomal targeting. *Cell*. 120:73–84. doi:10.1016/j.cell.2004.11.013.

Ritz, D., M. Vuk, P. Kirchner, M. Bug, S. Schütz, A. Hayer, S. Bremer, C. Lusk, R.H.

Baloh, H. Lee, T. Glatter, M. Gstaiger, R. Aebersold, C.C. Weihl, and H. Meyer. 2011. Endolysosomal sorting of ubiquitylated caveolin-1 is regulated by VCP and UBXD1 and impaired by VCP disease mutations. *Nat. Cell Biol.* 13:1116–23. doi:10.1038/ncb2301.

Rogakou, E.P., D.R. Pilch, A.H. Orr, V.S. Ivanova, and W.M. Bonner. 1998. Double-stranded Brekas Induce Histone H2AX phosphorylation on Serine 139. *J. Biol. Chem.* 273:5858–5868. doi:10.1074/jbc.273.10.5858.

Rosenberg, R.N., W.L. Nyhan, and C. Bay. 1976. Autosomal dominant striatonigral degeneration: a clinical, pathological, and biochemical study of a new genetic disorder. *Trans. Am. Neurol. Assoc.* 101:78–80.

Rouiller, I., B. DeLaBarre, A.P. May, W.I. Weis, A.T. Brunger, R.A. Milligan, and E.M. Wilson-Kubalek. 2002. Conformational changes of the multifunction p97 AAA ATPase during its ATPase cycle. *Nat Struct Biol*. 9:950–957. doi:10.1038/nsb872.

Sanders, S.L., M. Portoso, J. Mata, J. Bahler, R.C. Allshire, and T. Kouzarides. 2004. Methylation of histone H4 lysine 20 controls recruitment of Crb2 to sites of DNA damage. *Cell*. 119:603–614. doi:10.1016/j.cell.2004.11.009.

Sasagawa, Y., A. Higashitani, T. Urano, T. Ogura, and K. Yamanaka. 2012. CDC-48/p97 is required for proper meiotic chromosome segregation via controlling AIR-2/Aurora B kinase localization in Caenorhabditis elegans. *J. Struct. Biol.* 179:104–111. doi:10.1016/j.jsb.2012.06.009.

Sato, Y., A. Yamagata, S. Goto-Ito, K. Kubota, R. Miyamoto, S. Nakada, and S. Fukai. 2012. Molecular basis of Lys-63-linked polyubiquitination inhibition by the interaction between human deubiquitinating enzyme OTUB1 and ubiquitin-conjugating enzyme UBC13. *J. Biol. Chem.* 287:25860–25868. doi:10.1074/jbc.M112.364752.

Sato, Y., A. Yoshikawa, H. Mimura, M. Yamashita, A. Yamagata, and S. Fukai. 2009. Structural basis for specific recognition of Lys 63-linked polyubiquitin chains by tandem UIMs of RAP80. *EMBO J.* 28:2461–2468. doi:10.1038/emboj.2009.160.

Satoh, T., A. Sumiyoshi, M. Yagi-Utsumi, E. Sakata, H. Sasakawa, E. Kurimoto, Y. Yamaguchi, W. Li, C.A.P. Joazeiro, T. Hirokawa, and K. Kato. 2014. Mode of substrate recognition by the Josephin domain of ataxin-3, which has an

endo-type deubiquitinase activity. *FEBS Lett.* 588:4422–4430. doi:10.1016/j.febslet.2014.10.013.

Schols, L., P. Bauer, T. Schmidt, T. Schulte, and O. Riess. 2004. Autosomal dominant cerebellar ataxias: clinical features, genetics, and pathogenesis. *Lancet. Neurol.* 3:291–304. doi:10.1016/S1474-4422(04)00737-9.

Schuberth, C., and A. Buchberger. 2008. UBX domain proteins: Major regulators of the AAA ATPase Cdc48/p97. *Cell. Mol. Life Sci.* 65:2360–2371. doi:10.1007/s00018-008-8072-8.

Schwertman, P., S. Bekker-Jensen, and N. Mailand. 2016. Regulation of DNA double-strand break repair by ubiquitin and ubiquitin-like modifiers. *Nat Rev Mol Cell Biol*. 17:379–394. doi:10.1038/nrm.2016.58.

Shanbhag, N.M., I.U. Rafalska-Metcalf, C. Balane-Bolivar, S.M. Janicki, and R.A. Greenberg. 2010. ATM-dependent chromatin changes silence transcription in cis to DNA double-strand breaks. *Cell*. 141:970–981. doi:10.1016/j.cell.2010.04.038.

Shao, G., D.R. Lilli, J. Patterson-Fortin, K.A. Coleman, D.E. Morrissey, and R.A. Greenberg. 2009. The Rap80-BRCC36 de-ubiquitinating enzyme complex antagonizes RNF8-Ubc13-dependent ubiquitination events at DNA double strand breaks. *Proc. Natl. Acad. Sci. U. S. A.* 106:3166–3171. doi:10.1073/pnas.0807485106.

Sharma, N., Q. Zhu, G. Wani, J. He, Q. Wang, and A.A. Wani. 2014. USP3 counteracts RNF168 via deubiquitinating H2A and gammaH2AX at lysine 13 and 15. *Cell Cycle*. 13:106–114. doi:10.4161/cc.26814.

Siegel, R.L., K.D. Miller, and A. Jemal. 2016. Cancer statistics. *CA Cancer J Clin*. 66:7–30. doi:10.3322/caac.21332.

Sims, J.J., and R.E. Cohen. 2009. Linkage-Specific Avidity Defines the Lysine 63-Linked Polyubiquitin-Binding Preference of Rap80. *Mol. Cell*. 33:775–783. doi:10.1016/j.molcel.2009.02.011.

Sobhian, B., G. Shao, D.R. Lilli, A.C. Culhane, L.A. Moreau, B. Xia, D.M. Livingston, and R.A. Greenberg. 2007. RAP80 targets BRCA1 to specific ubiquitin structures at DNA damage sites. *Science*. 316:1198–1202. doi:10.1126/science.1139516.

Song, C., Q. Wang, and C.-C.H. Li. 2003. ATPase activity of p97-valosin-containing

protein (VCP). D2 mediates the major enzyme activity, and D1 contributes to the heat-induced activity. *J. Biol. Chem.* 278:3648–3655. doi:10.1074/jbc.M208422200.

Spasser, L., and A. Brik. 2012. Chemistry and biology of the ubiquitin signal. *Angew. Chemie - Int. Ed.* 51:6840–6862. doi:10.1002/anie.201200020.

Spratt, D.E., H. Walden, and G.S. Shaw. 2014. RBR E3 ubiquitin ligases: new structures, new insights, new questions. *Biochem. J.* 458:421–37. doi:10.1042/BJ20140006.

Stark, J.M., A.J. Pierce, J. Oh, A. Pastink, and M. Jasin. 2004. Genetic steps of mammalian homologous repair with distinct mutagenic consequences. *Mol. Cell. Biol.* 24:9305–9316. doi:10.1128/MCB.24.21.9305-9316.2004.

Stewart, G.S., S. Panier, K. Townsend, A.K. Al-Hakim, N.K. Kolas, E.S. Miller, S. Nakada, J. Ylanko, S. Olivarius, M. Mendez, C. Oldreive, J. Wildenhain, A. Tagliaferro, L. Pelletier, N. Taubenheim, A. Durandy, P.J. Byrd, T. Stankovic, A.M.R. Taylor, and D. Durocher. 2009. The RIDDLE syndrome protein mediates a ubiquitin-dependent signaling cascade at sites of DNA damage. *Cell*. 136:420–434. doi:10.1016/j.cell.2008.12.042.

Stewart, G.S., T. Stankovic, P.J. Byrd, T. Wechsler, E.S. Miller, A. Huissoon, M.T. Drayson, S.C. West, S.J. Elledge, and A.M.R. Taylor. 2007. RIDDLE immunodeficiency syndrome is linked to defects in 53BP1-mediated DNA damage signaling. *Proc. Natl. Acad. Sci. U. S. A.* 104:16910–16915. doi:10.1073/pnas.0708408104.

Stolz, A., W. Hilt, A. Buchberger, and D.H. Wolf. 2011. Cdc48: A power machine in protein degradation. *Trends Biochem. Sci.* 36:515–523. doi:10.1016/j.tibs.2011.06.001.

Stucki, M., J.A. Clapperton, D. Mohammad, M.B. Yaffe, S.J. Smerdon, and S.P. Jackson. 2005. MDC1 Directly Binds Phosphorylated Histone H2AX to Regulate Cellular Responses to DNA Double-Strand Breaks. *Cell*. 123:1213–1226. doi:10.1016/j.cell.2005.09.038.

Sun, Y., X. Jiang, S. Chen, N. Fernandes, and B.D. Price. 2005. A role for the Tip60 histone acetyltransferase in the acetylation and activation of ATM. *Proc. Natl. Acad. Sci. U. S. A.* 102:13182–13187. doi:10.1073/pnas.0504211102.

Sy, S.M.H., J. Jiang, W.S. O, Y. Deng, and M.S.Y. Huen. 2013. The ubiquitin specific

protease USP34 promotes ubiquitin signaling at DNA double-strand breaks. *Nucleic Acids Res.* 41:8572–8580. doi:10.1093/nar/gkt622.

Thorslund, T., A. Ripplinger, S. Hoffmann, T. Wild, M. Uckelmann, B. Villumsen, T. Narita, T.K. Sixma, C. Choudhary, S. Bekker-Jensen, and N. Mailand. 2015. Histone H1 couples initiation and amplification of ubiquitin signalling after DNA damage. *Nature*. 527:389–393. doi:10.1038/nature15401.

Todi, S. V, B.J. Winborn, K.M. Scaglione, J.R. Blount, S.M. Travis, and H.L. Paulson. 2009. Ubiquitination directly enhances activity of the deubiquitinating enzyme ataxin-3. *EMBO J.* 28:372–82. doi:10.1038/emboj.2008.289.

Truong, L.N., Y. Li, L.Z. Shi, P.Y.-H. Hwang, J. He, H. Wang, N. Razavian, M.W. Berns, and X. Wu. 2013. Microhomology-mediated End Joining and Homologous Recombination share the initial end resection step to repair DNA double-strand breaks in mammalian cells. *Proc. Natl. Acad. Sci. U. S. A.* 110:7720–7725. doi:10.1073/pnas.1213431110.

Vaz, B., S. Halder, and K. Ramadan. 2013. Role of p97/VCP (Cdc48) in genome stability. *Front. Genet.* 4:60. doi:10.3389/fgene.2013.00060.

Vekaria, P.H., T. Home, S. Weir, F.J. Schoenen, and R. Rao. 2016. Targeting p97 to Disrupt Protein Homeostasis in Cancer. *Front. Oncol.* 6:181. doi:10.3389/fonc.2016.00181.

Verma, R., R. Oania, R. Fang, G.T. Smith, and R.J. Deshaies. 2011. Cdc48/p97 mediates UV-dependent turnover of RNA Pol II. *Mol. Cell*. 41:82–92. doi:10.1016/j.molcel.2010.12.017.

Di Virgilio, M., E. Callen, A. Yamane, W. Zhang, M. Jankovic, A.D. Gitlin, N. Feldhahn, W. Resch, T.Y. Oliveira, B.T. Chait, A. Nussenzweig, R. Casellas, D.F. Robbiani, and M.C. Nussenzweig. 2013. Rif1 prevents resection of DNA breaks and promotes immunoglobulin class switching. *Science*. 339:711–5. doi:10.1126/science.1230624.

Wang, B., and S.J. Elledge. 2007. Ubc13/Rnf8 ubiquitin ligases control foci formation of the Rap80/Abraxas/Brca1/Brcc36 complex in response to DNA damage. *Proc. Natl. Acad. Sci. U. S. A.* 104:20759–20763. doi:10.1073/pnas.0710061104.

Wang, B., S. Matsuoka, B.A. Ballif, D. Zhang, A. Smogorzewska, S.P. Gygi, and S.J. Elledge. 2007. Abraxas and RAP80 form a BRCA1 protein complex required

for the DNA damage response. *Science*. 316:1194–1198. doi:10.1126/science.1139476.

Wang, J., A. Aroumougame, M. Lobrich, Y. Li, D. Chen, J. Chenj, and Z. Gong. 2014. PTIP associates with artemis to dictate DNA repair pathway choice. *Genes Dev.* 28:2693–2698. doi:10.1101/gad.252478.114.

Wang, Y., N. Zhang, L. Zhang, R. Li, W. Fu, K. Ma, X. Li, L. Wang, J. Wang, H. Zhang, W. Gu, W.-G. Zhu, and Y. Zhao. 2016a. Autophagy Regulates Chromatin Ubiquitination in DNA Damage Response through Elimination of SQSTM1/p62. *Mol. Cell*. 63:34–48. doi:10.1016/j.molcel.2016.05.027.

Wang, Z., H. Zhang, J. Liu, A. Cheruiyot, J.-H. Lee, T. Ordog, Z. Lou, Z. You, and Z. Zhang. 2016b. USP51 deubiquitylates H2AK13,15ub and regulates DNA damage response. *Genes Dev.* 30:946–959. doi:10.1101/gad.271841.115.

Watanabe, S., K. Watanabe, V. Akimov, J. Bartkova, B. Blagoev, J. Lukas, and J. Bartek. 2013. JMJD1C demethylates MDC1 to regulate the RNF8 and BRCA1-mediated chromatin response to DNA breaks. *Nat. Struct. Mol. Biol.* 20:1425–1433. doi:10.1038/nsmb.2702.

Weaver, B.A.A., and D.W. Cleveland. 2006. Does aneuploidy cause cancer? *Curr. Opin. Cell Biol.* 18:658–667. doi:10.1016/j.ceb.2006.10.002.

Weinstock, J., J. Wu, P. Cao, W.D. Kingsbury, J.L. McDermott, M.P. Kodrasov, D.M. McKelvey, K.G. Suresh Kumar, S.J. Goldenberg, M.R. Mattern, and B. Nicholson. 2012. Selective Dual Inhibitors of the Cancer-Related Deubiquitylating Proteases USP7 and USP47. *ACS Med. Chem. Lett.* 3:789–792. doi:10.1021/ml200276j.

Wiener, R., X. Zhang, T. Wang, and C. Wolberger. 2012. The mechanism of OTUB1-mediated inhibition of ubiquitination. *Nature*. 483:618–22. doi:10.1038/nature10911.

Wilcox, A.J., and J.D. Laney. 2009. A ubiquitin-selective AAA-ATPase mediates transcriptional switching by remodelling a repressor-promoter DNA complex. *Nat. Cell Biol.* 11:1481–1486. doi:10.1038/ncb1997.

Wilson, M.D., S. Benlekbir, A. Fradet-Turcotte, A. Sherker, J.-P. Julien, A. McEwan, S.M. Noordermeer, F. Sicheri, J.L. Rubinstein, and D. Durocher. 2016. The structural basis of modified nucleosome recognition by 53BP1. *Nature*. 536:100–103. doi:10.1038/nature18951.

Winborn, B.J., S.M. Travis, S. V. Todi, K.M. Scaglione, P. Xu, A.J. Williams, R.E. Cohen, J. Peng, and H.L. Paulson. 2008a. The deubiquitinating enzyme ataxin-3, a polyglutamine disease protein, edits Lys63 linkages in mixed linkage ubiquitin chains. *J. Biol. Chem.* 283:26436–26443. doi:10.1074/jbc.M803692200.

Winborn, B.J., S.M. Travis, S. V Todi, K.M. Scaglione, P. Xu, A.J. Williams, R.E. Cohen, J. Peng, and H.L. Paulson. 2008b. The deubiquitinating enzyme ataxin-3, a polyglutamine disease protein, edits Lys63 linkages in mixed linkage ubiquitin chains. *J. Biol. Chem.* 283:26436–26443. doi:10.1074/jbc.M803692200.

Woodfield, S.E., R.J. Guo, Y. Liu, A.M. Major, E.F. Hollingsworth, S. Indiviglio, S.B. Whittle, Q. Mo, A.J. Bean, M. Ittmann, D. Lopez-Terrada, and P.E. Zage. 2016. Neuroblastoma patient outcomes, tumor differentiation, and ERK activation are correlated with expression levels of the ubiquitin ligase UBE4B. *Genes Cancer*. 7:13–26. doi:10.18632/genesandcancer.97.

Wu, H., S.L. Pomeroy, M. Ferreira, N. Teider, J. Mariani, K.I. Nakayama, S. Hatakeyama, V.A. Tron, L.F. Saltibus, L. Spyracopoulos, and R.P. Leng. 2011a. UBE4B promotes Hdm2-mediated degradation of the tumor suppressor p53. *Nat. Med.* 17:347–355. doi:10.1038/nm.2283.

Wu, J., Y. Chen, L.-Y. Lu, Y. Wu, M.T. Paulsen, M. Ljungman, D.O. Ferguson, and X. Yu. 2011b. Chfr and RNF8 synergistically regulate ATM activation. *Nat. Struct. Mol. Biol.* 18:761–768. doi:10.1038/nsmb.2078.

Wu, J., M.S.Y. Huen, L.-Y. Lu, L. Ye, Y. Dou, M. Ljungman, J. Chen, and X. Yu. 2009. Histone ubiquitination associates with BRCA1-dependent DNA damage response. *Mol. Cell. Biol.* 29:849–860. doi:10.1128/MCB.01302-08.

Xia, D., W.K. Tang, and Y. Ye. 2016. Structure and function of the AAA+ ATPase p97/Cdc48p. *Gene*. 583:64–77. doi:10.1016/j.gene.2016.02.042.

Xia, Y., G.M. Pao, H.-W. Chen, I.M. Verma, and T. Hunter. 2003. Enhancement of BRCA1 E3 ubiquitin ligase activity through direct interaction with the BARD1 protein. *J. Biol. Chem.* 278:5255–5263. doi:10.1074/jbc.M204591200.

Xu, P., D.M. Duong, N.T. Seyfried, D. Cheng, Y. Xie, J. Robert, J. Rush, M. Hochstrasser, D. Finley, and J. Peng. 2009. Quantitative Proteomics Reveals

the Function of Unconventional Ubiquitin Chains in Proteasomal Degradation. *Cell*. 137:133–145. doi:10.1016/j.cell.2009.01.041.

Yang, H., J.-J. Li, S. Liu, J. Zhao, Y.-J. Jiang, A.-X. Song, and H.-Y. Hu. 2014. Aggregation of polyglutamine-expanded ataxin-3 sequesters its specific interacting partners into inclusions: implication in a loss-of-function pathology. *Sci. Rep.* 4:6410. doi:10.1038/srep06410.

Yang, K., R. Guo, and D. Xu. 2016. Non-homologous end joining: advances and frontiers. *Acta Biochim. Biophys. Sin. (Shanghai).* 48:632–640. doi:10.1093/abbs/gmw046.

Yao, T., and R.E. Cohen. 2002. A cryptic protease couples deubiquitination and degradation by the proteasome. *Nature*. 419:403–407. doi:10.1038/nature01071.

Ye, Y. 2006. Diverse functions with a common regulator: Ubiquitin takes command of an AAA ATPase. *J. Struct. Biol.* 156:29–40. doi:10.1016/j.jsb.2006.01.005.

Yin, Y., A. Seifert, J.S. Chua, J.-F. Maure, F. Golebiowski, and R.T. Hay. 2012. SUMO-targeted ubiquitin E3 ligase RNF4 is required for the response of human cells to DNA damage. *Genes Dev.* 26:1196–1208. doi:10.1101/gad.189274.112.

Zhang, F., Q. Fan, K. Ren, and P.R. Andreassen. 2009. PALB2 functionally connects the breast cancer susceptibility proteins BRCA1 and BRCA2. *Mol. Cancer Res.* 7:1110–1118. doi:10.1158/1541-7786.MCR-09-0123.

Zhang, J., J.M. Dewar, M. Budzowska, A. Motnenko, M.A. Cohn, and J.C. Walter. 2015. DNA interstrand cross-link repair requires replication-fork convergence. *Nat. Struct. Mol. Biol.* 22:242–247. doi:10.1038/nsmb.2956.

Zhang, W., Z. Qin, X. Zhang, and W. Xiao. 2011. Roles of sequential ubiquitination of PCNA in DNA-damage tolerance. *FEBS Lett.* 585:2786–2794. doi:10.1016/j.febslet.2011.04.044.

Zhang, X.-F., Q.-Z. Pan, K. Pan, D.-S. Weng, Q.-J. Wang, J.-J. Zhao, J. He, Q. Liu, D.-D. Wang, S.-S. Jiang, H.-X. Zheng, L. Lv, C.-L. Chen, H.-X. Zhang, and J.-C. Xia. 2016. Expression and prognostic role of ubiquitination factor E4B in primary hepatocellular carcinoma. *Mol. Carcinog.* 55:64–76. doi:10.1002/mc.22259.

Zhang, Y., Y. Lv, Y. Zhang, and H. Gao. 2014a. Regulation of p53 level by UBE4B in breast cancer. *PLoS One*. 9:e90154. doi:10.1371/journal.pone.0090154.

Zhang, Z., H. Yang, and H. Wang. 2014b. The histone H2A deubiquitinase USP16 interacts with HERC2 and fine-tunes cellular response to DNA damage. *J. Biol. Chem.* 289:32883–32894. doi:10.1074/jbc.M114.599605.

Zhong, X., and R.N. Pittman. 2006. Ataxin-3 binds VCP/p97 and regulates retrotranslocation of ERAD substrates. *Hum. Mol. Genet.* 15:2409–2420. doi:10.1093/hmg/ddl164.

Zhu, Q., N. Sharma, J. He, G. Wani, and A. a Wani. 2015. USP7 deubiquitinase promotes ubiquitin-dependent DNA damage signaling by stabilizing RNF168. *Cell Cycle*. 4101:37–41. doi:10.1080/15384101.2015.1007785.

Zimmermann, M., and T. de Lange. 2014. 53BP1: pro choice in DNA repair. *Trends Cell Biol.* 24:108–117. doi:10.1016/j.tcb.2013.09.003.

Zimmermann, M., F. Lottersberger, and S.B. Buonomo. 53BP1 Regulates DSB Repair Using. 2.

APPENDIX – PUBLICATIONS

During my DPhil, some of my work has contributed towards the following publications:

Lessel, D., B. Vaz, S. Halder, P.J. Lockhart, I. Marinovic-Terzic, J. Lopez-Mosqueda, M. Philipp, J.C.H. Sim, K.R. Smith, **J. Oehler**, E. Cabrera, R. Freire, K. Pope, A. Nahid, F. Norris, R.J. Leventer, M.B. Delatycki, G. Barbi, S. von Ameln, J. Högel, M. Degoricija, R. Fertig, M.D. Burkhalter, K. Hofmann, H. Thiele, J. Altmüller, G. Nürnberg, P. Nürnberg, M. Bahlo, G.M. Martin, C.M. Aalfs, J. Oshima, J. Terzic, D.J. Amor, I. Dikic, K. Ramadan, and C. Kubisch. 2014. Mutations in SPRTN cause early onset hepatocellular carcinoma, genomic instability and progeroid features. *Nat. Genet.* 46:1239–44. doi:10.1038/ng.3103.

Baranes-Bachar, K., A. Levy-Barda, **J. Oehler**, D. A. Reid, E. Rothenberg, K. Ramadan, Y Ziv, and Y Shiloh. UBE4A-mediated protein ubiquitylation at sites of DNA damage is essential for optimal repair of double-strand breaks. *Mol. Cell.* In revision.